DETERMINATION OF OPTIMUM BLEND OF BIOETHANOL-PETROL MIXTURE USING ULTRASONICATION FOR ENVIRONMENTAL FRIENDLY FUEL

Diakanua Nkazi

A thesis submitted to the Faculty of Engineering and the Built Environment, University of the Witwatersrand, Johannesburg, in fulfilment of the requirements for the degree of Doctor of Philosophy.

Johannesburg, 2014

DECLARATION

I declare that this thesis is my own, unaided work. It is being submitted for the Degree of Doctor of Philosophy in the University of Witwatersrand, Johannesburg. It has not been submitted before for any degree or examination in any other University.

(Signature of candidate)

---------- day of----------2014

ABSTRACT

Increasing global energy demand as well as air quality concerns have in recent years led to the search for alternative clean fuels to replace fossil fuels. One such alternative is the blending of petrol (gasoline) with ethanol, which has numerous advantages such as ethanol's ability to act as oxygenate thus reducing the carbon monoxide emissions from the exhaust of internal combustion engines of vehicles. However, the hygroscopic nature of ethanol is a major concern in obtaining a perfectly homogenized petrol-ethanol fuel. This problem has led to the study of ways of homogenizing the petrol-ethanol mixtures. Therefore, this thesis aimed at enhancing the homogenization of petrol-ethanol mixture.

Ethanol concentration in ethanol-water mixture plays a key role in enhancing the homogenization of the fuel, thus the bioethanol employed in this study was dehydrated with silica gel using ultrasonication-enhanced adsorption. Afterwards, the dehydrated ethanol was used in studying the homogenization of the fuel blend.

Water removal from the bioethanol using ultrasonication-enhanced adsorption shows a 28% increase when compared to the water removal using magnetic-stirring-enhanced adsorption, During ultrasonication-enhanced adsorption, the estimated adsorption enthalpy was –1 592.82 J/mol (exothermic) and the entropy was -5.44 J/ K mol, indicating a non-ordered loading of water molecules in the adsorption site. In addition, a modified pseudo second order kinetic model given by $\frac{d\,q_t}{(q_t - q_e)^2} = \frac{1}{q_e}[\,cos\,(K-t) - t\sin(K-t)]\,dt$ was proposed for the ultrasonication-enhanced adsorption process. Effect of temperature during ultrasonication-enhanced adsorption was found to be directly proportional to the amplitude and the pulse rate. However, increase in the amplitudes at lower pulse rates resulted in better cavitation, and hence better adsorption.

Furthermore, during phase behavior of ethanol-petrol blend, volume fractions of ethanol and petrol were studied with respect to t the depth within the storage container to confirm homogenization of the blend and time of storage. The binodal curve of the ternary diagram shows an increase of homogeneous region indicating an improved interaction between water and petrol. Therefore, the interesting results regarding the homogenization of the fuel blends

resulted from using ultrasonication-enhanced blending were very promising, and could be a platform upon which further research efforts could be built on.

The concentration distribution in the reactor showed proof of cavitation formation since in both directions, the variation of concentration with both time and distance was found to be oscillatory. On comparing the profiles in both directions, the concentration gradient, diffusion flux, and energy and diffusion rates were found to be higher in the vertical direction compared to the horizontal direction. It was therefore concluded that ultrasonication creates cavitation in the mixture which enhances mass transfer and mixing of ethanol and petrol. The horizontal direction was found to be the diffusion rate limiting step which proposed that the blender should have a larger height to diameter ratio. It is however recommended that further studies be done on the rate-limiting step so as to have actual dimensions of the reactor.

Testing of the blended fuel in internal combustion engine showed an optimal performance of this fuel at 60 % volume ethanol content with higher fuel power. The results of fuel consumption and emissions (such as CO_2 and CO) trends confirm various reports in literature on the performance of ethanol/petrol blended fuel.

To my wife Kanabwingi Nkazi Bijou, my children and family members who stand close to me. For your love, encouragement and support, thank you.

ACKNOWLEDGMENTS

Foremost, I would like to be grateful to God who gives me strength, knowledge and ability to do research through Christ Jesus.

To Professor Sunny E. Iyuke I would like to express my sincere gratitude for the supervision of this project, his continuous encouragement, guidance and support enabled the completion of my research project. The three years under his supervision taught me to develop a scientific rigor and effectiveness.

I would also like to thank the Nanotechnology and Petroleum Research Group of the University of the Witwatersrand for their contribution. They were able to share their knowledge, dynamism and good funniness through our research group meeting.

I want to thank warmly Doctor J. Mulopo and Doctor G. Simante for their valuable suggestion, insightful advice and support.

I would like to extend a heartfelt thanks to Mr. M. Bruce for his laboratory assistance and materials facilities, his contribution helped the success of the laboratory experiments.

I will not forget all academics and supports staff for creating an exceptional environment in the school. These years spend together have been rich in events and friendships. I have found a second family that will be difficult to leave.

I would like to thank as well my brother Diakanua Diantantu and his wife Billy Ilunga, my brother Diakanua Yizila and his wife Nicole Yizila, my sister Diakanua Mbila, couple Fatuma Kanabwingi and Matand, couple Mosse Sav and Tandu's family for their support and motivation during this research project. Thanks to all my friends and people who helped make this project successful.

Table of contents

Contents **Page**

LIST OF FIGURES

Figure **Page**

LIST OF TABLES

Table **Page**

LIST OF SYMBOLS

Active surface area	A
Adsorbate concentration at time t	C_t
Adsorbate concentration in the liquid phase initially (t = 0)	C_{So}
Adsorbate concentration in the liquid phase at time t	C_{St}
Adsorbate concentration on the adsorbent initially and at time t	C_{At}
Adsorbate volume in solid phase	V
Adsorbent and adsorbate affinity coefficient	β
Adsorbent void fraction	ε_p
Adsorption Enthalpy change	ΔH_{Ads}
Adsorption Entropy change	ΔS_{Ads}
Adsorption Free Gibbs Energy	ΔG_{Ads}
Adsorption rate constant	k_{Ad}
Clearance volume	V_c
Connecting rod length	l
Constant which depend on the micropores distribution	D
Diffusion length	L
Diffusion time	τ_D
Effective diffusivity	D_{eff}
Effectiveness of the system	ε_{system}
Efficiency of the engine	η
Energy intensity of ultrasonication	I_{US}
Equilibrium adsorbate concentration	$C_{s\,eq}$
Exergies	a_i
Final adsorbate concentration	C_f
Fraction of ethanol or petrol	x_k
Ideal gas constant	R
Initial adsorbate concentration	C_0
Mass transfer coefficient	K_f
Maximal adsorption capacity	V_0
Power transferred to the reactor	P_{US}
Pressure	P

Property of the fuel mixture	ε_m
Property of pure ethanol	ε_k
Radius	r
Ratio of specific heats	γ
Solute diffusivity in the fluid	D_{AB}
Sound velocity	c
Specific heat at constant volume	C_V
Specific heat at constant volume	C_P
Temperature	T
Thermochemical availability	a_{th}
Tortuousity	τ
Turbulent flame factor	f
Ultrasonic pressure amplitude	P_o

CHAPTER 1: RESEARCH BACKGROUND

1.1 Introduction

Increasing demands in alternative clean fuels have resulted in different modifications on the existing production processes of well-known fuels, such as, petrol. These modifications include the blending of petrol with alcohols, such as, ethanol, pentanol and methanol. Alcohols are usually blended with petrol to increase the octane number, by acting as oxygenator to increase the fuel additive and as a replacement for compounds like Methyl Tertiary Butyl Ether (MTBE) (Hughes, 2009). Among the above mentioned alcohols, the mostly used alcohol is ethanol due to its significantly higher research octane number. In addition, ethanol adds oxygen to the blends, contains zero benzene and aromatics, and has low sulphur content, which increases the hydrocarbon blending value relative to petrol (DOESA, 2009). The ability of ethanol to act as an oxygenate reduces the carbon monoxide emissions and thus resulting in less greenhouse effects like global warming and this makes this research topic a relevant field of study.

In South Africa, ethanol is produced locally, thereby making it an easily accessible alternative source as a fuel blend. Ethanol is produced through fermentation process using renewable carbon source, such as, sugars as feedstock (Rutz et al, 2008; Walker, 2010). The use of ethanol is environmentally friendly due to its very low toxicity (Walker, 2010). At the same time, commercial production of synthetic ethanol from the Fischer-Tropsch process is undertaking by Sasol produces at Secunda, thus making ethanol readily available for petrol-ethanol blend process (DOESA, 2009). In spite of the enormous benefits of ethanol as a source of fuel, authors have complained that the use of ethanol is hampered by its high volatility, high cost of production, distribution issues, market complaints, quality assurance, and its hygroscopic nature (DOESA, 2009). .

However, despite these concerns, ethanol is the most promising octane-raising additive for petrol (Rasskazchikova et al., 2004). An evaluation made by Da Silva et al. (2005) shows the positive effect of the addition of oxygenates, such as, ethanol on the Reid vapor pressure (RVP), the anti-knock properties of gasoline, and octane ratings. The use of oxygenated additives led to improved burning in the combustion process, and reduction of emission of

carbon monoxide and the levels of aromatics compounds. Holley et al. (2006) conducted a study on the extinction of premixed flames of mixtures of liquid fuels (such as ethanol, methanol and hydrocarbon fuels) with air at atmospheric pressure. The mixture was considered because of their relevance to spark ignition engine. The experiments were performed in the counterflow configuration and the extinction strain rate was determined through the use of laser Doppler velocimetry and digital particle image velocimetry, and was numerically simulated using chemical kinetics and molecular transport. The results indicate that, for the same equivalence ratio, the ethanol and methanol flames are more resistant to extinction than the hydrocarbon flames under fuel-lean conditions.

Furthermore, blending bio-fuels with a petroleum-based fuel has dual advantage: (i) addition of a relatively small percentage will result in a substantial total volume of gasoline substitution, and (ii) the existing infrastructure for distributing fuels can be used without any modifications to it. When ethanol is mixed with water, liquid or in the form of humidity, ethanol absorbs some or all water until saturation point is reached. When a saturation point is reached, the ethanol-water phase separates, and petrol-ethanol solution form distinct layers in the tank. The change in temperature can also stimulate the phase separation.

Sonochemistry studies the methods for the generation of power ultrasound. It is used in liquid as the medium because sonochemistry is driven by acoustic cavitation which can only occur in liquids. The device is capable of converting mechanical or electrical energy into high frequency sound called transducer. There are four main types: liquid driven, gas driven, electromechanical and magnetically-driven vibrating bar.

The spectacular effects of cavitation phenomena (high temperature and pressure locally, strong acoustic streaming, high shear stress near the bubble wall) has been successfully exploited for various applications such as chemical mixing (in homogenous and heterogeneous systems), waste water treatment, biotechnology, polymer chemistry, etc.

I.2 Research problem and motivation

Of highest concern however is the hygroscopic nature of ethanol which leads to moisture being taken up by the fuel. The fact that water and alcohol are fully miscible means that this

nature can cause the alcohol and water to separate from petrol and form two distinct layers. This is a process commonly termed phase separation. During this process, alcohol and water are partially removed from petrol. These two are much denser than petrol and thus they tend to form a dense bottom layer consisting of some alcohol-soluble hydrocarbons. The petrol partially depleted of alcohol forms the upper less dense layer (Hughes, 2009). This behaviour of petrol blend can result in the bottom layer being stirred up and pumped into the vehicle thus stalling the engine. The second problem is that the upper layer will be reduced in octane value and not meet the specifications (Hughes, 2009).The process of phase separation is therefore a field of study in the fuel industry, and looking at the demand of fuel, there is an urgent need to control the effect of phase separation on the ethanol and petrol blend.

Several research reports have appeared in literature on various ways of mixing/blending fuels (Wilks, 2008), however, a few research has been conducted to investigate the relationship between mixing technique and water content during fuel blending

1.3 Objective

The main objectives of this research involving fuel blending and internal combustion processes are to:

- Investigate the effect of the ultrasonication on the phase behavior of ethanol-petrol blend;
- Develop ethanol dehydration process using adsorption enhanced by ultrasonication;
- Discuss the kinetic model of adsorption of water enhanced by ultrasonication;
- Study the horizontal and vertical ethanol-petrol blending profile using ultrasonication;
- Discuss the mixing hydrodynamic of ethanol-petrol mixture during the blending process;
- Study the internal combustion of ethanol-petrol fuel;
- Analyse the level of pollutants and emissions arising from the use of ethanol-petrol fuel that may cause environmental and health problems.

1.4 Research approach

A conceptual approach was taken to achieve the main goal of this study. The approach involves several steps. The steps are depicted in Figure 1.1. It is essential to dehydrate distilled bioethanol to meet required water content for homogeneous ethanol-petrol blend. The dehydrated ethanol was then blended with petrol, followed by testing of the ethanol-petrol fuel in the internal combustion.

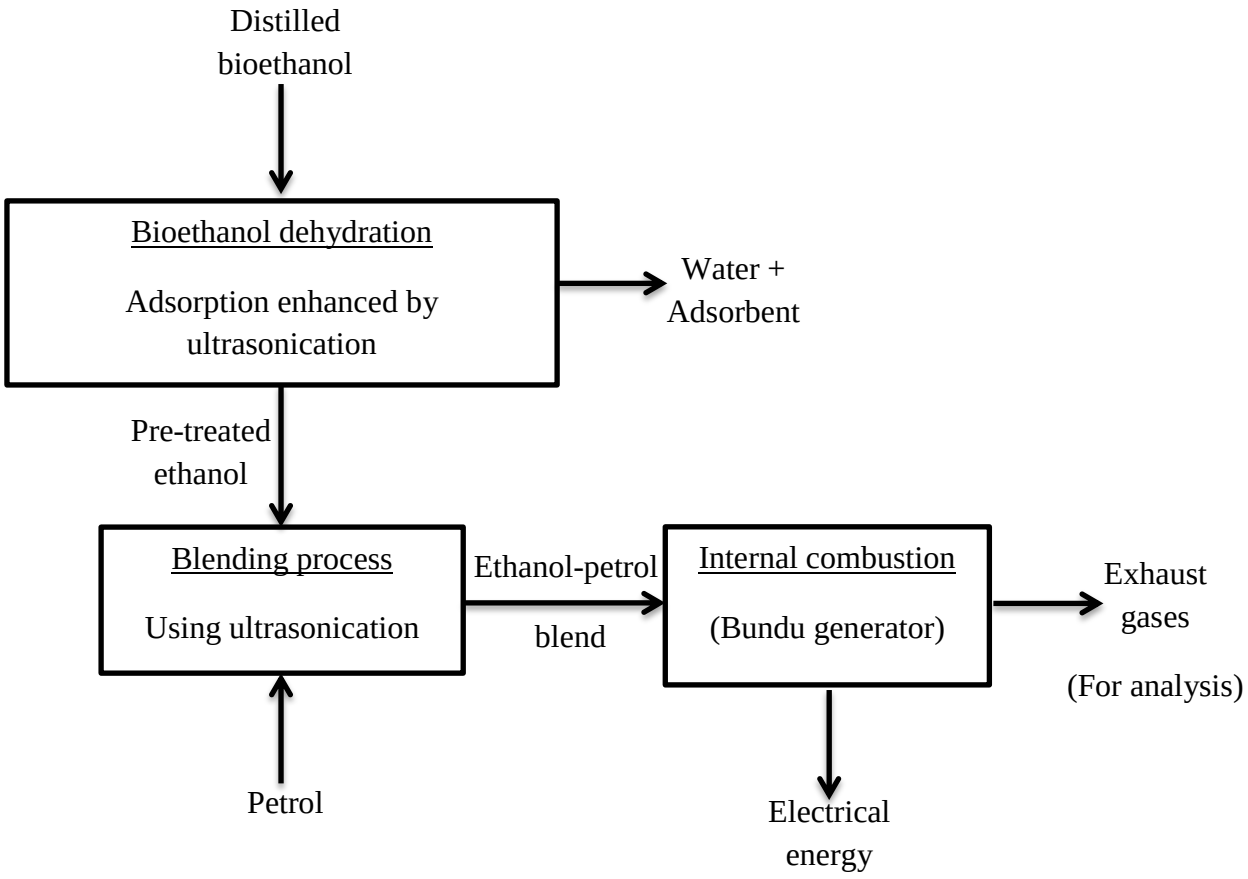

Figure 1.1: Conceptual approach employed in the study

1.5 Thesis outline

The layout of the thesis is as follows:

This thesis addressed problems related to the blending process enhanced by ultrasonication, and investigated the effect of the blend percentage and operating variables. The following chapters will discuss the issues related to the pre-process (dehydration of bioethanol), main process (blending of bioethanol-petrol mixture) and testing of fuel produced.

- Chapter 1 provides information on the background, and a short overview of fuel blend to understand the remainder of the thesis. This chapter discuss the research problem, objective of the research and the approach used to achieve the main goal of this study.

- Chapter 2 presents the necessary background on phase behavior of the possible fuel content such as water, bioethanol and petrol; the dehydration process by adsorption with summary of adsorption kinetics and adsorption mechanism; review of ethanol-petrol blend and ultrasonication process; and finally the internal combustion of blended fuel.

- Chapter 3 provides details of the experimental methods and analytical procedure used in this project. This chapter presents the range of blends used for phase behavior study through a ternary diagram and the sampling method for dehydration and blending processes.

- Chapter 4 presents the experimental results of the phase behavior of ethanol-petrol blend enhanced by ultrasonication, this include the dehydration process, and the testing of the blend in internal combustion engine.

- Chapter 5 lays out the discussion of the results presented in chapter 4, which can be used to better the understanding of the production of the bioethanol-petrol blend using ultrasonication-enhanced blending.

- Chapter 6 concludes this research project by proposing the fitting dehydration kinetics model and presents the mixing behavior of bioethanol/petrol blend. This analysis

provides a set of recommendations for better understanding of the blending process enhanced by ultrasonication.

During the course of this project two journal patents were filed and three papers were sent for publication

- Filed Patents:
  a. Blending bioethanol and petrol using cavitation for internal combustion engine "IYUKE 9 Pat", which explores the new technique of mixing two fuels components. Details of the blending technique enhanced by ultrasonication were discussed including the effect of the ultrasonication on the phase behaviour.

  b. Purification of ethanol "Iyuke Pat 14.1". This work explores the adsorption technique enhanced by ultrasonication.

- Manuscripts under review in scientific journals:

  1) Dehydration of bioethanol by adsorption enhanced by ultrasonication:

This paper discusses the effect of the adsorbent mass and ultrasonicator setting on the enhancement of adsorption of water.

  2) Mixing hydrodynamics of bioethanol and unleaded gasoline using ultrasonication:

The effect of operating variables such as pressure, temperature, concentration of ethanol at different positions from the ultrasonicator horn and time during ultrasonication-enhanced blending were discussed.

  3) Thermodynamics studies of bioethanol- gasoline blend using cavitation in internal combustion:

The exhaust gases such as CO_2, CO and NO_x were analyzed and discussed as function of ethanol content in the blended fuel.

CHAPTER 2: LITERATURE REVIEW

2.1 Phase behavior of ethanol-petrol blend using ultrasonication

Ethanol dissolves both in gasoline and water, so when water comes into contact with ethanol-petrol mixture, it is more likely that some of the ethanol dissolved in the petrol will move to the water side, decreasing the octane content of gasoline. The mixture of petrol and ethanol is capable of absorbing a certain amount of water and this eventually leads to a change in crucial properties of the mixture.

2.1.1 Characteristics of ethanol-petrol-water mixture

Due to increasing demand of new environmentally friendly fuels, ethanol is a good alternative fuel since its combustion produces less greenhouse gases emissions. The disadvantage of using ethanol instead of petrol is that ethanol has a low heating value compared to pure gasoline. The use of ethanol as a fuel source can reduce total dependency on crude oil. The addition of ethanol to petrol increases the octane content of the petrol and the formation of photochemical smog. The higher the ethanol content of the ethanol-petrol blend, the higher the rate of combustion (Anderson et al, 2010).

Ethanol is the hydrophilic substance; therefore it has a great attraction for water molecules. Water removes or decreases the ethanol content of gasoline and thus the octane content of gasoline is severely affected. Water has a negative effect on the engine of the vehicle, while small amounts of water in the solution with gasoline cannot cause any significant damage (Badrana et al, 2011).

As water dissolve in gasoline, the maximum amount of water that gasoline is capable of absorbing is reached and this indicate the equilibrium being achieved. At this point any excess water will not dissolve and this results in the formation of two separate phases with different composition of ethanol. The amount of water that gasoline is capable of absorbing depends on the temperature as well as on pressure of the fuel system (Hughes, 2009).

Water is denser than gasoline, so when water is mixed with gasoline, water settles to the bottom of the tank. In processing plants this requires the installation of control system at the bottom of the tank so that the operator is alerted when water is present at the bottom of the tank. The problem with these sensors is that if water is dissolved in the gasoline, it cannot be

detected and thus no further action can possibly be taken by the controller/ operator (Ejikeme, 2013).

Some ways of controlling phase separation include making a good choice of alcohol, using required amount of alcohol, using suitable solvents, using optimum blending temperature, blending appropriate hydrocarbon composition of petrol, and the amount of water (Hughes, 2009). In this study, mixing techniques were studied in order to enhance homogeneous mixing of water, ethanol and petrol. Ethanol is industrially produced with a purity of 95 to 99.9% with the balance being water and thus it is of importance to ensure a homogeneous mixture of petrol and ethanol prior to pumping into an engine.

The use of ethanol blended gasoline is specifically beneficial in winter due to absorption of water to prevent gas line freeze. Important point is that water in the gasoline should not be present in large amounts to cause damage to the engine. The contamination of gasoline by water in stations in most cases is caused by the rain and the seepage of ground water in the underground tank through tiny holes on the tank (Ejikeme, 2013).

Stirring is the most used method of blending petrol and ethanol, and this relies on the bulk movement of the fluids. Several research results comparing different mixing methods, such as impinging-jet micro mixing method, the use of stirred tank and high pressure homogenizing method, have been reported in literature (Donsi et al, 2010; Thoma et al, 2013) . These techniques are however compared in terms of energy demands in the emulsification of oil and water (Siddiqui, 2011). The results showed that for a given energy dissipation rate, ultrasonication gives the smallest emulsion drop size and this was comparable to that of the high-pressure homogenizer at a lesser ultrasonicator energy (Siddiqui, 2011). Silverson rotor-stator device was found to give the biggest droplets for similar energy dissipation rate while Impinging-jet micro mixer gave intermediate drop sizes (Siddiqui, 2011). It can be concluded from the information above that ultrasonication has the ability to produce a homogeneous mixture at low energies.

Hydrous gasoline may be advantageous since its use reduces amount of greenhouse gases that are released from the engine, for example CO_2 and NOx emissions due to slow burning inside the engine. Depending on the amount, the addition of ethanol in gasoline causes significant damage on the metals that are in use in gasoline engines due to decreased polarisation. The same comment applies when water is present in the gasoline as a contaminant. The corrosion caused is localized type corrosion (Lou, 2010).

2.1.2 Phase behavior of ethanol-petrol blend

A chemically and structurally stable system can be homogeneous or heterogeneous depending on the miscibility or immiscibility of phases involved in the blend (Vukovic et al, 1999). These behaviours are influenced by chemical composition, temperature and interactions between substances. The higher the free energy the more the system shows a homogeneous mixture.

Ethanol-petrol mixture is essentially immiscible with water, while ethanol can mix in both water and petrol due to its polar and non-polar groups (Bridgeman, 1933). The mixture formed two phases depending on the water content; therefore the phase behavior depends on the qualitative description and quantitative phases in the mixtures. The phase behaviour is represented in a diagram (ternary diagram) that reflects the compositions of the substances involved in the system. The nodal curve shows the limit between phases (Homogeneous and heterogeneous phases) in the ternary diagram, which determines at which compositions the phases separate.

Breaux (2012) found that the increase of water in the blended fuel reduce the ignition probability and the exhaust gas temperature. Egebäck (2005) stated that during the phase separation, water absorbs ethanol from the blended fuel, and may compete with the petrol-oil to reduce the lubricating ability of the lubricating oil in two-stroke engine. Therefore water content needs to be controlled to avoid negative effect of the fuel blend.

2.1.3 Ternary diagram for ethanol-petrol blend

The convenient way of studying phase behavior is by the use of the triangular diagrams. The ternary diagram essentially contains sloping straight lines which are referred to as tie lines, and the curved line known as the binodal curve. The points on this line and above represent the single phase that does not split into two immiscible phases whereas the area that lies below this curve represents the formation of two phases that are at equilibrium with each other**.**

Triangular diagram

The physical phase behavior of ternary systems for mixing, distillation and liquid-liquid extraction can be represented, at constant temperature and pressure, on an equilateral triangle ternary diagram. This representation uses the fact that the sum of the three distances that represented the component concentrations of the ternary system, from an inner point is constant. The ternary-phase diagram shows a completely mixed system at equilibrium and does not explain the mixing process. The binodal curve indicates the limit at which the three liquid components exist as a single phase. Let note that petrol is a complex mixture of hydrocarbons, therefore the phase behavior when mixed with water and ethanol may be influenced by its composition.

Figure 2.1 shows water-ethanol-petrol ternary diagram at 18 ^{0}C developed by kyriakides et al. (2012) in term of volume fraction.

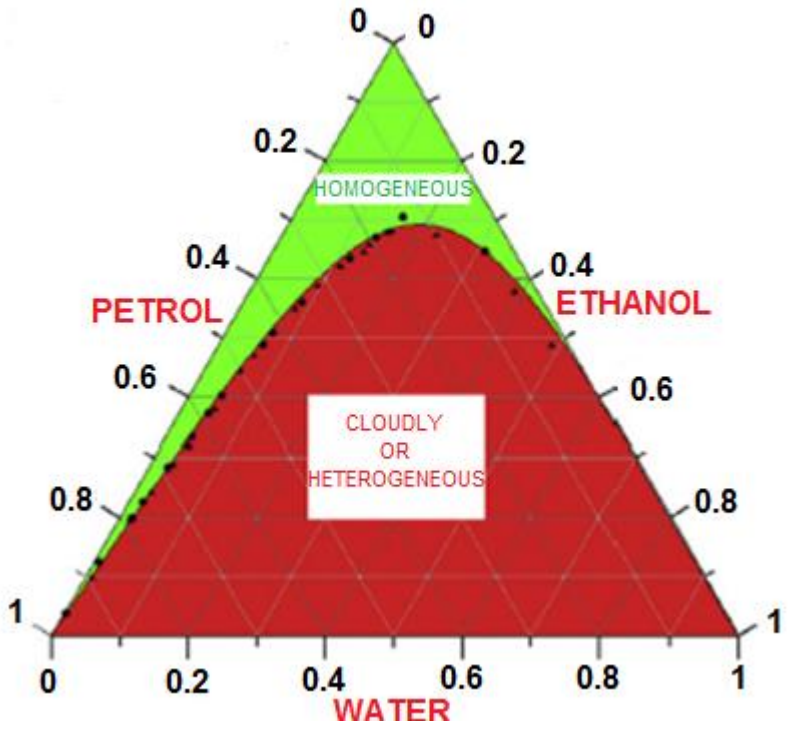

Figure 2.1: Ternary diagram for water-ethanol-petrol mixture (Kyriakides et al., 2012)

Phase behaviour of a mixture is affected by some variables, which eventually result in different binodal curves in a ternary diagram. These factors are (De Oliveira et al, 2000):

- ✓ The volumetric ratio or the composition of the representative point of the system in the ternary diagram;
- ✓ Temperature which has a significant effect on the phase behavior (increase in temperature increases the miscibility of petrol-water system);
- ✓ Chemical nature of the ternary components

2.2 Ethanol-petrol mixture using ultrasonicator-enhanced blending

Addition of oxygenates to petrol can increase the octane number of petrol to the required level. According to Rasskazchikova et al. (2004), the spectrum of oxygenates used is broad such as ethers- methyl tert-butyl, methyl tert-amyl, ethyl tert-butyl, and diisopropyl. Alcohols such as methanol, ethanol, and some higher alcohols have been used to boost the octane number of petrol (Felton et al, 1987). Additionally, these additives have a high blending octane number, low volatility, minimum carbon formation, and low petrochemical activity (Furey et al, 1991). The most used oxygenates are alcohols because alcohol-petrol blends have properties comparable to traditional petroleum fuels. The commonly used alcohols are methanol and ethanol. The use of methanol, despite its high blending octane number, is discouraged in many countries, due to its high toxicity, volatility, and hygroscopicity (Rasskazchikova et al., 2004).

Rasskazchikova et al. (2004) further states that ethanol became more competitive as a result of the introduction of new continuous fermentation manufacturing processes instead of the old cyclic/ batch in one hand, the gradual increase in petrol price (Rodrigo et al, 2009) in the other hand. In addition, ethanol is less hygroscopic, less toxic and possesses higher heat of combustion and lower evaporation rate when compared to methanol. The above mentioned advantages of ethanol contributed towards its use. It is therefore obvious that the use of ethanol in fuel blending could contribute to the reduction of air pollution, while at the same time, maintaining, and perhaps, also improving engine performance in the modern vehicle. The growing interest in ethanol is also due to the possibility of manufacturing it from renewable plant feedstock (Rasskazchikova et al., 2004).

2.2.1 Dehydration of bioethanol by ultrasonication-enhanced adsorption

As discussed in Chapter 1 of this thesis, removal of water is essential to enhance the homogeneous mixing of ethanol-petrol blend. Therefore, dehydration of ethanol (bio-ethanol), whereby water is removed is required before fuel blending.

In this study, dehydration of bioethanol using adsorption process was investigated. Industrial adsorption techniques are employed for largely separation processes such as: gas recovery, solvent recovery, ultra-purifications, fine chemicals and bio-separations. The industrial adsorption techniques may be classified as follow:

- Adsorbate concentrations, these techniques are based on the removal of trace contaminants from a bulk process;
- Adsorption process, this type may use a cyclic batch or continuous counter-current process and it is based on the modes of operation in the adsorption phenomena;

- Adsorbent regeneration processes: Regeneration methods use a chemical or physical agent that reverse the process, and the industrial techniques employed for this type are Temperature swing adsorption (TSA) and Pressure swing adsorption (PSA).

One of the current industrial methods, based on adsorption, applied for the dehydration of ethanol is pressure swing adsorption (PSA) and some drawback (Cavalcante, 2000) with TSA and PSA are:

- ✓ TSA: The mechanical energy is more expensive than the heat of adsorption, the operation is done at very low pressure, and the desorption occurs at low purity;
- ✓ PSA: There is inefficient usage of the energy available and the adsorbent activity is less efficient. Also in the liquid system, high latent heat flux of interstitial fluid should be added.

Due to the challenges facing the use of TSA and PSA, this study investigates the adsorption process under pressure waves and temperature generated by cavitation process. The system uses an adsorbent disperses in the liquid phase. To enhance the dehydration of bioethanol via

adsorption technique, two mixing-enhanced methods, mixing with magnetic stirrer and mixing with ultrasonication, were investigated and compared. The ultrasonication-enhanced dehydration of bioethanol uses ultrasound energy in liquid phases to promote the mixing. In addition, silica gel was used as adsorbent in the dehydration process.

2.2.1.1 Adsorption of water on silica-gel

Adsorption is a mass transfer process, in which molecules (adsorbate) from gas or liquid phase interact with and attach to surface of a solid (adsorbent) (Wu, 2004). The transport process of water toward the adsorbent in this case is driven by attraction force. The polar bond formed between the adsorbate and the adsorbent as seen in Figure 2.1 allows purification or dehydration of ethanol by removing undesirable material such as water in gaseous or liquid phase.

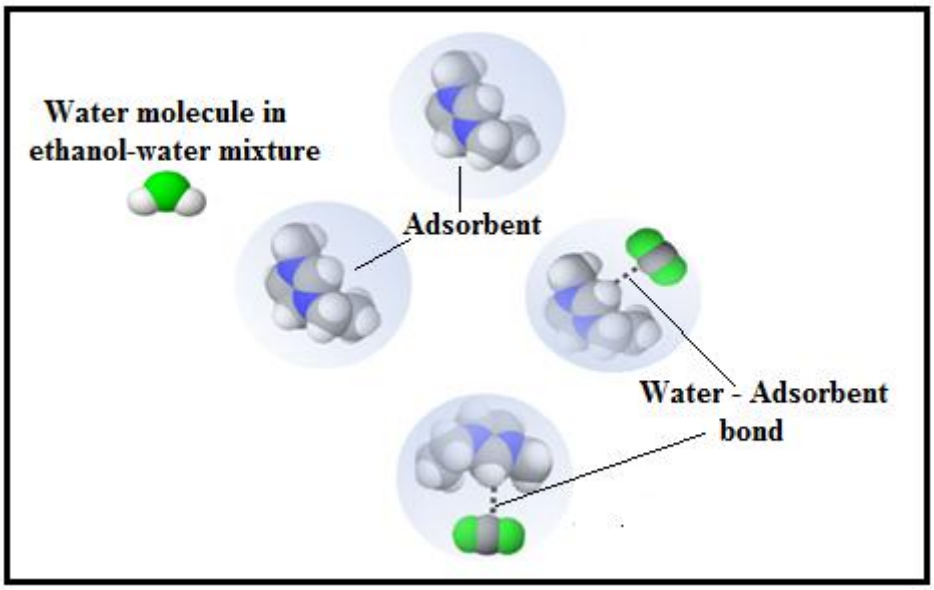

Figure 2.2: Adsorption process

Based on the type of contact between adsorbate and adsorbent and the quantity of energy involved during the adsorption process, two types of adsorption have been identified: physical adsorption (physisorption) and chemical adsorption (chemisorption) (Rachidi, 1994; Mechrafi, 2002). Due to low energy exchange between the adsorbent and the adsorbate on the solid surface, physical adsorption occurs and is mainly caused by van der waal forces between the adsorbate and the adsorbent (Desjardins, 1990). The attraction is not fixed to a

specific site and the adsorbate is relatively free to move on the surface. This is relatively reversible and capable of multilayer adsorption.Since physisorption is reversible; it does not affect the chemical nature of the adsorbate molecules (Madani, 2004).

Chemical adsorption occurs via chemical interaction between the adsorbate and certain functional groups on the surface of the adsorbent. Therefore the adsorption process depends on the functional groups present on the adsorbent and not the surface area. Adsorbed molecules are not free to move on the surface. There is a high degree of specificity and typically a monolayer is formed. The process is seldom reversible due to a stronger perturbation of the molecular electronic structure with formation of chemical bonds between adsorbate and adsorbent. Chemisorption occurs at higher temperature and required more energy. Table 2.1 presents the comparisons between physical adsorption and chemical adsorption.

Table 2.1: Comparison between physisorption and chemisorption

Physisorption	**Chemisorption**
Molecules are adsorbed on available sites	Molecules are adsorbed on active sites only
Adsorbates are molecules	Adsorbates are atoms or radicals
Multiple layers	Single layer
Attraction is a result of Vander Waal's force	Attraction is a result of bonds
Forces are weak but act on long distance	Forces are strong but act on short distance
Reversible	Irreversible
Adsorption temperature must be below the boiling point of the adsorbate	Occurs at any temperature
Heat of adsorption is less than 50 KJ/ mol	Heat of adsorption can be more than 100 KJ/ mol (Christmann, 2012)

2.2.1.2 Adsorption mechanism

The adsorption mechanism that dominated the ultrasonication-enhanced dehydration of bioethanol via adsorption technique is physisorption of water onto silica gel. It is probable that the mechanism employed had also some potential of chemical adsorption, but the

contribution of chemisorption to the overall adsorption is negligible. The attractive forces depend on the adsorbent geometry and electronic properties of the adsorbent and adsorptive. Adsorption occurs when the attraction between the solute and the solvent is less than the interaction with the adsorbent. The adsorption process of solute on the solid adsorbent involves: :

- ✓ the transport of the solute in the fluid phase to the adsorbent surface through diffusion or bulk motion (mass transfer);
- ✓ the transport of the solute from the surface to the adsorbent pores (Intragranular diffusion).

The attachment of solute to the adsorbent and transfer of the solute into adsorbate pores; this mechanism depends on (Cheremisionoff et al, 1978; Wu, 2004):

1. the physical and chemical properties of the adsorbent;
2. the physical and chemical properties of the adsorbate;
3. the amount of the adsorbate, and the process parameters.

Intraparticle (intragranular) diffusion can be characterized by an effective diffusivity (D_{eff}), given by:

$$D_{eff} = D_{AB}\, \varepsilon_p / \tau \qquad (2.1)$$

Where D_{AB} is the solute diffusivity in the fluid, ε_p is the adsorbent void fraction, and τ is its tortuosity. If the adsorbent radius is given by r (in metre), (D_{eff}/r^2) can be approximated by the following relationship:

$$\frac{C_t - C_0}{C_f - C_0} \approx \frac{6}{\sqrt{\pi}} \left(\frac{D_{eff}\, t}{r^2}\right)^{\frac{1}{2}} - 3\frac{D_{eff}\, t}{r^2} \approx 1 - \frac{6}{\pi^2}\, e^{-\pi^2 D_{eff} \frac{t}{r^2}} \qquad (2.2)$$

Where C_t, C_0, and C_f are the adsorbate concentration at time t, the initial adsorbate concentration, and the final adsorbate concentration, respectively.

Therefore the effective diffusivity may be determined from the gradient of the graph of $\ln\left[\frac{C_f - C_t}{C_f - C_0}\right] against\ time\ t$ given by the following equation.

$$\ln[\frac{C_f - C_t}{C_f - C_0}] = \ln\left(\frac{6}{\pi^2}\right) - \pi^2 D_{eff}\frac{t}{r^2} \quad (2.3)$$

2.2.1.3 Factors affecting water adsorption

A number of factors can influence the adsorption process, including the adsorptions capacity and kinetics (Perrat, 2001; Mekaoui, 2001). The adsorbate molecule size, polarity and its solubility affect the transport process toward the adsorbent surface. In addition, pressure (for gas-phase adsorption), surface area and structure of the adsorbent, temperature of the medium do influence the adsorption process.

If the size of the adsorbate is less than the pore diameter of the adsorbent, the solute can diffuse easily in the porous and reach the adsorption site. Lundelius' rule state that adsorption of a solute is inversely proportional to its solubility in the solvent. The greater is the solubility of adsorbate molecule in the solvent, the smaller is its extent of adsorption. At the same time, the selectivity domain in which adsorption occurs may depend on the type of interaction between the adsorbate and the adsorbent. Therefore the adsorption of water (polar molecule) on a solid with polar terminal on the adsorption site will show higher adsorption capacity. In term of the surface area of the adsorbent, the greater the specific area of the solid, the greater would be its adsorbing capacity. Adsorption processes are generally exothermic therefore the increase in temperature decreases the attachment adsorbate – solid. Also, an increase in pressure causes an increase in the magnitude of adsorption of an adsorbent

2.2.1.4 Adsorption models for water-silica gel

Various models are used to discuss the adsorption process of water on silica gel (Hui et al, 2002), but the thermodynamic and the kinetic models were used to discuss the effect of ultrasonication on the adsorption process of water-silica gel.

Thermodynamics of surface adsorption

Adsorption process is exothermic and the heats released might be the result of the energetically favourable interactions (the electrostatic attractions and the intermolecular forces) between the adsorbate and adsorbent species. The adsorption energy (E_n) required to the transfer of the solute molecules from the liquid phase to the solid phase can be expressed as:

$$E_n = -RT \ln \frac{C_{solute\ in\ bulk\ solution}}{c_{soute\ in\ solid}} \tag{2.3}$$

Polanyi's theory

The existing of potential field around the adsorbent surface facilitates the adsorption process, and the adsorption potential needed to compress the vapour from its equilibrium pressure to the saturated pressure is given by (Zoubir, 2007; Dubinin et al, 1947; Polany et al, 1970):

$$E_n = \int_{P_{equil}}^{P_{sat}} V\, dP = \int_{P_{equil}}^{P_{sat}} \frac{R\,T}{P} dP = RT \ln\left(\frac{P_{sat}}{P_{equil}}\right) \tag{2.4}$$

Equation of Dubinin and Radushkevich

Dubinin and Radushkevich (Zoubir, 2007; Dubinin et al, 1947; Polany et al, 1970) proposed the relationship between the fraction of the molar volume occupied by the adsorbate and adsorption potentials. The proposed equation is applied to micropores and is given by the following:

$$V = V_0\, e^{-D\,[\frac{T}{\beta}\ln\left(\frac{P_{sat}}{P_{equil}}\right)]^2} \tag{2.5}$$

Where V_0, V, D and β are the maximal adsorption capacity, the adsorbate volume in solid phase, the constant which depend on the micropores distribution of the adsorbent, and adsorbate affinity coefficient, respectively.

The adsorption thermodynamics is characterized by the temperature, energies and pressures. This process is spontaneous; therefore ΔG is negative and is given by the following expression:

$$\Delta G_{ad\,m} = \Delta \mathrm{H}_{ad\,m} - \mathrm{T}\Delta S_{ad\,m} \tag{2.6}$$

The thermodynamic quantities may be determined from the heat released during the process and the adsorbate amount. The measured heat corresponds to the molar enthalpy which can be measured at different temperature using isosteric method (Zoubir, 2007). The adsorbate potentials at equilibrium in both phases become equals for a given filling of adsorbent and the isosteric adsorption enthalpy and entropy can be determine from the gradient and y-intercept of $\ln\frac{P}{P_0}$ $against$ $\frac{1}{T}$ from the following equation:

$$\ln\frac{\mathrm{P}}{\mathrm{P_0}} = \frac{\Delta \mathrm{H_{ad\,m}}}{\mathrm{R}}\,\frac{1}{\mathrm{T}} - \frac{\Delta \mathrm{S_{ad\,m}}}{\mathrm{R}} \tag{2.7}$$

The above relation from isosteric method resembles the differential equation in respect of T of the Clausius-Clapeyron relation given by:

$$\Delta H_{ad\,m} = -RT^2\,\frac{\partial}{\partial T}\left(ln\frac{P}{P_0}\right) \tag{2.8}$$

Design of adsorption process

Batch adsorbers are suitable for liquid phase adsorption, where the specific area of the adsorbent, the temperature and the adsorption time are determining factors for the separation process. The adsorption time depends on the adsorbate concentration, adsorbent size, mixing energy and the viscosity of the liquid phase. The first step on the adsorption design is to find an expression from the mass balance equation followed by the optimal time for the adsorption process.

If the adsorbate volume is negligible compare to the liquid phases; the total volume may be assumed to be constant. Also if C_{So}, C_{St}, are the adsorbate concentration in the liquid phase at t = 0, and at time, t, respectively; and C_{Ao} and C_{At} are the adsorbate concentration in the liquid phase on the adsorbent at t = 0 and at time t, respectively; then the mass balance equation can be written as follow:

$$m\,C_{Ao} + V\,C_{So} = m\,C_{At} + V\,C_{St} \tag{2.9}$$

Where m is the mass of the fresh adsorbent in mg, and V is the volume of the liquid phase in mL.

Equation (2.9) can be written as follow:

$$m\,(C_{Ao} - C_{At}) = V\,(C_{St} - C_{So}) \tag{2.10}$$

If Equation (10) is divided by by V C_{So}, it gives:

$$\frac{m}{V}\left(\frac{C_{Ao}}{C_{So}} - \frac{C_{At}}{C_{So}}\right) = \frac{C_{St}}{C_{So}} - 1 \tag{2.11}$$

Further simplification of Equation (11) gives:

$$\tau\, y_o - \tau\, y = x - 1 \tag{2.12}$$

and,

$$y = y_o + \frac{1}{\tau}\,(1 - x) \tag{2.13}$$

where $y_o = \frac{C_{Ao}}{C_{Ao}^{eq}}$, $y = \frac{C_{At}}{C_{At}^{eq}}$, $x = \frac{C_{St}}{C_{So}}$, $C_{Ao}^{eq} \equiv$ adsorbate concentration in the adsorbent phase initially (t = 0), C_{At}^{eq} adsorbate concentration in the adsorbent phase at time t and $\tau \equiv$ distribution rate $= \frac{m}{V}\frac{C_{Ao}^{eq}}{C_{So}}$. Therefore the distribution rate can be determined by graphical method using Equation (2.13).

With the use of Equation (16), the contact time during the adsorption can be determined. The adsorption rate in term of mass transfer in the liquid phases is given by following expression:

$$-\frac{dC_{St}}{dt} = k_f \left(C_{St} - C_{eq}\right) \tag{2.14}$$

By integrating the differential Equation (2.14) and solve for time t gives the expression of the contact time (2.16).

$$\frac{\mathrm{dC_{St}}}{(C_{eq} - C_{St})} = k_f \, dt \tag{2.15}$$

And,

$$t = \frac{1}{k_f} \int_{C_{So}}^{C_{So}^{eq}} \frac{dC_{St}}{(C_{eq} - C_{St})} \tag{2.16}$$

Also the mass transfer coefficient can be determined by solving the differential equation (2.15) at a time t.

Adsorption mechanism during ultrasonication-enhanced adsorption

The adsorption of water molecule from liquid phase to a solid phase may be explained by heterogeneous mechanism; the adsorbates diffuse to the adsorbent disperse in the reactor as depicted in Figure 2.3. The mechanisms involved during the ultrasonication-enhanced adsorption process are:

- Solute transport from the solvent (liquid phase) to the solid surface;
- Transport of the solute molecule through the adsorbent pores; and
- Adsorption on the adsorbent site.

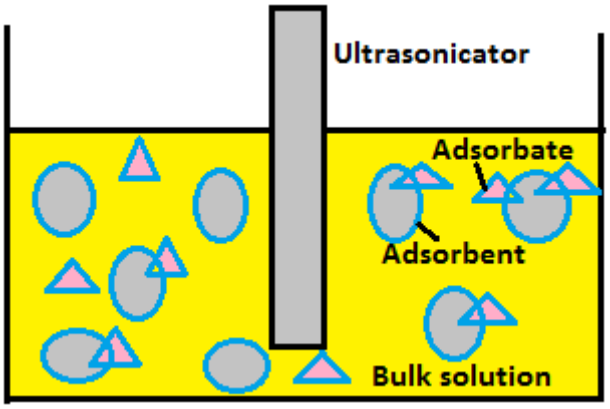

Figure 2.3: Schematic of adsorptions mechanism

Kinetic studies facilitate the understanding of the adsorption mechanism. The adsorption time depends on the factors discussed above, but it may be optimized by the adsorption kinetics. The rate at which the solute adsorbed on the solid surface gives the kinetic models of the process. At an isothermal condition, the kinetic model is given by the following expression (Qiu et al, 2009):

$$\frac{d\,C}{d\,t} = k_{Ad}(C_{s\,eq} - C_{s\,t})^n \tag{2.17}$$

Where $C_{s\,t}$, $C_{s\,eq}$, k_{Ad} and n are the adsorbate concentration at time t, the equilibrium adsorbate concentration, the rate constant and the order of reaction, respectively.

If the adsorption reaction is zero order, the kinetic model should be written as:

$$dC = k_{Ad}\,dt \tag{2.18}$$

$$C_{s\,t} = k_{Ad}\,t + constant \tag{2.19}$$

At initial stage, time t = 0, the concentration of the solute in adsorbate phase is zero, i.e. Cst(t=0)=Cs0=0, therefore the above equation become:

$$C_{s\,eq} = k_{Ad}\,t_{eq} \;\; and \;\; C_{s\,t} = k_{Ad}\,t \tag{2.20}$$

Then the adsorption rate constant can be determined from the gradient of the linear graph of the concentration plotted against time.

The equation of the first order adsorption shows the proportionality relationship between the rate of concentration and the concentration of the solute in adsorbate phase, and is given by the following expression (Ho, 2004):

$$\frac{d\,C}{d\,t} = k_{Ad}\,(C_{s\,eq} - C_{s\,t}) \tag{2.21}$$

The solution of Equation (2.21) is given as follow:

$$\ln(C_{s\,eq} - C_{s\,t}) = -k_{Ad}\,t + \beta \tag{2.22}$$

Applying the boundary conditions:

$c_{s\,t} = 0\ at\ t = 0\ ;\qquad \beta = \ln C_{s\,eq}$

Equation (2.22) becomes:

$$\ln(C_{s\,eq} - C_{s\,t}) = -k_{Ad}\,t + \ln C_{s\,eq} \tag{2.23}$$

Therefore the adsorption rate constant can be determined from the gradient of the straight line graph of $\ln(C_{s\,eq} - C_{s\,t})$ against time.This model was presented by Ho (2004) to describe the adsorption kinetic process of liquid-solid, where the kinetic equations were based on the adsorption capacity. This model is also referred to as pseudo-first-order rate equation.

The adsorption model of the second order express the rate of adsorption as a function of squared of the concentration of the solute in the adsorbate phase, and is given by the following expression:

$$\frac{d\,C}{d\,t} = k_{Ad}(C_{s\,eq} - C_{s\,t})^2 \quad (2.24)$$

Solving Equation (24) gives:

$$\int \frac{d\,C_{s\,t}}{(C_{s\,eq} - C_{s\,t})^2} = \int k_{Ad}\,d\,t \quad (2.25)$$

$$\frac{1}{(C_{s\,eq} - C_{s\,t})} = k_{Ad}\,t + \beta \quad (2.26)$$

Applying the boundary condition ($C_{s\,t} = 0\ at\ time\ t = 0$) to Equation (2.26), the second order adsorption model become:

$$\frac{1}{(C_{s\,eq} - C_{s\,t})} = k_{Ad}\,t + \frac{1}{C_{s\,eq}} \quad (2.27)$$

$$\frac{1}{C_{s\,t}} = \frac{1}{C_{s\,eq}^2 k_{Ad}}\frac{1}{t} + \frac{1}{C_{s\,eq}} \quad (2.28)$$

The adsorption kinetic constant can be determined from the gradient of the graph $\frac{1}{C_{s\,t}}\ against\ \frac{1}{t}$.

This model was introduced by Ho (2006), and was called pseudo-second order rate equation to distinguish kinetic equations based on adsorption capacity from concentration of solution.

Zeldowitsh kinetic model (Elovich equation)

This model was established by Zeldowitsh (Qiu, 2009) to describe the adsorption of gases on the solid surface; but in recent years, researchers had used that model in liquid-solid

adsorption. This kinetic model describes the rate of the adsorbate concentration as exponential function of time. The Elovich's equation is given by the following expression:

$$\frac{d\,C}{d\,t} = \alpha\, e^{-\gamma\, C_{s\,t}} \tag{2.28}$$

$$\int_0^{C_{s\,t}} e^{\gamma C}\, d\,C = \int_0^t \alpha\, d\,t \tag{2.29}$$

$$e^{\gamma C_{s\,t}} = \alpha\gamma\, t + 1 \tag{2.30}$$

If α γ t >> 1 as suggested by Chien and Clayton (1980), α and γ can be determined from the gradient and y-intercept of the graph $C_{s\,t}\ against \ln t$ given by the following expression:

$$C_{s\,t} = \frac{1}{\gamma}\ln \alpha\,\gamma + \frac{1}{\gamma}\ln t \tag{2.31}$$

The adsorption kinetics is thermodynamically limited describing the relationships between the adsorbed species and the fluid phase. All the above models were investigated for ultrasonication-enhanced adsorption process to describe the process, and also estimate the kinetic parameters for the suitable model for the process.

2.2.2 Ultrasonication technique and ethanol-petrol blend

This section provides a short overview of ethanol-petrol blend and ultrasonication process. With the use of ultrasonication, ethanol-petrol blending is dramatically enhanced.

2.2.2.1 Chemical and physical characteristics of ethanol and petrol blends

In order to understand the nature of ethanol-petrol blended fuel it is essential to understand the characteristics of polar solvent and hydrocarbons, their differences, and how these products interact. Petrol is hydrophobic and has a flash point of approximately - 43 ^{0}C, with variation in octane rating (IAFC, 2008). Petrol has a specific gravity ranging between 0.72 and 0.76, indicating that it is less dense than water and thus floats on top of water. Its auto-ignition temperature is between 280 °C and 456 °C, and it has a boiling point between 38 °C and 204 °C depending on fuel composition (IAFC, 2008). Ethanol is a polar substance, which is water-soluble and has flash point of 13°C. Ethanol is less dense than water with a specific gravity of 0.79. However, its hydrophilic nature makes it to be miscible with water. Ethanol has an auto-ignition temperature of 423°C, and a boiling point of 78°C. Ethanol is less toxic than gasoline or methanol (IAFC, 2008).

According to Chen et al. (2011), ethanol has been used in automobile engines since the nineteenth century. However, the discovery of cheaper, petroleum based petrol, ultimately replaced it. Table 2.2 presents a comparison of the chemical and physical properties of bioethanol and petrol fuel.

Mueller et al. (2009) describes how, during the late 1970s, the phase-out of leaded gasoline began. In the late 1970s, when the use of leaded gasoline was prohibited, Methyl *tert*-butyl ether (MTBE) and ethanol were then added to the gasoline to improve the octane rating and to reduce emissions. However, ethanol recently surpassed MTBE as the additive of choice, becoming the most attractive oxygenate due to the environmental and health concerns associated with MTBE. The use of MTBE and ethanol as oxygenates enhances the octane number of gasoline (Da Silva et al., 2005) . However, the use of MTBE has been restricted due to its high solubility in water, its toxic effect and degradation products, which are causes for environmental concern (da Silva et al., 2005).

Table 2.2: Chemical and physical properties for bio-ethanol and petrol fuel (IAFC, 2008; Sheet, 2008)

Fuel property	**Bio-ethanol**	**Gasoline**
Molecular formula	C_2H_5OH	C_4–C_{12}
Molecular weight (g/mol)	46.07	100–105
Carbon (mass %)	52.2	85–88
Hydrogen (mass %)	13.1	12–15
Oxygen (mass %)	34.7	2.7
Density15/15 °C (kg/l)	0.79	0.72–0.775
Boiling point (°C)	78	27–225
Vapour pres.(kPa) at 38 °C	15.9	48–103
Specific heat (kJkg_1K_1)	2.4	2
Viscosity (mPa s) at 20 °C	1.19	0.37–0.44
Low heating val., 103 (kJ/l)	21.1	30–33
Auto ignition temp. (°C)	423	257
Research octane number	108.6	98
Motor octane	92	87
(R + M)/2	100	92.5
Cetane	–	5–20
Flammability lim. (Vol %)	4.3/19	1.4/7.6
Water tolerance (Vol %)	Compl. miscible	Negligible
Stoichiometric air/fuel	9	14.7
Aromatics (Vol %)	–	35
Carbonyl (ppm) as C–O	567	–
Carbonyl (ppm) as acetone	1117	–
Carbonyl (ppm) as acetaldehyde	893	–
Sulphur (mg/kg)	<0.8	10
Copper (mg/kg)	<0.1	–

Blending ethanol with petrol has multiple effects. Ethanol increases the heat output of the unleaded petrol, which produces more complete combustion, resulting in slightly lower emissions from unburned hydrocarbons (Chen et al., 2011). The higher the concentrations of ethanol, the more the fuel has polar solvent-type characteristics with corresponding effects on conducting fire suppression operations (Chen et al., 2011). However, even at high concentrations of ethanol, minimal amounts of water will draw the ethanol out of the blend away from the petrol. Ethanol and petrol are very similar in specific gravity and thus the two differing fuels mix readily with minimal agitation, but the blend is more of a suspension than a true solution. Ethanol has a greater affinity for water than it does for petrol, which means that over time, without agitation, petrol will be found floating on a layer of an ethanol/water solution. Table 2.3 shows the characteristics of different ethanol-petrol blends (Tangka et al., 2011).

Table 2.3: Properties of gasoline fuel blended with various percentages of ethanol (Average values) (Tangka et al. 2011)

sample code	% Ethanol	% Gasoline	Flash point (^{0}C)	vapour pressure (kpa at 37.8^{0}C)	Energy density (MJ/L)	Octane number	Specific gravity
E0	0	100	-65	36	34.2	91	0.7474
E10	10	90	-40	38.9	33.182	93	0.7508
E20	20	80	-20	39	32	94	0.7605
E30	30	70	-15	38	31.5	95	0.7782
E40	40	60	-13.5	35.6	30	97	0.7792
E50	50	50	-5	34	29	99	0.7805
E60	60	40	-1	31	28	100	0.7812
E70	70	30	0	28	27	103	0.7823
E80	80	20	5	24	26.5	104	0.7834
E90	90	10	8.5	18	23.6	106	0.784
E100	100	0	12.5	9	23.5	129	0.789

Bayraktar (2005) highlights the most attractive properties of ethanol which include the fact that it can be produced from renewable energy sources such as agricultural feedstock. It also has a high octane number and flame speed. According to Anderson, et al. (2012), the octane rating of fuel refers to the fuel's ability to resist auto-ignition and knock in a spark-ignited engine. The higher the octane rating of the fuel, the greater its desirability. Therefore an ethanol-gasoline blend fuel is more practical than ethanol alone (more fuel consumption) and could improve engine performance and decrease exhaust emissions. Turner et al. (2011) further corroborates this by describing how bio-ethanol is an attractive fuel for internal combustion engines due to its renewable nature and resultant reduction of CO_2 emissions. It also has a higher octane rating and enthalpy of vaporization when compared to standard gasoline.

This then allows for use of increased compression ratios and the possibility of more favorable spark timings, thereby increasing engine efficiency (Aina, 2012). Anderson, et al. (2012) also reported that the physical properties of ethanol provide significant improvement when added to petrol. A number of studies have been conducted on correlations between oxygenate additives to petrol, and the corresponding pollutant concentrations in the engine exhaust gas. It has been reported that the addition of oxygenates resulted in a decrease in exhaust emissions (Song, et al., 2006). Da Silva, et al. (2005) further reported that pollutants of greatest significance when considering an operation of an internal combustion engine are carbon monoxide (CO), unburned (or partially oxidized) hydrocarbons, nitrogen oxides and particulate matter. According to Da Silva (Da Silva et al, 2005) the use of oxygenated fuels decreases the emission of carbon monoxide (CO) and unburned hydrocarbons from car exhausts. Furthermore, studies conducted by Al-Hasan (Al-Hasan, 2003) have shown that ethanol as a fuel additive to unleaded petrol results in improved engine performance and a significant decrease in the exhaust emissions of CO and unburned hydrocarbons. The addition of ethanol results in an increase in the thermal efficiency of engine operation (Anderson, et al., 2012). Mirom et al (1986) showed that the completeness of fuel combustion increases in the presence of oxygenates, and emission of carbon monoxide and hydrocarbon (partly burnt) is reduced by 32.5% and 14.5%, respectively. Also, due to the use of oxygenates, the environmental and performance characteristics of gasoline are improved and motor fuel supplies are broadened due to use of non-petroleum feedstock (Rasskazchikova et al., 2004).

According to Anderson, et al. (2012), there are some disadvantages associated with the addition of ethanol to petrol. These disadvantages include potential increase (or decrease) of the RVP, alteration of distillation properties, and prevention of transportation in pipelines due to the risk of water-induced phase separation. Furthermore, the net heating value of ethanol is less than that of petrol, and there is also a reduction in the volumetric fuel economy and travel range on a tank of fuel (Anderson, et al., 2012). The most appropriate feedstock for the production of bioethanol are agricultural products, such as, sugar cane and grains, agricultural solid wastes, and cellulosic materials (such as wood and coal) (Bayraktar, 2005). Lignocellulosic biomass can be converted to bioethanol by hydrolysis and subsequent fermentation (Binod, 2011). Thermochemical processes may also be employed in the production of bioethanol in which gasification is followed either by fermentation or by a catalyzed reaction.

Ethanol-gasoline blends are, however, sensitive to moisture and have a tendency to separate into two layers when exposed to relatively small volumes of water. On exposure to water, the ethanol-petrol blend will at first absorb the water until a point at which the quantity of water added is greater than its solubility in the blend. Then a separate layer forms. The problem associated with this phase separation is that the ethanol preferentially partitions into the aqueous layer, resulting in an ethanol-rich aqueous layer and ethanol-deficient petrol layer. This ethanol-deficient gasoline layer then has a reduced octane rating and may not function satisfactorily as a fuel (Mueller et al., 2009). Therefore, the problem is not the formation of the aqueous layer, but with the resulting change in the fuel composition and the negative impact this has on its performance as a fuel.

2.2.2.2 Ultrasonication process for producing ethanol-petrol blended fuel

Ultrasound is defined as sound waves at high frequencies >20 KHz and this sound is normally transmitted through a medium by inducing vibration of the molecules through which it is traveling (Karshafian, 2010). Ultrasound can be classified into two distinct types: low amplitude type ultrasound and high amplitude ultrasound. Of interest in this study is the high power ultrasound, which usually involves lower frequencies of around 20-100 KHz and high amplitudes of range 12-320 μm. At these ranges, greater acoustic energy can be generated, inducing cavitation in liquids (Tabada, 2008).

When ultrasound wave propagates in a medium, such as, a liquid or slurry, it produces cavitation. Cavitation is an important aspect of ultrasonication since it has the capacity to generate powerful hydro-mechanical shear forces in the bulk liquid, which disintegrate nearby particles by extreme shear forces (Tabada, 2008). The disintegration of these particles will therefore result in perfect mixing between the two liquids (Tabada, 2008). Another important aspect of ultrasonication in mixing is acoustic streaming which has been shown to enhance heat and mass transfer, reaction rates, emulsification, and depolymerization (Tabada, 2008). The enhancement in mass transfer and reaction rates is therefore of importance in this study, and makes ultrasonication a relevant field of study in solving the problems highlighted in the previous sections of this Chapter.

Ultrasonic cavitation is a very effective type of dynamic agitation based on the growth and implosive collapse of bubbles in liquid due to ultrasonic vibrations (Jansen et al, 2010). Cavitation results from pre-existing weak points in the liquid, such as gas-filled crevices in suspended particulate matter or transient micro bubbles from prior cavitation events (Kenneth, 1994). As ultrasound passes through a liquid, the expansion cycles exert negative pressure on the liquid, pulling the molecules away from one another. Where the ultrasonic energy is sufficiently intense, the expansion cycle creates cavities in the liquid when the negative pressure exceeds the local tensile strength of the liquid, which varies according to the type and purity of liquid (Jansen et al, 2010). Under the proper conditions, these bubbles undergo a violent collapse, generating very high pressures and temperature as shown in Figure 2.4. It is this behaviour that makes this study relevant to the solution of phase separation.

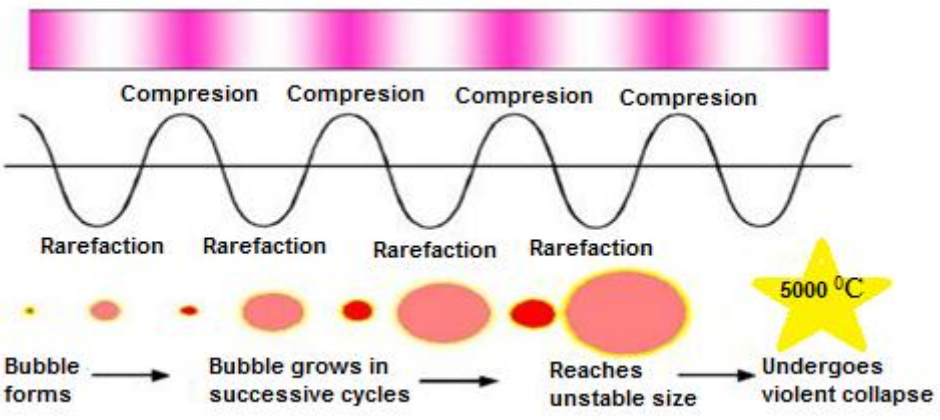

Figure 2.4: Growth and imploding cavitation bubbles (Suslick, 2004)

Furthermore, during cavitation a temporary localized hot spot is created due to the compression of bubbles. Hence, the collapse of these bubbles results in intense local heating and high pressures, suggesting that cavitation rarefaction can be used to generate extraordinary physical and chemical conditions in otherwise cold liquids (Suslick et al., 1999). Similarly, Vanhille et al (2012) described acoustic cavitation as the effect which takes place when a sufficiently high-amplitude ultrasonic signal is propagating in a liquid. The authors also described the stable cavitation as the creation and oscillation of gas bubbles in the liquid whilst inertial cavitation is characterized by the release of a large amount of energy when bubbles collapse. Neppiras (1984) also described cavitation as an event which occurs whenever a new surface, or cavity, is created within a liquid. A cavity can be described as any bounded volume, be it empty or containing gas or vapor, with at least a part of the boundary being a liquid . The presence of a sound field precipitates not only the formation and expansion but also contraction of cavities. According to Neppiras (1984), acoustic cavitation is a term primarily used to describe cases involving both expansion and contraction of cavities or bubble nuclei. In addition, cavitation can be described as the generation, subsequent growth and collapse of the cavities releasing large magnitudes of energy over a very small location, thus causing very high energy densities which could be instrumental in the intensification of chemical processing applications (Gogate, 2008). Furthermore, the generation of free radicals during the cavitation process, as a consequence of the dissociation of vapors trapped in the cavitating bubbles, results in either the intensification of chemical reactions or the propagation of a particular reaction under ambient conditions (Gogate, 2008). The cavitation may also cause the generation of local turbulence and liquid micro-circulation (acoustic streaming) in the reactor, resulting in the improvement of the rate of transport processes (Gogate, 2008). It is this particular aspect of cavitational reactors which intensifies physical processing applications and chemical processes, which are mass transfer limited.

There are a number of ways in which ultrasonic radiation differs from conventional energy sources (heat, light or ionizing radiation) including duration, pressure and energy per molecule (Suslick et al., 1999). Indeed, the exceptionally large local temperatures and pressures combined with the heating and cooling rates resulting from the collapse of bubbles generated by cavitation provides a unique mechanism for generating high energy chemistry (Suslick, et al., 1999). The generation of acoustic cavitation involves the superimposition of a time-varying, generally sinusoidal, pressure on the steady ambient pressure (Neppiras, 1984).

Two types of cavitation are highlighted by Neppiras (1984): transient and stable. Transient cavitation is used to describe the violent response to an applied sound field whilst stable cavitation applies to a rather gentle response, depending on the pressure levels and other ambient conditions. Additionally, Gogate (2008) highlighted four main types of cavitation as acoustic cavitation, hydrodynamic cavitation, optic cavitation and particle cavitation. In acoustic cavitation, the pressure variations in the liquid are altered using sound waves, typically ultrasound. Sonochemistry is the term applied to the chemical changes taking place as a consequence of cavitation resulting from the passage of sound waves. Hydrodynamic cavitation is the term applied when pressure variations are used to induce cavitation while optic cavitation results from the rupturing of the liquid continuum using photons of high intensity light (laser) (Gogate, 2008). Particle cavitation describes the cavitation which is generated by the beam of the elementary particles. However, any acoustic and hydrodynamic cavitations produce the intensity necessary for chemical or physical processing (Gogate, 2008).

According to Gogate (2008), there are two primary effects associated with cavitation in homogenous liquid phase reactions. Foremost, it is highly improbable that the resultant cavity would enclose a vacuum. It is far more likely that the cavities will instead contain vapour from the liquid medium or dissolved volatile reagents or gases. On collapse, these vapours will be subject to extreme conditions of high temperatures and pressures, resulting in the fragmentation of molecules and the generation of highly reactive radical species. These radical species then either react within the collapsing bubble or after they have travelled into the bulk liquid. Gogate (2008) then describes the second effect associated with cavitation in homogenous liquid phase reactions as the in-rush of the liquid to fill the void, which is formed on the sudden collapse of the bubble. This phenomenon then produces shear forces in the surrounding bulk liquid, which have the capacity to break the chemical bonds of any materials that are dissolved in the fluid, or agitate the boundary layer facilitating the transport.

According to Suslick, et al. (1999), there are a number of chemical and physical consequences associated with high intensity sound. Figure 2.5 is a schematic representation of these chemical and physical effects.

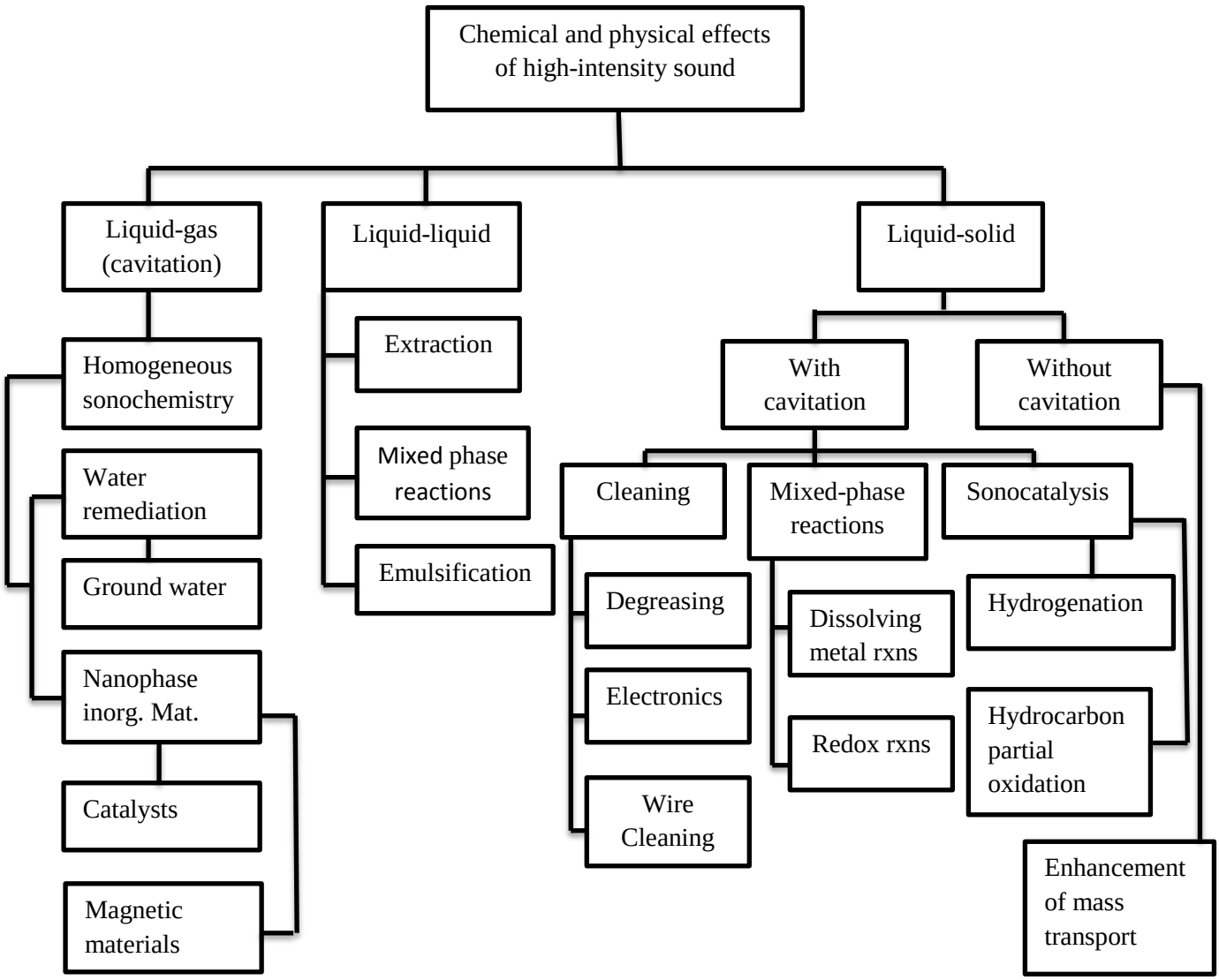

Figure 2.5: Classification of the chemical and physical effects of ultrasound (Suslick et al, 1999)

The primary benefit associated with acoustic cavitation is its ability to concentrate acoustic energy in small volumes which then results in temperatures of 1000 K, pressures in the GPa range, local accelerations 12 orders of magnitude higher than gravity, shock waves, and photon emission (Louisnard et al, 1999). However, acoustic cavitation involves an extensive array of temporal and spatial scales, and is thus highly complex to measure. Acoustic cavitation is difficult to control, to predict, and to scale up (Louisnard et al, 1999).

2.2.2.3 Diffusion mechanism in ethanol-petrol blending

Diffusion is the movement of molecules from medium of higher concentration to medium of lower concentration. The rate of diffusion can be affected by many parameters including temperature, molecular weight, and bulk convection. Transverse and vertical diffusion are the most relevant mechanisms of mass transfer in the mixing of ethanol and gasoline using an ultrasonicator. The effect of horizontal and vertical diffusion on ethanol-petrol blend was investigated in this study to determine the dominant diffusion. The one with the slow diffusion rate is the limiting step in the process and therefore it can be controlled to alter the system.

On studying diffusion in liquid- liquid phase mixture, the driving force for the diffusion mechanism is the temperature of the system and composition (Pertler et al, 1996). Diffusion has been studied in the turbulent mixing of rivers, ocean and lakes and it has been shown that horizontal diffusion is normally faster compared to vertical diffusion (Imboden et al, 1988). It is also shown that vertical diffusion is dependent of the depth and stratification of the lake, ocean or river (Imboden et al, 1988). This fact about horizontal and vertical diffusion will therefore serve as a hypothesis for this research.

Fick's first law relates the diffusive flux to the concentration field, by postulating that the flux goes from a region of higher concentration to region of lower concentration, with a magnitude that is proportional to the concentration gradient. The equation below describes Fick's first law of diffusion:

$$J = -D\frac{dC}{dx} \tag{2.32}$$

Equation (2.32) explains that the diffusive flux is proportional to the existing concentration gradient. Figure 2.6 gives an illustration of Fick's law.

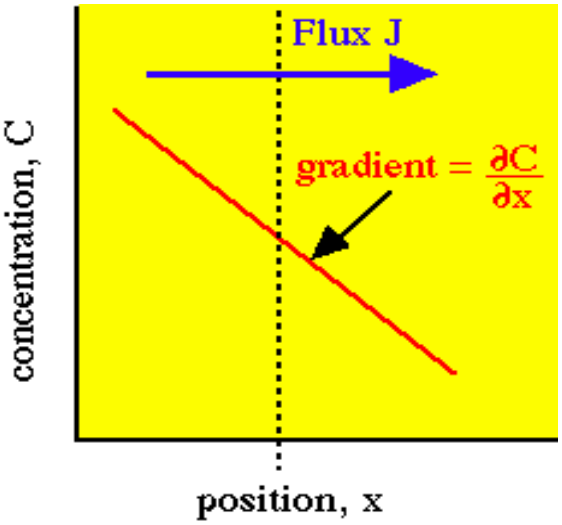

Figure 2.6: Graphical representation of gradient of concentration

The negative sign in Equation (2.32) indicates that flow occurs from regions of higher concentration to region of lower concentration. The flux (J) can be given in units of moles.cm^{-2}s^{-1}, atoms.cm^{-2}s^{-1} or other similar equivalents. The diffusivity (D) is expressed in cm^{2}.s^{-1}.

Fick's second law predicts how diffusion causes the concentration to change with time thus the fuel mixing process can be quantified by the diffusivity coefficient (D) after which the rate of diffusion is described according to Fick's second law:

$$\frac{dC}{dt} = -D_L\left(\frac{d^2C}{dx^2} + \frac{d^2C}{dy^2}\right) \tag{2.33}$$

Equation (2.33) can therefore be used to calculate the overall rate of diffusion of a certain material that diffuses in both directions that is vertical and transverse directions. Since the mechanism behind ultrasonic mixing is diffusion, the time taken for diffusion of a liquid until a point where a homogeneous mixture is achieved can be related to the diffusion length of the liquid. This relationship is shown in Equation (2.34) below where the diffusivity of the liquid can be obtained from Equation (2.33). Equation (2.34) below was adapted from Goksen, (2004):

$$T_D = \frac{L^2}{D} \tag{2.34}$$

Where T_D is the diffusion time (s), L is the diffusion length (m); and D is the diffusivity.

Equation (2.34) shows that, industrially it is possible to improve the kinetics of mixing by reducing the diffusion length required for mixing or increasing the contact area between the two different liquids while keeping the volume constant (Goksen, 2004). This way of controlling the kinetics of mixing may therefore be applied on the limiting diffusion that is either the horizontal or vertical diffusion. The length that maximises the kinetics will therefore be used to directly determine the geometry of the mixing tank. One way of increasing the contact area between the two liquids is to inject one liquid into the other through nozzles and this creates micro plumes of the injected fluid in the host fluid and thus decreasing the diffusion length (Goksen, 2004).

2.2.2.4 Energy distribution during the blending process

One of the most important aspects of sonication is the intensity of the sonication energy distribution within a reactor. More often, the energy knowledge about the ultrasonic energy transferred to the cell is available; however this knowledge is insufficient for describing the situation within the sonication reactor (Klima, 2007). The intensity distribution of the sonication energy can however be predicted based on the knowledge of the spreading of the ultrasound which includes reflections and superposition.

Different studies have shown that the sound field is strongly non-uniform and thus describe the formation of standing waves whose position depends strongly on the liquid level in the sonication reactor. Kimura et al (2000) has confirmed the validity of this theory by showing that almost all the ultrasonic energy is consumed within a small volume near the ultrasonic horn (Klima et.al, 2007). The experimental setup in this study is similar to the one described by Klima,et.al (2007), and thus for such an arrangement it can be assumed that the highest local intensity value is reached in the close vicinity of the horn. The energy intensity value is

therefore given by the power transferred to the reactor through the tip of the transducer divided by the active surface area of the tip as given by Equation (2.35):

$$I_{US} = \frac{P_{US}}{A} \tag{2.35}$$

Where I_{US} is the energy intensity of ultrasonication; P_{US} is the power transferred to the reactor; and A is the active surface area.

From Equation (2.35) it can be shown that the intensity is inversely proportional to the area it spreads into, and thus a decrease in the intensity is expected with an increase in distance from the sonication horn. This approach however limitation has and thus the behaviour can be changed significantly due to multiple reflections at the cell boundaries. Hence for specific cell dimensions, higher intensities can be recorded at regions further away from the horn, thus resulting in a non-linear energy profile. The intensity distribution is also equivalent to the distribution of acoustic pressure amplitude in the reactor (Klima, 2007) and this relationship is shown in Equation (2.36):

$$I_{US}(r) = \frac{{P_o}^2(r)}{2\rho c} \tag{2.36}$$

Where r is the spatial variable ($r = [x, y, z]$), ρ is the density of medium, c is the sound velocity in this medium and ${P_o}^2$ is the ultrasonic pressure amplitude.

This relationship shows that by measuring the pressure distribution in the reactor, the energy intensity can also be analysed from the results. In this study, pressure distribution in the reactor was measured as a means to investigating the energy intensity distribution (see Chapter 4 for details).

2.3 Testing of ethanol-petrol blended fuel in internal combustion engine

Numerous studies on the testing of ethanol-petrol blended fuel in internal combustion engines have been done, and results have shown that ethanol-petrol-based engines are more efficient

than pure gasoline-based engines. Bayraktar (2005) investigated the effect of ethanol on the engine performance and the carbon monoxide emissions. In his investigation, he looked at the effect of ethanol composition in the ethanol-petrol blended fuel. From the study, he discovered that ethanol composition of 7.5% led to better engine performance, and reduction in carbon monoxide emissions. Using theoretical model, the author also speculated that better engine performance and less CO emissions were achieved when the ethanol composition of the ethanol-petrol fuel was 16.5%.

In the same vein, Lin et al. (2012) also conduct a study on the effect of different ethanol-petrol composition on the performance of internal combustion engine. This study focused on fuel energy efficiency and pollution analysis under different loadings. The efficiency was expressed as thermal efficiency of the generator. From the study, the researchers found that ethanol addition to petrol reduced the emissions. In addition, it was found that particle number concentration increased with the load and decreased with the increase in the percentage of ethanol in the ethanol-petrol blend. The reduction in CO, NO_X and total emission when E60 (fuel blend with 60 % ethanol) was used was found to be 86%. They also found that small generator thermal efficiency increased with the increase in the content of ethanol in the blend.

Similarly, Koc et al (2009) showed that ethanol addition does not only improve efficiency and emission reduction but also increase the compression ratio of the engine without knock occurrence. Other studies that were also done showed similar results. For example, Rakopoulos et al (2005) reported an improvement in the efficiency of internal combustion engine when ethanol-petrol blended was used. Yacoub et al (1998) also showed an enhancement in the performance of an engine operated with ethanol-petrol blend and even showed the characteristic performance of C_1 (methanol) to C_5 (pentanol) petrol blends. Sung et al (1983), Award et al (2012), and Hasan (2002) reported a similar deduction from their studies.

2.3.1 Thermodynamic Models of Internal Combustion Engine

Performance of an internal combustion engine using different fuels can be analyzed using first and second laws of thermodynamics .In a combustion process, fuel and oxidizer react to obtain products of different composition. The actual path by which this transformation takes place is understood only for simple fuels, such as hydrogen and methane. For fuels with

more complicated structure, the details are not well defined. First law of thermodynamics can be used to relate the end states of mixtures undergoing a combustion process; its application does not require that the details of the process be known. Energy balance in the cylinder is made with the aim of obtaining power and efficiency with the aid of first law. The Otto cycle is a popular way of analyzing an engine using first law of thermodynamics.

The Otto Cycle

It is well known that the performance of an engine is analyzed using the engine cycle depicted schematically in Figure 2.7 and Figure 2.8. The engine cycle enables easy determination of engine performance parameters, such as, mean indicated pressure, mean effective pressure, thermal efficiency and fuel consumption

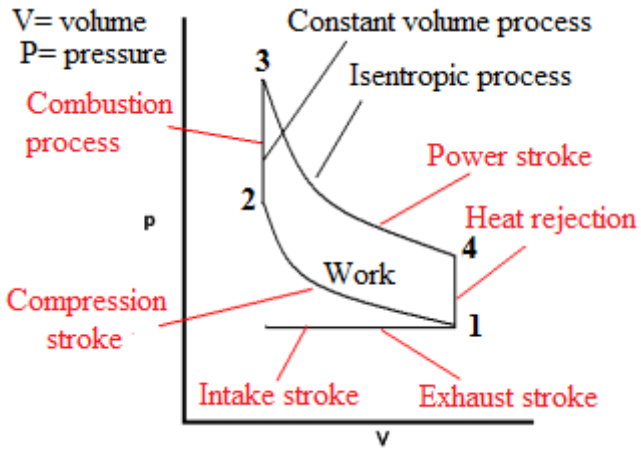

Figure 2.7: Ideal Otto Cycle (Hago W. and Morin A., 2010)

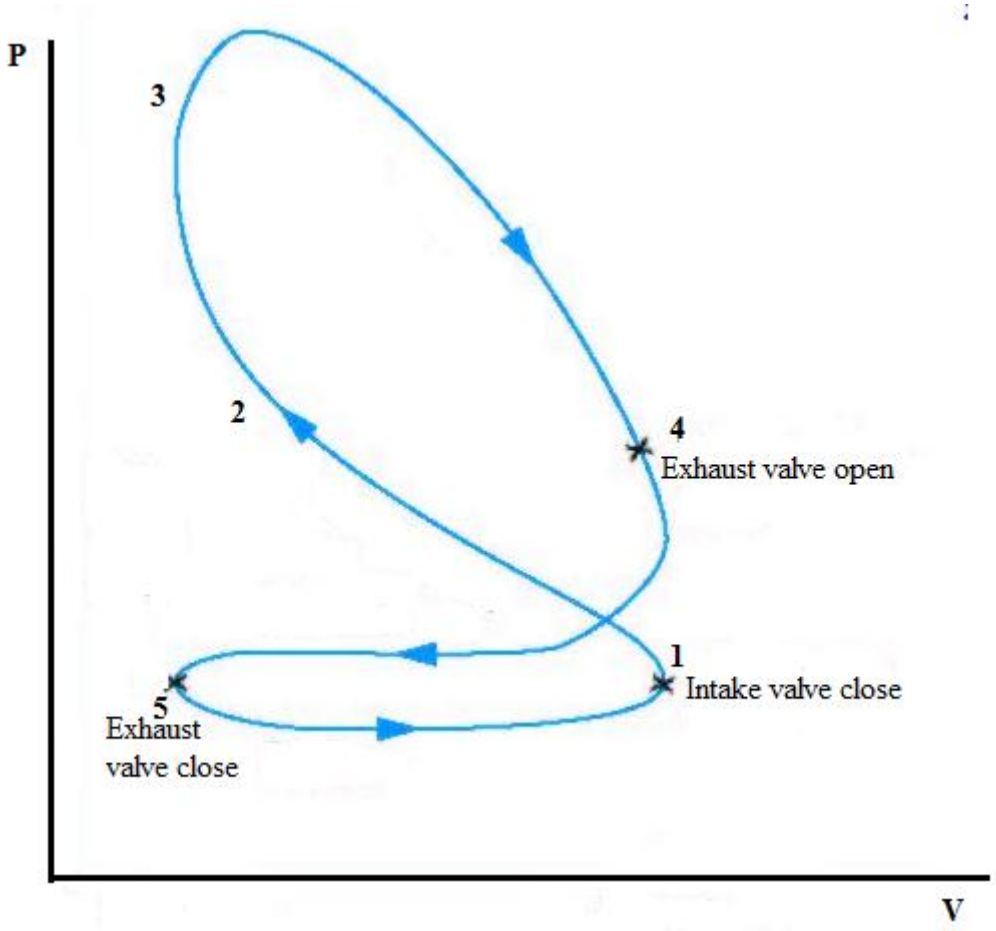

Figure 2.8: Real Otto Cycle (Hago et al, 2010)

In Figure 2.7 and Figure 2.8, Process 1-2 represents isentropic compression as the piston moves from bottom dead center to top dead center.

Process 2-3 is a constant volume heat transfer to the air fuel mixture from an external source while the piston is at top dead center. This process is the ignition and the subsequent rapid burning.

Process 3-4 is an isentropic expansion and Process 4-1 completes the cycle with constant-volume heat rejection.

Once the cycle has been determined for each fuel mixture, the mean effective pressure (mep) and thermal efficiency are determined as follows:

$$mep = \frac{net\ work\ for\ one\ cycle}{displacement\ volume} \tag{2.37}$$

$$\eta = 1 - \left(\frac{1}{r}\right)^{k-1} \quad (2.38)$$

$k = C_p/C_V$, for constant heat capacities

The net work for one cycle is given by:

$$W_{Cycle} = (u_3 - u_4)\text{-}(u_2 - u_1) \quad (2.39)$$

Where u = is the internal energy

Theoretical determination of the Otto cycle from first law

Thermodynamic models of the real engine cycle have served as effective tools for complete analysis of engine performance and sensitivity to various operating parameters (Rakopoulos, 2006). From first law of thermodynamics, the Otto cycle, which is mostly used for analyzing the performance of the engine in the generation of electricity from various fuels, can be produced using mathematical models. The mathematical models which have been developed include zero-dimensional models or single-zone models, two-zone, four-zone or even multi-zone models (Borgnakke, 1986). The single zone models are simple as they consider the engine to be made up of a uniform mixture of gases while the two zone models divide the working fluid in the engine into two zones (burned and unburned) (Rakopoulos, 2005).

Computer simulations of internal combustion engine cycles are used because they aid in design studies, in predicting trends, in serving as diagnostic tools, in analyzing the data that are obtainable from experiments, and in helping one to understand the complex processes that occur in the combustion chamber (Maher et al, 2004). The most frequently used model is the quasi-dimensional model which is the double zone model. It is used because it is believed to predict the performance of the engine well when compared to the single zone models

(Rakopoulos, 2005). The equations governing the rate of fuel consumption, temperatures and pressures for the quasi–dimensional model are shown below.

The mass burning rate was modelled by the following equation (Heywood, 1988):

$$\frac{dM_b}{dt} = A_{fl}.\rho.ST \tag{2.40}$$

The turbulent flame front speed (ST) was modelled by the following equation (Heywood, 1988):

$$ST = SL.f.\frac{\rho_u/\rho_b}{[(\rho_u/\rho_b)-1]Xm_b+1} \tag{2.41}$$

Where f is the turbulent flame factor, defined as:

$$f = 1 + 0.0018 \times rpm \tag{2.42}$$

The laminar flame front speed for mixtures of hydrocarbon and/or alcohol, air, and residual gas could be modelled by the following equation (Yu et al., 1986):

$$SL = SL_O \left(\frac{T_u}{T_O}\right)^{\propto} \left(\frac{P}{P_O}\right)^{\beta} \left(1 - 2.06{X_r}^{0.77}\right) \tag{2.43}$$

Where:

$$\propto = 2.18 - 0.8(\emptyset - 1) \tag{2.44}$$

$$\beta = -0.16 + 0.22(\emptyset - 1) \tag{2.45}$$

$$SL_O = B2 + B3(\emptyset - B1) \tag{2.46}$$

Values of B1, B2 and B3 are given by Heywood (1988) for both ethanol and petrol.

Using Equation (2.40) to Equation (2.46), the rate of change of mass of fuel in the engine's cylinder can be estimated.

As mentioned above, the Otto cycle is useful for analyzing engine's performance. Assuming ideal gas behavior, the compression stroke of the spark ignition engine can be simulated using the following equations:

$$PV = nRT \tag{2.47}$$

$$\frac{dP}{d\theta} = \left[-\left(1 + \frac{R}{C_V}\right) P \frac{dV}{d\theta} - \frac{R}{C_V}\right] / V \tag{2.48}$$

From Heywood (1988), the volume of the cylinder at any crank angle can be defined as:

$$V = V_C \left\{1 + \frac{1}{2}(r_c - 1)[R + 1 - cos\theta - (R^2 - sin^2\theta)^{0.5}]\right\} \tag{2.49}$$

Where V_C= the clearance volume.

$$R = \frac{l}{a} \tag{2.50}$$

l =Connecting rod length, a=crank radius

Differentiating Equation (48) with respect to the crank angle gives:

$$\frac{dV}{d\theta} = V_C \left\{\frac{1}{2}(r_c - 1)[sin\theta - 0.5(-2sin2\theta)]\right\} \tag{2.51}$$

Equation (2.47) to Equation (2.51) can be simulated using computer software like MATLAB and the obtained results can be compared with the experiment results.

The following simplifying assumptions are made in order to model the performance of the combustion engine according to the first law of thermodynamics.

Assumptions:

(a)Spatial homogeneity of pressure (for two-zone models)

(b) Spatial homogeneity of temperature (for the whole cylinder or for each zone considered)

(c) Working fluid is considered an ideal gas

(d) Gas properties (enthalpy, internal energy, etc.) are modelled using polynomial relations with temperature (and pressure)

(e) Heat released from combustion is distributed evenly throughout the cylinder

(f) Blow-by losses are not taken into account

(g) Enthalpy associated with pressure of injected fuel is usually not significant and hence ignored

(h) Spatially averaged, instantaneous (time resolved) heat transfer rates are used to estimate heat transfer to the cylinder walls

(i) Dissociation is neglected

(j) No heat transfer occurs between burned and unburned zones

(k) Work required to transfer fluid from the unburned zone to the burned zone is negligible.

Models for mixture properties

Combustion of the fuel-air mixture inside the engine cylinder is one of the processes that control engine power, efficiency, and emissions (Heywood, 1988). The gas species (e.g. oxygen, nitrogen, fuel vapour, carbon dioxide, carbon monoxide, water vapour) that make up the working fluids in the internal combustion engines can usually be treated as ideal gases by using an Ideal gas equation:

$$PV = mRT = m\frac{R}{M}T = nRT \tag{2.52}$$

Where p is the pressure, V the volume, m the mass of gas, T the temperature, R the universal gas constant, M the molecular weight, and n the numbers of moles.

The mixture of petrol and ethanol properties can be determined from individual properties if they are known using the following equation:

$$\epsilon_m = \sum \epsilon_k x_k \tag{2.53}$$

ϵ_m is the property of the mixture, ϵ_k is the property of pure ethanol or petrol and x_k is the fraction of ethanol or petrol.

Fuel to air ratio is defined by:

$$\left(\frac{F}{A}\right)_{sm} = \sum \frac{\epsilon_k x_k (F/A)_{sk}}{\epsilon_k x_k} \tag{2.54}$$

The low heating value of the fuel mixture as given by Bayraktar (2005) is:

$$LHV_m = \frac{\sum \epsilon_k x_k LHV_k}{\sum \epsilon_k x_k} \tag{2.55}$$

Fuel-air equivalent ratio is given by:

$$\emptyset_m = \emptyset_G \frac{(F/A)_{sG}}{(F/A)_{sm}} \sqrt{\frac{\epsilon_m}{\epsilon_G}} \tag{2.56}$$

The chemical reactions occurring in the cylinder can be approximated by the following reactions:

Petrol combustion

$$C_8H_{18} + N_2 + 10O_2 \rightarrow CO_2 + 7CO + 9H_2O + 2NO \tag{2.57}$$

$$N_2 + O_2 \rightarrow 2NO \qquad (\Delta H_{rxn} = 90.43 kJ/mol) \tag{2.58}$$

Bio-ethanol combustion

$$C_2H_5OH + N_2 + 3.5O_2 \rightarrow CO_2 + CO + 3H_2O + 2NO \tag{2.59}$$

Overall combustion reaction

$$C_8H_{18} + C_2H_5OH + 2N_2 + 13.5O_2 \rightarrow 2CO_2 + 8CO + 12H_2O + 4NO \quad (2.60)$$

Thermodynamic of internal combustion engine from second law of thermodynamics analysis models

An internal combustion engine can be analyzed as an open system which exchanges heat and work with its surrounding environment. By applying second law of thermodynamics, an expression for the maximum useful work that the engine can deliver can be derived. According to the first law of thermodynamics,

$$\Delta Q - \Delta W_v = \Delta H \quad (2.61)$$

Where ΔW_v is the useful work transfer to the environment and $\Delta H = H_P - H_R$
From the second law of thermodynamic, the heat transfer ΔQ is given as follows:

$$\frac{\Delta Q}{T_A} \leq \Delta S \quad (2.62)$$

Where T_A is the temperature of the surrounding and ΔS is the entropy
Combining the above Equation (2.61) and Equation (2.62) results in:

$$\Delta W_v \leq -(\Delta H - T_A \Delta S) \quad (2.63)$$

Maximum work will be obtained when the pressure and temperature of the products equal that of the atmosphere.

Under these conditions:

$$\Delta W_{v\,max} = -(\Delta G)_{T_A P_A} \quad (2.64)$$

Where: $(\Delta G)_{T_A P_A}$ is the Gibbs free energy at atmospheric temperature, and pressure and it will be at its maximum at the complete combustion of the fuel.

A measure of the effectiveness of any internal combustion engine is the ratio of the actual work delivered compared with this maximum work. This ratio is termed, the availability conversion efficiency:

$$\eta = \frac{\Delta W}{\Delta W_{v\,max}} = \frac{\Delta W}{-(\Delta G)_{T_A P_A}} \tag{2.65}$$

The performance of internal combustion engine in producing power using different fuels can also be analysed using the second law of thermodynamics. The second law of thermodynamics analysis applies availability (exergy) equations in the engine cylinder. Availability exists in the form of chemical availability, flow availability, thermal availability, mechanical availability and fuel availability.

Availability of a system in a given state is the maximum amount of useful work that can be produced due to the interaction with the environment. Exergy unlike energy can be destroyed by processes such as combustion, friction and mixing.

Different models for estimating fuel chemical availability are:

$$a^o_{fch} = -(\Delta G)^o_{T_0, P_0} = 1.0286(\Delta H)^o_{T_0, P_0} = 1.0286 LHV \tag{2.66}$$

$$a_{fch} = LHV\left[1.0401 + 0.01728\frac{y}{z} + 0.0432\frac{p}{z} + 0.2196\frac{q}{z}(1 - 2.0628)\right] \tag{2.67}$$

$$a_{fch} = LHV\left(1.04224 + 0.011925\frac{y}{z} - \frac{0.042}{z}\right) \tag{2.68}$$

Equation (2.66) is used to estimate chemical availability for octane (Caton, 2000), Equation (2.67) is used for fuels of the form $C_z H_y O_P S_q$(Rakopoulos*et al*, 2005), and Equation (2.68) is used for liquid fuels of the form $C_z H_y$ (Stepanov, 1994, Rakopoulos*et al*, 2005).

Another form of availability that is often considered is thermochemical availability and it is given by:

$$a_{th} = E + P_O V - T_O S - G_O \tag{2.69}$$

When the system moves from one state to another, the change in exergy can be defined by (Lior et al, 1988):

$$\Delta a_{th} = C_P(T_{n+1} - T_n) - T_n \left[C_P ln\left(\frac{T_{n+1}}{T_n}\right) + Rln\left(\frac{P_n}{P_i}\right)\right] \tag{2.70}$$

The availability balance can be made on the inlet manifold and the exhaust manifold for each fuel composition and the results can be used to estimate the efficiency of the engine for different fuel composition using Equation (2.71) (Rakopoulos *et al*, 2005):

$$\eta = \frac{availability\ out\ in\ products}{availability\ in} \tag{2.71}$$

The efficiency for one cycle for a four stroke engine using second law is defined as (Heywood, 1988, Rokopoulos et al, 2005):

$$\eta = \frac{W_{ind}}{m_f a_{fch}} \tag{2.72}$$

Using these equations different types of fuels can be investigated and compared to increase the economical use of the fuel.

Theoretical determination and analysis of the Otto cycle from second law

Lior and Rudy (1988) discussed the use of the second law to analyze spark ignition engines. The efficiencies they found using the second law of thermodynamics can be compared with the results obtained from first law and the experimental results to determine the models for engines performance. The thermodynamic states (state 1, 2, 3 and 4 in Figure 2.7) are determined as follows:

As mentioned above, the second law of thermodynamics deals with exergy when the analysis of the internal combustion engines is being performed. Therefore, the exergy of the feed fuel is found first using Equation (2.66) and Equation (2.67):

Since there is no transfer of mass in or out of the engine's cylinder during a single cycle, the exergy of the fuel enclosed in the cylinder needs to be found as follows (Lior et al, 1988):

$$a_{fch,closed=a_{fch}-(P-P_i)v} \tag{2.73}$$

Where:

v= specific volume (volume/mol)
P_i= the partial pressure of the components (ethanol and petrol once vaporized) determined using Roult's law as follows:

$$P_i = x_i P \tag{2.74}$$

The specific volume is calculated from equations of state like the ideal gas equation for ideal gases:

$$v = \frac{RT}{P} \tag{2.75}$$

Where: R is the ideal gas constant
T is the temperature
P is the pressure in the cylinder

The compression stroke (1 – 2) is often assumed to be an isentropic process and the following equations are therefore used to find the pressure and temperature at state 2:

$$T_1 {V_1}^{\gamma-1} = T_2 {V_2}^{\gamma-1} \tag{2.76}$$

$$P_2 = P_1 \left(\frac{v_1}{v_2}\right)\left(\frac{T_2}{T_1}\right) \tag{2.77}$$

Where:

T_2 = Temperature at state 2

P_1 and P_2 = Pressure at state 1 state 2

γ = ratio of specific heats i.e.

$$\gamma = \frac{C_P}{C_V} \tag{2.78}$$

Where:

C_V= is the specific heat at constant volume

C_P= is the specific heat at constant volume

$C_P$and $C_P$as a function of temperature for the components involved which are: Unleaded petrol (C_8H_{18}), Bio-ethanol (C_2H_5OH) , water (H_2O), carbon dioxide (CO_2), carbon monoxide (CO), nitrogen oxide (NO), Nitrogen (N_2), Oxygen (O_2) have been presented in Appendix D.

C_V is related to the C_P by the following expression:

$$C_V = C_P - R \tag{2.79}$$

The C_V expressions are also presented in Appendix J as temperature dependent.

If during combustion, the cylinder is assumed to be a perfect insulator i.e. adiabatic system, the maximum temperature which results as a consequence of combustion can be used to determine the pressure at state 3. Equation 2.80 is used to determine the temperature.

$$H_R = H_P \tag{2.80}$$

Where;

H_R = enthalpy of the reactants (Ethanol and petrol)

H_P = enthalpy of the products

The enthalpies are related to temperature by the heat capacities as follows:

$$H_i = N_i * [H^o{}_{fi} + \int_{To}^{T} C_p dt] \tag{2.81}$$

Where:

H_i= enthalpy of species i

$H^o{}_{fi}$ = enthalpy of formation

N_i = mass of species i

And the enthalpy of the mixture (reactants (H_R) or products (H_P)) is defined by:

$$H_R \; or \; H_P = \sum H_i \tag{2.82}$$

Knowing the temperature allows the determination of pressure from Equation (2.77), which results from the division of ideal gas equations at state 2 and state 3:
The final part of the ideal cycle, process 3 – 4, involves an isentropic expansion of the combustion products. This is the expansion which is the work producing phase of the cycle. The temperature and pressure of the isentropic expansion are estimated the same way as the temperature and pressure were estimated at the end of isentropic compression.

Knowing the pressure and the temperature at each state allows the determination of the total exergy (thermochemical and chemical) using Equation (2.69) and Equation (2.70).From the exergies calculated at each state the effectiveness of the system for each type of fuel can be determine using Equation (2.84):

$$\in_{system} = \frac{(a_3 - a_4) - (a_2 - a_1)}{a_{in}} \tag{2.84}$$

Where:

$a_2 - a_1$ = Exergy added during compression
$a_2 - a_3$ = Exergy lost during combustion
$a_3 - a_4$ = Exergy extracted during expansion
a_4 = Exergy lost from exhaust

CHAPTER 3: EXPERIMENTAL AND RESEARCH METHODOLOGY

The bioethanol used in this study was produced in the Biotechnology laboratory of the school of chemical and metallurgical engineering/ university of the Witwatersrand by fermentation of pre-treated corn cobs produced between 12-15 % ethanol which was distilled to 85% v/v ethanol using Syawala (2013) and Kiss (2013) methods. However, further dehydration of the bioethanol was necessary before ethanol-petrol blending in order to produce homogeneous blend that falls within homogenous region of the ternary diagram. The following experimental steps were used to meet the objective of this project.

- The first step of this study was to investigate the effect of ultrasonic energy on the bioethanol-petrol-water phase behaviour; this provides the qualities of the ethanol needed to be used for the blending process with an ultrasonicator;

- The second step was the pre-treatment of distilled bioethanol by adsorption of water with silica-gel stimulated by ultrasound;

- The third was the blending process with its profile on the vertical and horizontal directions;

- Finally the investigation of the ultrasonicated ethanol-petrol fuel in the performance of internal combustion engine.

Figure 1.1 describes schematically the processes used in this project to meet the research objective. The pre-process allows dehydration of bioethanol required for homogeneous water-ethanol-petrol fuel. The main process consists of mixing the blended components in the first place and finally the testing of the fuel blend in internal combustion. Engine unleaded petrol 95 used in this study was purchased from Braamfontein TOTAL filling station, Johannesburg – South Africa. Bioethanol were characterized in terms of ethanol concentration measured by high performance liquid chromatography (HPLC). The bioethanol and petrol used were characterised in terms of viscosity, density and colour as seen in table 3.1.

Table 3.1: Characteristics of bioethanol and petrol used in this project

	Ethanol concentration % (Using HPLC)	Viscosity mPa s at 26 ^{o}C (using Ostwald viscometer)	Density at 26 ^{o}C	Colour
Bioethanol	84.00 ± 2.01	1.16	0.77	Transparent
Petrol	-	0.38	0.75	Greenish

3.1 Determination of phase behavior of ethanol-petrol blend using ultrasonication

The setup to investigate the phase behaviour consisted of a glass blender, a thermometer and an ultrasonicator. The ultrasonicator horn is 33 cm high with diameter of 0.7 cm, and operates at 24 kHz. The thermometer was placed at 3 cm from the ultrasonicator horn which was placed in the center of the reactor. The experimental set up for the phase behaviour of petrol-ethanol-water is depicted in Figure 3.1.

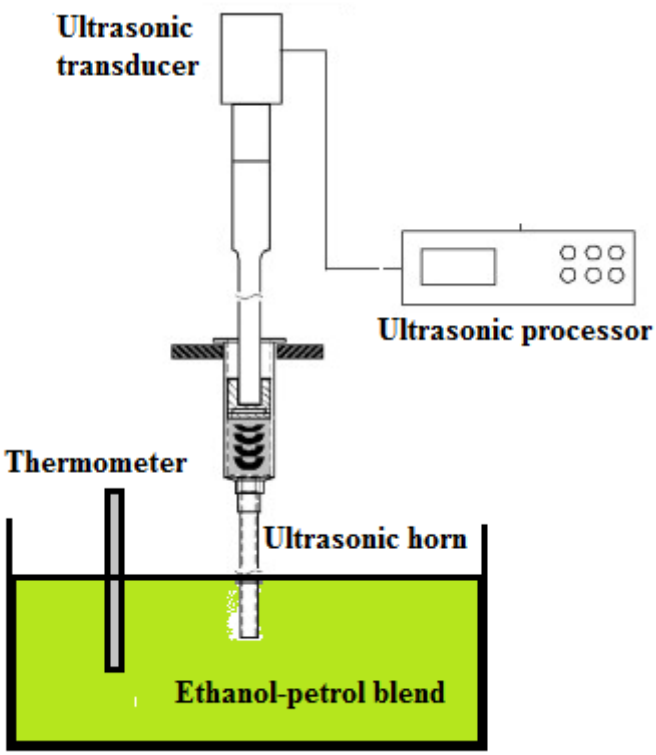

Figure 3.1: Experimental set up for determination of phase behaviour of ethanol-petrol blend

The experiment was performed using a desired composition of the mixture. Two hundred and seventy-two samples were prepared from estimated binodal curves on the region above and below the existing curve as plotted on the work done by Kyriakides (2012) and De Oliveira (2000). The ternary components were mixed using ultrasonicator-enhanced blending in various proportions according to the data presented in Table A.1 in the Appendix A. The ternary diagram of the mixtures used to investigate the phase behaviour is provided in Figure 3.2.

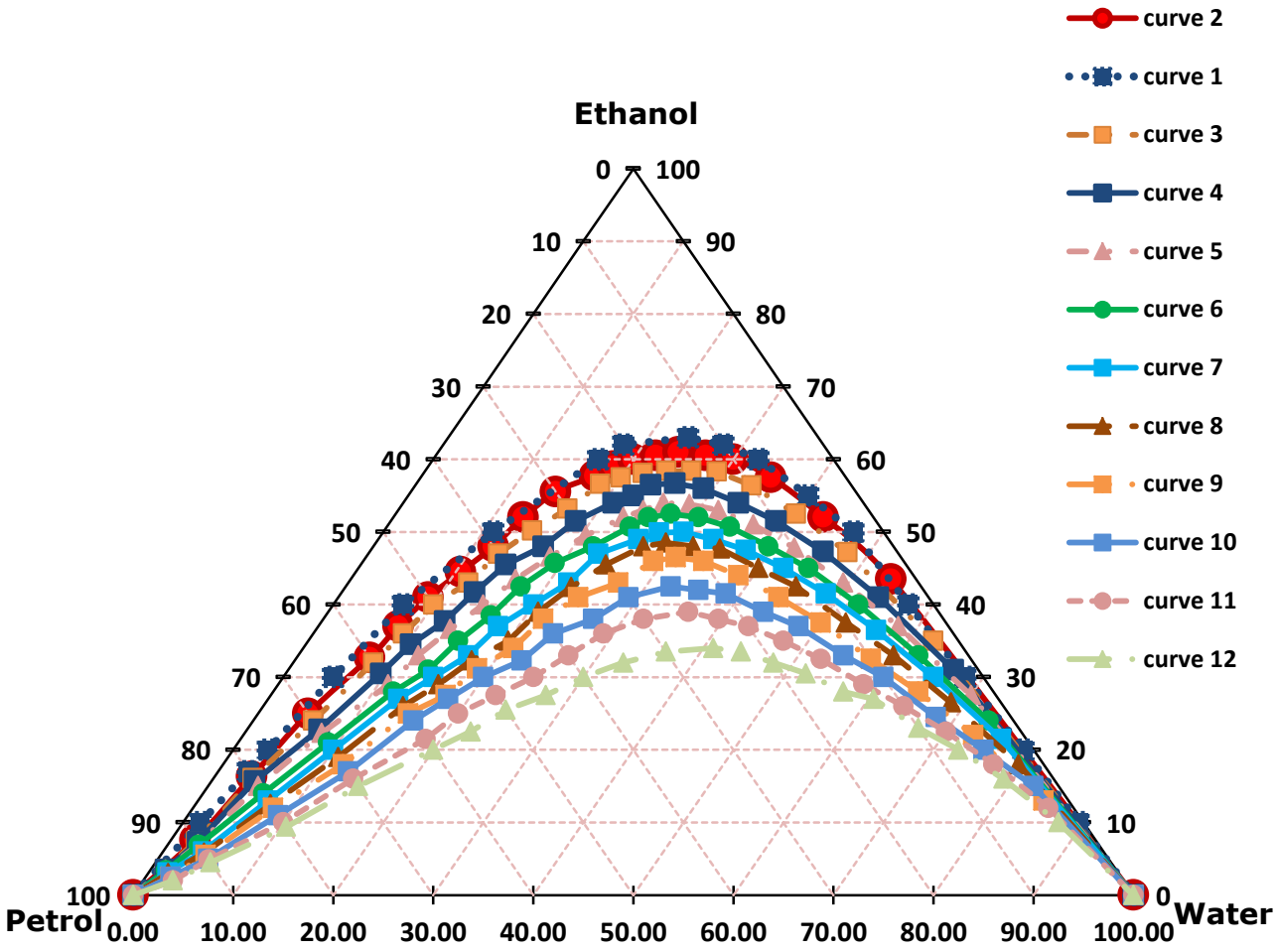

Figure 3.2: Ternary diagram of the investigated petrol-ethanol-water mixture

3.2 Production of ethanol-petrol blend using ultrasonication-enhanced blending

Details of the procedure employed in the production of ethanol-petrol blend in this study can be obtained from Figure 1.1; the procedure includes dehydration of ethanol before blending of the dehydrated bioethanol with petrol. In addition, parameters affecting the blending process, such as, pressure and temperature were investigated.

3.2.1 Dehydration of bioethanol by ultrasonication-enhanced adsorption process

During the dehydration, four different concentration of water in ethanol were investigated. The resulting bio-ethanol concentrations were 85, 90, 95 and 98% by volume. Silica gel was used as the adsorbent, and the adsorption was enhanced using magnetic stirring and ultrasonication to evaluate adequately the effect of ultrasonication on the adsorption.

3.2.1.1 Magnetic-stirring-enhanced water adsorption on silica-gel

Figure 3.3 shows the experimental setup for magnetic-stirring-enhanced adsorption of the dehydration of bio-ethanol. The stirring was expected to enhance mass transfer between adsorbate and adsorbent. Before performing the experiment, the beaker was insulated with foil to reduce heat loss, then ethanol-water mixture was stirred, and the temperature was recorded at intervals of 5 minutes for 30 minutes.

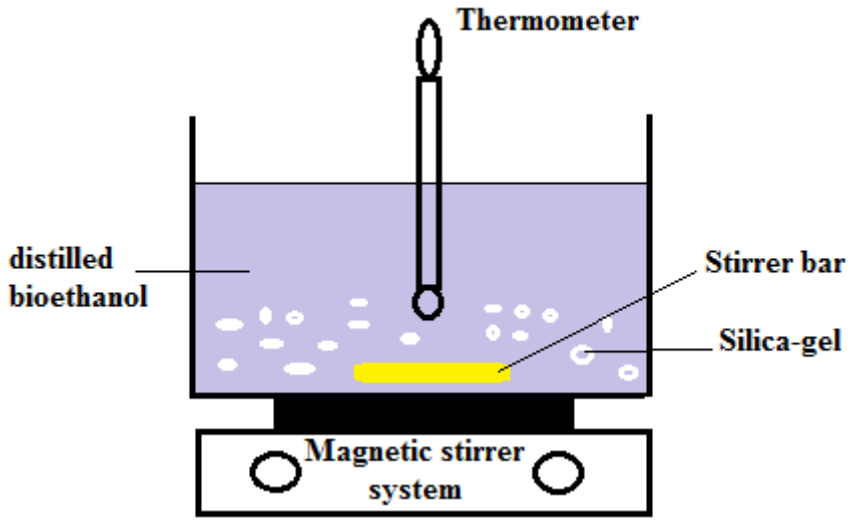

Figure 3.3: Adsorption-enhanced with magnetic stirrer

3.2.1.2 Ultrasonication-enhanced dehydration of bio-ethanol on silica-gel

Figure 3.4 depicts the experimental setup for ultrasonication-enhanced dehydration of bio-ethanol via adsorption on silica gel. The ultrasonicator probe was immersed in the solution and switched on, and then silica gel was added in the adsorption reactor. The time was recorded at intervals of 5 minutes for 30 minutes. The temperature in the adsorption reactor was also recorded, and the samples were kept for analysis. Every run was conducted using fresh solution of water-ethanol mixture and silica gel.

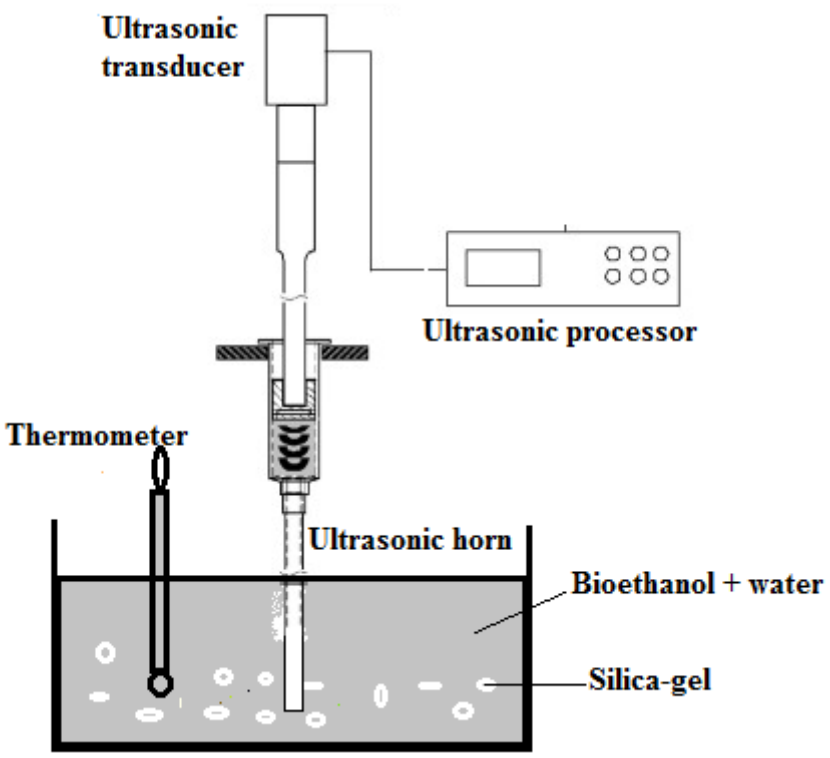

Figure 3.4: Experimental setup of ultrasonication-enhanced adsorption

3.2.2 Ethanol-petrol blend via ultrasonication techniques

The approach taken in the experimental section focussed on meeting the objectives outlined in Chapter 1. This included setting up a batch blender with marked points at different radii and height ranging from 1 to 4 cm. Thermometers were then placed at the 1 cm, 3 cm, and 4 cm marks. The ultrasonicator horn was place in the center of our blender. The experimental set up for the ultrasonication-enhanced blending of ethanol and petrol is depicted in Figure 3.1.

Petrol and ethanol were then blended in various proportions ranging from 10 to 30 % ethanol. For each experiment, the volume of petrol under investigation was first poured into the batch blender. The ultrasonicator horn was then lowered to approximately 2 cm below the surface of the petrol before being switched on. The temperature of the petrol was maintained at 26 °C, and then the appropriate volume of ethanol was added to the petrol at a constant rate. The temperature readings and the times were recorded for blending analysis.

In all the experiments performed, the horizontal and vertical axis was defined with respect to the ultrasonicator horn as outlined below.

- **Horizontal direction**

Samples were taken using pipette at horizontal distance from the ultrasonicator probe moving outward to the blender wall, as depicted in Figure 3.5.

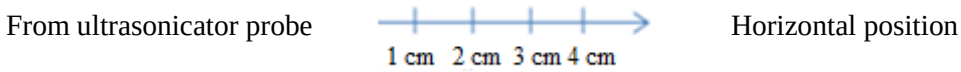

Figure 3.5: Horizontal position for measurement

To study the horizontal mixing profiles, samples were collected in the horizontal direction at different points. To determine the distance between the points, circles of different diameters were drawn on a piece of paper and the paper was placed underneath the blender. The radii were varied from 1 to 4 cm from the center of the blender as explained above. At each distance, samples were collected at different ultrasonication times of 60, 120, 180, 240, 300 and 360 seconds. After collecting the sample a new sample was prepared for the next position. The procedure was repeated for the other points.

- **Vertical direction**

Samples were taken at vertical distance from the tip of the ultrasonicator probe moving upward to the mixture surface as depicted in Figure 3.6.

Vertical position

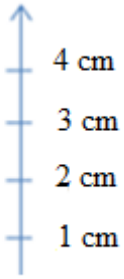

From bottom of the ultrasonicator horn

Figure 3.6: Vertical position for measurement.

To study the vertical mixing profiles, the samples were collected in the vertical direction using pipette. A vertical marked at different height varying from 1 to 4 cm was displayed on the side of the blender. The same procedure of sample collection was observed as discussed on the horizontal direction sample collection. In all the samples, the temperature and pressure of the mixture were measured at each collected sample point and time specified above.

3.3 Combustion of Ethanol-petrol blend in internal combustion engine

More ethanol-petrol blend with different composition of ethanol (0 %, 20 %, 40%, 60 %, 80 %, and 100 %) were prepared using ultrasonication-enhanced blending method for internal combustion test. A liter of the blended fuel was added in the generator tank and then the engine was switched on. The volumes of the fuel in the tank were measured at different time for fuel consumption using a meter deep in a fuel tank, and the temperatures of the exhaust pipe were also measured to map the change in temperature with times. The exhaust gases were collected and its compositions were analyzed using a gas chromatography(GC) equipped with a flame ionization detector (FID) and a thermal conductivity detector (TCD). The internal combustion engine (AC generator) shown in Figure 3.7 was used to study the combustion process during the internal combustion of the blended fuel. The engine specifications were summarized in Table 3.2.

Figure 3.7: Power generator (Sinemaster IG2600 BUNDU POWER)

Table 3.2: Specification and characteristics of the internal combustion engine

Model type	KG166 (Single cylinder, air-cooled 4 stroke, gasoline engine)
Displacement (Borex Stroke)	171 cc (66x50 mm)
Compression ratio	8.5:1
Rated power (kW/(r/min))	3.3/3600
Ignition system	Transistor-Controlled Ignition **(**TCI**)**
Spark plug	Bosch - WR7DC
Starting system	Recoil starter
Fuel type	Automotive unleaded gasoline
Fuel consumption (g/kW-h)	500
Lube oil	CD grade or SAE 10W-30, 15W-40
Fuel tank capacity (L)	4.6
Continuous running time	3 hours (at rated output)
Overall dimension (L x W x H) mm (inches)	564 x317 x 453 (22.2 x 12.5 x 17.8)
Dry weight (kg (lbs))	26 (57.2)

3.4 Quantification and analytical techniques

The data collected were analyzed in terms of concentrations, pressure and temperature of the blended fuel. The concentrations in liquid and gas phases were analysed using the High Performance Liquid Chromatography (HPLC) and Gas Chromatography (GC), respectively. The pressure in the blender was measured with the oscilloscope (Tektronix 2445B).

3.4.1 Analysis with high performance liquid chromatography (HPLC)

An Agilent HPLC (Agilent 1200 Series HPLC System) was used for the analysis of samples collected during the blending experiments. The HPLC used is shown in Figure 3.8.

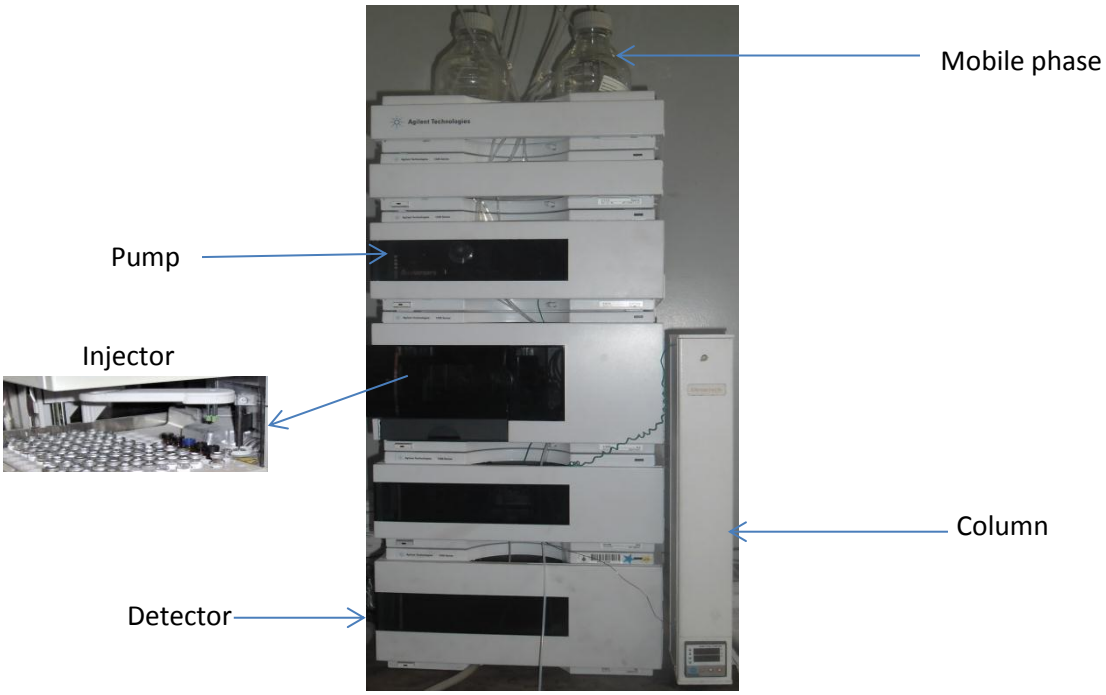

Figure 3.8: A High-Pressure Liquid Chromatography (HPLC)

1. **Mobile phase**: the solvent reservoir bottle was filled up to 90 ml of acetonitrile as the mobile phase for ethanol analysis. HPLC grade of acetonitrile was 99 % pure for mobile phase, with a dilution factor of 2.
2. **Pump:** The role of the pump is to force the mobile phase through the liquid chromatograph at a specific flow rate, expressed in millilitres per min (mL/min). For the analysis the flow rate was 10 mL/min.

3. **Injector:** The injector serves to introduce the liquid sample into the flow stream of the mobile phase. The injector sample volume was set to 20µL.
4. **Column**: An Eclipse XDB-C18 column (Length x internal diameter: 4.6 ×150 mm, particle size: 5 µm) maintained at 25^0C was used.
5. **Detector:** The detector provides an output to a computer that result in the liquid chromatogram (i.e., the graph of the detector response). An example of the graph of the detector response can be found in Appendix C.

Before using the HPLC for the analysis, the equipment was calibrated using the method described in Appendix C. The concentration samples that were collected were poured into sample bottles of about 1.5 ml using a pipette and placed on the HPLC loading tray. To perform the analyses for the horizontal sampling, all 72 vials were firstly loaded into the HPLC loading tray and placed in the HPLC. The pump was then switched on and a purging time of 10 minutes was allowed to let the pump warm up and stabilize. Once the pump stabilized and all the icons on the computer screen turned green, the analysis was started. The same procedure was done for the vertical direction samples. The retention time for the analysis of ethanol was set to be between 1.7-1.8 min. The results given by the HPLC are in terms of the area under the curve thus using the calibration curve described in Appendix C below the area obtained was automatically interpolated to find the concentration that lies within the calibration curve for the given area and the results obtained from the HPLC can be found in Appendix C

3.4.2 Measurement with oscilloscope

The pressure distributions in the blended fuel and the blender were measured indirectly using an oscilloscope shown in Figure 3.9 and the full method of how the equipment was used is described in details in Appendix C.

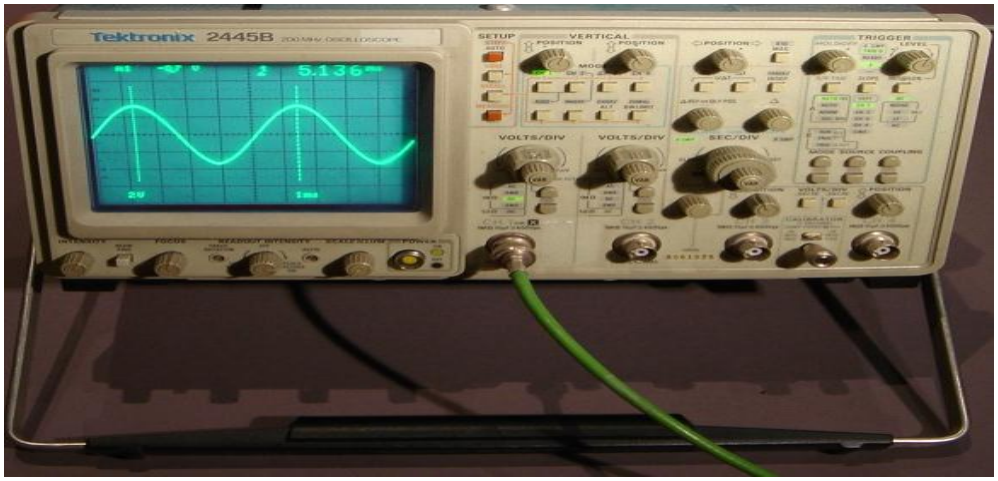

Figure 3.9: Typical oscilloscope used for pressure analysis (Tektronix 2445B Oscilloscopes**)**

The oscilloscope signal sensor probe was used to sense the voltage distribution in the mixture. The oscilloscope voltage reading was given in volts /division, and thus prior to the experiment, the equipment volatage reading was set to 1 division. The time was also given as seconds /division and this reading was also set to 1 division. The waves shown in the screen give the voltage reading as the probe senses the voltage distribution in the solution per time.

Ethanol and petrol mixtures of 30%, 20% and 10 % ethanol were prepared as explained in 3.2.2. During the sonication period, the oscilloscope probe was first held in the reactor at a 1cm horizontal distance from the ultrasonication horn. At this specific position, the voltage was read and recorded from the oscilloscope for different sonication times of 60, 120, 180, 240, 300 and 360 seconds. This procedure was repeated for a 2 cm, 3 cm and 4 cm horizontal distances while the ultrasonicator and oscilloscope settings were kept constant. The same experiment was performed for the same vertical distances from the horn and the voltage was read from the oscilloscope. The voltage readings for all samples were then converted to pressure using the conversion factor given as:

$$1\text{Pa} = 25.4\mu\text{volts} \tag{3.1}$$

3.4.3 Analysis with Gas Chromatography (GC)

The exhaust gases from the internal combustion engine were analyzed as a function of the blended ratio using a Bruker GC 430 with schematic shown in the Figure 3.10.

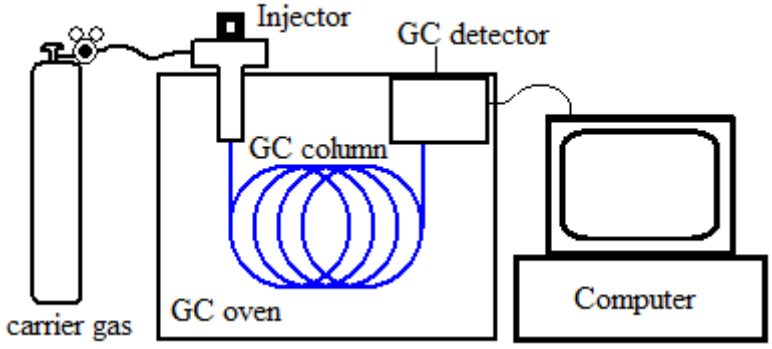

Figure 3.10: Schematic of the GC used for the analysis

The experiments were carried out on a Bruker 430gas-chromatograph. The separation was performed on a Shincarbon ST 80/100 packed column, with a length of 2 m, inner diameter of 2.00 mm. Nitrogen was used as a carrier gas with an initial flow of 20 ml/min. Samples were injected in splitless mode through the injector set at 100 °C. In the GC temperature program the initial temperature was 100 °C and was raised to 250 °C with a rate of 15 °C/min, and maintained for 3 minutes.

Before the analysis, the GC was calibrated and the detailed calibration procedure is provided in Appendix C. The GC provides the composition of gases as area percentage (the area under the peak which result as a consequence of gas detection divided by the sum the areas under all the peaks). The area percentages were converted to concentration percentages which were used in the mass balance.

CHAPTER 4: RESULTS

4.1 Phase behavior of ethanol-petrol blend using ultrasonication

The results of the investigation of the phase behavior of bioethanol-petrol blend are given in term of ternary diagram and water tolerance profile plot.The blended fuel was stored in water bath at 26 ^{O}C controlled by a thermostat for two weeks. The data in Table A.2 of Appendix A gives the composition of the binodales curve of the stable blend at the end of the storage time. The ternary diagram and the water tolerance against petrol content are given in Figure 4.1 through Figure 4.3.

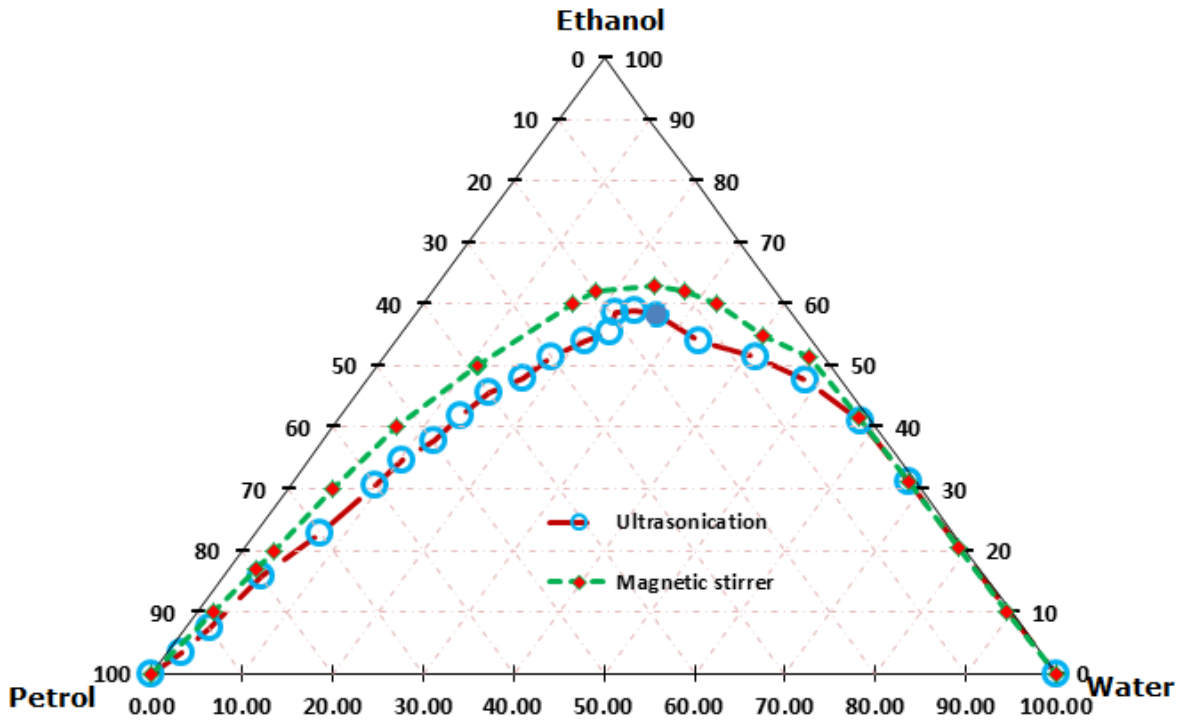

Figure 4.1: Ternary diagram of ultrasonicated and stirred ethanol-petrol-water mixture at 26 ^{O}C

Contour plot and surface plot depicted in Figure 4.2 and Figure 4.3, respectively.

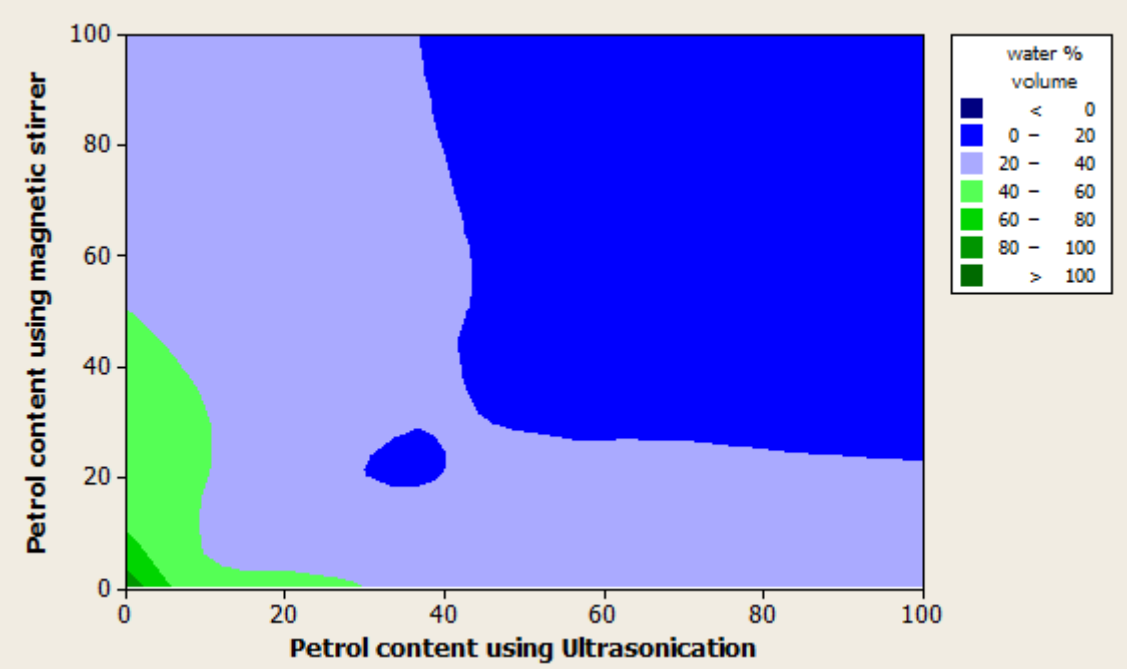

Figure 4.2: Contour plot for water content as function of petrol content

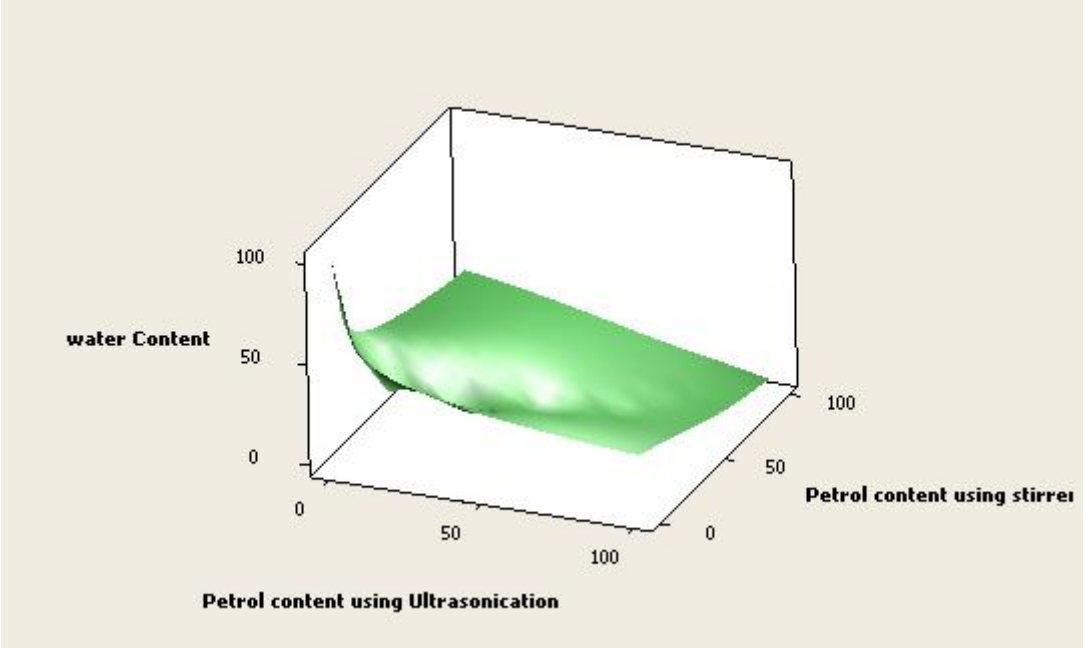

Figure 4.3: Surface plot for water content as function of petrol content

During the storage of ethanol-petrol blend, the volume fraction of ethanol and petrol were measured at different points within the storage container and times for homogeneity test, Figures 4.4 and Figure 4.5 show the volume fraction measurement of E50 and E60 with depth and time in the storage container.

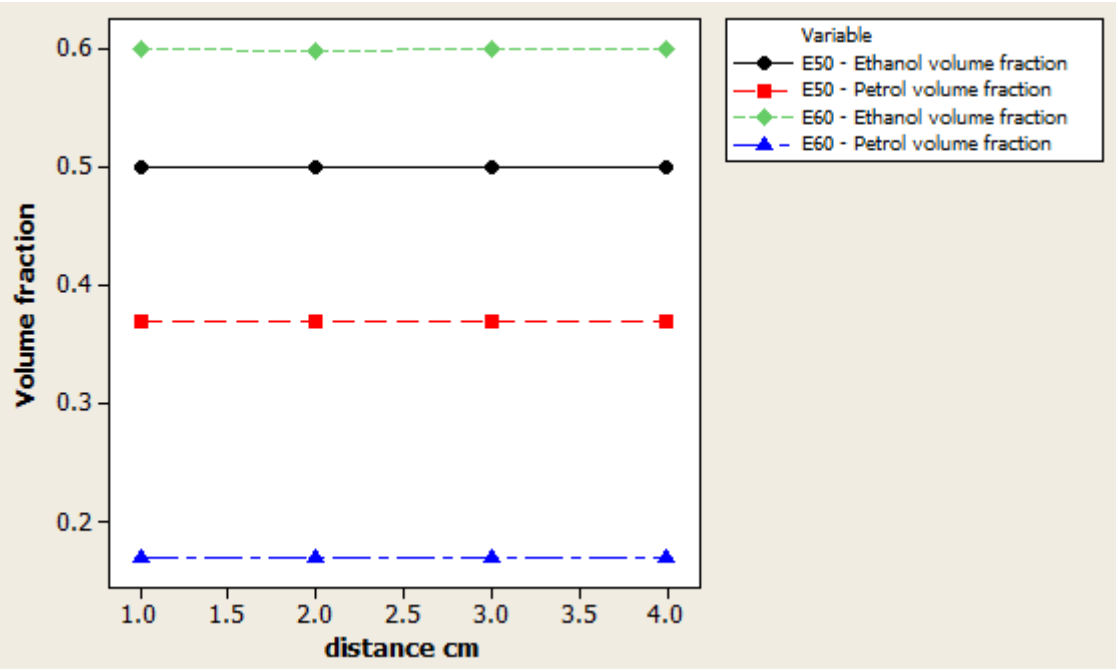

Figure 4.4: Ethanol and petrol volume fraction with depth

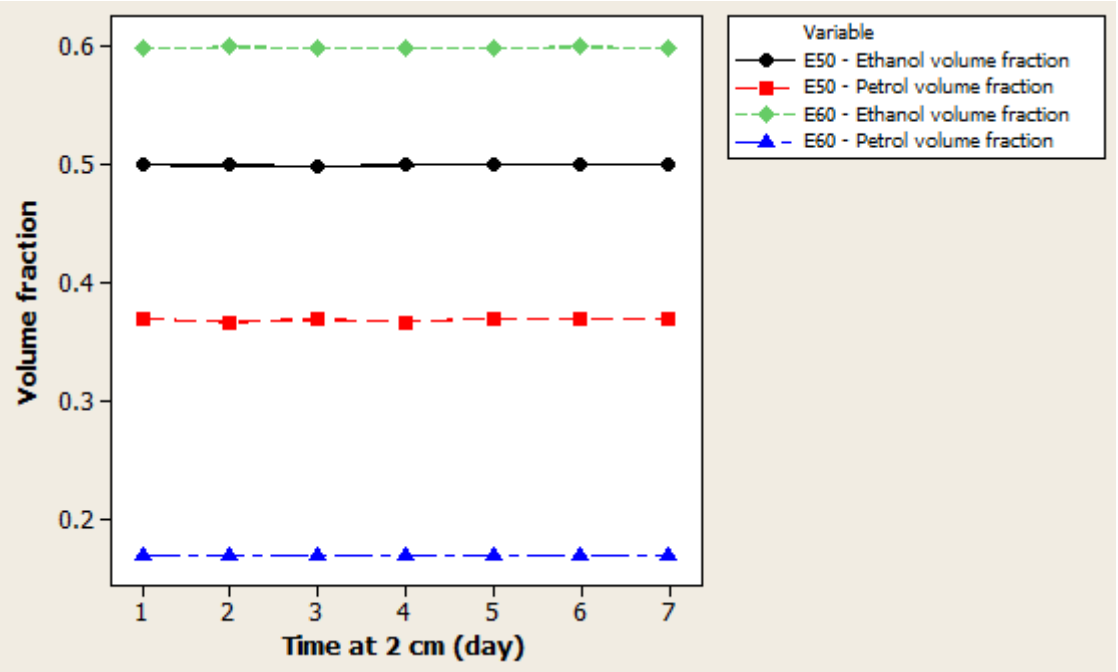

Figure 4.5: Volume fractions of ethanol-petrol blend with time during the storage at 2 cm depth

4.2 Ethanol-petrol mixture using ultrasonication-enhanced blending

The blending process was studied in terms of concentration, bulk pressure and temperature. The results of ultrasonication-enhanced adsorption were first reported followed by the results of the blending process, which are given below.

4.2.1 Dehydration of bioethanol mixture prior to blending

4.2.1.1 Ultrasonication-enhanced dehydration via adsorption methods

The effect of ultrasound on dehydration of the bioethanol was investigated by comparing the adsorption of water by silica gel using ultrasonicator and stir bar, both reactors operating with the same amount of ethanol. The ultrasonicator was set at 0.5 pulse rate and 50 % of amplitude. Figure 4.6 shows that the relative amount of water adsorbed is higher with the use of ultrasound energy.

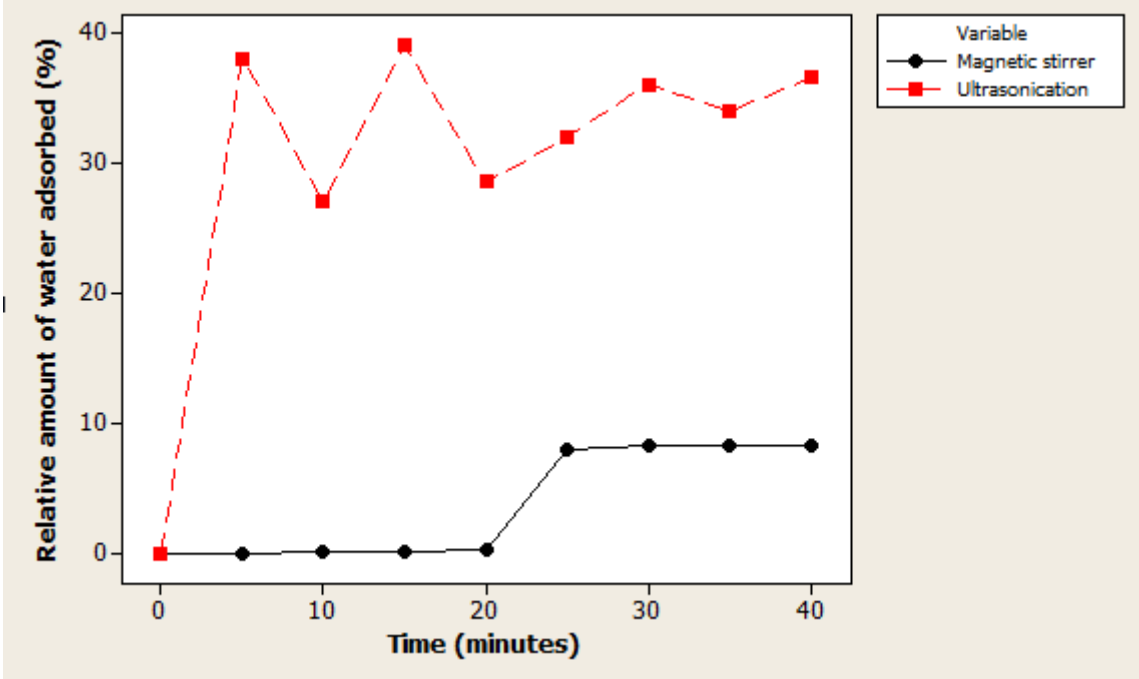

Figure 4.6: Relative amount of water adsorbed against time

4.2.1.2 Enthalpy change during ultrasonication-enhanced adsorption of water

The enthalpy change during the adsorption process was also investigated, and Figure 4.7 gives the estimation of the adsorption enthalpy and entropy changes. Figure 4.7 was plot from the data collected at 0.5 amplitude and 0.5 pulse rate (ultrasonicator setting) which can be found in Appendix B.2. This data cannot be compared to literature because no such experiments have been reported.

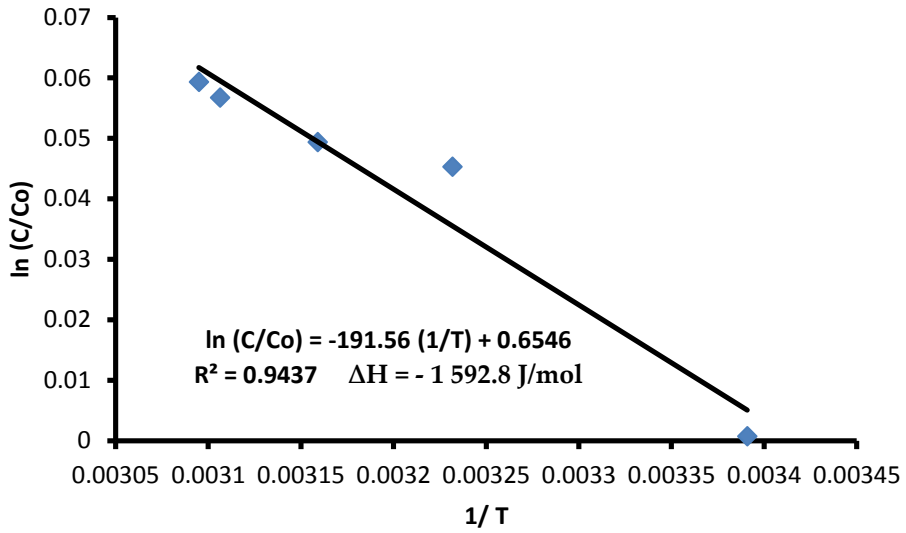

Figure 4.7: Calculated adsorption enthalpy and entropy changes

4.2.1.3 Effect of operating variables on enhancement of dehydration of bioethanol

Figure 4.8 and Figure 4.9 show the ethanol concentration profile and temperature during the dehydration of bioethanol using ultrasonication-enhanced adsorption

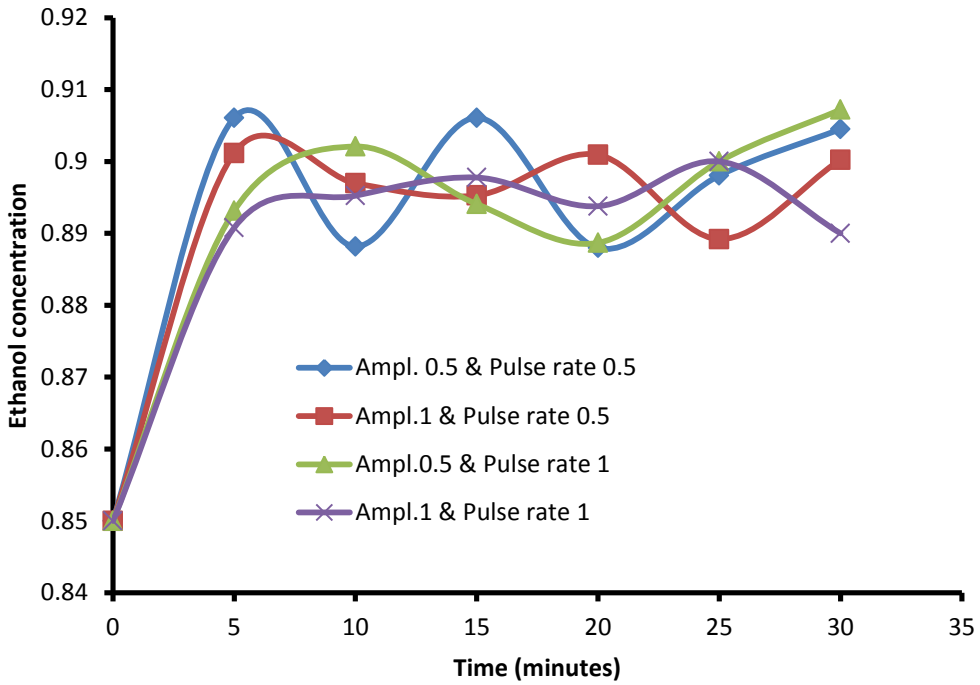

Figure 4.8: Ethanol Concentration profiles at varied ultrasonicator settings

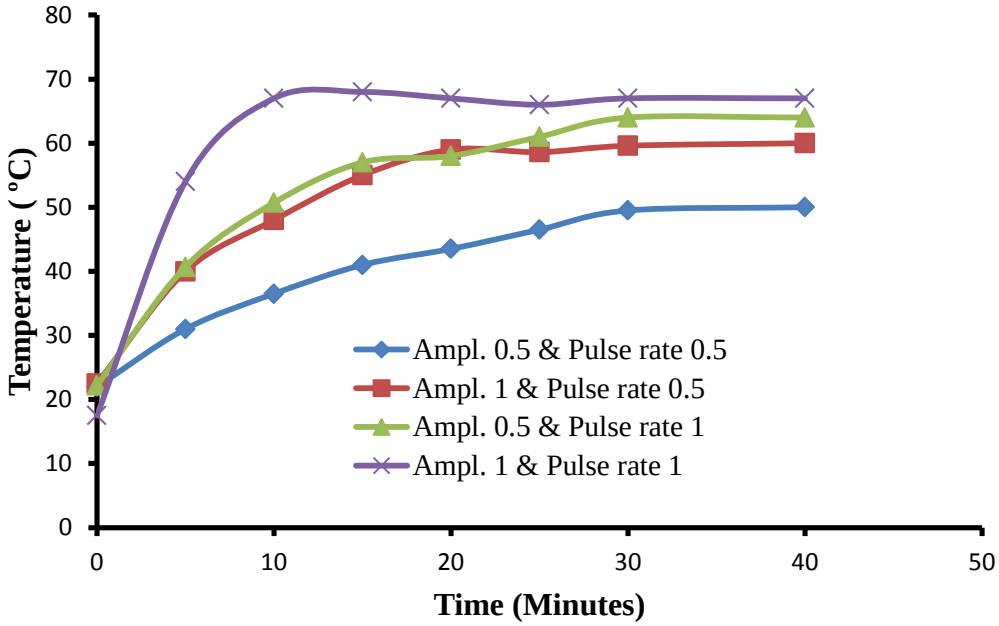

Figure 4.9: Temperature profiles at varied ultrasonicator pulse rate and amplitude

4.2.1.4 Kinetics of ultrasonication-enhanced dehydration using adsorption

In order to fit the kinetic model describing the process, a second order kinetic model was chosen based on studies done by Qiu *et al*. (2009) and Sekharao *et al*, (2011). They also claimed that second order kinetic is best suited for organic mixtures, such as high concentration bio-ethanol mixtures. In order to fit the kinetics, the adsorptive capacity was calculated using equation (2.28), the linear plot of the adsorption as a function of time was found using the equation below .

$$\frac{t}{q_t} = \frac{1}{V_o} + \frac{1}{q_e}t \text{ (Pseudo second order kinetic model re-arranged)} \quad (4.1)$$

derived from, $\frac{dq_{(t)}}{dt} = k_{p2}(q_t - q_e)^2$, and intergrated with the boundry conditions : $q_t = q_t \; and \; 0$ at t = t and 0, respectively. Where q is the adsorptive capacity, k is the adsorption capacity constant and $V_0 = K_{P2}(q_e)^2$ and the subscribts '0', 'e' and t are at time = 0, equilibruim and time rerspectively.

By plotting t against t/q_t, the linear plot shown in Figure 4.10 should give the corrected constants of the kinetic model, from which the model can be checked if it agrees with the experimental results.

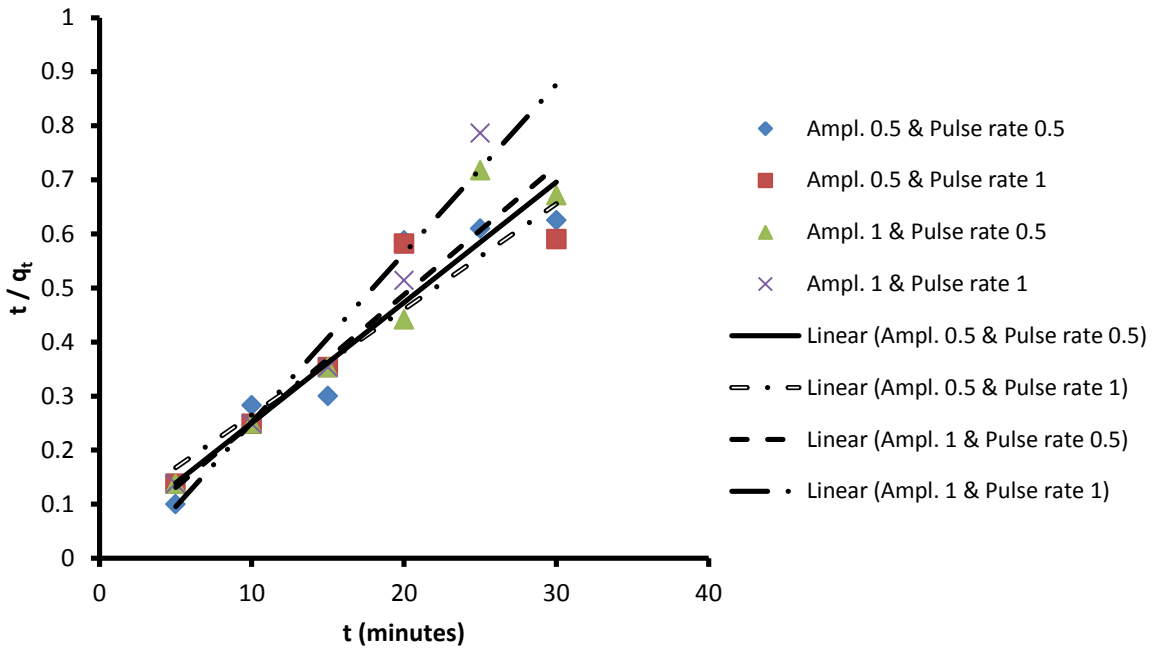

Figure 4.10: Time over adsorptive capacity (t/q_t) versus time (t)

From Figure 4.10, the constants of the kinetic model were estimated. Figure 4.11 compares the experimental and the estimated adsorptive capacity.

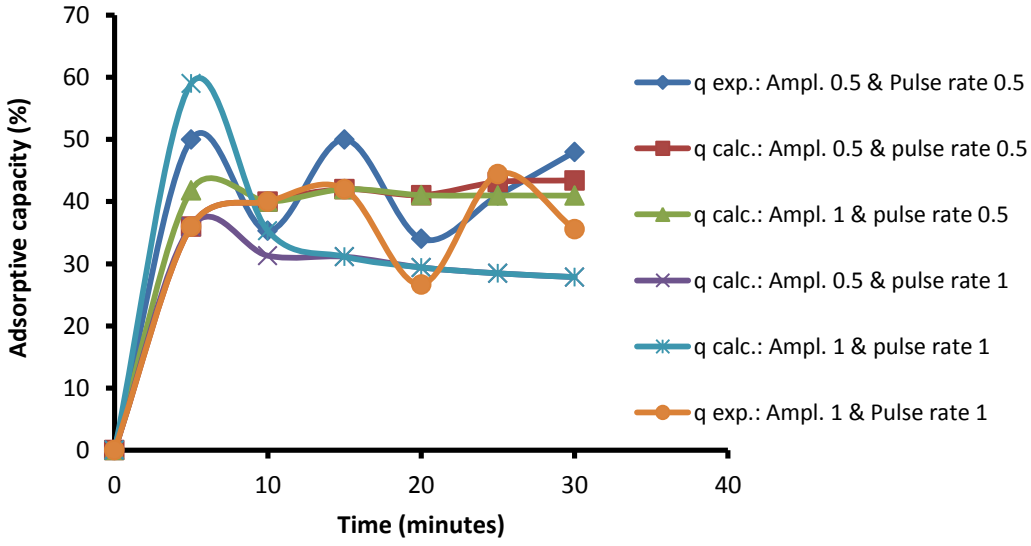

Figure 4.11: Calculated and experimental adsorption capacity

4.2.2 Effect of ultrasonicator position during ultrasonication-enhanced blending

4.2.2.1 Pressure profile

To investigate the ultrasonicator energy distribution in the blender, the pressure was measured at different distances from the horn using an oscilloscope as explained in the experimental method of this thesis. The relationship between pressure and intensity of energy is given by the Equation (2.35) in Chapter 2. This equation shows that the pressure distribution in the reactor is directly proportional to the energy and thus the pressure profiles describe the energy profiles. The data used to plot the figures for pressure profile with positions can be found in Appendix C.1. To understand the energy distribution, horizontal and vertical pressures were measured and the results are given below. The pressure profiles were obtained at different horizontal positions using the ultrasonic probe. Figure 4.12, Figure 4.13 and Figure 4.14 (obtained from data presented in Tables C.1, C.2 and C.3 of Appendix C.1) are the experimental results. The figures show that the pressure decreases with horizontal position from the ultrasonicator probe.

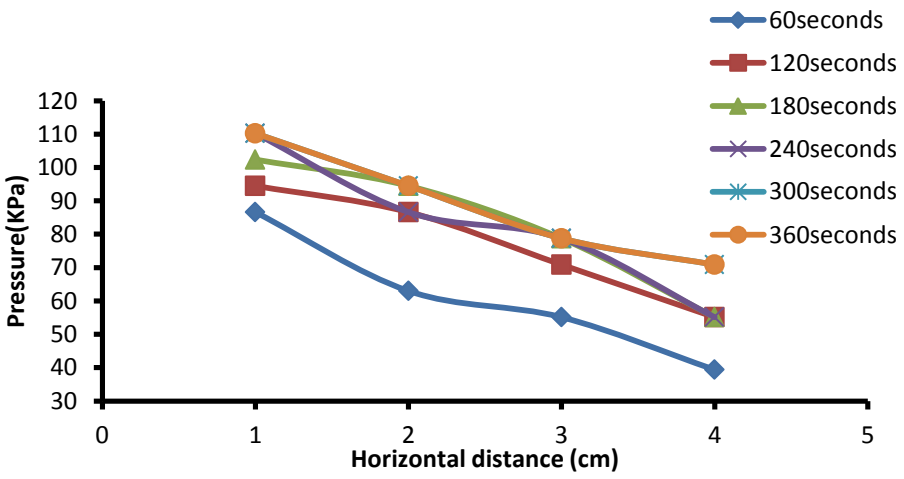

Figure 4.12: Variation of pressure with horizontal distance for E10 blend

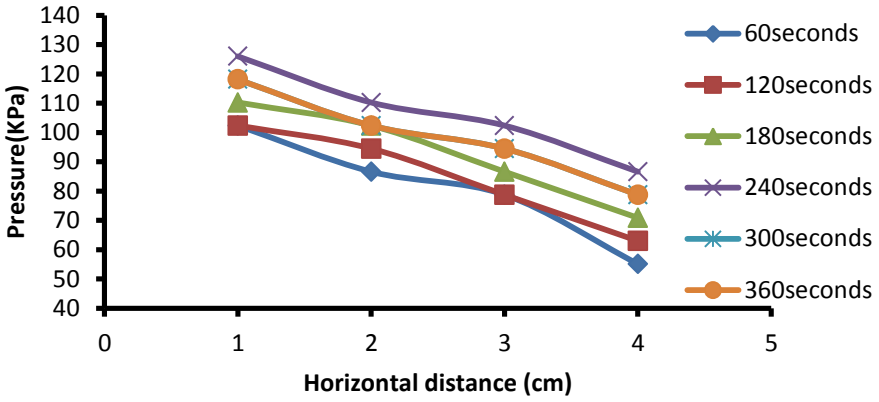

Figure 4.13: Variation of pressure with horizontal distance for E20 blend

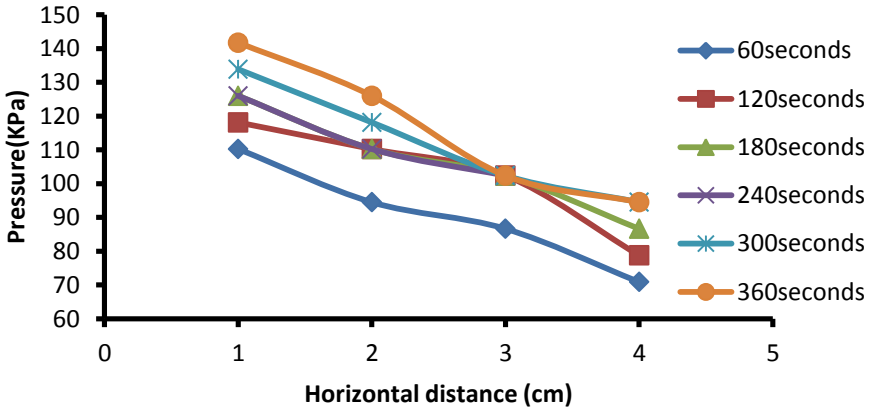

Figure 4.14: Variation of pressure with horizontal distance for E30 blend

The effect of the amount of ethanol in mixture on the pressure distribution was also studied, and thus pressure variation with the horizontal position was plotted at different ethanol–petrol blend. In all the figures, it can be seen that the E30 blend has the highest pressures followed by E20 blend and the lowest being E10 blend. Figure 4.15, Figure 4.16, Figure 4.17, Figure 4.18 and Figure 4.19 show the pressure profile against horizontal position for ethanol- petrol blend at specific time.

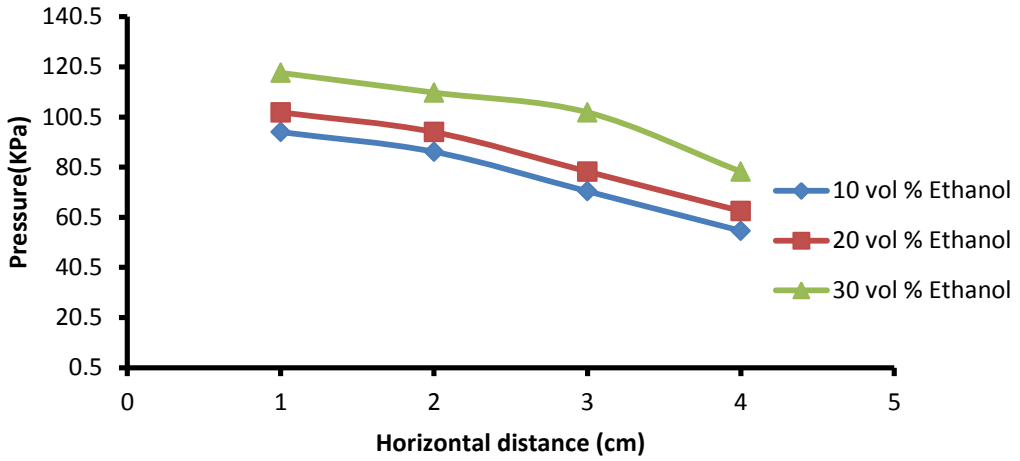

Figure 4.15: Variation of pressure with horizontal distance at 120 seconds

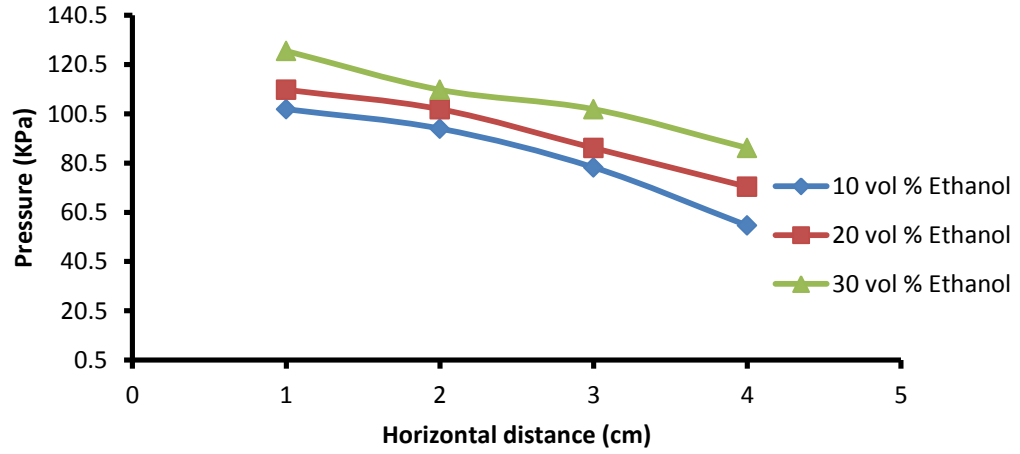

Figure 4.16: Variation of pressure with horizontal distance at 180 seconds

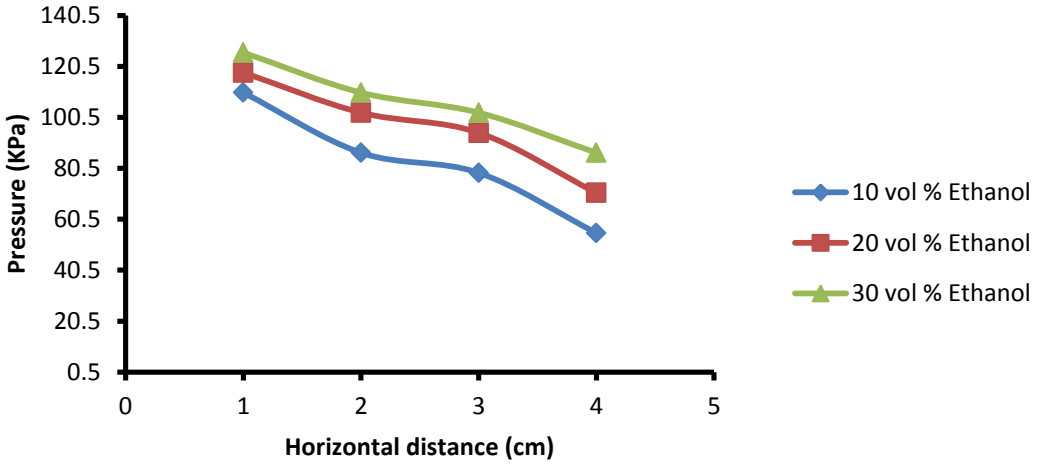

Figure 4.17: Variation of pressure with horizontal distance at 240 seconds

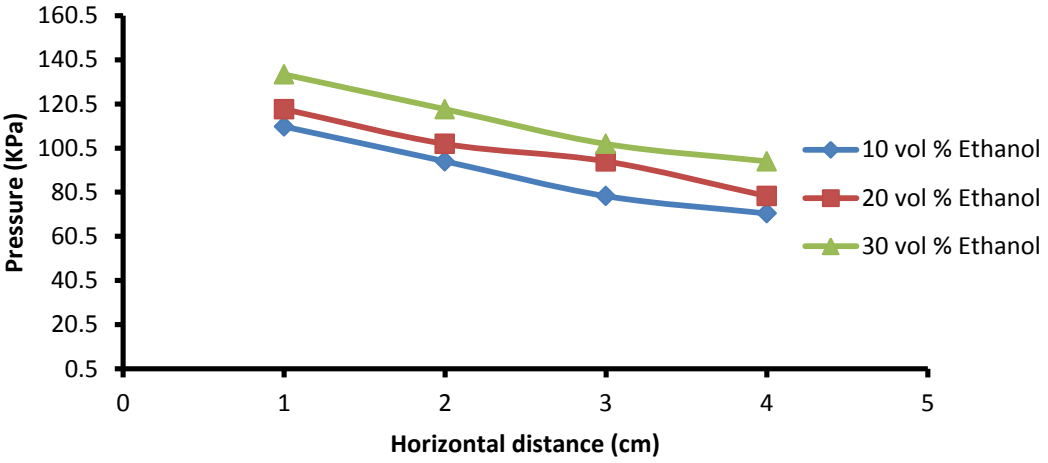

Figure 4.18: Variation of pressure with horizontal distance at 300 seconds

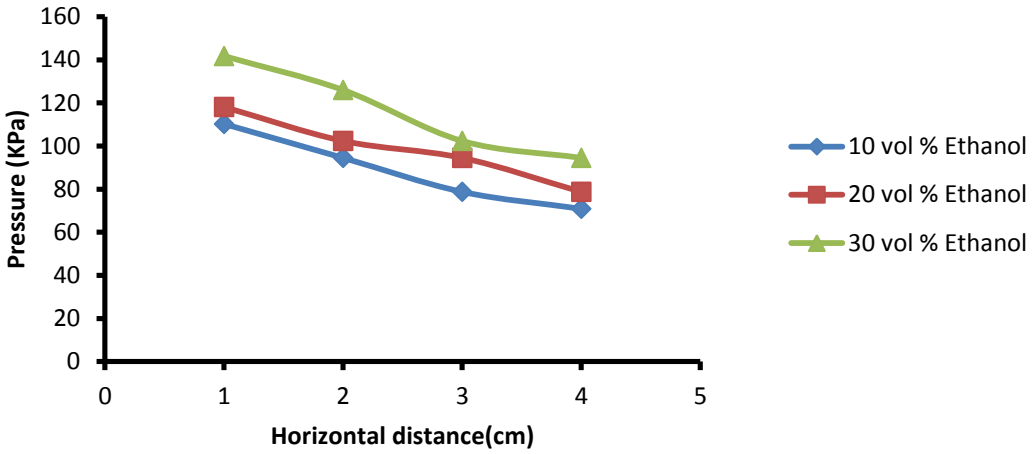

Figure 4.19: Variation of pressure with horizontal distance at 360 seconds

The pressure distribution in the vertical direction was also analysed as done in the horizontal direction where the tables used to plot the figures of pressure as function of time and distance can be found in Appendix C.1. Figure 4.20 through 4.22 show the change in pressure with depth for E10, E20 and E30 using ultrasonication-enhanced blending. It can be seen from the figures the pressure increases with the distance. The mixing time yield the highest pressure when mixing was done for 360 sec and the lowest when mixing was done for 60 sec. This is evident in the Figure 4.20 and Figure 4.22. In Figure 4.21 a slight deviation of pressure is seen for 360 sec sonication, which is initially higher and gradually decreases.

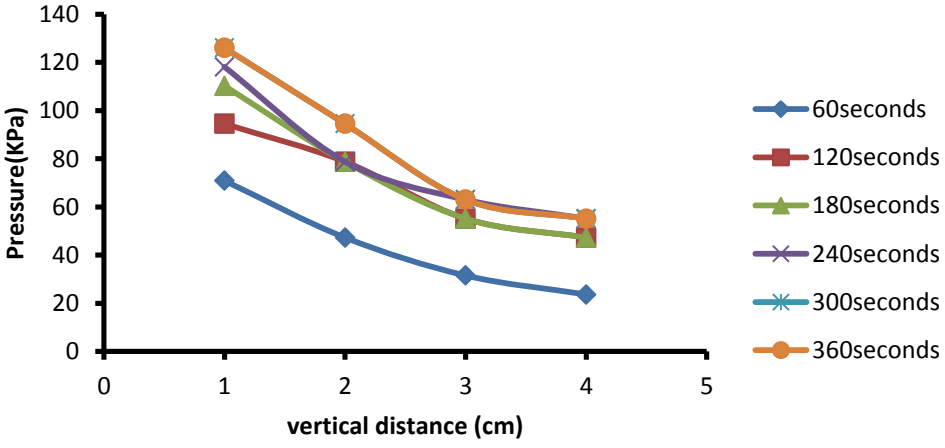

Figure 4.20: Variation of the pressure with vertical distance for E10

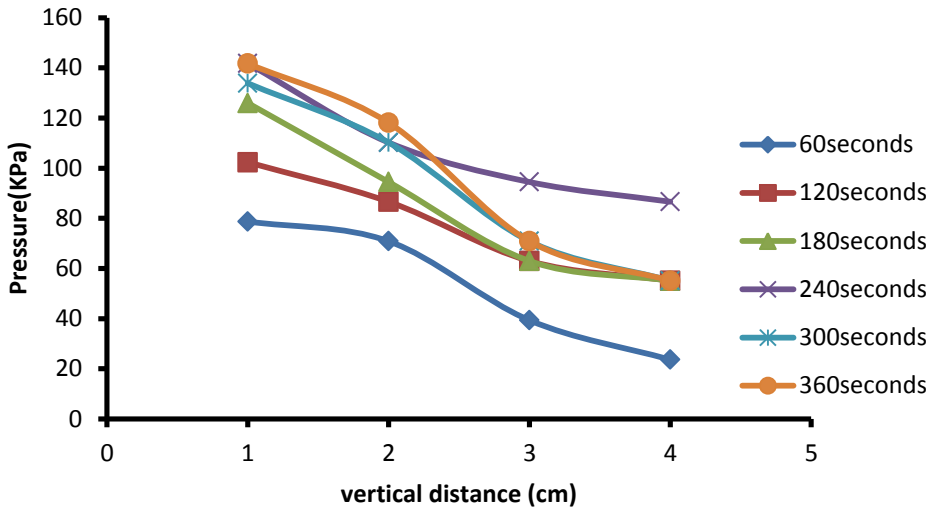

Figure 4.21: Variation of the pressure with vertical distance for E20

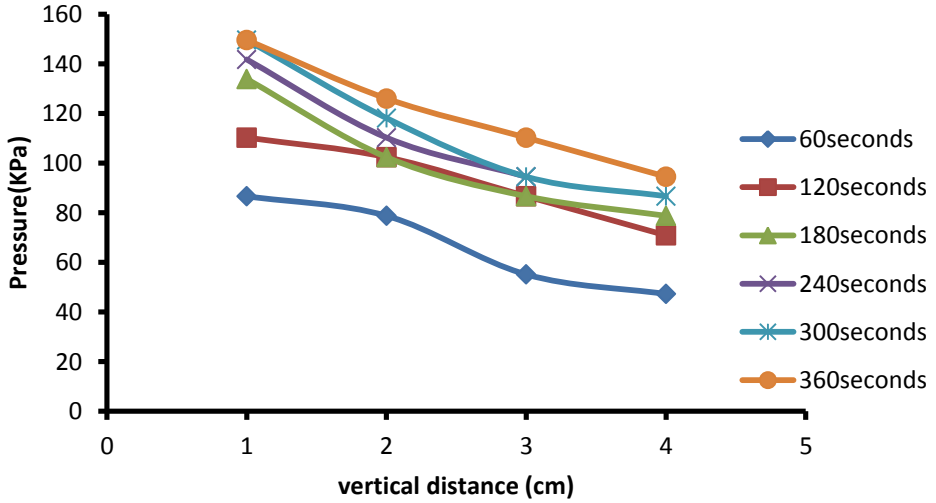

Figure 4.22: Variation of the pressure with vertical distance for E30

Figures 4.23 through 4.27 show a plot of pressure as a function of distance for different ethanol and petrol blends at different ultrasonic time. The graph shows that the solution of 30% ethanol has the highest pressure in comparison to the 10 % and 20% volume ethanol. This relationship is shown for all ultrasonic times of 60 to 360 seconds.

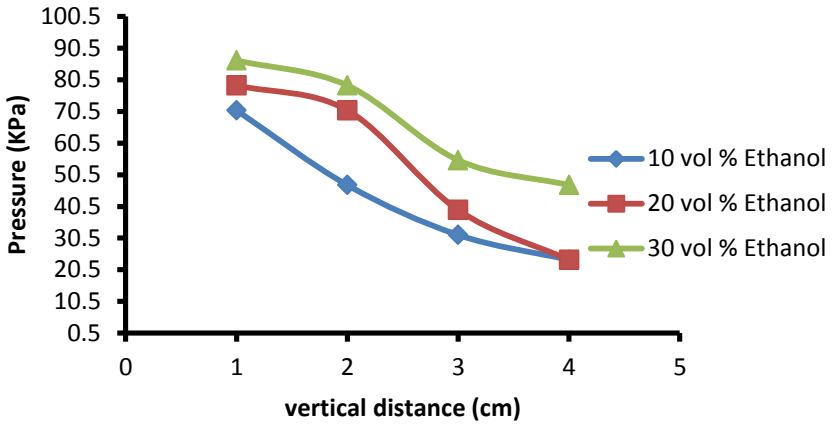

Figure 4.23: Variation of the pressure with distance at 60 seconds

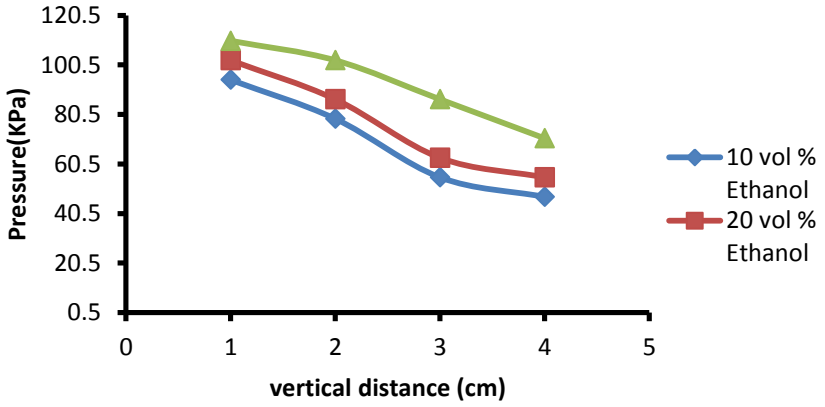

Figure 4.24: Variation of the pressure with distance at 120 seconds

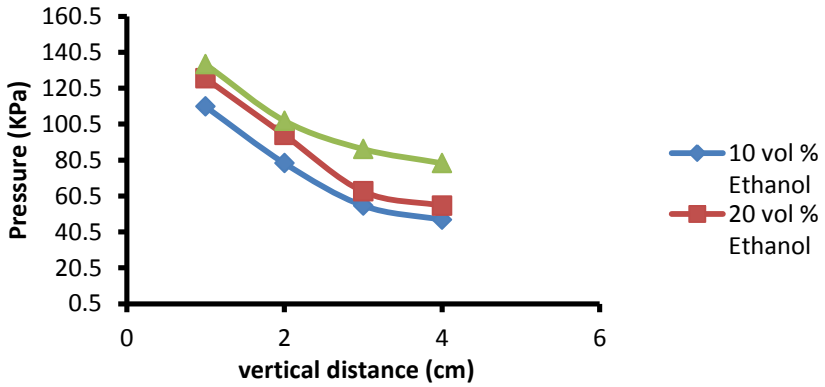

Figure 4.25: Variation of the pressure with distance at 180 seconds

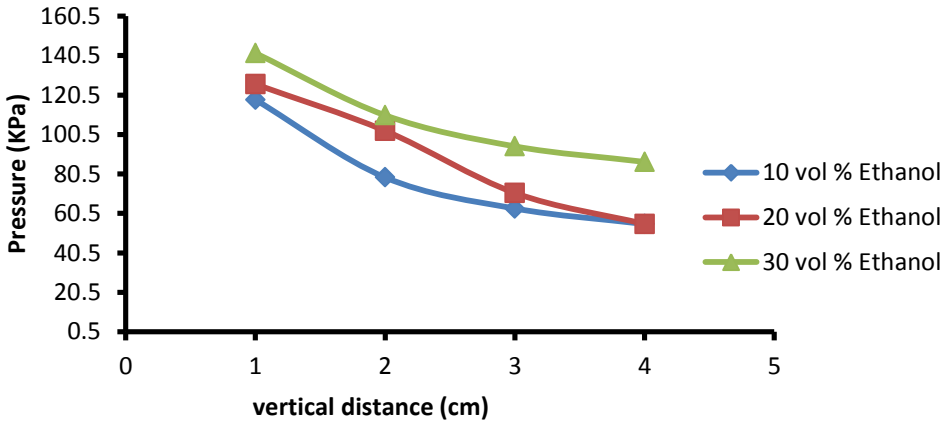

Figure 4.26: Variation of the pressure with distance at 240 seconds

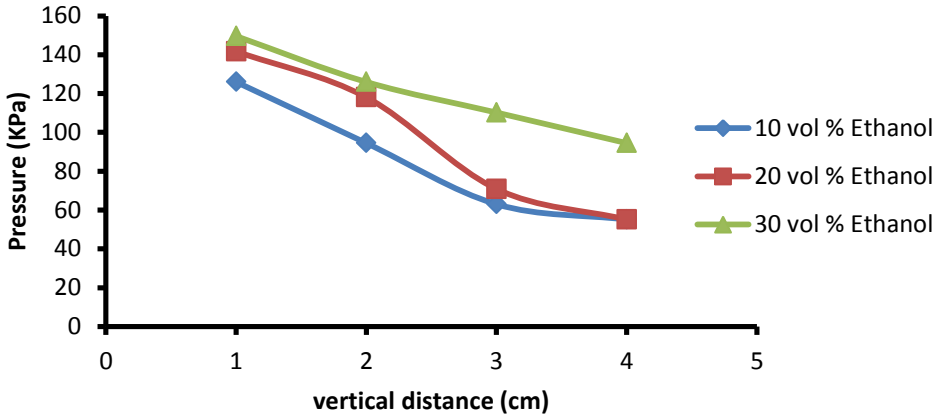

Figure 4.27: Variation of the pressure with distance at 360 seconds

4.2.2.2 Temperature profile

The temperature profile within the blender was investigated to investigate the thermal distribution in the mixing vessel. Expectedly the temperature profile wave-like according to the intensity of energy distribution discussed in the literature.

The temperature change with the horizontal distance was measured and recorded described in Chapter 3. Figures 4.28 through 4.30 show the temperature as a function of the horizontal direction. In these figures, it can be seen that highest temperature was achieved when ultrasonication time is the longest.

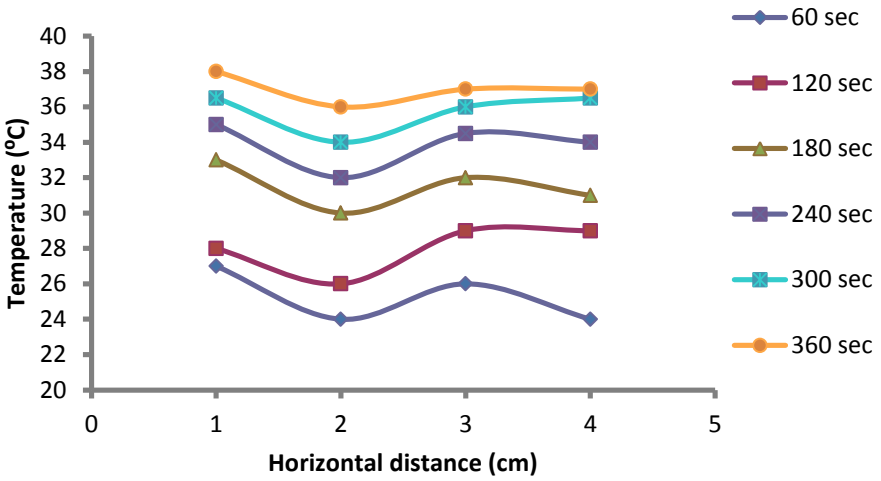

Figure 4.28: Variation of temperature with distance for blended fuel E10

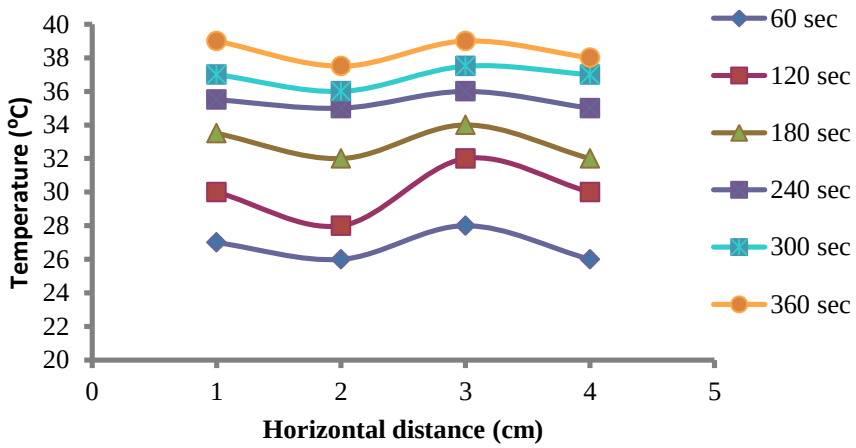

Figure 4.29: Variation of temperature with distance for blended fuel E20

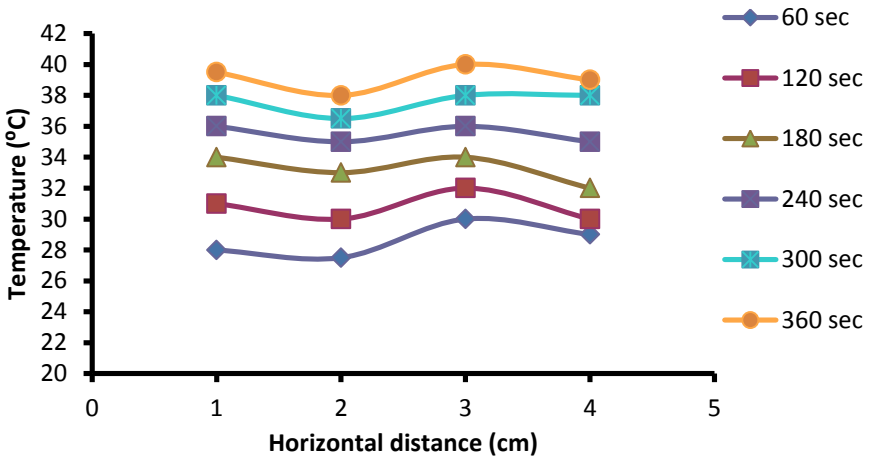

Figure 4.30: Variation of temperature with distance for blended fuel E30

The temperature distribution in the reactor/ mixing vessel as a function of the vertical distance in the mixer was also investigated to see how well the energy is distributed across the reactor to form the cavities and homogenize the mixture. Detailed information about the investigation can be obtained from Appendix C.2. Figures 4.31 through 4.33 show the relationship between temperature and the vertical distance for different ultrasonication times for E10, E20 and E30. It can be seen from these figures that temperature decreased with an increase in distance from bottom of the ultrasonicator probe to the top of the mixer in the upward direction. Also Figures 4.31 through 4.33 show that temperature increased with a decrease in the depth of the ultrasonicator. The temperature increased from about 34^{o}C to about 41^{o}C as the depth decreased from 4 cm to 1 cm when the ultrasonication time was 360 seconds. Similar trend was observed for ultrasonication times of 300 seconds, 240 seconds, 180 seconds, 120 seconds and 60 seconds. .

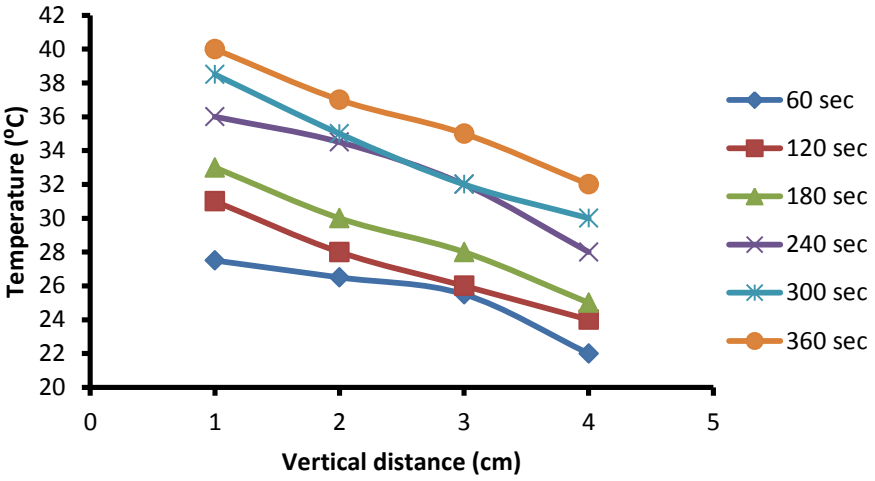

Figure 4.31: Temperature as function of vertical distance for blended fuel E10

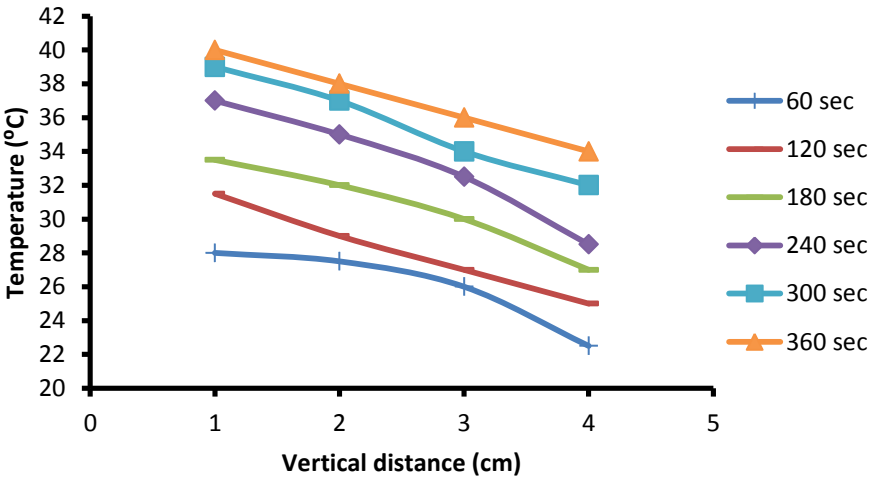

Figure 4.32: Temperature as function of vertical distance for blended fuel E20

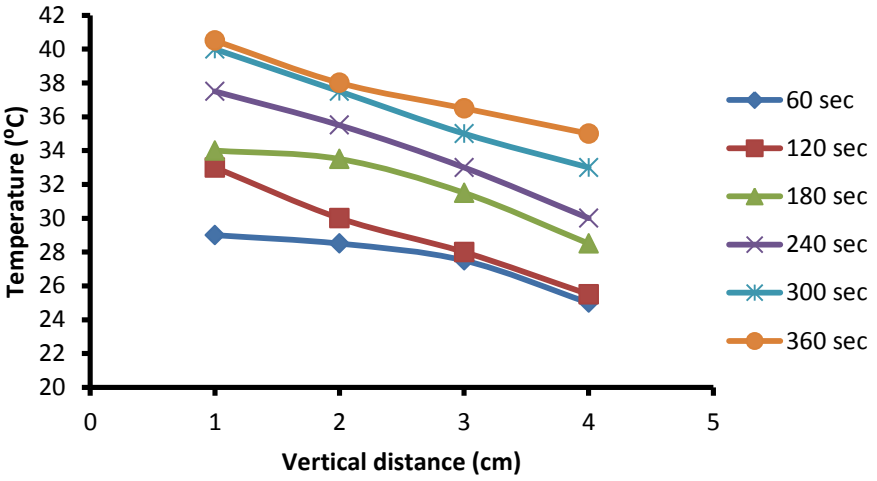

Figure 4.33: Temperature as function of vertical distance for blended fuel E30

4.2.2.3 Concentration gradient during ultrasonication-enhanced blending

To investigate the concentration gradient due to diffusion in the horizontal and vertical directions, samples of fuel mixture were collected at different positions horizontally and vertically from the ultrasonicator horn. The ethanol concentration as a function of the horizontal and vertical distance from the horn was analysed with HPLC as explained in Chapter 3.

Figures 4.34 through 4.36 show ethanol concentration as a function of the horizontal distance from the ultrasonicator horn. Similarly, Figures 4.42 through 4.44 depict ethanol concentration as a function of the vertical distance from the ultrasonicator horn. Figures 4.34 through 4.36 below show the relationship of concentration as a function of distance for different sonication time for the E10, E20 and E30 blend. Figure 4.34 depicts that at specific ultrasonication times, the ethanol concentration profile with distance is a wave function. There is however no specific trend on how the waves change with the ultrasonication times and this will be explained in the discussion section. Figure 4.35 and 4.36 also show that the concentration profile with distance is a wave function.

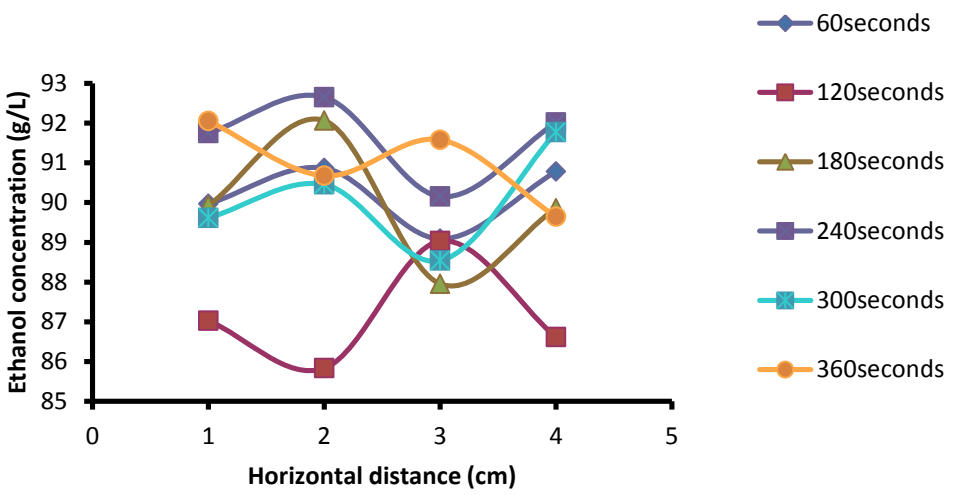

Figure 4.34: Concentration as function of distance for E10 blend

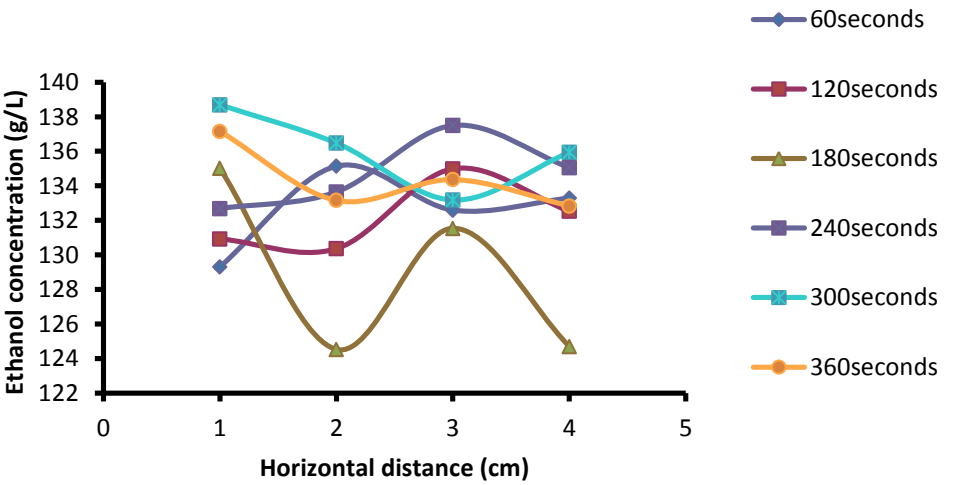

Figure 4.35: Concentration as function of distance for E20 blend

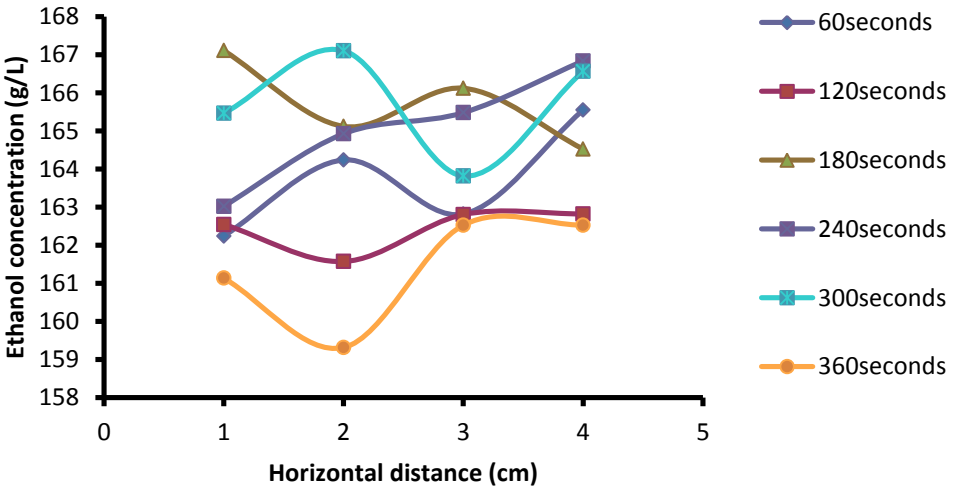

Figure 4.36: Concentration as function of distance for E30 blend

The effect of ethanol volume in the mixture on the concentration profile was also analysed Figures 4.37 through 4.41 show that the highest concentrations were recorded for the E30 blend followed by E20 blend and lastly E10 blend having the lowest concentration. The concentration profile depicted by the E30, E20 and E10 blends were also seen in the plot of concentration with distance at a specific time. Below are the figures for the effect of amount of ethanol on the concentration with time and distance, and the data used to plot the graphs can be found in in appendix C.

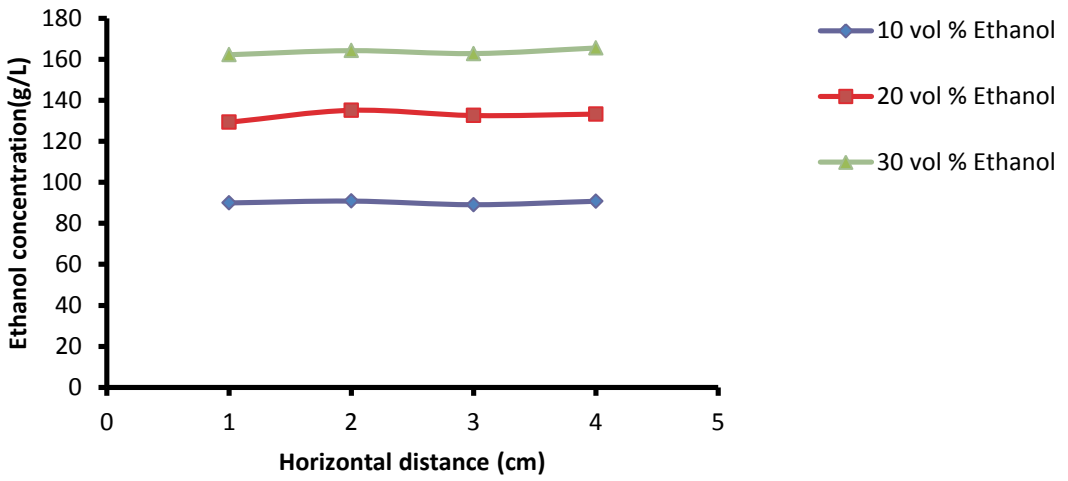

Figure 4.37: Ethanol concentration as function of horizontal distance for 60 seconds

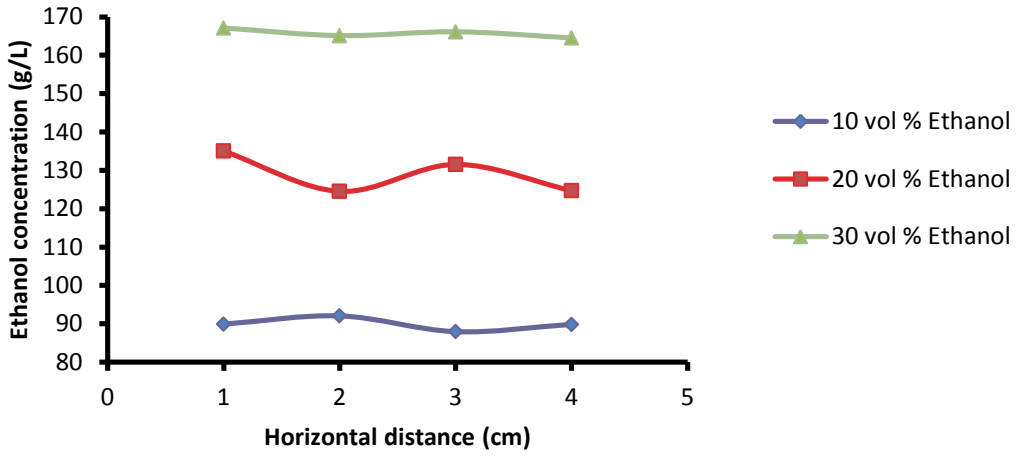

Figure 4.38: Ethanol concentration as function of horizontal distance for 180 seconds

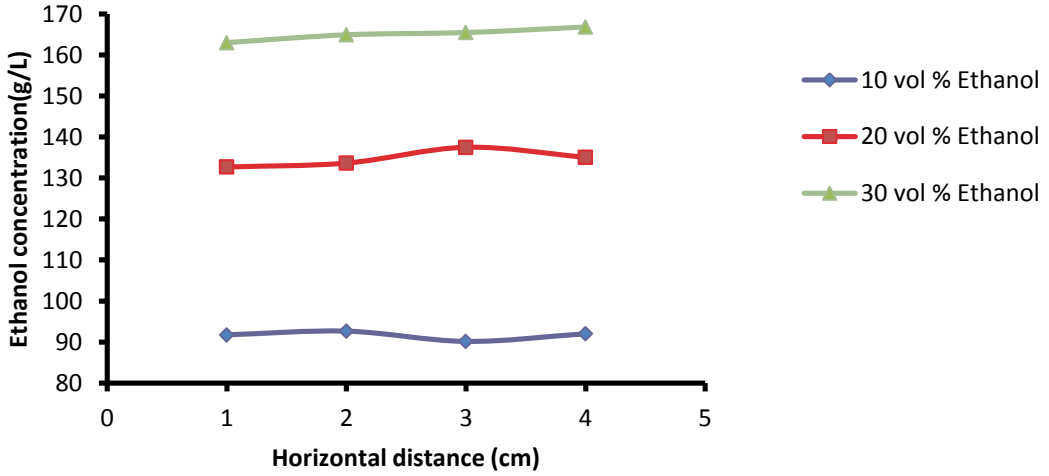

Figure 4.39: Ethanol concentration as function of horizontal distance for 240 seconds.

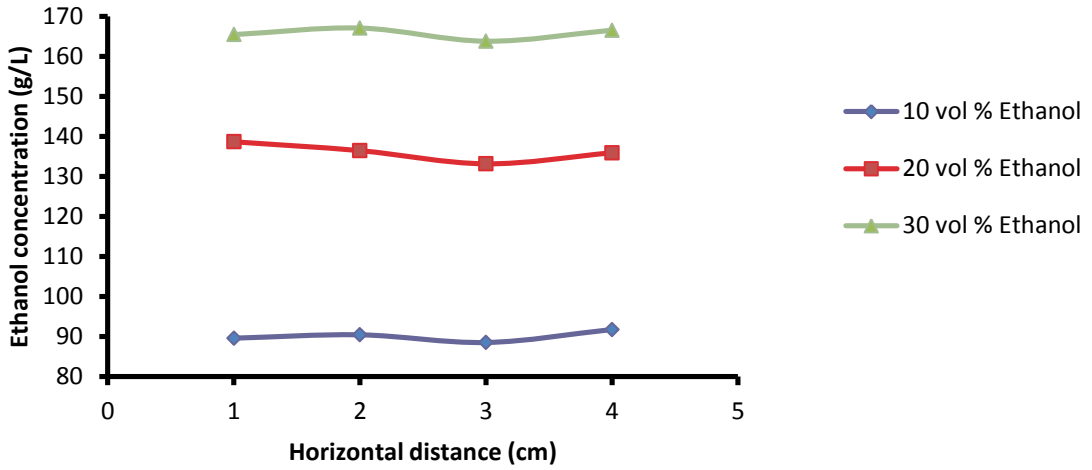

Figure 4.40: Ethanol concentration as function of horizontal distance for 300 seconds.

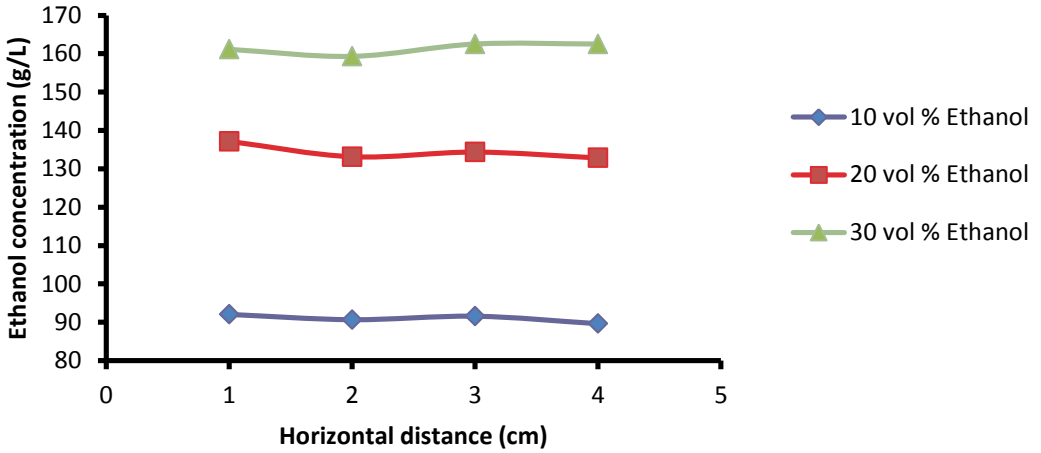

Figure 4.41: Ethanol concentration as function of horizontal distance for 360 seconds.

Mixing liquids using the ultrasonication technique is governed by diffusion and this occurs in both the horizontal and vertical direction. The mass transfer on the vertical direction was therefore also studied and the data used to plot the concentration profile obtained from the HPLC in the vertical direction can be found in appendix C.3.

Figures 4.42 through 4.44 show the concentration profile as a wave function for all the different ultrasonication times. The amplitude of oscillations describes the concentration gradient in the vertical direction as discussed in the horizontal direction. There is however no

consistent relationship between the waves amplitude and the sonication times as shown below.

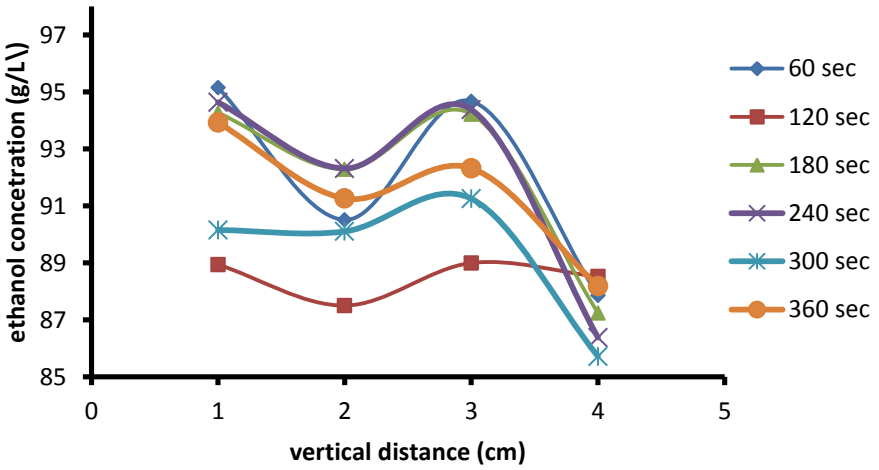

Figure 4.42: Ethanol concentration as a function of vertical distance for E10 blend

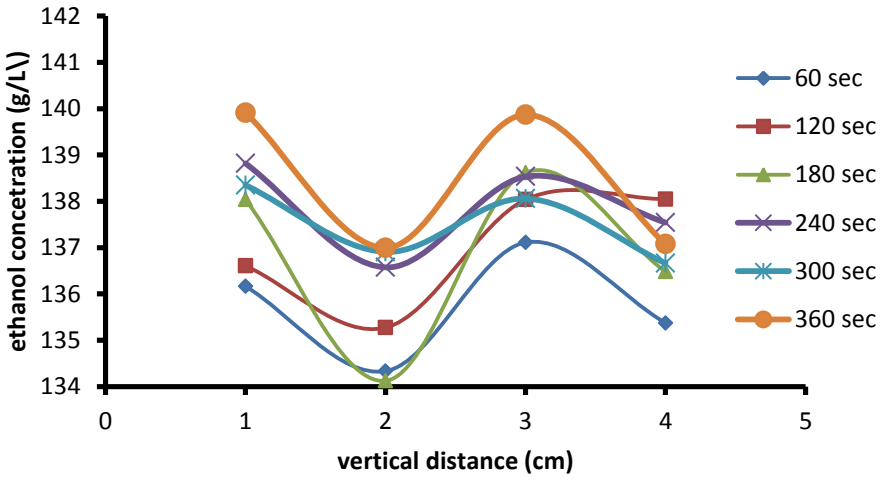

Figure 4.43: Ethanol concentration as function of vertical distance for E20 blend

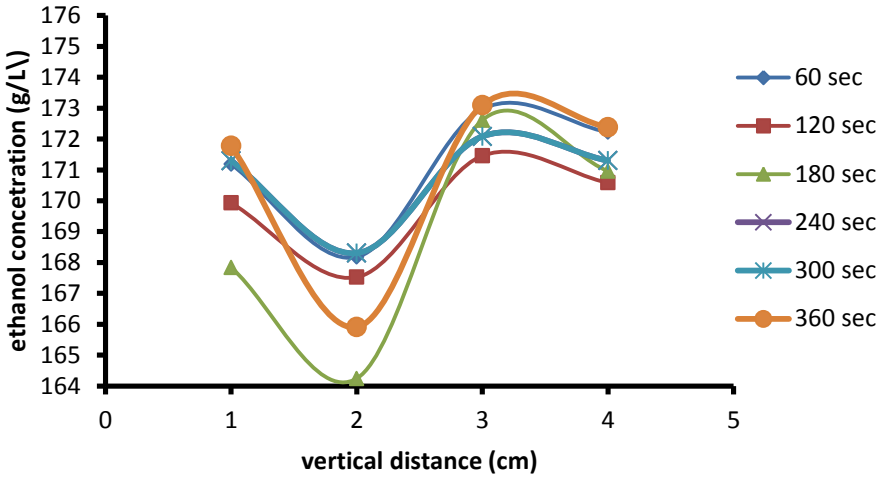

Figure 4.44: Ethanol concentration as function of vertical distance for E30 blend

As done in the horizontal direction, the effect of the amount of ethanol in the mixture on cavitation was also investigated in the vertical direction. Figures 4.45 through 4.50 below give the variation of concentration with time and distance for the three ethanol blends of different viscosity and density due to the amount of ethanol in the mixture. The highest viscosity is witnessed as the amount of ethanol is increased as explained in the horizontal profile of this thesis.

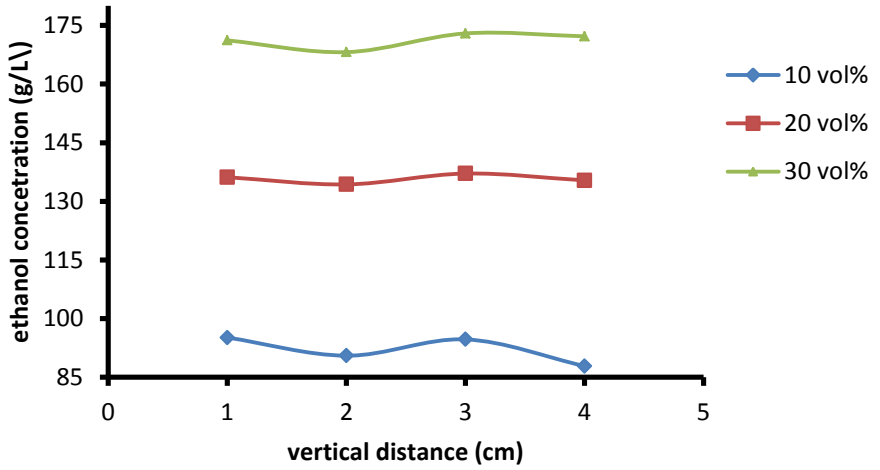

Figure 4.45: Ethanol concentration as function of vertical distance for various blend composition for 60 seconds

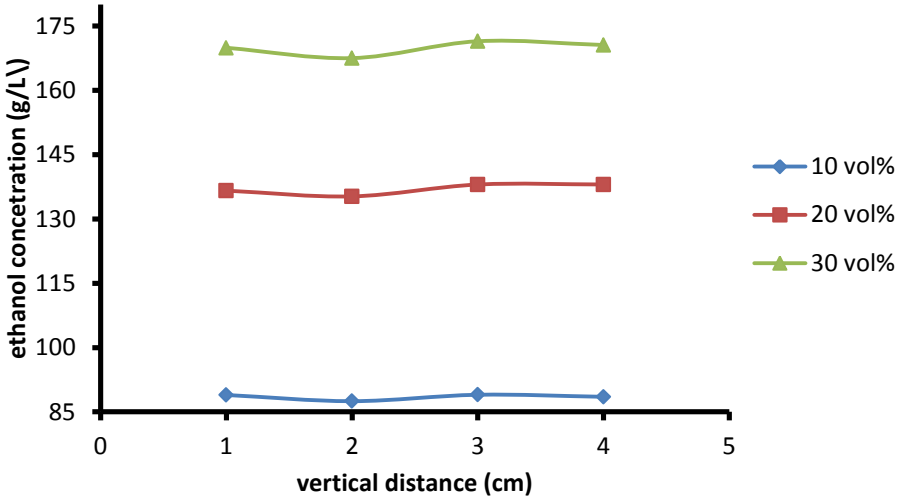

Figure 4.46: Ethanol concentration as function of vertical distance for various blend composition for 120 seconds

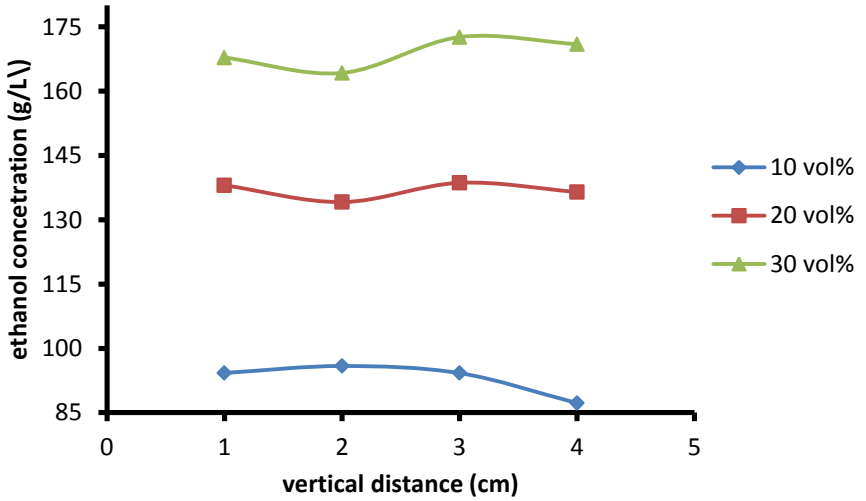

Figure 4.47: Ethanol concentration as function of vertical distance for various blend composition for 180 seconds

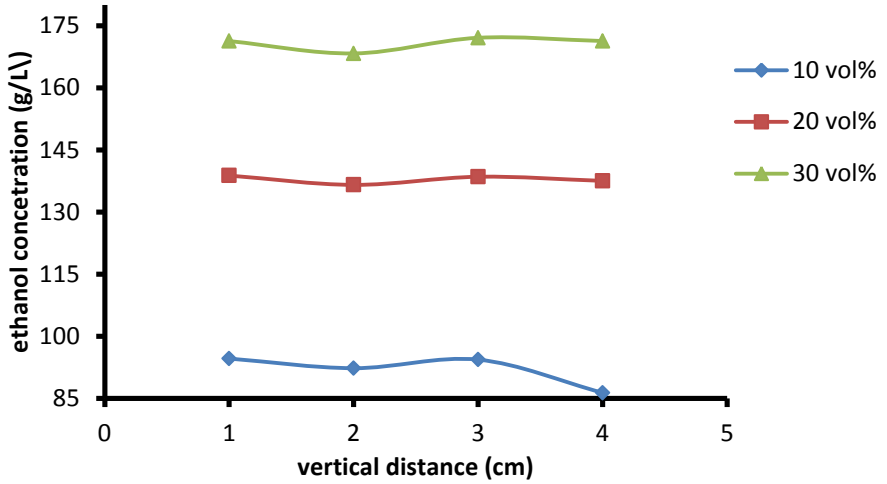

Figure 4.48: Ethanol concentration as function of vertical distance for various blend composition for 240 seconds

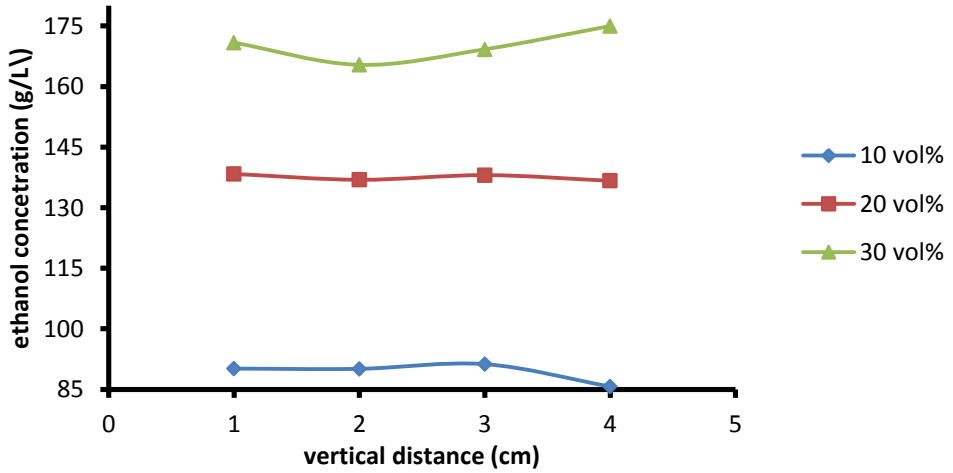

Figure 4.49: Ethanol concentration as function of vertical distance for various blend composition for 300 seconds

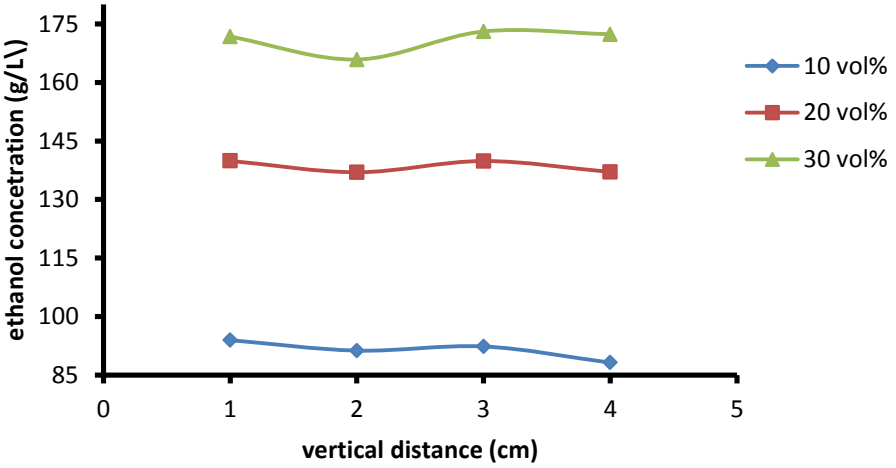

Figure 4.50: Ethanol concentration as function of vertical distance from the ultrasonicator horn for 360 seconds

4.2.2.4 Effect of ultrasonication on the vertical and horizontal concentration gradient

The figures 4.51 through 4.53 show the relationship of concentration profile with distance in a horizontal and vertical distance. Contour plots (with Akima's polynomial method) of Figures 4.51 through 4.53 show the concentration gradient for different ethanol-petrol blends at 360 seconds. Figures at different time which show similar profile can be found in appendix C.3.

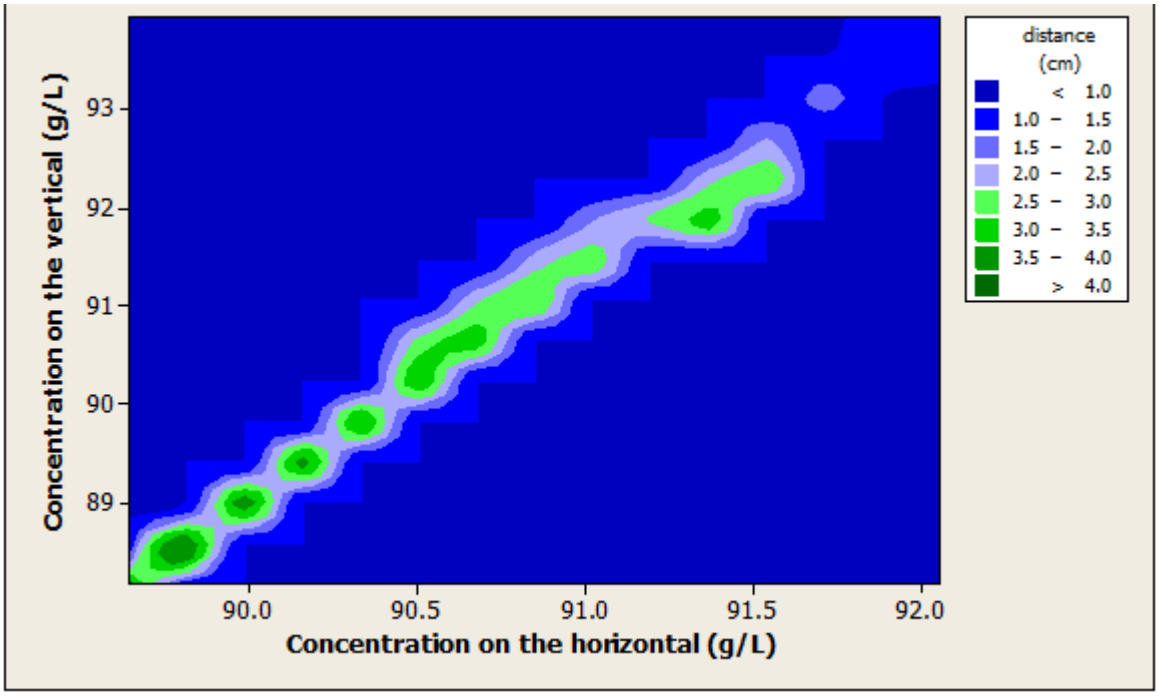

Figure 4.51: Concentration as function of horizontal and vertical distance for E10

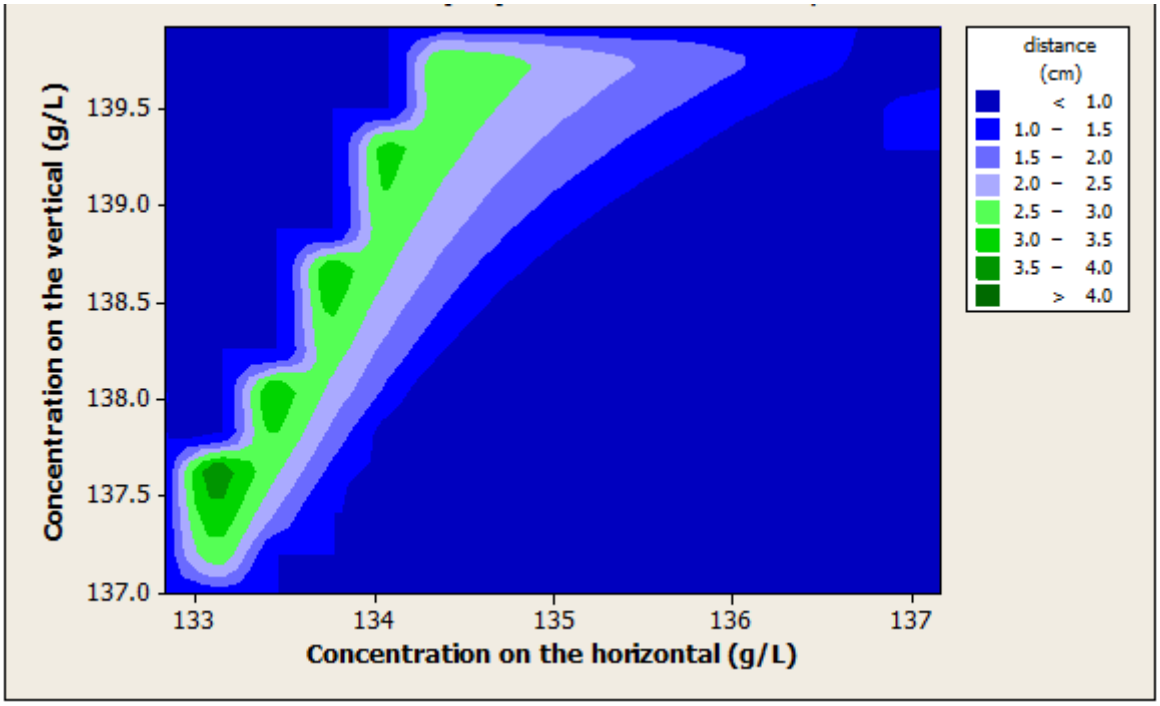

Figure 4.52: Concentration as function of horizontal and vertical distance for E20

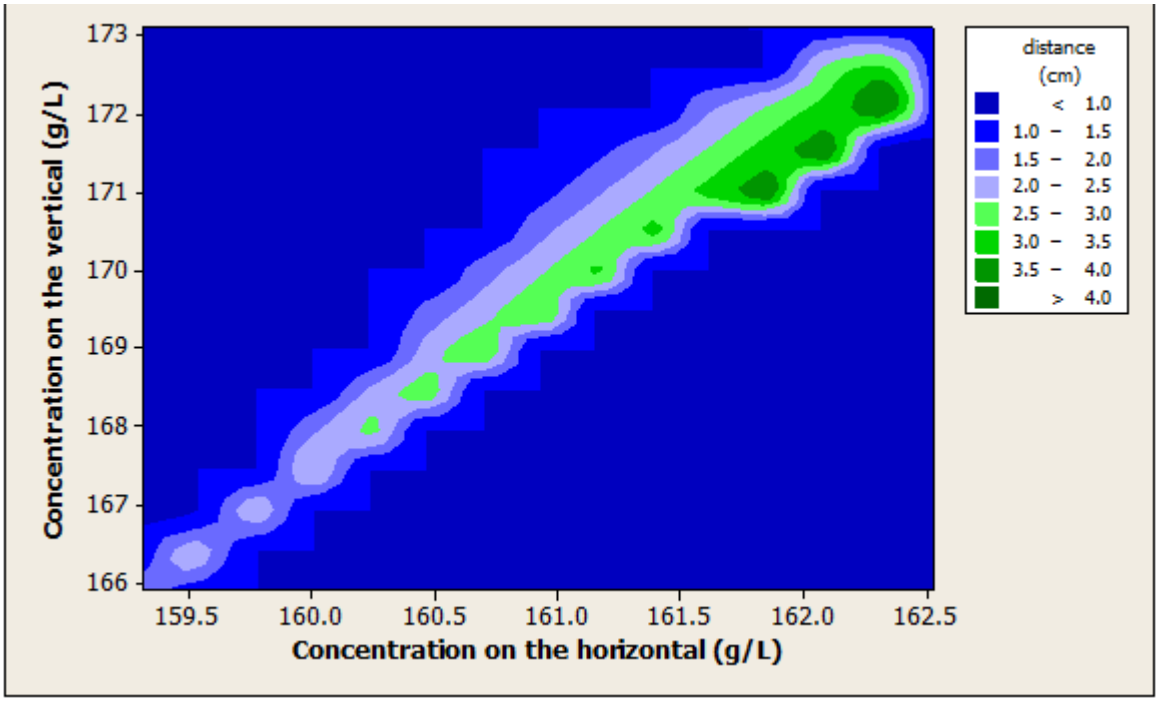

Figure 4.53: Concentration as function of horizontal and vertical distance for E30

4.2.3 Effect of time on the performance of ultrasonication-enhanced blending

4.2.3.1 Change in pressure with time

The change of pressure with time during ultrasonication-enhanced blending was also investigated to understand the variation of pressure during the process. Figures 4.54 through 4.56 show the relationship between pressure and time for different horizontal positions at a specific ethanol-petrol blend. This relationship describes the distribution of the intensity of energy with time.

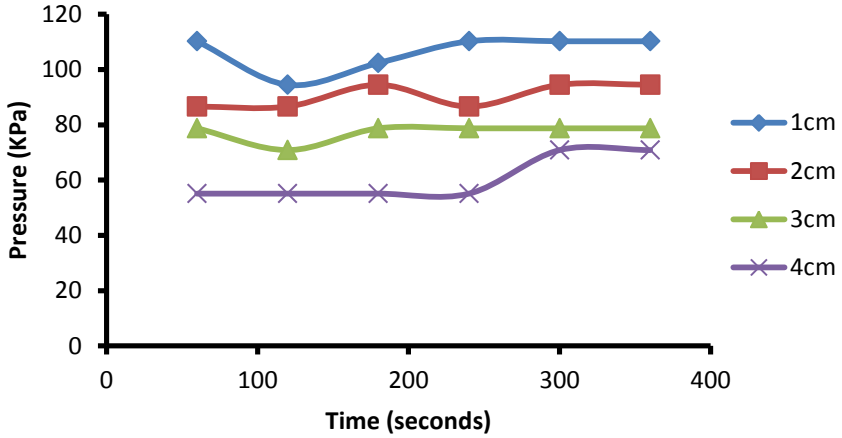

Figure 4.54: Horizontal variation of pressure with time for blended fuel E10

Figure 4.54 shows a nearly as wave like trend for pressure at the horizontal direction, the trend is more visible on the 1 and 2 cm distance. As the sonication time increased a constant pressure is reached. The constant pressure for all the position can be seen when sonication of the mixture was done for about 300 seconds.

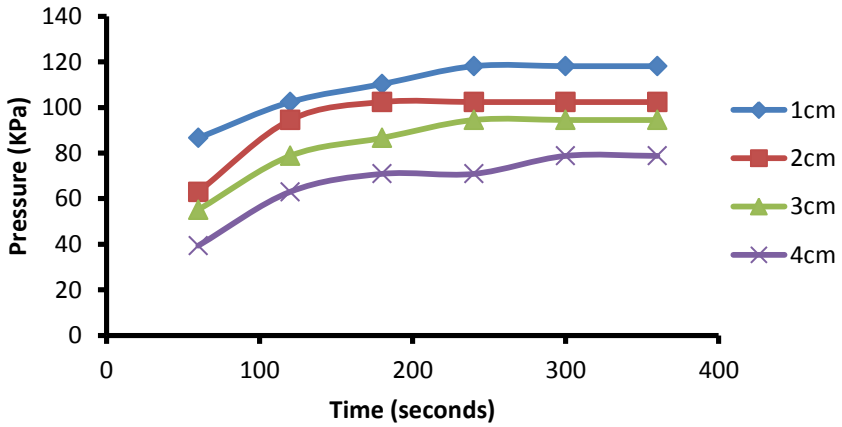

Figure 4.55: Horizontal variation of pressure with time for blended fuel E20

Figure 4.55 shows that pressure increase with time in a non-linearly relationship then after some time of sonication a constant pressure is reached. The constant pressure for 1, 2 and 3 cm was reached at about 240 seconds and for 4cm it was reached at 300 seconds.

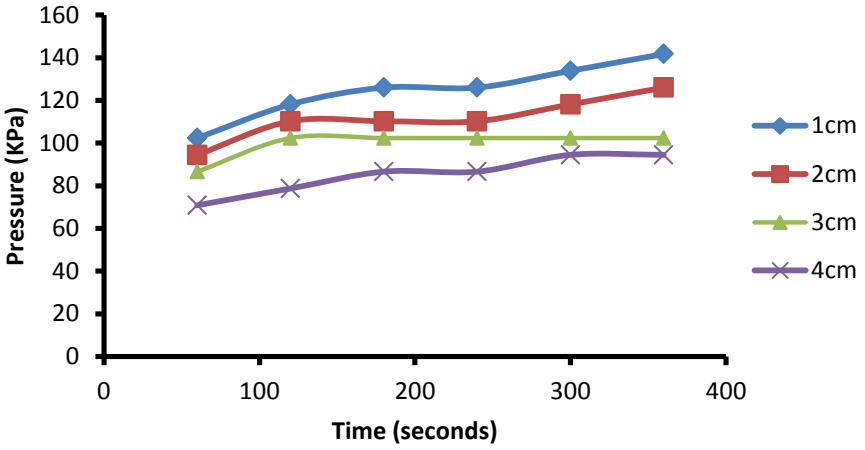

Figure 4.56: Horizontal variation of pressure with time for blended fuel E30

Figure 4.56 shows that at the beginning of the sonication of the mixture pressure increases then as time progresses the pressure shows a small change until it reaches a constant. For 1 and 2 cm at 240 seconds the pressure starts to increase with sonication time while for 3 and 4 cm the pressure at about 240 seconds it reaches a constant.

The pressure distribution in the blender was also studied to show the rate of pressure distribution in the vertical direction. The pressure distribution is also related to the energy distribution since the pressure is experienced due to the effect of ultrasound energy. The tables in the pressure of Appendix C.1 give the data used to plot the graphs.

Figures 4.57 to 4.59 show a plot of pressure as function of sonication time at different position for E10, E20 and E30 blends. It can be seen in figure 4.57 that pressure increase with time then reaches a constant at 300 sec for all positions. In Figure 4.58 it can be seen that pressure increase with sonication time without constant pressure for 1cm and 2cm and in Figure 4.59 it can be seen that a constant pressure is only reached for 1cm.

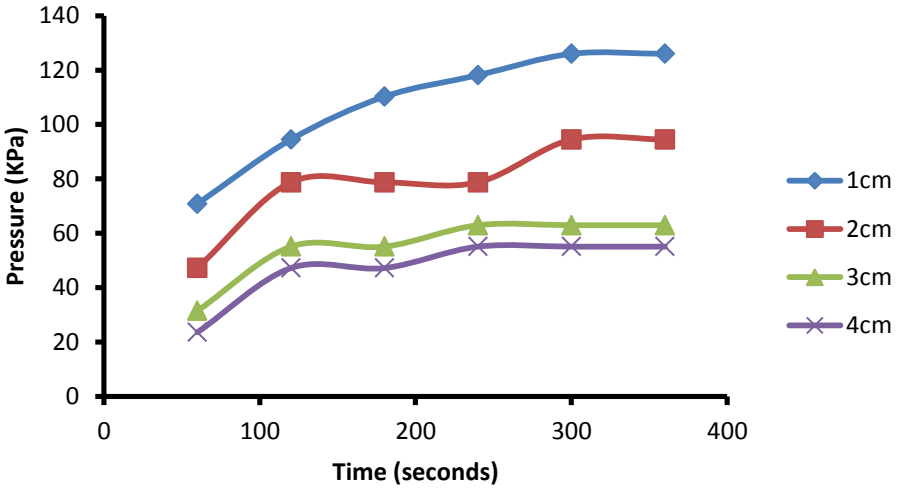

Figure 4.57: Vertical variation of the pressure with time for blended fuel E10

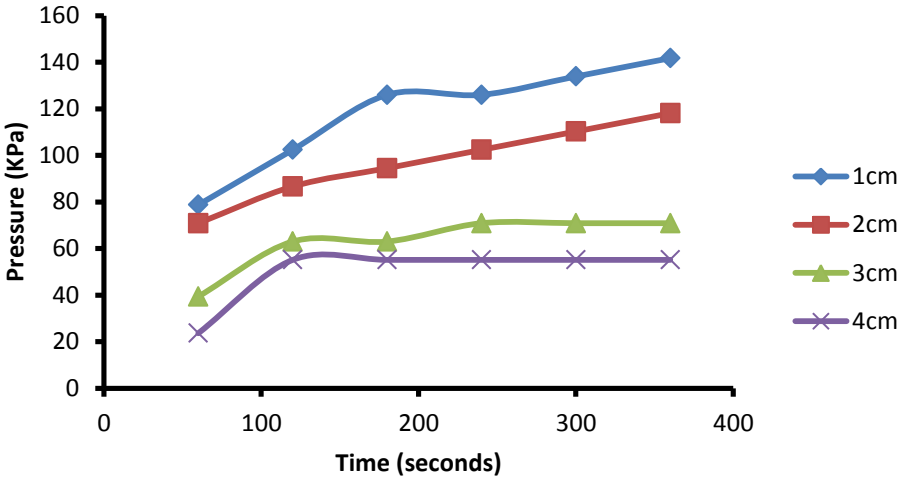

Figure 4.58: Vertical variation of the pressure with time for blended fuel E20

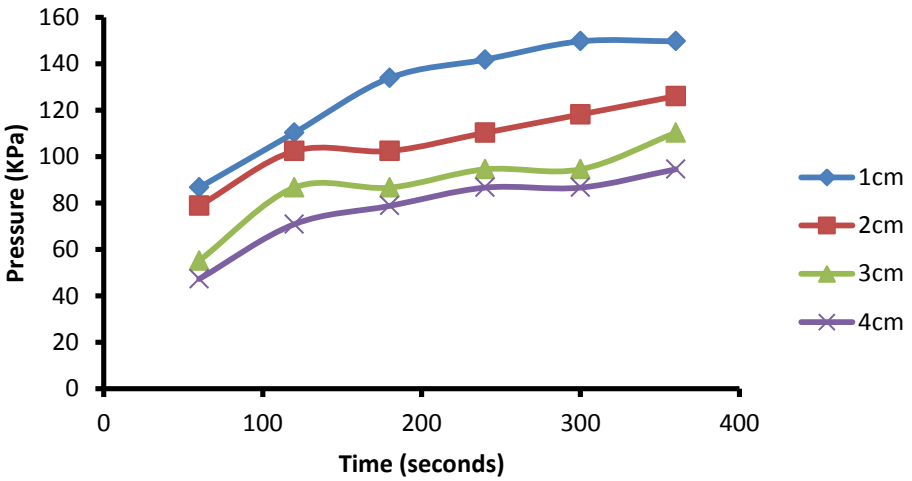

Figure 4.59: Vertical variation of the pressure with time for blended E30

Figures 4.60 through 4.63 show a plot of pressure as a function of time for different ethanol and petrol blends at specific position. It can be depicted that pressure increase in a non-linear relationship with sonication time. Also the solution of 30 vol % ethanol has the highest pressures in comparison to the 20 and 10 volume % ethanol solutions.

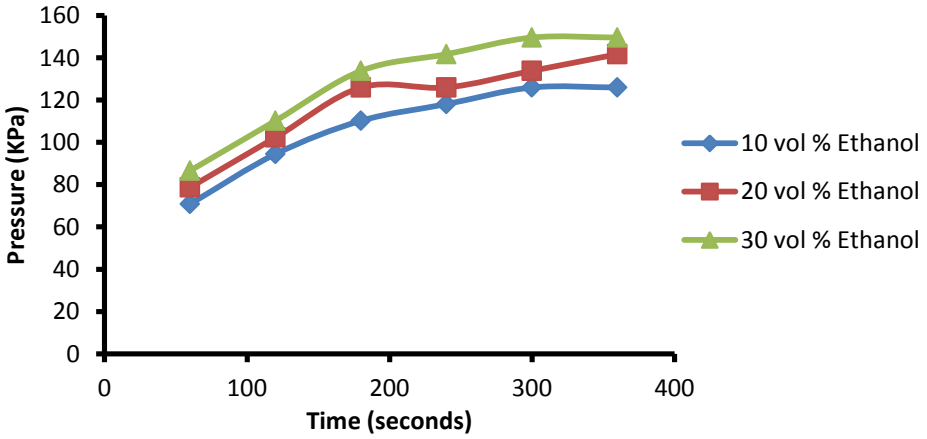

Figure 4.60: Variation of the pressure with time at 1 cm

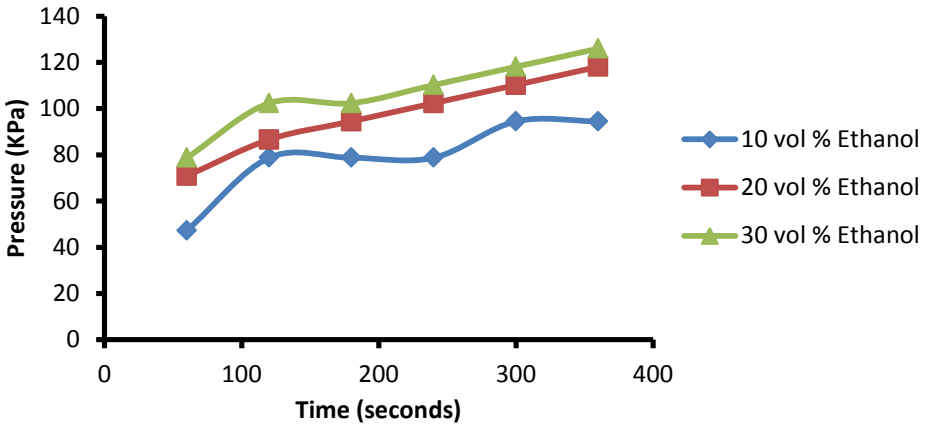

Figure 4.61: Variation of the pressure with time at 2 cm

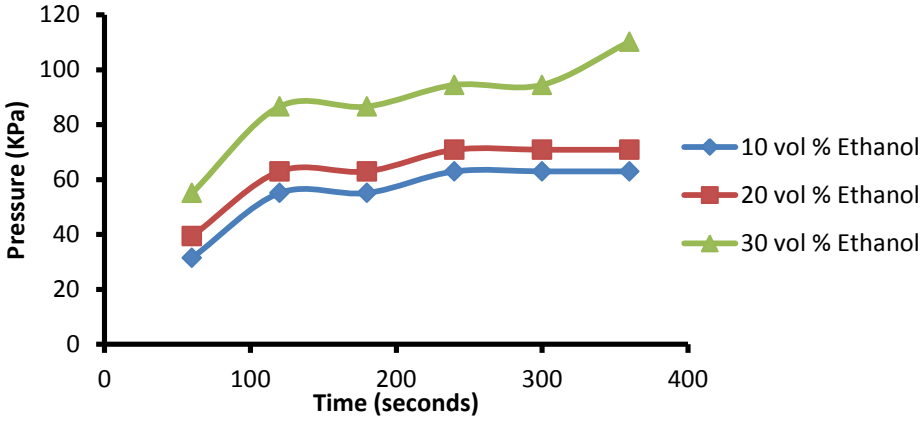

Figure 4.62: Variation of the pressure with time at 3 cm

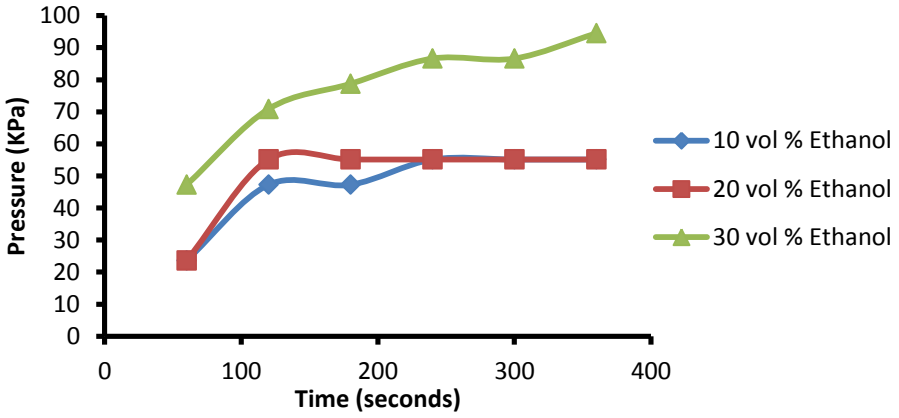

Figure 4.63: Variation of the pressure with time at 4 cm

4.2.3.2 Variation of temperature with time

The variation of temperature with time was also studied so as to investigate the heat transfer rates in the reactor. Figures 4.64, 4.65 and 4.66 show that concentration increase in a non-linear relationship with sonication time.

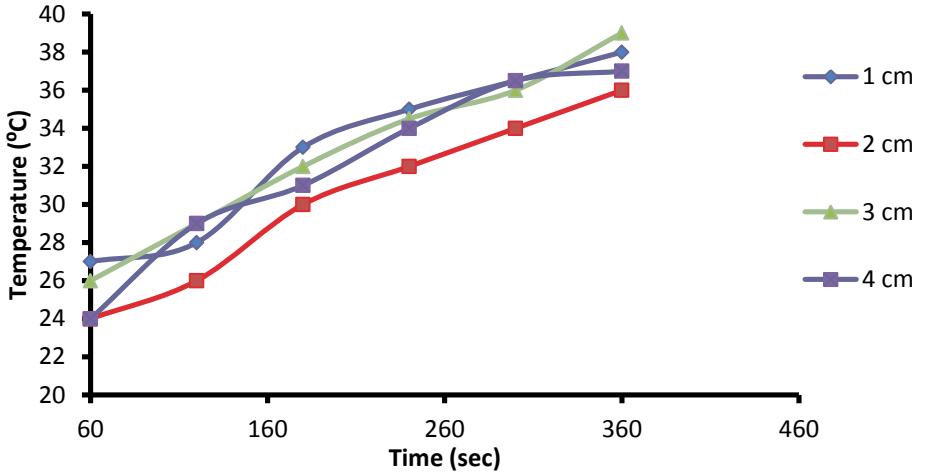

Figure 4.64: Horizontal variation of temperature with time for E10

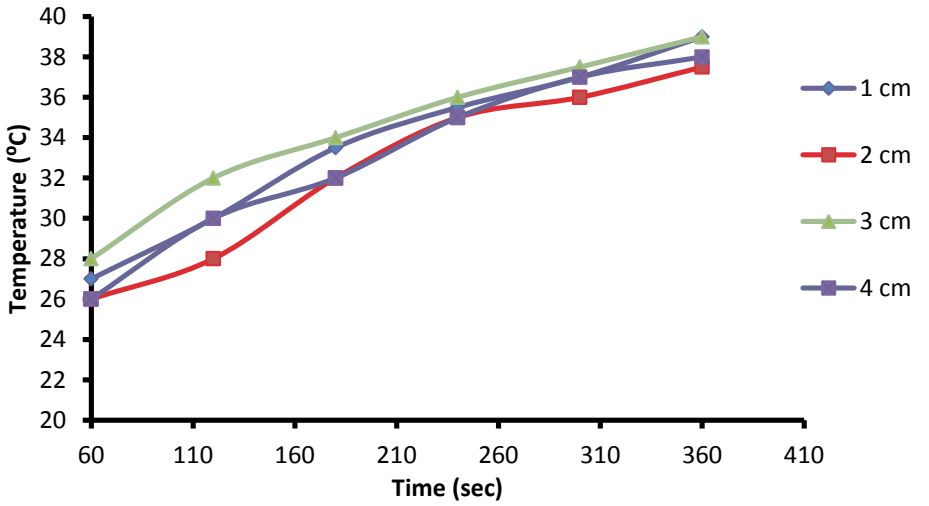

Figure 4.65: Horizontal variation of temperature with time for E20

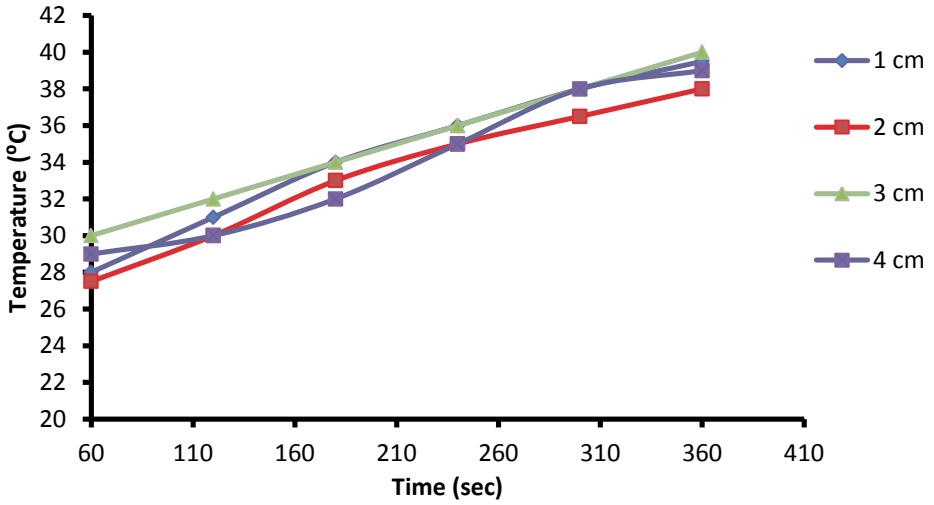

Figure 4.66: Horizontal variation of temperature with time for E30

The rate of heat transfer in the vertical direction was also studied to show how fast the energy is propagated through the solution in the vertical direction. The data collected during the experiment can be found in appendix C.2 and this data was plotted to show the rate of heat transfer shown in figures 4.67, 4.68 and 4.69. Also it can be seen from figures 4.67 through 4.3.46 that the temperature is highest for 1 cm and lowest at 4 cm.

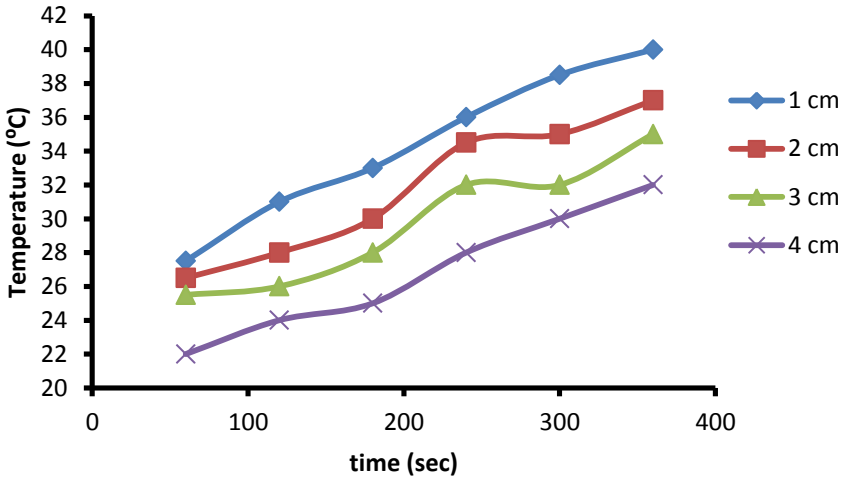

Figure 4.67: Temperature on the vertical as function of time for E10 blend

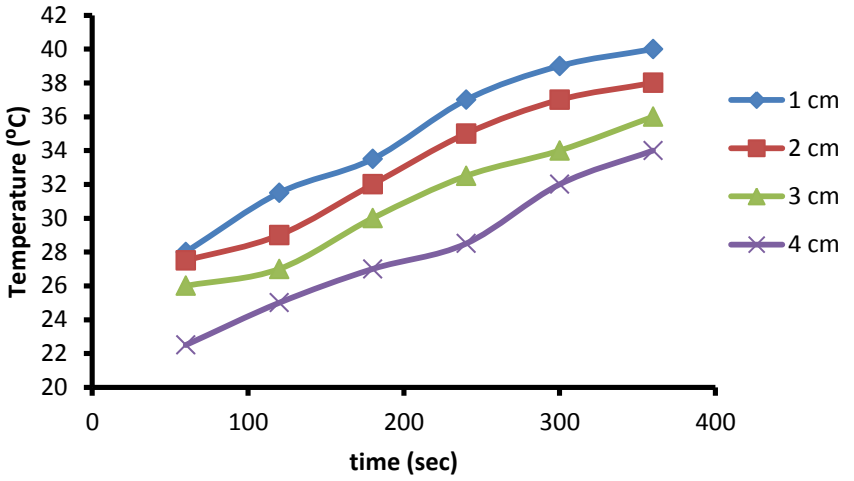

Figure 4.68: Temperature on the vertical as function of time for E20 blend

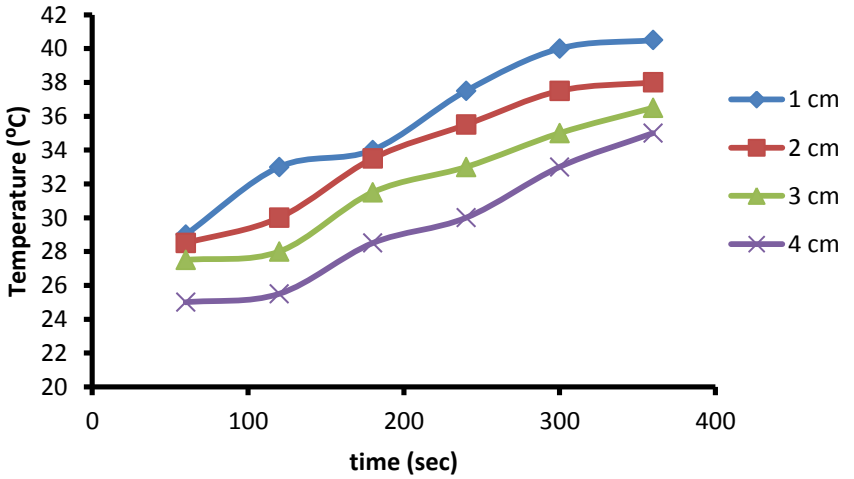

Figure 4.69: Temperature as function of time for E30 blend

4.2.3.4 Change in concentration with time

To investigate the diffusion kinetics in the horizontal direction, the ethanol concentration variation with sonication time was analysed. The three figures below show the variation of concentration with time for different distance for E10, E20 and E30 blends. Figures 4.70, 4.71 and 4.72 show that the variation of ethanol concentration with time on the horizontal direction is generally a wave function similar to the one seen with respect to distance. The waves show a continuous increase at some points while a continuous decrease is witnessed at other points.

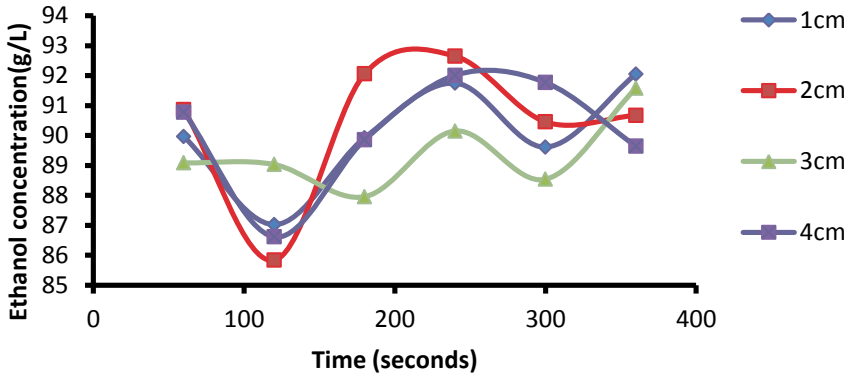

Figure 4.70: Horizontal variation of ethanol concentration as function of time for E10 blend

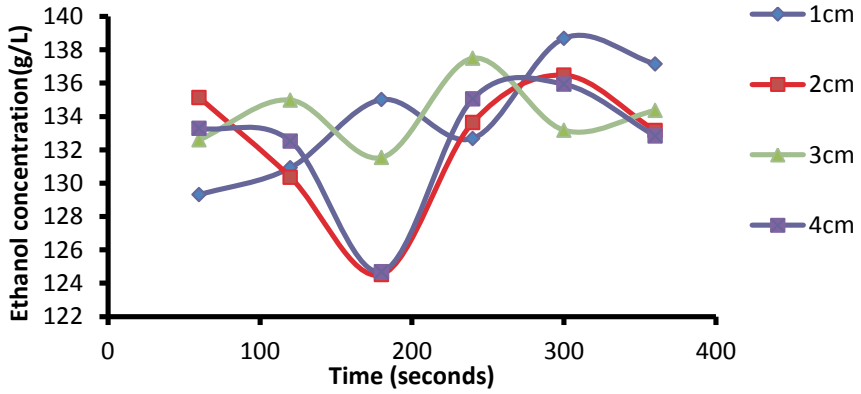

Figure 4.71: Horizontal variation of ethanol concentration as function of time for E20 blend

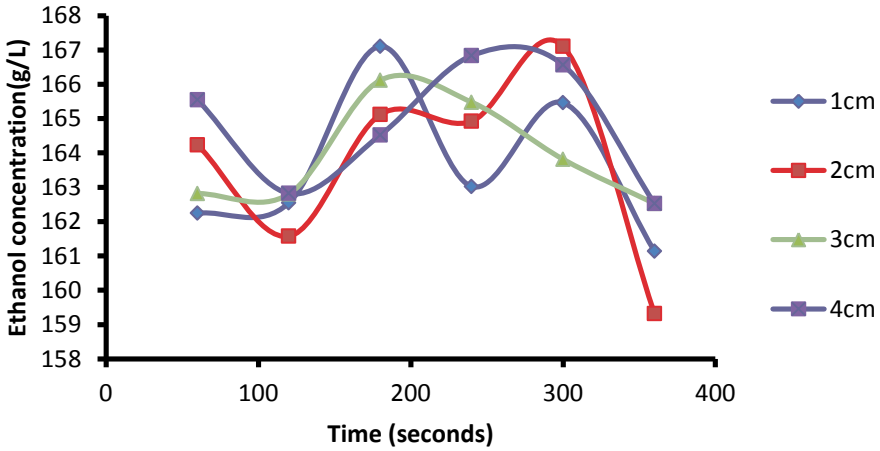

Figure 4.72: Horizontal variation of ethanol concentration as function of time for E30 blend

The formation of cavities in the vertical direction was also studied as done in the horizontal direction and thus the data given in Appendix C.3 was used to generate the graphs shown in Figures 4.73, 4.74 and 4.75.

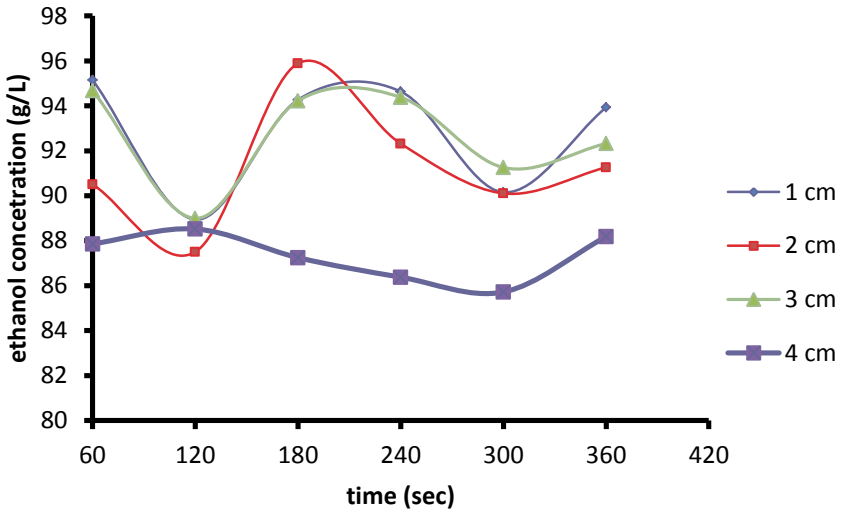

Figure 4.73: Vertical variation of ethanol concentration as function of time for E10 blend

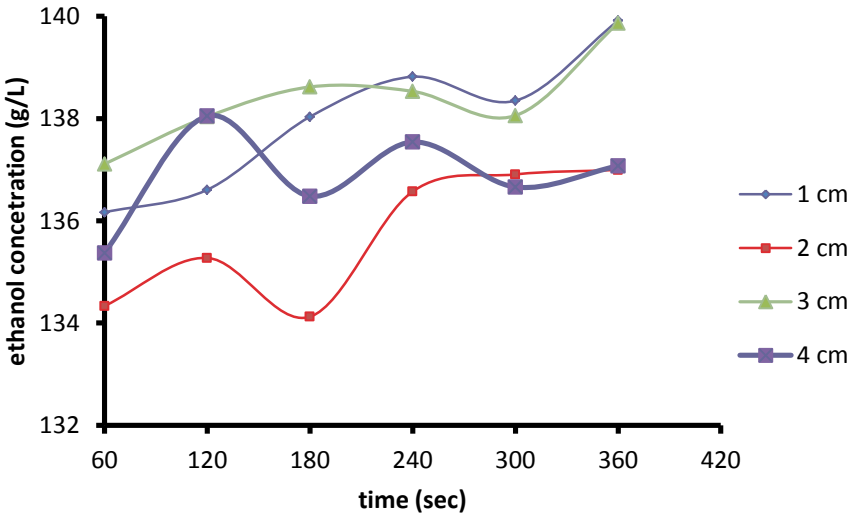

Figure 4.74: Vertical variation of ethanol concentration as function of time for E20 blend

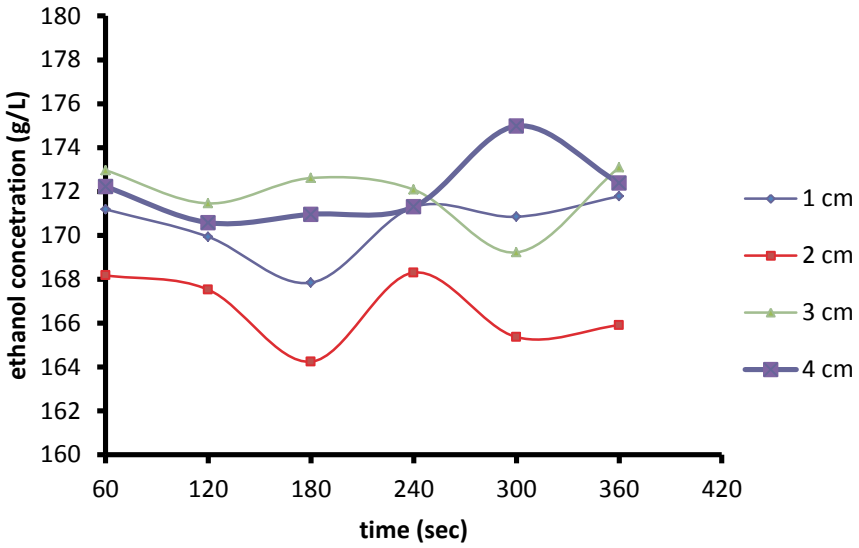

Figure 4.75: Vertical variation of ethanol concentration as function of time for E30 blend

4.2.3.5 Diffusion rate limiting step

To investigate the effect of ultrasonication on the diffusion flux as well as determine the diffusion rate limiting step the vertical and the horizontal direction, the pressure variation and the mixing efficiency in both direction was compared. Contour plots (with Akima's polynomial method) seen in Figures 4.76 through 4.79 give the pressures comparison of E10, E20 and E30 at a distance of 3 cm and mixing efficiency.

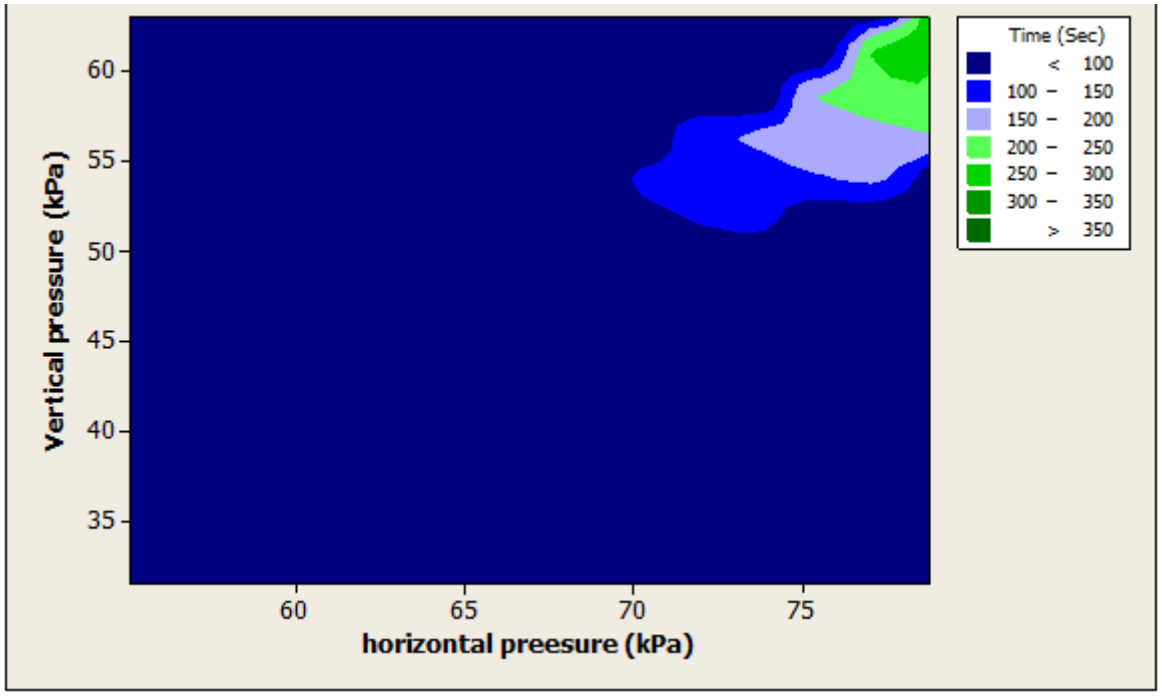

Figure 4.76: Horizontal pressure against vertical Pressure at different time for E10

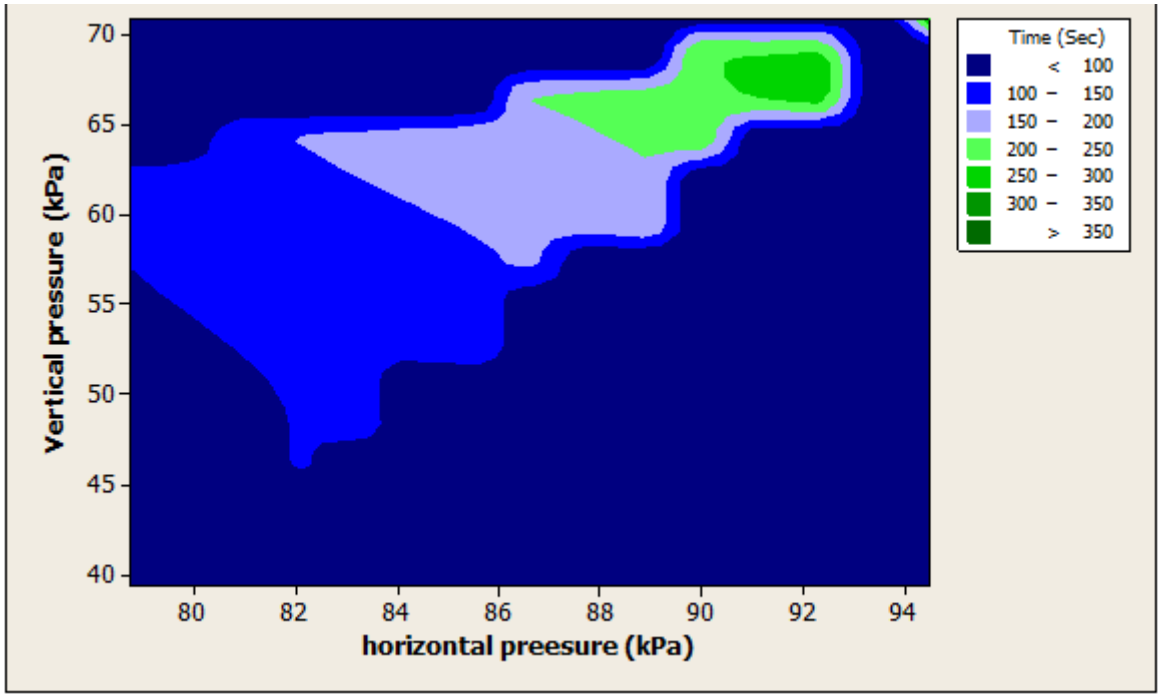

Figure 4.77: Horizontal pressure against vertical Pressure at different time for E20

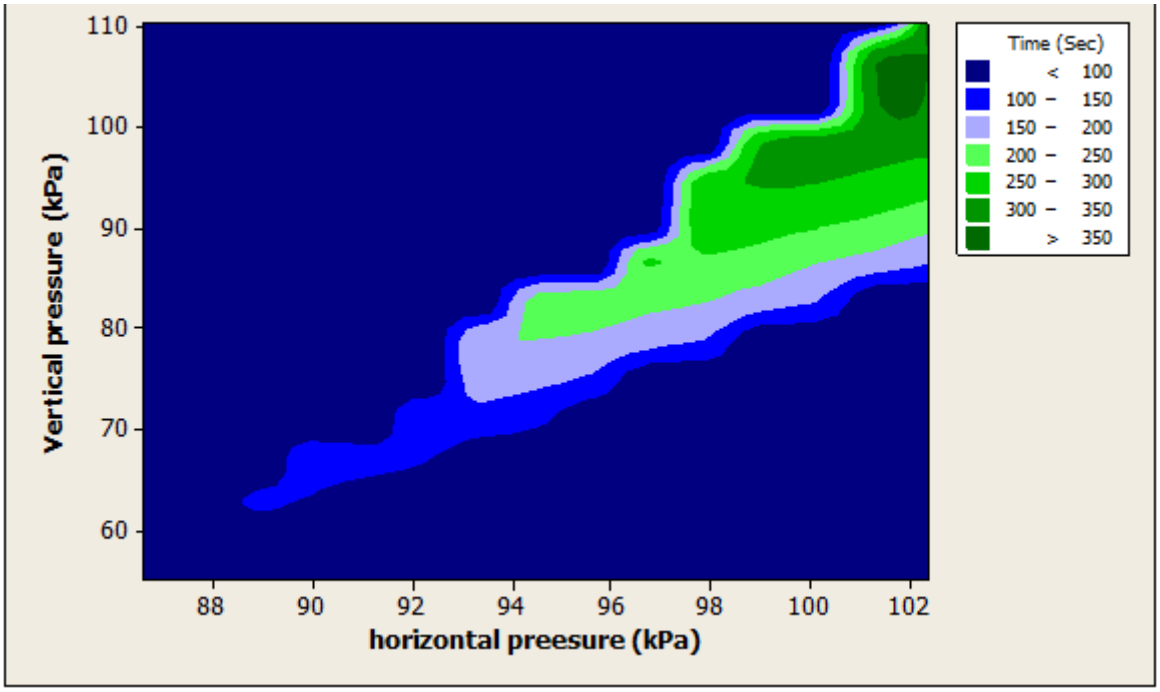

Figure 4.78: Horizontal pressure against vertical Pressure at different time for E30

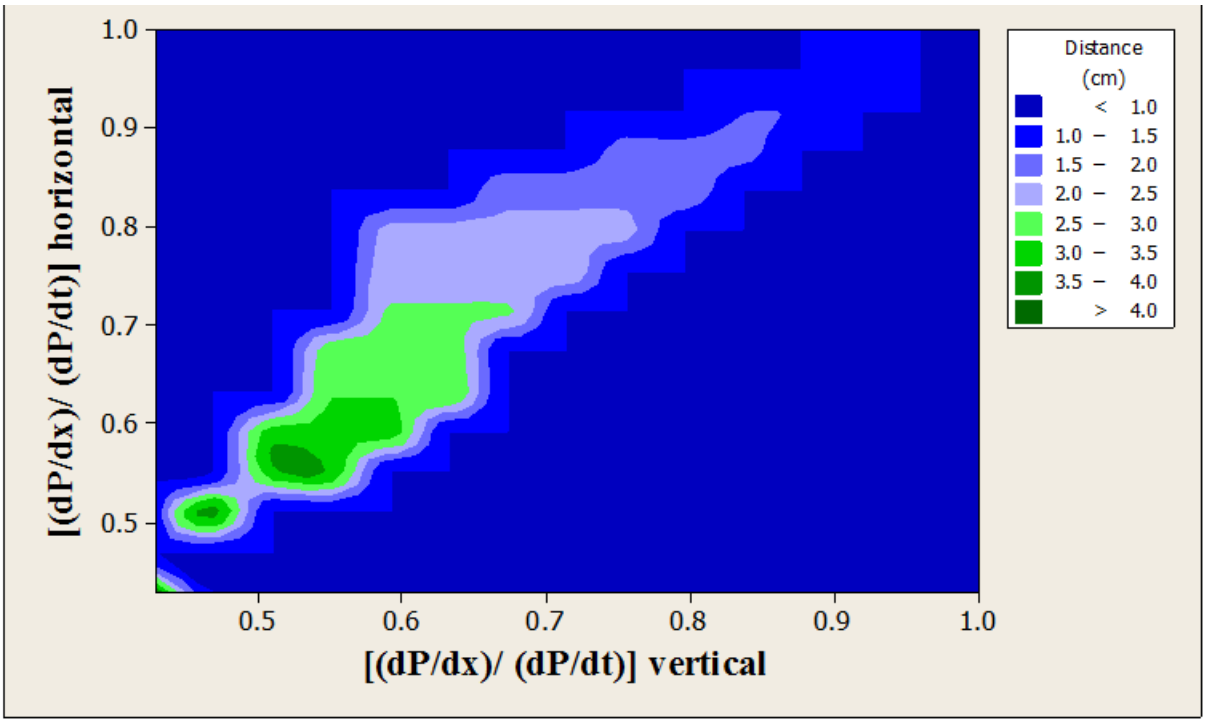

Figure 4.79: Horizontal mixing efficiency against vertical mixing efficiency for E10

4.3 Testing of ethanol-petrol blend in internal combustion engine

During combustion, heat is released and this heat is then converted to work by one means or another. Substances, which can undergo combustion, are called fuels. Ethanol and petrol are examples of these fuels. A good fuel is one that is readily available, cheap, burns easily, has a high calorific value and is environmentally friendly. Results of the thermodynamic studies of the testing of blended fuel in an internal combustion engine are presented in this section.

Equation (4.1) and Equation (4.2) give the combustion reactions of ethanol and petrol, respectively. In addition, Equation (4.3) gives the overall combustion reaction. Reactions 4.1 and 4.2 show the combustion reactions of both the ethanol and petrol. Reaction 4.3 is the overall reaction of the fuel blend.

$$C_2H_6O + 3O_2 \rightarrow 2CO_2 + 3H_2O \quad (4.1)$$

$$2C_8H_{18} + 25O_2 \rightarrow 16CO_2 + 18H_2O \quad (4.2)$$

$$C_2H_6O + 2C_8H_{18} + 28O_2 \rightarrow 18CO_2 + 21H_2O \quad (4.3)$$

Due to difference in composition, the different fuel blends will be consumed at different rates. The fuel consumption rate is directly affected by the heating value of the particular fuel. Figure 4.80 shows the fuel consumption rate at different proportions of ethanol and petrol.

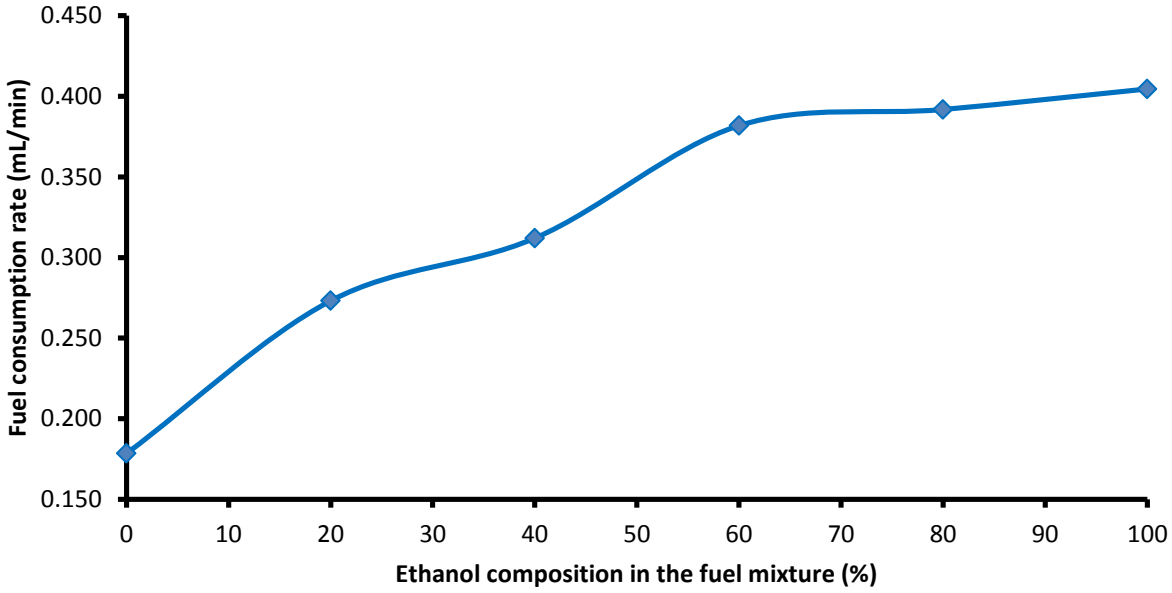

Figure 4.80: Fuel consumption rate as a function of fuel composition

Figure 4.81 shows the exit gas temperature of fuel and the consumption rate with some Ethanol composition.

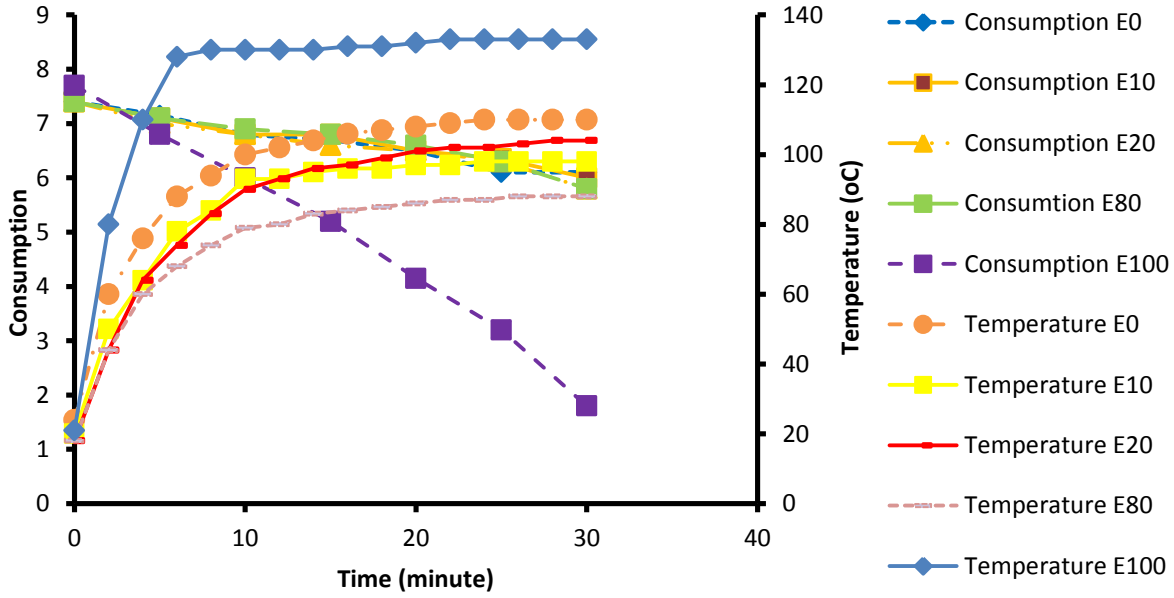

Figure 4.81: Consumption rate and temperature profile

With the adverse effects of exhaust gases on the environment, it is therefore important to obtain a fuel that result in the least amount of pollutants. Carbon dioxide is the greenhouse gas that contributes to climate change which has resulted to several natural disasters around

the globe. Figure 4.82 shows the composition of CO_2 in the exhaust mixture as a function of ethanol content in the fuel blend.

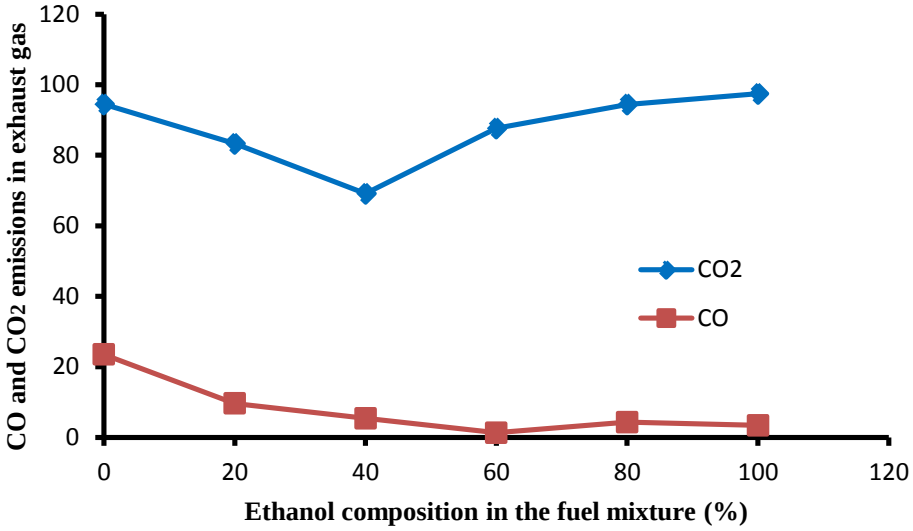

Figure 4.82: CO_2 and CO emissions as a function of ethanol composition in the fuel blend

During the combustion process, some of the oxygen molecules react with nitrogen molecules to form nitrogen (II) oxide (also known as nitric oxide). The nitrogen oxide is formed according to Equation (4.4):

$$N_2 + O_2 \rightarrow 2NO \qquad (4.4)$$

The kinetics of the above mentioned reaction is such that the production of nitric oxide increases with increasing temperature during combustion (EFD, 1993). Figure 4.83 shows the concentration of nitric oxide in the exhaust gas mixture as determined from the code presented in appendix.

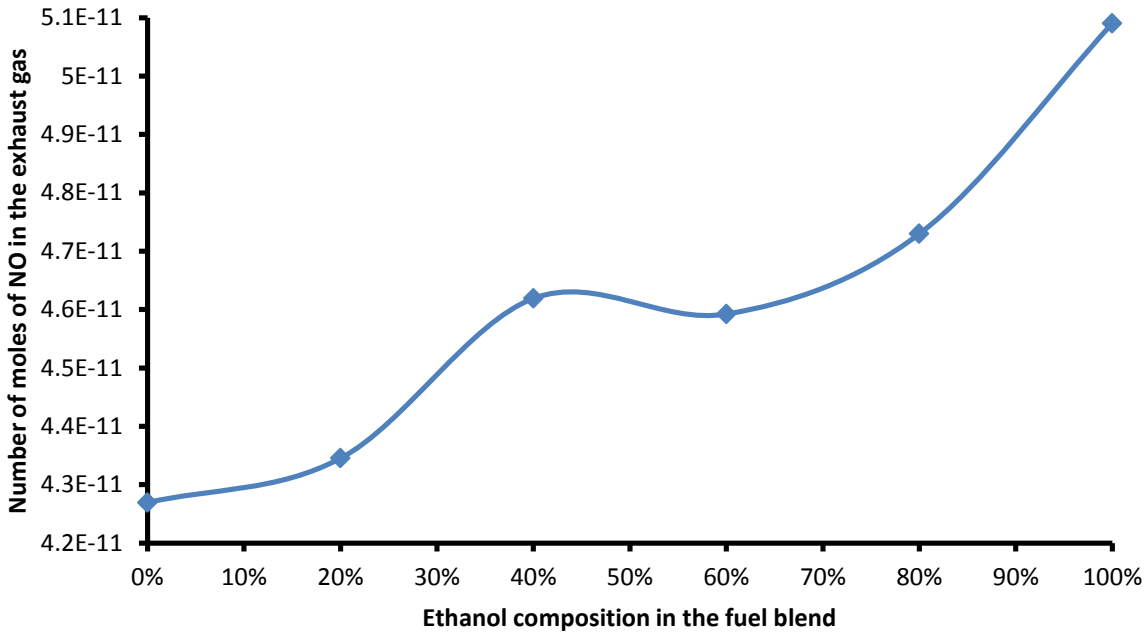

Figure 4.83: Concentration of nitric oxide in the exhaust gas as a function of ethanol in the fuel mixture

Figure 4.84 shows the fuel power of the different ethanol/petrol blends. Fuel power is a product of the mass of fuel consumed and its calorific value, which is the heat released during combustion, according to Equation (4.5).

$$FP = m_f \times CV \tag{4.5}$$

Where: FP is the Fuel power, in kW; m_f is the mass of fuel consumed, in kg/s; CV is the Calorific value of the fuel, in kJ/kg

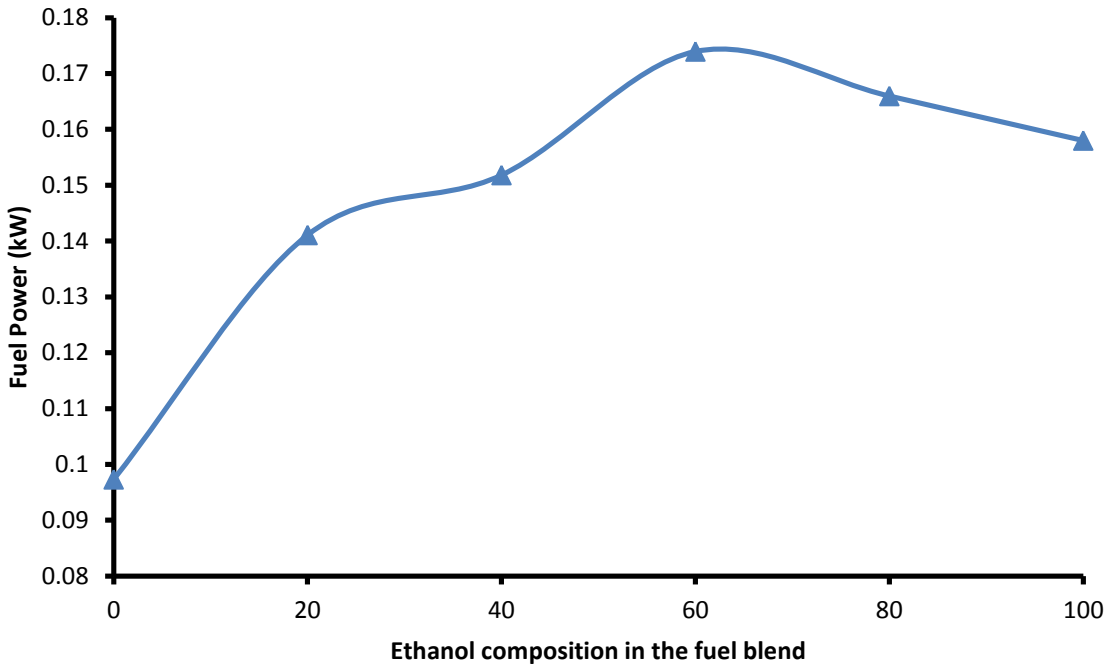

Figure 4.84: Curve showing the fuel power as a function of ethanol composition in the fuel blend

CHAPTER 5: DISCUSSION

5.1 Phase behavior of ethanol-petrol blend using ultrasonication

From Figure 4.1, the binodal curves show the effect of ultrasonication in blending ethanol and petrol. The increased in homogeneous region indicates higher tolerance of water compare to the non-sonicated blended fuel, indicating an improved interaction between water and petrol. The effect of ultrasonication on phase separation and eventually on the stability of the blend is shown also in Figure 4.2 and Figure 4.3, where the petrol content decreases exponentially with an increase of water tolerance. The increase of water tolerance in ethanol-petrol blend could be as attributed to the following:

- The water solubility in organic phase depends on the temperature; therefore the increase in temperature improves the compatibility of the petrol-ethanol-water mixture (Gramajo et al, 2004; Johanem et al, 2009) which was achieved during the ultrasonication process by implosion of cavities;
- Aromatics and alkenes interact with water through π bonds (Neagu et al, 2010). The cavitation process induced during the ultrasonication was able to break the bond (Gong et al., 1998), and increase the alkene content of the fuel. The gases collected show higher concentration in hydrogen and the test in saturated hydrocarbon show an increase in unsaturated hydrocarbon.

The decrease in water and ethanol content were observed in some of the sample, this could be attributed to the breakage of water or ethanol molecules. Therefore more research needs to be done on the free radical mechanism and the storage stability at different temperatures for logical conclusion.

In order to visualize the interaction effects of water with petrol mixture during the ultrasonication-enhanced blending, contour and surface plots are used (see Figure 4.2 and Figure 4.3). An increase in petrol content showed a negative trend on water tolerance, whereas a minimum water tolerance was seen around 40 % petrol content with ultrasonication and 20 % with magnetic-stirring enhanced blending. Water tolerance was similar for ultrasonicated blend with higher petrol content and for stirred blend with low petrol. The water interaction with more organic content is explained above. These results

suggested that ultrasonication-enhanced blending could sufficiently increase water tolerance in ethanol-petrol-water blends.

Density of the mixture during storage was employed to quantitatively characterize the homogeneity of the blended fuel. A homogenous fuel should be defined as a mixture where the chance of picking a fuel component is equal throughout the whole fuel mixture (i.e. the density distribution does not change with position and time [$\frac{d\rho(x,t)}{dx} = 0$]). Egermann (1980) and Yip et al. (1977) reported that ordered mixtures do not show concentration variation of components when sampling at different points.

Equations (5.1) through (5.7) were used to estimate the density of the blended mixture, which was compared to the average density of the sample obtained at different positions in the storage tank.

$$mass\ of\ the\ mixture\ at\ x = \sum_i^n mass_i\ at\ x \tag{5.1}$$

$$density\ of\ the\ mixture \times volume\ total = \sum_i^n density\ of\ i \times volume\ of\ i \tag{5.2}$$

$$\rho_{mixt} \times V_{tot} = \rho_E \times V_E + \rho_w \times V_w + \rho_P \times V_P \tag{5.3}$$

$$\rho_{mixt} = \rho_E \times \chi_E + \rho_W \times \chi_W + \rho_P \times \chi_P \tag{5.4}$$

$$\rho_{mixt} = (\rho_E - \rho_W)\chi_E + (\rho_P - \rho_W)\chi_P + \rho_W \tag{5.5}$$

$$\frac{d\rho_{mixt}}{dx} = (\rho_E - \rho_W)\frac{d\chi_E}{dx} + (\rho_P - \rho_W)\frac{d\chi_P}{dx} \tag{5.6}$$

or

$$\frac{d\rho_{mixt}}{dt} = (\rho_E - \rho_W)\frac{d\chi_E}{dt} + (\rho_P - \rho_W)\frac{d\chi_P}{dt} \tag{5.7}$$

The ethanol-petrol blends with $\frac{d\chi_E}{dt} \approx 0\ and\ \frac{d\chi_P}{dt} \approx 0$ are homogeneous mixture because the ethanol and petrol distributions are the same in the blended fuel. Therefore the volume fraction of ethanol and petrol are constant. Figure 4.4 and Figure 4.5 show the volume fractions of ethanol and petrol for E50 and E60. The χ_{E50} and χ_{E60} were respectively 0.49960 and 0.59904, with the coefficients of variation (CV) 1.6 x 10^{-6} and 3.0 x 10^{-4} respectively. The CVs are closer to zero indicating the uniformity of data. The volume fractions of ethanol and petrol were fairly constant at any point and at different times in the storage tank.

Therefore, the blended fuels above the binodal curve were homogeneous as the $\frac{d\rho_{mixt}}{dt} = 0\ and\ \frac{d\rho_{mixt}}{dx} = 0$, and Equation (4.6) and Equation (4.7) may be used to estimate the parameters of the homogeneous mixture.

5.2 Ethanol-petrol mixture using ultrasonication-enhanced blending

The blending process discussed in this section including the dehydration of bioethanol enhanced by ultrasonication. Pressure, temperature and ethanol concentration profile describe the characteristics of the ethanol-petrol mixture. The energy and concentration distribution during ultrasonication-enhanced blending was also discussed in this section.

5.2.1 Dehydration of bioethanol-water mixture using adsorption prior to blending

Figure 4.6 shows that the ultrasonication enhances adsorption more than using a magnetic stirrer to enhance adsorption of water on the silica gel. The generated pressure and temperature in the adsorption vessel system allow water molecules adsorption on the adsorbent surface. The trend of ultrasonication enhanced adsorption shows a wave function due to the ultrasound energy distribution in the adsorption reactor, which has been proven in the literature to be a wave functions (Mason et al, 2002). Assuming the adsorption occurs in ideal solution, the adsorption enthalpy (ΔH_{Ads}) of 1,592.82 J/ mole of water was determined from the slope of the graph in Figure 4.7. The constant ΔH_{Ads} can be explained by a uniform potential field providing a homogeneous adsorption site at the sorbent surface. The sign of ΔH_{Ads} (-) and ΔS_{Ads} (- 5.44 J/ K moles) show that the adsorption enhanced by ultrasonication is a non-spontaneous process ($\Delta G_{Ads} > 0$) at temperature T greater than 292.792 K. The dispersion force due to the interaction between adsorbate molecules with oxygen atoms of the silica-gel contributed to this energy (as the polarizability of Si^{+4} is smaller, i-e 0.048 x 10^{-2} compared to the polarizability of oxygen (Ridha, 2009; Lasaga, 1982); the negative value of the entropy shows that the loading manner of water molecules in the adsorption site involves gain in disorder. The adsorption entropy obtained during the ultrasonication-enhanced adsorption in this study contradicts the sign of the entropy reported by Ridha (2009) where filling of adsorbate in adsorbent pore occurred in an ordered way. The contradiction could be attributed to the conditions at which Ridha (2009) performed the experiment. For Ridha

(2009), the adsorption was carried out at a constant temperature without ultrasonication. But in this study, ultrasonication was used to enhance the adsorption and during the process temperature distribution was not constant.

The influence of the pulse rate was observed in Figures 4.8 and 4.9 whereby an increase in the pulse rate decreases the oscillations in results and they follow a more consistent nature in terms of how they increase and decrease, thus being more constant. At a higher pulse rate the cavitations are less aggressive as seen on Figure 4.8 thus the changes seen are less as said by Hesson (2003). And at a lower pulse rate the cavitations are more aggressive and this can be seen from Figure 4.8 for the pulse rate of 0.5 series whereby the oscillations in results are the greatest thus showing the cavitations effect (Hesson, 2003).

As shown in Figure 4.9 the temperature rise of the curve with a pulse rate of 0.5 and amplitude of 0.5 was the lowest of all the curves. It is followed by the curve with pulse rate of 0.5 and amplitude of 1. The temperature rise for the pulse rate of 1 and amplitude of 0.5 is higher than that of pulse rate of 0.5 at amplitude of 0.5 and 1. The temperature rise for pulse rate of 1 and amplitude of 1 was higher than the rest. The temperature for the pulse rate of 1 and amplitude of 1 became constant after 15 minutes at 66.5 ºC.

The temperature rise as stated from the literature was due to cavitation. When the cavities implode in liquids heat escapes the cavity during the collapse which is quenched by the low temperature liquid. Thus temperature rise was proportional to amplitude. This was supported by literature that at high amplitude temperature increase is faster. But as stated in the literature review care must be taken as high amplitude can lead to rapid deterioration of ultrasonic transducer resulting in liquid agitation instead of cavitation (Santos *et al*., 2009).

From Figure 4.10, it can be seen that the experimental data almost gave a perfect linear fit with the model except for two points when the pulse was increased to 1 at 25 and 30 minutes. The linear equations of $\frac{t}{q}$ against t, at different operating conditions, fitted the second order kinetic with coefficients of determinations (R^2) greater than 0.8.

Table 5.1: Trend line equations with coefficient of determination values

y = 0.0222 x + 0.0283 R^2 = 0.8955 Ampl. = 0.5 & Pulse rate = 0.5	y = 0.0195 x + 0.0699 R^2 = 0.8744 Ampl. = 0.5 & Pulse rate = 1
y = 0.0238 x + 0.0122 R^2 = 0.9338 Ampl. = 1 & Pulse rate = 0.5	y = 0.0442 x + 0.2123 R^2 = 0.8858 Ampl. = 1 & Pulse rate = 1

From Figure 4.11, it was observed that the calculated kinetics was found to resemble the behaviour of the adsorption with sonication but without the oscillating concentrations. In order to achieve the oscillating concentrations as viewed by the experimental results, one would need a trigonometric function such as sine or cosine added to the kinetic model.

What can be seen in the model is that at a higher pulse rate, the amount of water removed decreases with time. This could be attributed to the constant vibrations during the process, resulting therefore in a breakage of water molecule due to the effect of cavitation as reported by Costa (2009). Costa stated that the energy released during the implosion of cavities is sufficient for the following reaction to occur:

$$H_2O \rightarrow H\bullet + HO\bullet \quad (5.8)$$

$$H\bullet + H_2O \rightarrow H_2 + HO\bullet \quad (5.9)$$

$$HO\bullet + HO\bullet \rightarrow H_2O_2 \quad (5.10)$$

$$H\bullet + HO\bullet \rightarrow H_2O \quad (5.11)$$

$$H\bullet + H\bullet \rightarrow H_2 \quad (5.12)$$

This regeneration of water molecule may have a negative effect during the dehydration process. The broken pulse allows the molecule of water to reach the adsorbent surface and better adsorption as observed.

The pseudo second order model did not fit the experimental data perfectly (R^2 = 0.26) but followed the same pattern as the experimental model, in a linear fashion and asymptotes at the average concentration, at lower sonication pulse rate of 0.5. Based on the kinetic model at higher sonication pulse rates, the absorptivity is expected to decrease. This can be seen to

agree with the experimental data depicted in Figure 4.8, where the concentration seems to decrease at higher pulse rates. In order to quantify the degree of fit of the model onto the data the coefficient of determination was calculated to be 0.26, indicating that the model and the data do not agree with each other. , based on the equation given by (Investopedia, 2013) to calculate the R^2.

Proposed kinetic model of ultrasonication enhanced adsorption

The proposed kinetic model of adsorption enhanced by ultrasonication is a modified pseudo-second order equation (Qiu et al, 2009) given by the following equation:

$$\frac{d\,q_t}{(q_t - q_e)^2} = \frac{1}{q_e}[\,cos\,(K-t) - t\sin(K-t)]\,dt \qquad (5.13)$$

The solution of the above equation by considering the boundary conditions ($q_t = 0$ at t =0 and $q_t = q_t$ at time t) is given as follow:

$$\frac{1}{q_e - q_t} - \frac{1}{q_e} = \frac{t}{q_e}\cos(K-t) \qquad (5.14)$$

$$q = q_e + \frac{q_e}{t\cos(K-t) - 1.0} \qquad (5.15)$$

The solution of the proposed kinetic model was obtained using Eureqa Pro (Nutonian software). This solution satisfied the experimental data and gives the values of the constants of the model.

$$q = 41.2 + \frac{41.2}{t\cos(5.67-t) - 1.0} \qquad (5.16)$$

The graph of the adsorptive capacity in Figure 5.1 compares the experimental plot and the calculated from equation 5.16, with R^2 goodness of fit = 0.9208, maximum error = 0.0141, mean absolute error = 0.00204 and complexity = 15.

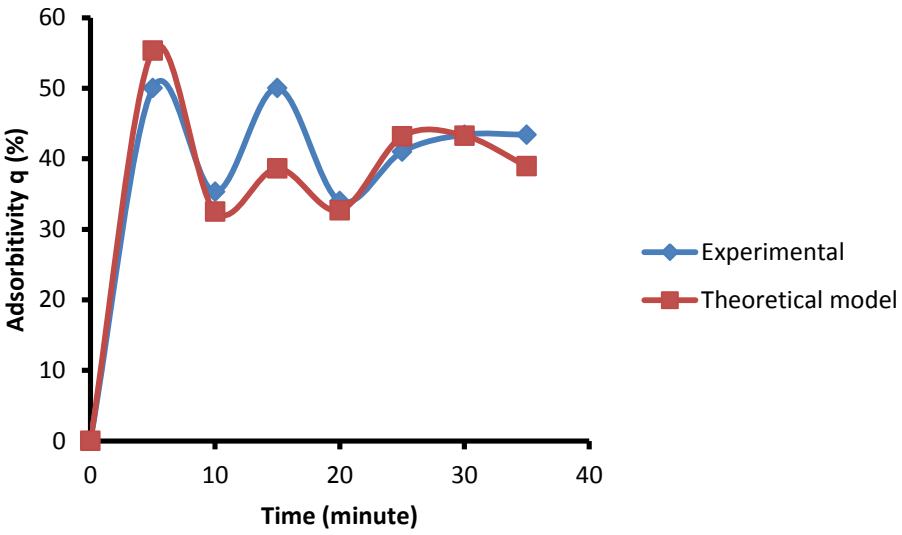

Figure 5.1: Calculated and experimental adsorptive capacity curve (Amplitude: 0.5 and pulse rate: 0.5)

5.2.2 Effect of ultrasonicator position during ultrasonication-enhanced blending

As shown in the Figures 4.12 through 4.14, the pressure decreases non-linearly with horizontal position from the ultrasonicator probe. This behaviour can be explained by the relationship between pressure and intensity of energy as shown in Equation (2.35). Equation (2.35) shows that the intensity of energy decrease as the area in which the wave spread into increases. The acoustic energy is more concentrated close to the ultrasonicator probe. Therefore as the distance increases from the probe to the surface of the reactor, the energy intensity is less concentrated. Similarly, Kimura et al. (1996) reported that almost all the ultrasonic energy is consumed within a small volume near the ultrasonicator horn, attributed to the non-consistent behaviour with respect to ultrasonication time due to non-uniform formation and growth of cavities within the reactor. Furthermore, several reports in literature have shown that the behaviour can be described by the formation of standing waves whose position depends strongly on the liquid level in the sonicated cell (Klima et al, 1999). . Thus, the results presented in this report are in agreement with results of Kimura et al (1996). However, the experimental results show a non-linear and a decrease in pressure when moving horizontally away from the ultrasonicator horn. This behaviour may be due to multiple reflections at the reactor boundaries (Klima et al, 1999) resulting in high pressures at the reactor edges. Despite the non-wave behaviour of horizontal pressure with distance, it can

however be concluded that the highest local intensity value is reached in the close vicinity of the horn.

The results shown in Figures 4.15 through 4.19 show that the E30 blend have the highest pressures compared to E10 blend. Thus this behaviour can be explained by the effect of physical properties of the mixture such as viscosity, density and surface tension. A liquid at high viscosity and density if the energy is sufficient to initiate cavitation, the solution has the ability to store high energy compared to a low viscosity mixture. When the bubbles in the mixture implode, they release this high energy which in turn results in high temperatures and high pressures as seen in the above graph for a 30% ethanol. This phenomenon therefore explains the high pressure recorded for a 30% mixture compared to the low viscous 20% and 10% ethanol. Therefore this also indicates that the energy supplied by the ultrasonicator with the settings mentioned in the method section delivered enough energy to induce cavitation.

The decrease in pressure with vertical distance from the bottom of the ultrasonicator probe to the top (see Figures 4.20 through 4.22) could be attributed to the rapid mixing at the bottom of the ultrasonicator probe when compared to the mixing at the top of the probe. Thus more cavitation occurs at the tip of the ultrasonicator probe and results to higher pressure. The energy dissipation by the oscillation of bubbles in the vertical direction is assumed to be by irreversible process of heat and mass transfer. Therefore lower pressure and temperature were recorded at a distance away from the tip of the probe.

The relationship between pressure and vertical distance shown in Figures 4.23 through 4.27 is the same as the one seen in the horizontal results and thus the trend is also due to that high density liquid can store a large amount of energy once cavitation is initiated. The imploding cavitation bubbles have tremendous amount of energy to be released when it implodes (James, 2012) thus resulting to high pressure and temperature. The 30% ethanol solution has a higher density compared to the 20 and 10 % ethanol solutions which explains the high pressures recorded for that mixture (see Figures 4.23 through 4.27). The energy supplied by the ultrasonicator for this experiment was sufficient to initiate cavitation thus the 30% solution showed high pressure due to its ability to store more energy. However, further research should be conducted to determine the factors that contribute to the behavior shown by high viscous and dense solutions of ethanol and petrol blends.

The wave profile shown in Figures 4.28 through 4.30 was expected since the ultrasonic energy is a wave of compressions and rarefactions that propagate through the liquid mixture. It was however expected that the waves would show a temperature decrease with the horizontal distance from the horn as obtained by Saez et.al (2006).This expectation could be attributed to higher energy experienced close to the energy emitter source, which in this case is the ultrasonicator horn, resulting in low temperatures away from the horn. However, the experimental results show no consistent decrease in the temperature with distance and this thermal distribution within the reactor can be explained by the existence of a reflection on the walls of the reactor, which means that high temperatures can also be recorded at distances close to the reactor walls.

The amplitude size of the oscillations describe the gradient of heat transfer with distance and thus the Figures 4.28 through 4.30 do not show a specific trend in amplitudes since amplitudes are almost of the same size at specific times and specific blends. The equality of the amplitudes may be due to the same sonication settings used during the experiment, indicating that the intensity was the same through all mixtures.

The energy input delivered by sonicator to the liquid is sufficient to initiate cavitation, and the cavitation formed will store large amount of energy. Therefore when the cavitation bubbles implode, tremendous amount of energy will be released. Each collapsing bubble can be considered as a microreactor in which local temperatures of several thousand degrees, and pressures greater than one thousand atmospheres (>1000 atm) are created instantaneously (Hugo, 2009). The behaviour can also be explained by the effect of fluid properties on heat transfer rate. Heat transfer is often better in liquids of low viscosity than in liquids of high viscosities (Abdou, 2012; Moorthy, 2012). This means that Liquids that have a low viscosity generally allow heat to pass through them faster, and thus the heat from the E20 and E10 blends was lost faster, resulting in low temperatures (see Figures C.1 through C.6 in appendix C). High viscous liquids like the E30 ethanol-petrol blend on the other hand do not allow swift transfer of heat.

As shown in Figures 4.31 through 4.33, the ultrasonicator probe was placed 1 cm above the base of the reactor, thus the mixing happens much more frequently at the bottom of the probe because more cavitation occurs and rapid collision of the molecules with the base surface of the reactor in comparison to when moving upwards from the ultrasonicator probe. The

temperature is higher at the bottom of the ultrasonicator probe because rapid vibration occurs at the tip of the ultrasonicator probe thus causing cavitation; the formation and violent collapse of microscopic bubbles occurs which produce local hot spot thus increasing temperature in the liquid medium (Jarupan, 2002). The temperature is the highest for when the mixing was done for 360 seconds because as the time of sonication increases, the energy input increases. The occurrence of cavitation is more and therefore the temperatures are higher when time of sonication is increased.

Report from Tangka et al (2011) on the physical properties of different petrol and ethanol blends showed that density E10, E20 and E30 were 750.8 kg/m^3, 760.5 kg/m^3 and 778.2 kg/m^3 , respectively. Therefore it is expected that highest temperature will be recorded for E10 when compared to E30 because of the lowest density of E10 since temperature of a liquid is inversely proportional to its density as shown in Figures C.7 through C.11. Also another reason for this expectation could be attributed to the higher energy content of petrol when compared to the energy content of ethanol. The temperature is the highest for the E30 blend compared to the other two ethanol-petrol blends. This is because in a solution of high density and viscosity, when the energy is sufficient to cause initial cavitation, the formed cavitation bubbles store large amount of energy that is released when the cavitation bubbles implode, thus resulting in high temperatures.

As shown in Figures 4.34 through 4.36, the concentration variation with the horizontal distance from the horn is a wave at specific sonication times and ethanol volumes. This concentration profile can be explained by the ultrasonic mixing phenomenon of cavitation. During the sonication of the ethanol and petrol mixture at high intensities, the sound waves propagate into the mixture resulting in alternating high pressure and low pressure cycles. During the low pressure cycle, waves create small vacuum bubbles or voids in the mixture and these bubbles can reach a point where they can no longer absorb energy and thus collapse violently during a high pressure cycle (Hielscher, 2005). The growth of bubbles results in higher concentration while the collapse results in low concentration due to ethanol splitting and thus the combination of this effect is a wave concentration profile.

The concentration gradient for all Figures 4.34 through 4.36 can be related to the size of the amplitudes of the oscillations but however the graphs do not show any generalised amplitude

size variation with either distance or sonication times. Energy can be lost at different points due to friction. In addition, the growth and implosion of bubbles are non-uniform, which also can affect amplitudes at different points. The other reason why the amplitude size is not the same is that reflections of the reactor walls lead to the wave superposition effect that results in an increase and a decrease in wave amplitude at a point where multiple waves are combined (Raman, 2006). In case of an ultrasonic transducer, the amplitude of oscillation describes the intensity of acceleration, and thus factors affecting intensity distribution also affect the amplitude size.

The behaviour depicted in Figures 4.37 through 4.41 was expected because E30 blend contains a large amount of ethanol in comparison to the other blends, though the sonication was operated at the same settings. In Figures 4.37 through 4.41, the wave amplitude is much smaller for E30 when compared to the other two blends, indicating that the concentration gradient is much smaller for 30% ethanol. The amplitude generally shows that the concentration gradient is quite low for E30 sample and thus mass transfer due to diffusion is affected. Due to the time limit of this study, factors influencing concentration gradient during ultrasonication-enhanced blending could not be investigated. As a recommendation, further studies are necessary to determine factors that might be influencing the concentration gradient.

The wave behaviour witnessed in the vertical direction (see Figure 4.42 through 4.44) is due to the fact that as the ultrasound energy is emitted into the blender, bubbles form at the emitter point and propagate throughout the blender, and the propagation is affected by bubble size, external pressure amplitude and surrounding environment(Xi, 2012). These bubbles can explode at any point in the reactor due to the liquid compressibility through acoustic radiation that shows a damping effect of the bubble oscillation (Brennen, 1995). The damping effect means that the bubble oscillation is non-uniform and thus at a specific point in the reactor, the amplitudes of the wave is not equal due to the non-uniform intensity of cavitation. The concentration gradient in the vertical direction however does not show any specific trend for the different sonication times and this may be due to the random loss of energy due to turbulence and friction at some points in the vertical direction.

The behaviour seen in Figures 4.45 through 4.50 was expected as mention in the effect of the amount of ethanol blends on the concentration as discussed on the horizontal direction. The

E30 blend has a higher viscosity and density compared to the other two mixtures and thus the intensity of ultrasonication was expected be lower in a more viscous mixture. Assuming cavitation had already been initiated however, the more vicious mixture was expected to have had the ability to store more energy compared to the other two mixtures. The experimental results however do not show any of these expectations and this might be due to energy loses experienced differently thus showing no clear effect of the physical properties on cavitation.

The highest gradient in the vertical direction can indicate that the flux is greater in the vertical direction than the horizontal direction according to Fick's first law, and this is more pronounced for E.20 (see Figures 4.51 through 4.53). The gradient can be related to the rate of diffusion by Fick's second law, which shows that concentration within a volume is directly proportional to the local curvature of the concentration gradient. Thus the rate of diffusion will be faster in the vertical direction.

5.2.3 Effect of time on the performance of ultrasonication-enhanced blending

The increase in pressure with time witnessed in Figures 4.54 through 4.56 can be explained by the intensity of mixing. As the mixing is done for a longer time, more energy intensity is applied resulting in high pressures in the mixture as well as high temperatures as the cavitation bubbles explode. This explosion of bubble is more violently compared to a shorter ultrasonication time, indicating that the pressure in the reactor will be higher with time. Therefore more cavitation bubbles are formed when sonication is done for a long period, and as a result the pressure increases. The increase in pressure was witnessed more in the 20% and 30% mixtures compared to the 10% mixture. In Figures 4.54 through 4.56, the pressure in the reactor seems to reach a constant value at each specific position in the last three or two minutes.

As shown in Figures 4.57 through 4.59, the increase in pressure with the ultrasonication time, while keeping all the ultrasonicator settings constant, is because as time for sonication is increased the amount of energy input is increased and more cavitation bubbles are formed. The increase in the sonication time increases the number of cycle, and thus increasing the number of bubbles formed in the solution. When the cavitation bubbles collapse they release energy, and conditions of high pressure and temperature are created. The constant pressure is

an indication that the energy distribution in the solution is uniform and a true solution may be achieved. The constant pressure also indicates the stopping time for the sonication.

The E30 blend has the highest pressure in Figures 4.60 through 4.63 and this may be high density liquid requires additional energy to initiate cavitation but once cavitation is initiated the imploding cavitation bubble have tremendous amount of energy to be release when it implode thus resulting to high pressure and temperature. The E30 solution was found to have a density of 778.2 kg/m^3 and E10 density of 750.8 kg/m^3 according to Tangka (2011). The energy supplied by the ultrasonicator for this experiment was sufficient to initiate cavitation thus the E30 solution showed high pressures compared to E10.

Similarly, the same behavior was observed for the variation of pressure with horizontal distance, and thus the trend is also due to that high density liquid can store a large amount of energy once cavitation is initiated. The imploding cavitation bubbles have tremendous amount of energy to be release when it implode (James, 2012.) thus resulting to high pressure and temperature. The 30% ethanol solution has a higher density compared to the other two blends which explains the high pressures recorded for that mixture. The energy supplied by the ultrasonicator for this experiment was sufficient to initiate cavitation thus the 30% solution showed high pressure due to its ability to store more energy.

The increase in temperature with time as seen in figure 4.64, 4.65 and 4.66 was expected since the more the mixture is exposed to the ultrasonicator the more the energy introduced in the mixture. This energy is directly proportional to temperature since bubbles exposed to this energy tend to explode more violently resulting in higher temperatures experienced in the mixture as the sonication time increases. When the mixing using the ultrasonicator was done for a long period of time the number of cycle increase thus resulting to more cavitation bubbles being formed. The increase in temperature is as a result of the cavitation bubble imploding and releasing the energy which contributes to high pressures and temperatures.
Similarly, Figures 4.67 through 4.69 show an increase of temperature with ultrasonication time, this is due to the increase in the energy input. As the sonication time is increased the more cavitation occurs thus when cavitation bubbles implode they result to an increase in temperature.

The wave function shown in Figures 4.70 through 4.72 is due to the ultrasonic energy distribution in the reactor which has been proven in literature to be a wave function. Despite the formation of waves as explained, the concentrations of ethanol in the reactor seem to be increasing with time at some specific positions from the horn. This increase in concentration is not evident in all the profiles as a decrease in concentration is also witnessed especially for the 30 % ethanol-petrol blend. This non uniform behaviour is due to the fact that the ethanol cavities grow and explodes in a non-uniform pattern. This gradual decrease of concentration with time might be due to the disintegration of ethanol bonds due to cavitation thus resulting in low concentrations at some positions. As the ultrasonication process, water bonds in the mixture also break and this result in low concentration of ethanol being recorded with time at some positions.

The amplitudes size of the oscillations in these three graphs gives the concentration gradient with time which in turn describes the rate of diffusion in the horizontal direction. Ultrasonication is known to increase the rate of diffusion and thus the wave function shows that cavities occur in the mixture which means diffusion rate is affected throughout the mixture.

The wave function seen in Figures 4.73 through 4.75 shows that cavitation occurs in the mixture enhancing mass transfer. The amplitude sizes define the rate of change of concentration with time which can in turn be linked to the rate of diffusion. The lowest amplitude sizes for each blend are however witnessed at the 4cm distance from the horn and this is due to that energy of ultrasonication is lower at that point.

5.2.4 Diffusion rate limiting step

The contour plots seen in figures 4.76 through 4.79 and Appendix C.25 show that the rate of pressure distribution is higher on the vertical direction compared to the horizontal direction. However the pressure reaches on the horizontal shows higher amplitude due to the transport direction, growth and collapse of bubbles. The mixing efficiency (α) is defined as the ratio of energy gradient to kinetic energy (Holford et al, 1999). At depth point and around the ultrasonicator horn, the mixing was more efficient ($\alpha \approx 1$), and α horizontal was higher because the low rate of energy on this direction. This conclusion can also be related to energy distribution which supports the results obtained for concentration showing that the

rate of diffusion is faster in the horizontal direction compared to the vertical direction. Below the diffusion on the horizontal will be discussed for different ethanol content in the fuel blend.

Coefficient of diffusion

The mass transfer equation combines gross fluid motion (convection) with diffusion (ruled by Fick's law) to promote the transport of the minor component (ethanol) through the major fuel element (petrol). And is given by an homogenous second differential equation as follows:

$$\frac{\partial \mathrm{C}}{\partial t}\frac{\partial x}{\partial x} - D\frac{\partial^2 \mathrm{C}}{\partial x^2} + v\frac{\partial \mathrm{C}}{\partial x} + \mu\,\mathrm{C} = 0 \tag{5.17}$$

Where C = C(x,t) denotes a permeate concentration, with x the longitudinal distance and t time, and the constants D, v, and μ are respectively diffusion, longitudinal fluid velocity, decay coefficient.

$$2v\frac{\partial \mathrm{C}}{\partial x} - D\frac{\partial^2 \mathrm{C}}{\partial x^2} + \mu\,\mathrm{C} = 0 \tag{5.18}$$

The solution of differential Equation 4 using the Laplace transform is given by the following steps:

$$-D\,\mathrm{C}_x'' + 2v\,\mathrm{C}_x' + \mu\,\mathrm{C}_x = 0 \tag{5.19}$$

$$D\,\mathcal{L}\left[\mathrm{C}_x''\right] + 2v\,\mathcal{L}[\mathrm{C}_c'] + \mu\,\mathcal{L}[\mathrm{C}_x] = 0 \tag{5.20}$$

$$-D\,[S^2Y(S) - S\mathrm{C}_x(0) - \mathrm{C}_x'(0)] + 2v\,[S\,Y(S) - \mathrm{C}_x(0)] + \mu\,Y(S) = 0 \tag{5.21}$$

$$[\mathrm{C}_x'(0) = 0]\ and\ [\mathrm{C}_x(0) = \mathrm{C}_o]$$

$$\mathrm{Y(S)} = \frac{-\mathrm{D\,S\,C_o} + 2\,\mathrm{v\,C_o}}{-\mathrm{D\,S^2} + 2\,\mathrm{v\,S} + \mu} = \frac{-2\frac{\mathrm{v\,C_o}}{\mathrm{D}} + \mathrm{C_o S}}{(\mathrm{S} - \frac{\mathrm{v}}{\mathrm{D}})^2 - (\frac{\mathrm{v}^2}{\mathrm{D}^2} + \frac{\mu}{\mathrm{D}})} \tag{5.22}$$

$$\mathrm{C}\,(x, t_a) = \mathcal{L}^{-1}\,[Y(S)]$$

$$\mathrm{C}\,(x, t_a) = k_1\,e^{\frac{x\,[v - \sqrt{(D\mu + v^2)}\,]}{D}} + k_2\,e^{\frac{x\,[\sqrt{(D\mu + v^2)} + v\,]}{D}} \tag{5.23}$$

The theoretical and the experimental convection and diffusion equation were plotted in figure 5.2. Perturbation was observed at $\frac{\partial^2 C}{\partial x^2} = 2$, this could be due to a wave behavior from ultrasonication. The R^2 values suggest that theses equations could explain the observed phenomena.

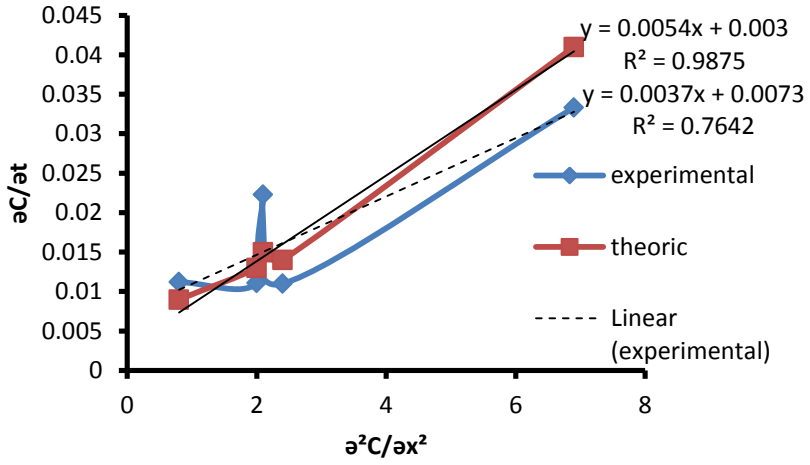

Figure 5.2: $\frac{\partial C}{\partial t}$ against $\frac{\partial^2 C}{\partial x^2}$ for experimental and theoretical coefficient of diffusion

The various ratios of ethanol and petrol blended for 420s using the ultrasonicator and the experimental coefficients of diffusion for each blend are presented in Table 5.2:

Table 5.2: Coefficient of diffusion for various ethanol-petrol blends

Ethanol petrol blends (Vol %)	Experimental Coefficient of diffusion	Theoretical Coefficient of diffusion	% deviation
5% Ethanol	37×10^{-4}	54×10^{-4}	31
10% Ethanol	20.9×10^{-4}	18×10^{-4}	17
15% Ethanol	47.3×10^{-4}	53.7×10^{-4}	12
20% Ethanol	60.2×10^{-4}	69×10^{-4}	13
25% Ethanol	68.1×10^{-4}	72×10^{-4}	5

Table 5.2 suggests that the increase of ethanol in the blend increase the diffusion coefficient. Therefore, the 25 % ethanol fuel blend had the highest Coefficient of diffusion.

5.3 Testing of ethanol-petrol blend in internal combustion engine

Figure 4.80 shows that as the ethanol content increases in the fuel mixture, there is an increase in the rate of fuel consumption rate. The rate of consumption of gasoline was 0.178 mL/min, whereas the consumption rate of pure ethanol was 0.405 mL/min, indicating an increase of 126 % in the consumption of fuel. Ethanol contains an oxygen atom, therefore it is said to be a partially oxidised fuel. As a result, it has a lower heating value. Because of this, more fuel is required to obtain the same performance when ethanol or ethanol-gasoline blends are used.

Figure 4.82 shows the emission of pollutants during the fuel testing. It can be seen from the figure that as the ethanol composition increases in the blend, there is a decrease in the CO_2 emissions. The emissions decrease until an optimal value is reached at 40 % ethanol, after which there is a steady increase in the emission. There was a 25.33 % decrease in CO_2 emissions when an ethanol (40 %)/petrol (60 %) blend was used as a fuel as compared to the emission for the usage of pure petrol. At lower compositions of ethanol in the fuel blend, there is formation of carbon monoxide, which competes with the formation of carbon dioxide, thus leading to a reduction in the formation of carbon dioxide. However at 40 % ethanol, the formation of carbon dioxide reaches its lowest value and starts to increase steadily. This increase is as a result of improved combustion in the engine. The improved combustion could be attributed to the increase of ethanol content in the fuel blend, which lowers the heating value of the fuel, leading to its complete combustion.

Another compound that has adverse effects on the people's health and the environment is carbon monoxide. This compound forms together with carbon dioxide during incomplete combustion of fuel during the combustion process. A chromatogram of a typical exhaust gas obtained from a GC showing that addition of ethanol to the fuel blend leads to a significant reduction of carbon monoxide from the exhaust emissions is included in Appendix D. The chromatogram of an exhaust gas formed from a fuel with 0 % ethanol and a carbon monoxide peak with a retention time of 1 minute (see Appendix D).

The addition of ethanol to petrol reduces the formation of carbon monoxide to levels that are beyond the detectable limit of the gas chromatography (see Appendix D). The composition

of ethanol in the fuel blend is increased to 60 %, there is no distinct carbon monoxide peak at a retention time of 1 minute.

When the ethanol percentage was increased, the CO_2 concentrations also increased as shown in GC spectrum (see appendix D), indicating more complete combustion with ethanol percentage increase in the blends. It was expected that the composition of carbon dioxide would increase steadily as ethanol percentage was increased (Yusaf et al (2009), Hsieh et al (2001), Al-Hasan (2001)). The concentration of CO_2 was expected to increase because of decreasing carbon monoxide concentration in the exhaust. However, during the analysis of the gas samples using the GC, the concentration of CO could well be detected when there was no ethanol in the blend as shown in Appendix Figure D.1 and Figure D.2. Figure D.3 of the Appendix shows a CO peak while Appendix Figure D.4 shows none. There were a number of things that could have caused the CO_2 concentration to decrease when ethanol percentage was increase from 0% to 40%. These include the contamination of the gas by air during collection, also during the analysis of the gas samples the contamination of the gas could have resulted from the presence of the air in the tube connected to the GC at which the gas was introduced.

From Figure 4.83 it can be seen that there is an increase in the nitrogen oxide (NO) as the composition of ethanol in the fuel blend is increased. This is a result of increased in combustion efficiency by increasing ethanol in the fuel. As the increase in temperature favour the formation of NO, which could react with CO (produced by incomplete combustion) to regenerate N_2. NO emissions depend on the combustion chamber condition such as temperature and fuel additive (Yusaf et al, 2009; Turner, 2010).

The concentration nitrogen oxide (NO) could not be measured as it was present in very small amounts hence no peak indicating the presence of NO during gas analysis was observed. Therefore, the concentration of NO was estimated from equilibrium data as shown in appendix D. It was expected that the concentration of NO would increase as the percentage of ethanol was increased (Bayraktar (2005); Yusaf et al (2009)). The increasing temperature favoured the formation of NO since this formation was found to be endothermic as shown by reaction (4.4).

From Figure 4.84, the indicated power increases with increasing ethanol %. The indicated power was expected to increase due to an increase in mean effective pressure in the cylinder,

resulting from the temperature increase with increasing percentage of ethanol in the blend. From the ideal gas law (see Equation (2.47), an increase in temperature results to an increase in pressure. Thus, increase in temperature in the cylinder with increasing ethanol percentage led to increase in mean effective pressure.

Fuel power was also used to analyze the effect of varying ethanol/petrol blends during combustion. Fuel power is defined as the product of fuel consumption and calorific value. The exhaust gas temperature depends on the combustion temperature which is influenced by the heating value of the fuel. As ethanol has a low heating value compared to petrol, the results of exhaust gas temperature showed a decrease with an increase of ethanol content (Ansari, 2002). However the fuel consumption showed an increase with increasing ethanol content in the blend and with time (see Figure 4.81). This could be explained by the low energy content of ethanol compare to petrol. The energy's power decrease at higher ethanol content, due to the dependency of energy power over the energy content; therefore the fuel consumption is affected (Egeback et al, 2004-2005)

Figure 4.84 shows an increase in the fuel power with increasing ethanol percentage from 0% to 60% and a decreased from 60% to 100% ethanol content in the blends. This decrease could be attributed to the high calorific value of petrol compared to ethanol. From 60% to 100% ethanol in the blend, fuel consumption becomes outweighed by the decrease in the calorific value of the mixture resulting from the decrease in petrol percentage in the blends resulting to the decrease in fuel power.

The fuel power increased as the composition of ethanol in the blend increased. However, the fuel power reached an optimal value at 60 % ethanol content in the fuel bend and declined slightly thereafter (see Figure 4.84). The reason for the increase is mainly due to the fact that ethanol is an oxygenated fuel and it is therefore consumed much more rapidly during combustion process (Launder, 2001). Since the calorific value of ethanol (26.828 MJ/kg) is much lower than that of petrol (44.125 MJ/kg), there is a decrease of the fuel power as the fuel becomes richer in ethanol and leaner in petrol (Bartok, 2004). Thermal efficiency is not affected to a large extent by increasing ethanol content in the petrol/bio-ethanol blend. From the definition of thermal efficiency (heat converted to work), it was observed that the heat produced at any blend was converted to heat at almost the same ratio resulting to a constant thermal efficiency as depicted in Figure 4.84 despite the increase in ethanol percentage in the blends.

CHAPTER 6: CONCLUSIONS AND RECOMMENDATIONS

6.1. Conclusions

This study shows that the ultrasonication process enhances the blending of petrol-ethanol-water mixture, and the homogeneity of ethanol-petrol blend was characterized by the density distribution of the mixture within the storage container and with time.

Ultrasonication improves adsorption capacity of silica gel by 35% when used to adsorb water from solutions of 85% vol. ethanol on average. It was found that an increase in the amplitude of the ultrasonication seemed to reduce the amount of water being adsorbed and the calculated adsorption capacity. This was due to desorption and adsorption which was continually occurring due to the pulse generated by the ultrasonication, and also the breakage and regeneration of water.

Under increased amplitudes (higher sound pressure) the pressure effects of adsorption are observed to increase the adsorption, at lower concentrations of ethanol, and induce the adsorption at higher concentrations. The amplitude can thus be seen as the breakthrough variable for adsorption, because by increasing the amplitude at higher concentrations adsorption and desorption behaviour of the system occurs. This agrees with what is obtainable from literature as the amplitude of the waves has to be sufficient in order to break the molecular bonds. Increasing the amplitude increases the force by which the cavitation occurs and in so doing increases the adsorption capability of the silica gel.

Based on the kinetic model at higher ultrasonication pulse rates, the absorptivity is expected to decrease. The modified pseudo second order model proposed $\frac{d\,q_t}{(q_t - q_e)^2} = \frac{1}{q_e}[\,cos\,(K - t) - t\sin(K - t)]\,dt$ fitted the experimental data.

The pressure in both horizontal and vertical direction was found to be decreasing with distance in a non-linear relationship. The mixture of high viscosity and density (E30 blend) had the highest temperature and pressure in both directions. The concentration profile is a wave function for both horizontal and vertical direction. It can therefore be concluded that ultrasonication has an impact on both the horizontal and vertical diffusion since the concentration profiles are waves confirming the formation of cavitation in the mixture. Ultrasonication increases temperatures and pressures which in turn enhances diffusion rate

and thus mixing possibilities of ethanol and petrol. The experimental results on the concentration gradient concludes that if the reactor geometry was to be proposed, it will have a greater height than the radius since the vertical diffusion seem to be favoured.

The lower energy content of ethanol affect the fuel consumption, but it compensates by the improved of combustion efficiency and environmental pollution. The addition of ethanol to petrol increases the fuel power and indicated power and also leads to a decrease in carbon monoxide and increase in carbon dioxide, NO emissions. Optimal performance of the fuel is observed when the blend contains 60 % ethanol. At this proportion, the highest fuel power is observed and moderate carbon dioxide and nitric oxide emissions are also observed.

6.2 Recommendations

It is recommended that further studies should be undertaken on such as:

1. The influence of ultrasonicator parameters and mixing mechanism should be done in order to understand the effect of ultrasound on the phase behaviour;

2. Stability of different blends of ethanol-petrol at different temperature;

3. Establishment of optimum operating variables, such as, the amplitude, the pulse rate, the temperature, the pressure, the blending time and the frequency, that could be related to the force required to break the molecular bonds of ethanol-water mixtures at various concentrations;

4. The geometry of the mixer and the rate of diffusion in horizontal and vertical directions have to understand the effect of the ultrasonicator probe position on mixing. The effect of density and viscosity on ultrasonication-enhanced blending should be investigated.

REFERENCE

Abedini R. and Mousavi S. M, (2010): Preparation and Enhancing Of Materials Using Ultrasound Technique: Polymers, *Catalysts and Nanostructure Particles*. *Petroleum and coal*, 52(2), 81-98

Adewuyi Y.G., (2001): Sonochemistry: environmental science and engineering applications. *Ind. Eng. Chem. Res., 40, pp. 4681–4715.*

Aina T., Folayan C. O. and Pam G. Y., (2012) Influence of compression ratio on the performance characteristics of a spark ignition engine. *Advances in Applied Science Research*, 3 (4):1915-1922

Al-Hasan, M. (2003). Effect of ethanol-unleaded gasoline blends on engine performance and exhaust emission. *Energy Conversion and Management 44* , 1547-1561

Anderson J.E, DiCicco D.M, Ginder J.M, Kramer U., Leone T.G, Raney-Pablo H.E, and Wallington, T.J (2012): High octane number ethanol-gasoline blends: Quantifying the potential benefits in the United States. *Fuel 97*, 585-594.

Anderson J E, Kramer U, Mueller S A, Wallington T J., (2010): Octane numbers of ethanol-gasoline and methanol-gasoline blends estimated from molar concentrations. *Energy & Fuels*, 24: 6576–6585.

Asakura, Y., Yasuda, K., Kato, D., Kojima, Y., & Koda, S. (2008): Development of a large sonochemical reactor at high frequency. *Chemical Engineering Journal 139* , 339-343.

Azzouzi E.H.E., Madani M.E, Mekkaoui M., Belghiti M.A.E, Mohamadine E.M, Rabet, Mountacer H., Hourch A.E, Zrineh A., Azzouzi M.E., (2010): The effect of Cu and Cu-humic acids on the adsorption of imazethapyr herbicide by montmorillonite clay Biotechnologie, Agronomie, Société et Environnement, 2010, Vol.14(4), pp.659-665

Badrana O, Emeishb S, Abu-Zaidc M, Abu-Rahmaa T, Al-Hasana M, Al-Ragheba M., (2011): Impact of Emulsified Water/Diesel Mixture on Engine Performance and Environment. *Int. J. of Thermal & Environmental Engineering.* Volume 3, No. 1, 1-7

Bayraktar, H. (2005). Experimental and theoretical investigation of using gasoline-ethanol blends in spark-ignition engines. *Renewable energy 30* , 1733-1747.

Benson RS, Whitehouse ND., (1979) Internal combustion engines. Oxford: *Pergamon Press*, Vols 1 and 2.

Bhirud U.S., Gogate P.R., Wilhelm A.M., Pandit A.B., (2004): Ultrasonic bath with longitudinal vibrations: a novel configuration for efficient wastewater treatment. *Ultrason. Sonochem.*, 11, pp. 143–147.

Binod P., Janu K.U., Sindhu R., Pandey A., (2011): Hydrolysis of Lignocellulosic Biomass for Bioethanol Production. *Biofuels*, Burlington: Academic Press, pp. 229-250.

Borgnakke, C.; Puzinauskas, P.; Xiao, Y., (1986): Spark Ignition Engine Simulation Models; Department of Mechanical Engineering and Applied Mechanics. University of Michigan. *Technical Report, Report No. UM-MEAM*-86-35

Breaux B., (2012): The effect of elevated water content on ethanol combustion. M.Sc, Faculty of the Louisiana State University and Agricultural and Mechanical College. P 121

Bridgeman O.C, (1933): Solubility of Ethyl Alcohol in Gasoline *Ind. Eng. Chem., 25* (5), pp 523–525

Bridgwater, A. V., Meier, D., & Radlein, D. (1999): An overview of fast pyrolysis of biomass *Organic geochemistry , 30* (12), pp 1479-1493.

Brunauer S., Deming L.S., Deming W.E., Teller E., (1940): On the theory of the van der Waals adsorption. J. *Am. Chem. Soc*. 62, 1723

Bui S., Verykios X., Mutharasan R, (1985): In Situ Removal of Ethanol from Fermentation Broths. Selective Adsorption Characteristics. *Indian Eng. Chem. Process Des. Dev*., 24, 4, 1209-1213

Chacartegui C.M, Lopez J.E.G, Alfonso F.S, Aakko P., Hamelinck C, Vossen G.V., Kattenwinkel H, (2007): Blending ethanol in diesel. *BIOScope*, Lot 3b, 10-12

Caton J. A. (2000): On the destruction of availability (exergy) due to combustion processes – with specific application to internal-combustion engines. Energy vol. 25, pp. 1097–1117

Cavalcante-Junior C.L., (2000): Industrial adsorption separation processes fundamentals, modelling and application. *Latin American Applied Research* 30:357-364

Chen, R., Chiang, L., Chen, C., & Lin, T. (2011): Cold-start emissions of an SI engine using ethanol-gasoline blended fuel. *Applied Thermal Energy 31* , 1463-1467.

Christmann K., (2012): Thermodynamics and Kinetics of Adsorption. Institut für Chemie und Biochemie, Freie Universität Berlin. IMPRS-Lecture Series, 1-58

Da Silva, R., Cataluna, R., Weber de. Menezes, E., Samios, D., & Sartori Piatnicki, C., (2005): Effect of additives on the antiknock properties and Reid vapor pressure of gasoline. *Fuel 84* , 951-959.

Delgado J.A., Uguina M.A., Sotelo J.L., Agueda V.I., Garcia A., Roldan A. , (2012): Separation of ethanol-water liquid mixtures by adsorption on silicalite. *Chemical Engineering Journal* vol. 180 January 15, p. 137-144

Delgado J.A., Águeda V.I., Uguina M.A., Sotelo J.L., García A., Brea P., García-Sanz A. (2013): Separation of ethanol–water liquid mixtures by adsorption on a polymeric resin Sepabeads 207. *Chemical Engineering Journal* vol. 220. p. 89-97

Desjardins R. (1997): Water treatment. Presses inter Polytechnique, Editions of polytechnique university of montreal, Canada. 2nd review Edition, 304 p.

De Oliviera, E., Barker,J.F., Chatzis, I., (2000): Gasoline-water-ethanol interactions and fluid properties, in Proceedings of the 2000 Petroleum hydrocarbons and Organic Chemicals in Groundwater conference, Ground Water Publishing Company, Westerville, Ohio, pp. 11-23

DOESA, (2009): assessment of the blending value of bio-ethanol with local and imported petrol. Biofuel report, Department of Energy, South Africa, 14 p.

Donsi F, Wang Y, Li J, Huang Q., (2010): Preparation of Curcumin Sub-micrometer Dispersions by High-Pressure Homogenization. *J. Agric. Food Chem.*; 58: 2848-2853.

Egebäck K.E., Henke M., Rehnlund B., Wallin M., Westerholm R., (2005): Blending of Ethanol in Gasoline for Spark Ignition Engines – Problem Inventory and Evaporative Measurements. Stockholm University, ATRAX AB, Autoemission KEE Consultant AB, p 133

El-Awad M.M., Elseory A.M., El-Faroug M.O., (2012): Determining the Thermodynamic properties of fuel blends for use with air-fuel models of IC engines." Industrial and Mechanical Engineering, Dubai (ICTIME'2012) 24-25

Errico M., Rong B.G., (2012) Synthesis of new separation processes for bioethanol production by extractive distillation, Separation and Purification Technology, 96, 58-67.

Feng R., Y. Zhao, C. Zhu and T.J. (2002): Mason, Enhancement of ultrasonic cavitation yield by multi-frequency sonication. Ultrason. Sonochem., 9, pp. 231–236.

Ferguson C.R., (1986): Internal combustion engines, *applied thermosciences Wiley*, 17 Science - p. 546.

Furey, R. and Perry, K., (1991): Vapor Pressure Characteristics of M85 Methanol Fuels. *SAE international, Pap. Ser.*, N 912429, pp 11-15.

Furey, R., & King, J. (1981). Evaporative amd exhaust emissions from cars fuelled with gasoline containing ethanol or methyl tert-butyl ether. *SAE international, Pap. Ser., 810261*, pp 1200-1216.

Gallo W.L.R. and Milanez L.F., (1992): Exergetic Analysis of Ethanol and Gasoline Fueled Engines. SAE. Transactions, *Journal of Fuels & Lubricants*, Section 4, Vol. 101, pp 907- 914.

Giakoumis E.G., (1998): Transient operation of diesel engines. PhD thesis. National Technical University of Athens.

Gogate P R**,** Pandit A B**, (**2005**):** A review and assessment of hydrodynamic cavitation as a techmology for the future, *Ultrasonics Sonochemistry*, 12(1) 21-27**.**

Gogate P.R**,** Tayal R.K, Pandit A.B**, (**2006**).** Cavitation: a technology on the horizon**.** *Current Science*, 91, 35–46

Gogate, P. (2008). Cavitational reactors for process intensification of chemical processing applications: A critical review. *Chemical Engineering and Processing 47* , 515-527.

Gogate P.R., Sivakumar M. and Pandit A.B., (2004): Destruction of Rhodamine B using novel sonochemical reactor with capacity of 7.5 l. *Sep. Pur. Tech.*, 34, pp. 13–24.

Gogate P.R., Tatake P.A., Kanthale P.M. and Pandit A.B., (2002): Mapping of sonochemical reactors: review, analysis, and experimental verification. *AIChE J.*, 48, pp. 1544–1560.

Goksen G., Yaralioglu, Ira O Wygant, Theodore C Marentis, Butrus T Khuri-Yakub, (2004): Ultrasonic mixing in microfluidic channels using integrated transducers. Stanford University. *Analytical Chemistry*; 76(13):3694-8

Gramajo de Doz, M.B., Bonatti, C.M., and Solimo, H.N.. (2004): Water tolerance and ethanol concentration in ethanol-gasoline fuels at three temperatures. Energy and Fuels, 18, p. 334 – 337.

Hago W. and Morin A., (2010): An internal combustion engine with CO_2 capture. *Efficient hydrogen motors*, p. 7-9

Heywood JB., (1988): Internal combustion engine fundamentals. New York: McGraw-Hill. Technology & Engineering - 930 p.

Ho, Y.S., (2004): Citation review of Lagergren kinetic rate equation on adsorption reactions. *Scientometrics*, **59**(1): 171-177.

Ho, Y.S., (2006): Review of second-order models for adsorption systems. *Journal of Hazardous Materials*, **136**(3): 103-111

Holley A.T., Balteria A., Dong Y., Fan Y., Andac M.G., and Egolfopoulos F.N., (2006): Extinction of premixed flames of practical liquid fuels: experiments and simulations.Combustion and flame 144, 448-460. Horlock JH, Winterbone DE., (1986): The thermodynamics and gas dynamics of internal combustion engines, vol. II. Oxford: Clarendon Press; 1148–212

Hugo M. Santos, Carlos Lodeiro, Jose Luis Capelo, (2009): Power Ultrasound Meets Proteomics. *Wiley VCH Verlag GmbH&Co. KGaA*, 107-126.

Hughes K. (2009), "Treatise on alcohol-blended Gasoline phase separation and alcohol monitors". MSc Research and Development Engineer Research and Development Engineer Central Illinois. *Cim-tek,* p. 21

Hui T. C., Kim C. N., Chakraborty A., Nay M. O., Othman M.A., (2002): Adsorption Characteristics of Silica Gel + Water Systems. *J. Chem. Eng., 47*, 1177-1181

IAFC – (2008): Responding to Ethanol Incidents. Workshop, First Edition v. 7.21. United States of America

IBSA – (2010), Dialogue forum: Investigation into harmonization of IBSA biofuels specifications and standards. Birchwood hotel, Johannesburg, South Africa, p. 2

Ikegami T., Yanagishita H., Kitamotoa D., Negishi H, Haraya K., Sano T, (2002): Concentration of fermented ethanol by pervaporation using silicalite membranes coated with silicone rubber. *Desalination.* Volume 149, Issues 1–3, 49–54

Imboden D.M. and Joller T.H, (1984): Turbulent mixing in the hypolimnion of Baldeggersee (Switzerland) traced by natural randon- 222. Limnal. Oceanagr. 29:831-844.

Janssen R.A, Roffers S., Ehlert T.D., Ahles J.G., Rasmussen P.W., McNichols P.S., McCraw E.C., (2008): Ultrasonic liquid treatment chamber and continuous flow mixing system. Patent, US20080062811 A1

Jarupan K, (2002): Effect of Ultrasound, Temperature and Pressure Treatments on Enzyme Activity and Quality Indicators of Fruit and Vegetable Juices. MSc Eng. University of Berlin. P 138

James R. H. (2003): Fundamentals of Ultrasonic Cleaning. Hessonic Ultrasonic, Washington UT, p 18

Jerry E. Sinor, Bailey B.K., (1993): Current and Potential Future Performance of Ethanol Fuels. SAE international Technical papers, Paper Number: 930376.

Kanthale P.M., Gogate P.R., Pandit A.B. and Wilhelm A.M., (2003): Cavity cluster approach for quantification of cavitational intensity in sonochemical reactors. Ultrason. Sonochem., 10, pp. 181–189.

Karshafian R., (2010). On the Permeabilisation and Disruption of Cell Membranes by Ultrasound and Microbubbles. PhD thesis, Department of Medical Biophysics, University of Toronto. p. 123

Kiss A.A., Suszwalak D.J.P.C., Ignat R.M., (2013): Breaking azeotropes by azeotropic and extractive distillation in a dividing-wall column". Chemical Engineering Transactions, Vol. 35, 1279-1284

Klíma, J.; Frias-Ferrer, A.; González-García, J.; Ludvík, J.; Sáez, V.; Iniesta, J. (2007): Optimisation of 20kHz sonoreactor geometry on the basis of numerical simulation of local ultrasonic intensity and qualitative comparison with experimental results. *Ultrasonics - Sonochemistry* vol. 14 issue 1 January, p. 19-28.

Koc M., Sekmen Y.b, Topgu T., Yucesu H.S. (2009): The effect of unleaded-ethanol gasoline blends on engine performance and exhaust emissions in a spark-ignition engine. *Renewable Energy*, vol. 34, pp. 2101–2106.

Kukulji, N., & Kurevija, T. (2011)*:* Energy and Environmental Significance of an Alternative Fuels Utilization Produced with to Liquid Technology. *Survival Sustainability, Environmental Earth Sciences*. Springer Berlin, pp 435-445.

Kumar A., Kumaresan T., Pandit A.B., Joshi J.B., (2006): Characterization of flow phenomena induced by ultrasonic horn. *Chem. Eng. Sci.*, 61, pp. 7410–7420.

Kunnakorn, D.; Rirksomboon, T.; Siemanond, K.; Aungkavattana, P.; Kuanchertchoo, N.; Chuntanalerg, P.; Hemra, K.; Kulprathipanja, S.; James, R.B.; Wongkasemjit, S. (2013): Techno-economic comparison of energy usage between azeotropic distillation and hybrid system for water–ethanol separation. *Renewable Energy* vol. 51. p. 310-316.

Kyriakides A., Dimas V., Lymperopoulou E., Karonis D., Lois E.(2013), Evaluation of gasoline–ethanol–water ternary mixtures used as a fuel for an Otto engine. *Fuel*, 108, 208–215.

Lin W.Y., Chang Y.Y., Hsieh Y.R., (2010): Effect of ethanol-gasoline blends on small engine generator energy efficiency and exhaust emission, Journal of the Air & Waste Management Association, 60(2), 142-148.

Lior N., Rudy G. J., (1988): Second Law Analysis of an Ideal Otto Cycle. *Energy Conversion and Management*, Vol. 28, 4, pp. 327-334.

Lou X., (2010): Stress corrosion cracking and corrosion of carbon steel in simulated fuel-grade ethanol. PhD thesis, School of Materials Science and Engineering Georgia Institute of Technology. P 236

Louisnard O, Gonzalez-Garcia J, Tudela I, Klima J, Saez V, Vargas-Hernandez Y. (2009): FEM simulation of a sono-reactor accounting for vibrations of the boundaries. *Ultrasonics Sonochemistry*, 16(2):250-259.

Madani M., (2004): Contribution to the study of the adsorption of imazethapyr and catalyzed photodegradation of imazethapyr and diuron. PhD thesis. Univ. Mohammed V, Faculty of Rabat. 211p.

Mason T.J., (2000): Large scale sonochemical processing: aspiration and actuality. *Ultrason. Sonochem.*, 7, pp. 145–149.

Mason T.J., (2003): Sonochemistry and sonoprocessing: the link, the trends and (probably) the future. *Ultrason. Sonochem.*, 10 (2003), pp. 175–179.

Mechrafi E. (2002) Adsorption, desorption and mobility of herbicides in contact with organic and inorganic adsorbents. PhD: University Mohammed V, Faculty of Sciences, Rabat (Morocco).

Miron, W., Ragazzi, R., Hollman, T., Gallagher G., (1986): Ethanol-Blended Fuel as a CO Reduction Strategy at High Altitude. *SAE International*, Technical Paper 860530

Monnier H., Wilhelm A.-M., Delmas H., (1999): Influence of ultrasound on mixing on the molecular scale for water and viscous liquids. *Ultrason. Sonochem*., 6, pp. 67–74.

Monnier H., Wilhelm A.-M., Delmas H, (2000): Effects of ultrasound on micromixing in flow cell. *Chem. Eng. Sci.,* 55, pp. 4009–4020.

Mueller, S. A., Anderson, J. E., & Wallington, T. J. (2009): A classroom demostration of water-induced phase separation of alcohol-gasoline biofuel blends. *Journal of Chemical Education , 89* (9), 1045-1048.

Neppiras, E. (1984): Acoustic cavitation: an introduction. *Ultrasonics*, Volume 22, 1, 25–28

Olsson J., (2011): Fuel dispersion and bubble flow distribution in fluidized beds. Licentiate Thesis, Chalmers University of Technology; University of Borås (Sweden). p 61

Owen K, Coley T. (1995): Automotive fuels reference book, 2nd ed. Warrendale: Society of Automotive Engineers; pp 419–51.

Qiu H., Lu, L.V., Pan B, Zhang Q., Zhang W., Zhang Q-x., (2009): *Critical review in adsorption kinetic models, Journal of Zhejiang University Science A*. Volume 10 (5) , pp 716-724

Panagiotou T, Robert J. Fisher. (2013): Producing micron- and nano- size formulations for functional foods applications. *Functional Foods in Health and Disease;* 3(7):274-289

Pertler M., Blass E., (2004): Fickian Diffusion in Binary Mixtures That Form Two Liquid Phases. *AIChE Journal*, Volume 42, 4, 910-920.

Polany, M., Smisek M., Cerney S., (1970): Active carbon manufacture, properties and application. *Anal. Chem.*, 1970, *42* (14), pp 81A–81A

Rachidi M.H., K. Bahja K., Zrineh A., Hamad M., Zaydoun S., Ferhat M., (1999): Adsorption de l'octaéthylporphyrine de nickel sur les apatites phosphocalciques. *J.Chim. Phys*. Vol. 96, 4 p. 706-724

Rakopoulos CD, Giakoumis EG. (1997): Development of cumulative and availability rate balances in a multi-cylinder turbocharged IDI diesel engine. *Energy Convers Manag*.; 38:347–69.

Rakopoulos CD, Giakoumis EG. (2006), *Second law analyses applied to internal combustion engines operation.Progress in Energy and Combustion Science,* 32 pp. 2–47

Rasskazchikova T. V., Kapustin V. M., and Karpov S. A.. (2004): Ethanol as high-octane additive to automotive gasoline. Production and use in Russia and abroad. *Chemistry and Technology of Fuels and Oils,* Vol. 40, 4

Ravagnani M.A.S.S., Reis M.H.M., Filho R.M, Wolf-Maciel M.R., (2010): Anhydrous ethanol production by extractive distillation: A solvent case study. Proc Safe EnvironProtect2010; 88:67-73.

Rokhina E.V., Lens P., Virkutyte J., (2009): Low-frequency ultrasound in biotechnology: state of the art. Trends Biotech., 27 (2009), pp. 298–306.

Rutz, D., Janssen R., (2008): Biofuel Technology Handbook**.** - 2nd version, *WIP Renewable Energies*, Germany; 152p.

Servant G., Laborde J.L., Hita A., Caltagirone J.P. and Gerard A., (2003): On the interaction between ultrasound waves and bubble clouds in mono- and dual-frequency sonoreactors. *Ultrason. Sonochem.,* 10, pp. 347–355.

Segebarth, N., Eulaerts, O., Reisse, J., Crum, L. A., & Matula, T. J. (2002). Correlation between acoustic cavitation noise, bubble population, and sonochemistry. *J. Physical Chemistry B.* 106 , 9181-9190.

Sekhararao G.S.H., Prasad B., Wasewar K.L., (2011): *Batch Study, Equilibruim and Kinetics of Adsorption of Selenium using Rice Husk Ash,* Journal of Engineering Science and Technology ,Vol. 6, No. 5, 586 - 605

Siddiqui S.W, (2011): Mixing performance of various geometries -Emulsification perspective, School of Chemical Engineering, University of Birmingham

Sheet E.A.E., (2008): Improvement of Gasoline Octane Number by Blending Gasoline with Selective Components. MSc thesis, Chemical Engineering/Oil Refinery & Petrochemical Industry, University Of Technology 2008, Iraq. p 99

Sinnott R. K.(2005), *Chemical Engineering Design,* Elsevier Butterworth Heinemann vol. 6 ed.4.

Sivakumar M., Tatake P.A. and Pandit A.B., (2002): Kinetics of p-Nitrophenol degradation: effect of reaction conditions and cavitational parameters for a multiple frequency system. Chem. Eng. J., 85 (2002), pp. 327–338.

Song, C.-L., Zhang, W.-M., Pei, Y.-Q., Fan, G.-L., & Xu, G.-P. (2006). Comparitive effects of MTBE amd ethanol additions into gasoline on exhaust emissions. *Atmospheric Environment 40* , 1957-1970.

Stepanov V.S. (1994), *Chemical energy and exergies of fuel. Energy.* vol. 20 No. 3 pp. 235-242

Stone R. Introduction to internal combustion engines. 3rd ed. London: MacMillan; 1992.

Sung N. W. and Patterson D. J. (1983), Theoretical limits of engine economy with alternative automotive fuels. University of Michigan. *Intl J Energy Research*, v7, n 2.

Suslick, K., Didenko, Y., Fang, M., Hyeon, T., Kolbeck, K., McNamara III, W., et al. (1999). Acoustic cavitationand its chemical consequences. *Philosophical Transactions of the Royal Society of London* , 335-353.

Suslick K.S., (1994): The chemistry of Ultrasound, The year book of Science and the Future, Encyclopaedia Britannica: Chicago, pp 138-155

Syawala D.S., Wardiyati T., Maghfoer M.D., (2013): Production Of Bioethanol From Corncob and Sugarcane Bagasse With Hydrolysis Process Using Aspergillus niger

and Trichoderma viride". *Journal Of Environmental Science, Toxicology And Food Technology*. Volume 5, Issue 4 (2013), 49-56.

Tabada M., Montalbo-lomboy, (2008): Ultrasonic pretreatment for enhanced saccharification and fermentation of ethanol production from corn. PhD thesis, Iowa State University, Ames, Iowa

Tangka J. K., Berinyuy J. E., Tekounegnin and Okale A. N., (2011): Physico-chemical properties of bio-ethanol/gasoline blends and the qualitative effect of different blends on gasoline quality and engine performance. *Journal of Petroleum Technology and Alternative Fuels.* Vol. 2(3), pp. 35-44.

Tatake P.A. and Pandit A.B., (2002): Modelling and experimental investigation into cavity dynamics and cavitational yield: influence of dual frequency ultrasound sources. *Chem. Eng. Sci*., 57 (2002), pp. 4987–4995.

Thoma G., Swofford J., Popov V. and Som M., (1997), Sonochemical destruction dichloromethane and o-dichlorobenzene in aqueous solution using a near field acoustic processor. *Adv. Env. Res.*, 1, pp. 178–193.

Treybal T.E, (1981): *Mass-transfer operations*. 3rd edition. Singapore: McGraw-Hill

Turner, D., Xu, H., Cracknell, R. F., Natarajan, V., Chen, X. (2011): Combustion performance of bio-ethanol at various blend ratios in a gasoline direct injection engine. *Fuel* , pp 1999-2006.

Ugwoha, Ejikeme (2013) Impact of soil organic matter on groundwater contamination risks for ethanol and butanol blended gasoline. PhD thesis, University of Nottingham. P 255

Vanhille, C., Campos-Pozuelo, C. (2012): Acoustic cavitation mechanism: A nonlinear model. *Ultrasonics Sonochemistry 19* , 217-220.

Vichare N.P., Gogate P.R., Dindore V.Y., Pandit A.B., (2001), Mixing time analysis of a sonochemical reactor. *Ultrason. Sonochem*. 8, pp. 23–33

Virot, M., Chave, T., Nikitenko, S. I., Shchukin, D. G., Zemb, T., & Mohwald, H. (2010). Acoustic cavitation at the water-glass interface. *J. Physical Chemistry 114* , 13083-13091.

Wilks MR, (2008): The impact of blending techniques, feedstock choice, and analytical techniques on biodiesel blend accuracy", *inform*, Vol. 19 (12)

Wu J., (2004): Modelling adsorption of organic compounds on activated carbon A multivariate approach. PhD Thesis University of Neuchâtel, Schweiz p 84

Yacoub Y., Bata R., Gautam M., Martin D. (1998): The performance characteristics of C_1-C_5 alcohol-gasoline blends with matched oxygen content in a single cylinder SI engine. Proceedings of the Institution of Mechanical Engineers, 212 Part A, 363379

Zhang Y.H.P., (2008): Reviving the carbohydrate economy via multi-product lignocellulose biorefineries. *Journal of Industrial Microbiology & Biotechnology*, Vol. 35, No. 5, pp. 367-375,

Zoubir B., (2007): Modeling and study of the feasibility of a solar adsorption refrigerator MSc project Faculty of Engineering sciences, University of BATNA, p 26-27

Appendix

Appendix A: Tables of data for ternary systems

Table A.1: Percentage of ternary components used for phase behavior studies

Sample No	Ternary components (%)			Sample No	Ternary components (%)			Sample No	Ternary components (%)		
	ethanol	water	petrol		ethanol	water	petrol		ethanol	water	petrol
	Curve 1				Curve 5 cont.				Curve 9		
1	0	0	100	**93**	29.0	11.0	60.0	**181**	0.0	0.0	100.0
2	10	1.75	88.25	**94**	33.0	12.0	55.0	**182**	2.5	2.5	95.0
3	17	3	80	**95**	36.6	13.4	50.0	**183**	5.5	4.5	90.0
4	20	3.5	76.5	**96**	40.0	15.0	45.0	**184**	12.0	8.0	80.0
5	30	5	65	**97**	43.5	16.5	40.0	**185**	18.0	12.0	70.0
6	40	7	53	**98**	46.6	18.4	35.0	**186**	25.0	15.0	60.0
7	50	11	39	**99**	49.5	20.5	30.0	**187**	27.5	17.5	55.0
8	60.0	16.5	23.5	**100**	52.0	23.0	25.0	**188**	31.2	18.8	50.0
9	62.0	18.0	20.0	**101**	53.0	24.5	22.5	**189**	34.0	21.0	45.0
10	63.0	24.0	13.0	**102**	54.0	26.0	20.0	**190**	38.0	22.0	40.0
11	62.0	28.0	10.0	**103**	53.8	28.7	17.5	**191**	41.0	24.0	35.0
12	60.0	32.5	7.5	**104**	53.0	32.0	15.0	**192**	43.0	27.0	30.0
13	55.0	40.0	5.0	**105**	51.0	36.5	12.5	**193**	46.0	29.0	25.0
14	50.0	47.0	3.0	**106**	47.8	42.2	10.0	**194**	46.5	31.0	22.5
15	40.0	57.5	2.5	**107**	43.0	49.5	7.5	**195**	46.0	34.0	20.0
16	30.0	68.2	1.8	**108**	37.0	58.0	5.0	**196**	44.0	38.5	17.5
17	20.0	79.0	1.0	**109**	27.5	70.0	2.5	**197**	41.0	44.0	15.0
18	10.0	89.5	0.5	**110**	0.0	100.0	0.0	**198**	37.5	50.0	12.5
19	0.0	100.0	0.0					**199**	32.5	57.5	10.0
								200	28.0	64.5	7.5
	Curve 2				Curve 6			**201**	22.0	73.0	5.0
20	0.0	0.0	100.0	**111**	0.0	0.0	100.0	**202**	13.0	84.5	2.5

21	7.6	2.4	90.0	**112**	3.4	1.6	95.0	**203**	0.0	100.0	0.0
22	16.3	3.7	80.0	**113**	6.9	3.1	90.0				
23	25.0	5.0	70.0	**114**	14.0	6.0	80.0				
24	32.7	7.3	60.0	**115**	21.0	9.0	70.0			**Curve 10**	
25	37.0	8.0	55.0	**116**	28.0	12.0	60.0	**204**	0	0.0	100.0
26	41.0	9.0	50.0	**117**	31.0	14.0	55.0	**205**	2.5	2.5	95.0
27	44.5	10.5	45.0	**118**	35.0	15.0	50.0	**206**	5	5.0	90.0
28	48.0	12.0	40.0	**119**	38.5	16.5	45.0	**207**	11	9.0	80.0
29	52.0	13.0	35.0	**120**	42.5	17.5	40.0	**208**	17	13.0	70.0
30	55.5	14.5	30.0	**121**	45.7	19.3	35.0	**209**	24	16.0	60.0
31	57.7	17.3	25.0	**122**	48.0	22.0	30.0	**210**	27	18.0	55.0
32	59.0	18.5	22.5	**123**	50.7	24.3	25.0	**211**	30	20.0	50.0
33	60.0	20.0	20.0	**124**	52.0	25.5	22.5	**212**	32.3	22.7	45.0
34	60.5	22.0	17.5	**125**	52.5	27.5	20.0	**213**	36	24.0	40.0
35	61.0	24.0	15.0	**126**	52.0	30.5	17.5	**214**	38	27.0	35.0
36	60.5	27.0	12.5	**127**	50.7	34.3	15.0	**215**	41	29.0	30.0
37	60.0	30.0	10.0	**128**	48.0	39.5	12.5	**216**	42.5	32.5	25.0
38	57.5	35.0	7.5	**129**	45.0	45.0	10.0	**217**	42	35.5	22.5
39	52.0	43.0	5.0	**130**	40.0	52.5	7.5	**218**	41.5	38.5	20.0
40	43.5	54.0	2.5	**131**	33.0	62.0	5.0	**219**	39	43.5	17.5
41	0.0	100.0	0.0	**132**	24.0	73.5	2.5	**220**	37	48.0	15.0
				133	0.0	100.0	0.0	**221**	33	54.5	12.5
		Curve 3						**222**	30	60.0	10.0
42	0.0	0.0	100.0					**223**	24.5	68.0	7.5
43	3.6	1.4	95.0					**224**	20	75.0	5.0
44	7.4	2.6	90.0			**Curve 7**		**225**	15	82.5	2.5
45	16.1	3.9	80.0	**134**	0.0	0.0	100.0	**226**	0	100.0	0.0
46	24.0	6.0	70.0	**135**	3.1	1.9	95.0				
47	32.0	8.0	60.0	**136**	6.0	4.0	90.0				
48	36.0	9.0	55.0	**138**	13.0	7.0	80.0			**Curve 11**	

49	40.0	10.0	50.0
50	43.0	12.0	45.0
51	47.0	13.0	40.0
52	50.2	14.8	35.0
53	53.2	16.8	30.0
54	56.6	18.4	25.0
55	57.5	20.0	22.5
56	58.1	21.9	20.0
57	58.4	24.1	17.5
58	58.4	26.6	15.0
59	58.3	29.2	12.5
60	56.4	33.6	10.0
61	52.5	40.0	7.5
62	47.2	47.8	5.0
63	35.0	62.5	2.5
64	0.0	100.0	0.0

Curve 4

65	0.0	0.0	100.0
66	3.5	1.5	95.0
67	7.3	2.8	90.0
68	15.7	4.3	80.0
69	22.8	7.2	70.0
70	30.5	9.5	60.0
71	34.5	10.5	55.0
72	37.7	12.3	50.0
73	41.7	13.3	45.0
74	45.5	14.5	40.0
75	48.0	17.0	35.0
139	20.0	10.0	70.0
140	27.0	13.0	60.0
141	30.0	15.0	55.0
142	33.0	17.0	50.0
143	37.0	18.0	45.0
144	40.0	20.0	40.0
145	43.0	22.0	35.0
146	47.0	23.0	30.0
147	49.0	26.0	25.0
148	49.9	27.6	22.5
149	50.0	30.0	20.0
150	49.0	33.5	17.5
151	47.5	37.5	15.0
152	45.0	42.5	12.5
153	41.5	48.5	10.0
154	36.5	56.0	7.5
155	30.0	65.0	5.0
156	21.5	76.0	2.5
157	0.0	100.0	0.0

Curve 8

158	0.0	0.0	100.0
159	3.0	2.0	95.0
160	5.8	4.2	90.0
161	12.5	7.5	80.0
162	19.0	11.0	70.0
163	26.0	14.0	60.0
164	29.0	16.0	55.0
227	0	0.0	100.0
228	2	3.0	95.0
229	4.9	5.1	90.0
230	10	10.0	80.0
231	16	14.0	70.0
232	21.5	18.5	60.0
233	25	20.0	55.0
234	27.5	22.5	50.0
235	30	25.0	45.0
236	33	27.0	40.0
237	36	29.0	35.0
238	38	32.0	30.0
239	39	36.0	25.0
240	38	39.5	22.5
241	37	43.0	20.0
242	35	47.5	17.5
243	32.5	52.5	15.0
244	29	58.5	12.5
245	26	64.0	10.0
246	22.5	70.0	7.5
247	18	77.0	5.0
248	12	85.5	2.5
249	0	100.0	0.0

Curve 12

250	0	0.0	100.0
251	2	3.0	95.0
252	4.5	5.5	90.0
253	9.4	10.6	80.0

76	51.5	18.5	30.0	**165**	32.3	17.7	50.0	**254**	15	15.0	70.0
77	54.0	21.0	25.0	**166**	35.0	20.0	45.0	**255**	20	20.0	60.0
78	55.0	22.5	22.5	**167**	39.0	21.0	40.0	**256**	22.5	22.5	55.0
79	56.5	23.5	20.0	**168**	42.4	22.6	35.0	**257**	25.5	24.5	50.0
80	56.7	25.8	17.5	**169**	45.5	24.5	30.0	**258**	27.5	27.5	45.0
81	56.0	29.0	15.0	**170**	48.0	27.0	25.0	**259**	30	30.0	40.0
82	54.0	33.5	12.5	**171**	48.5	29.0	22.5	**260**	32	33.0	35.0
83	51.5	38.5	10.0	**172**	48.0	32.0	20.0	**261**	33.5	36.5	30.0
84	47.3	45.3	7.5	**173**	47.7	34.8	17.5	**262**	34	41.0	25.0
85	41.0	54.0	5.0	**174**	45.0	40.0	15.0	**263**	33.5	44.0	22.5
86	31.0	66.5	2.5	**175**	42.5	45.0	12.5	**264**	32	48.0	20.0
87	0.0	100.0	0.0	**176**	37.5	52.5	10.0	**265**	30.5	52.0	17.5
				177	33.0	59.5	7.5	**266**	28	57.0	15.0
				178	26.5	68.5	5.0	**267**	27	60.5	12.5
		Curve 5		**179**	18.0	79.5	2.5	**268**	23	67.0	10.0
88	0.0	0.0	100.0	**180**	0.0	100.0	0.0	**269**	20	72.5	7.5
89	3.5	1.5	95.0					**270**	16	79.0	5.0
90	7.0	3.0	90.0					**271**	10	87.5	2.5
91	15.0	5.0	80.0					**272**	0	100.0	0.0
92	22.3	7.7	70.0								

Table A.2: Percentage of ternary components that show the effect of ultrasonication in enhancing blending

Sample No	Ternary components (%)			Sample No	Ternary components (%)		
	ethanol	water	petrol		ethanol	water	petrol
	None sonicated binodal curve				Sonicated binodal curve		
1	0	0	100	20	0.0	0.0	100.0
2	10	1.75	88.25	21	3.5	1.5	95.0
3	17	3	80	22	7.3	2.8	90.0
4	20	3.5	76.5	23	15.7	4.3	80.0
5	30	5	65	24	22.8	7.2	70.0
6	40	7	53	25	30.5	9.5	60.0
7	50	11	39	26	34.5	10.5	55.0
8	60.0	16.5	23.5	27	37.7	12.3	50.0
9	62.0	18.0	20.0	28	41.7	13.3	45.0
10	63.0	24.0	13.0	29	45.5	14.5	40.0
11	62.0	28.0	10.0	30	48.0	17.0	35.0
12	60.0	32.5	7.5	31	51.5	18.5	30.0
13	55.0	40.0	5.0	32	54.0	21.0	25.0
14	51.5	47.0	1.5	33	55.5	23.0	21.5
15	41.5	57.5	1.0	34	58.5	22.0	19.5
16	31.0	68.2	0.8	35	59.0	24.0	17.0
17	20.4	79.0	0.6	36	58.4	26.6	15.0
18	10.1	89.5	0.4	37	54.0	33.5	12.5
19	0.0	100.0	0.0	38	51.5	41.0	7.5
				39	47.5	48.5	4.0
				40	41.0	57.8	1.2
				41	31.0	68.1	0.9
				42	0.0	100.0	0.0

Appendix B: Dehydration of bioethanol by ultrasonication-enhanced adsorption

B.1 Amount of Silica required for the adsorption of water

As a basis for the experiment the amount of silica gel required to remove water was measured based on literature. (Sorbent systems, 2006) stated that the adsorption capacity of silica gel on water was 40% of the mass of the silica, thus the silica gel could adsorb up to 40% of its own mass. Assuming a 30ml solution was to be used the mass of silica was calculated based on the adsorptive capacity of 40% as follows;

Assume:

- 100% adsorption of water
- Density of water is 1g/ml at standard temperature and pressure, given that of silica gel is 2.2g/ml

By applying a mass balance over a batch system of 30ml solution at concentration of 85% volume ethanol, the mass of the water can be calculated as follows;

$$(0.15)(Volume\ of\ solution)(\rho_{water}) = \dot{m}_{water\ to\ be\ adsorbed}$$

$$(0.15)(30ml)(1g/ml) = \dot{m}_{water\ to\ be\ adsorbed}$$

$$\dot{m}_{water\ to\ be\ adsorbed} = 4.5g\ of\ water$$

This is the water that is to be adsorbed onto silica-gel, which is equivalent to the 40% of the dry mass of silica-gel. By applying the mass balance over the batch system, the mass of the silica gel could be calculated.

$$m_{water} + m_{silica\ gel} = m_{silica-gel\ and\ adsorbed\ water}$$

But it is given that the mass of water adsorbed accounts for 40% of mass of the dry silica-gel the above equation can be written as follows assuming all the water is adsorbed;

$$4.5g = (0.4)m_{silica\ gel}$$

$(0.4)m_{silica\ gel} = \frac{4.5}{0.4} = 11.25g$, it was done similarly for all other concentrations.

B.2 Ethanol Concentration calculations

The solutions where analysed using High Pressure Liquid Chromatography (HPLC) in order to detect and quantify the amount of water and ethanol in each sample. The samples were diluted, in a ratio of 1:2 (sample: dilatant) using methanol, which was also used as the mobile phase, in order to give a clearer distinction between the ethanol and water peaks.

The concentration results given by the HPLC were relative to the sample with units given as g/l, and had to be converted to volumetric concentrations using the densities of the liquids.

Example calculation, given from HPLC results;

Table B.1: concentrations of both ethanol and water obtained from the HPLC

Water (g/l)	Ethanol(g/l)
58.04	364.21

By dividing by 1000ml/l (conversion factor) then multiplying by the volume of sample and dividing by their individual densities the volumetric amounts of ethanol in the sample were calculated as follows;

Table B.2: Volume of the sample with the concentrations of ethanol and water

Volume of sample (ml)		0.5
density (g/ml)	ethanol	0.79
	water	1

$$Volume_{water} = (Conc._{HPLC}) \left(\frac{1000ml}{l}\right)^{-1} (Volume_{sample})(density\ (\frac{g}{ml}))^{-1}$$

$$Volume_{water} = (58.04\ (\frac{g}{l})) \left(\frac{1000ml}{l}\right)^{-1} (0.5ml)(1\ (\frac{g}{ml}))^{-1}$$

$$Volume_{water} = 0.03ml$$

Similarly the amount of ethanol which would represent the same concentration as that given by the sample from the HPLC was found, to be 0.24ml, thus giving a combined total volume of 27ml.

The volume concentration was then calculated by dividing the volume of ethanol/water by the total volume as follows: $Conc. = \frac{0.03ml}{27ml} = 0.09\ (9\%) water\ and\ 0.91\ (91\%) ethanol.$

B.3 Concentrations of ethanol using ultrasonicator from the readings obtained from the HPLC

Table B.3: Concentrations of ethanol using ultrasonicator

Initial concentration of 85% vol.												
				Concentration							**Concentration**	
		reading		**(g/ml)**		**mass**		**Volume**			**(vol. %)**	
Sample												
No.	**time**	**water**	**ethanol**	**water**	**ethanol**	**water**	**ethanol**	**water**	**ethanol**	**total**	**water**	**ethanol**
	0										0.15	0.85
1	5	50.36		0.05	0.38	0.03	0.19	0.03	0.24	0.27	0.09	0.91
2	10	58.04	364.21	0.06	0.36	0.03	0.18	0.03	0.23	0.26	0.11	0.89
3	15	50.36	383.79	0.05	0.38	0.03	0.19	0.03	0.24	0.27	0.09	0.91
4	20	90.01	563.63	0.09	0.56	0.05	0.28	0.05	0.36	0.40	0.11	0.89
5	25	49.95	347.57	0.05	0.35	0.02	0.17	0.02	0.22	0.24	0.10	0.90
6	30	50.49	377.79	0.05	0.38	0.03	0.19	0.03	0.24	0.26	0.10	0.90
	0											0.85
7	5	54.02	389.09	0.05	0.39	0.03	0.19	0.03	0.25	0.27	0.10	0.90
8	10	53.84	370.25	0.05	0.37	0.03	0.19	0.03	0.23	0.26	0.10	0.90
9	15	84.95	573.72	0.08	0.57	0.04	0.29	0.04	0.36	0.41	0.10	0.90
10	20	56.33	404.66	0.06	0.40	0.03	0.20	0.03	0.26	0.28	0.10	0.90
11	25	62.72	397.67	0.06	0.40	0.03	0.20	0.03	0.25	0.28	0.11	0.89

12	30	55.46	395.40	0.06	0.40	0.03	0.20	0.03	0.25	0.28	0.10	0.90
	0											0.85
13	5	55.71	367.86	0.06	0.37	0.03	0.18	0.03	0.23	0.26	0.11	0.89
14	10	48.81	355.23	0.05	0.36	0.02	0.18	0.02	0.22	0.25	0.10	0.90
15	15	57.60	384.08	0.06	0.38	0.03	0.19	0.03	0.24	0.27	0.11	0.89
16	20	61.49	387.77	0.06	0.39	0.03	0.19	0.03	0.25	0.28	0.11	0.89
17	25	71.73	370.88	0.07	0.37	0.04	0.19	0.04	0.23	0.27	0.13	0.90005
18	30	48.55	374.96	0.05	0.37	0.02	0.19	0.02	0.24	0.26	0.09	0.91
	0											0.85
19	5	65.72	423.49	0.07	0.42	0.03	0.21	0.03	0.27	0.30	0.11	0.89
20	10	53.11	358.57	0.05	0.36	0.03	0.18	0.03	0.23	0.25	0.10	0.90
21	15	58.76	407.59	0.06	0.41	0.03	0.20	0.03	0.26	0.29	0.10	0.90
22	20	61.42	408.26	0.06	0.41	0.03	0.20	0.03	0.26	0.29	0.11	0.89
23	25	57.05	349.51	0.06	0.35	0.03	0.17	0.03	0.22	0.25	0.11	0.89
24	30	67.00	371.68	0.07	0.37	0.03	0.19	0.03	0.24	0.27	0.12	0.88

B.3 Relative amount of water adsorbed

The amount of water adsorbed was calculated as the difference between the initial concentration and the concentration at each time interval. This gave the actual change in amount of water from the start till that point in time. This was then represented as a percentage in order to eliminate the varying water concentrations between the solutions.

$$relative\ amount = \frac{Conc._{initial} - Conc._{t}}{Conc._{Initial}}$$

$$relative\ amount = \frac{0.15 - 0.03}{0.15}$$

$$relative\ amount = 0.056082\ (37\%)$$

This shows the amount of water that has been removed relative to the amount which was there.

B.4 Adsorption Capacity Calculations

The adsorption capacity of an adsorbent, silica gel in this case, can be expressed as $Q_t = \frac{m_{adsorbed}}{m_{adsorbent}}$, thus by using the amount of silica gel used and the amount of water adsorbed onto the surface. Using the above concentrations of the 85% initial concentration experiments as an example this is how adsorptive capacity was calculated

$$Q_t = \frac{m_{adsorbed}}{m_{adsorbent}}$$

$$Q_t = \frac{(Conc._{initial} - Conc._{final})(vol._{solution})(\rho_{water})}{m_{silica\ at\ 85\%\ initial\ Conc.}}$$

$$Q_t = \frac{(0.15 - 0.03)(100ml)(1g/ml)}{11.25g}$$

$Q_t = 0.499$, similary it was done for all other experiments.

B.5 Effect of Temperature on Kinematic Viscosity

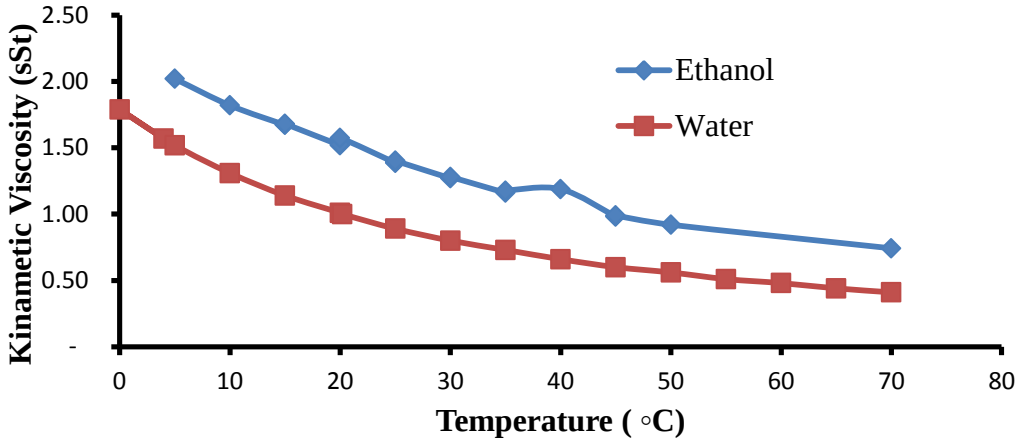

Figure B.1: Influence of temperature on kinematic viscosity

Table B.4: Viscosity calculations at initial concentration and final concentrations

	Viscosity			Viscosity	
Temperature	**ethanol**	**water**	**Temperature**	**ethanol**	**water**
5	2.0205	1.57	25	1.387	0.8
10	1.82	1.79	25	1.3913	0.73
15	1.6724	1.52	25	1.3965	0.66
15	1.676	1.31	25	1.4023	0.6
15	1.6812	1.14	30	1.27	0.56
20	1.519	1.01	30	1.28	0.51
20	1.527	1	35	1.1616	0.48
20	1.574	0.89	35	1.176	0.44

B.6 Raman spectrum

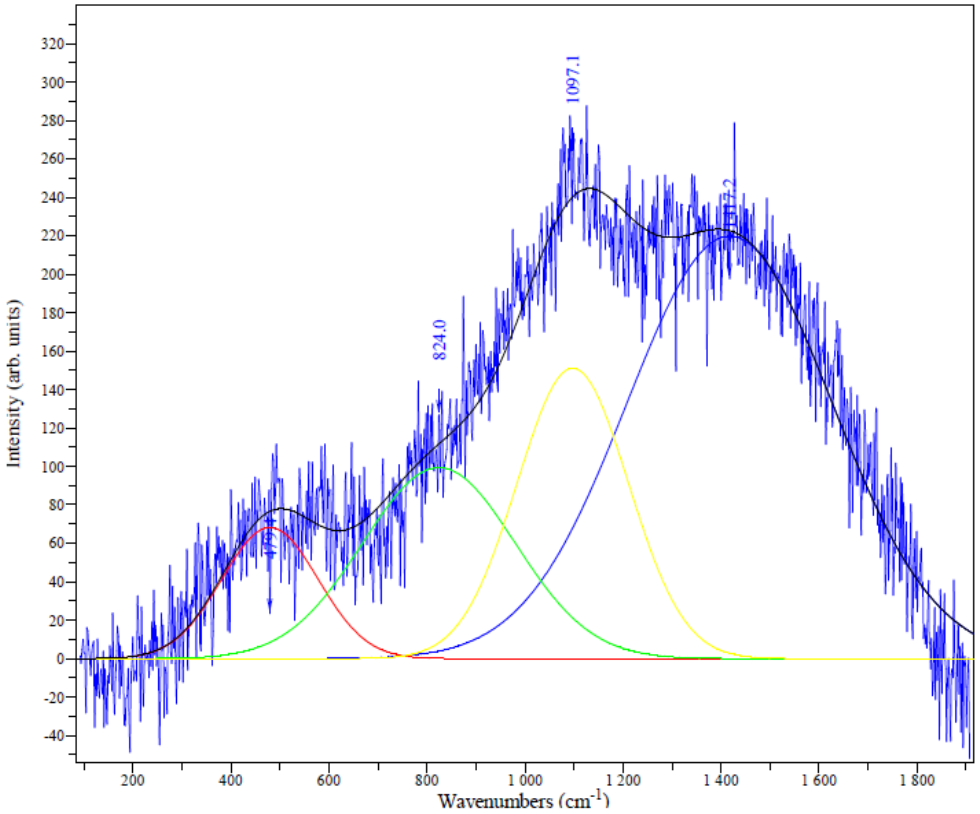

Silica gel Raman spectrum before the experiment

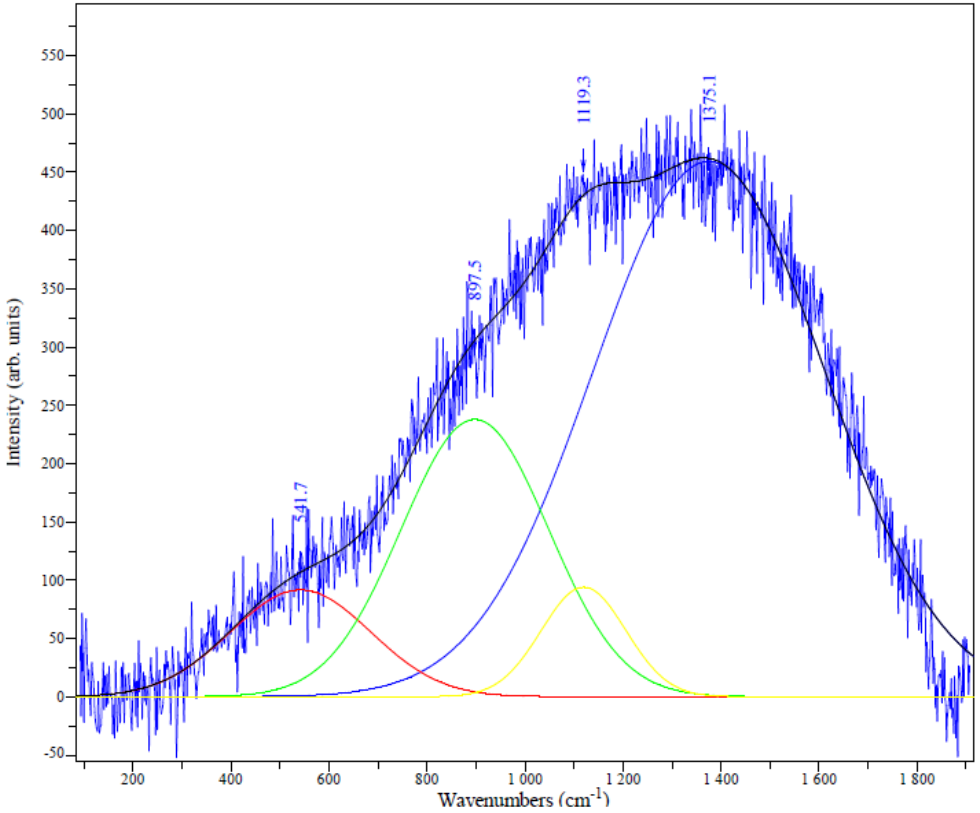

Silica gel Raman spectrum after the experiment

Figure B.2: The Raman spectrum of silica gel before and after the experiment

Table B.8: Calculation of model constants

	m	1/Vo	Vo	q[e]	K
85(0.5 Pulse Rate; 50% Amp.)	2.233	2.126	0.470	0.448	2.345
85(0.5 Pulse Rate; 100 % Amp.)	2.451	-0.298	-3.351	0.408	-20.139
85(1 Pulse Rate; 50% Amp.)	3.639	-4.433	-0.226	0.275	-2.988
85(1 Pulse Rate; 100% Amp.)	3.970	-11.376	-0.088	0.252	-1.385

Appendix C

C.1 Pressure profile

C.1.1 Horizontal variation of pressure with distance at different time

Table C.1.1: Horizontal variation of pressure with distance for E30

30% ethanol horizontal						
	Pressure(KPa)					
Distance	**60sec**	**120sec**	**180sec**	**240sec**	**300sec**	**360sec**
1 cm	102.3622	118.1102	125.9843	125.9843	133.8583	141.7323
2 cm	94.48819	110.2362	110.2362	110.2362	118.1102	125.9843
3 cm	86.61417	102.3622	102.3622	102.3622	102.3622	102.3622
4 cm	70.86614	78.74016	86.61417	86.61417	94.48819	94.48819

Table C.1.1 above gives the data for a 30 % ethanol mixture and this data was plotted to give a graph of pressure variation with distance at specific sonication times as shown in the figures discussed in the results and discussions.

Table C.1.2: Horizontal variation of pressure with distance for E20

20% ethanol horizontal						
	Pressure(KPa)					
Distance	**60sec**	**120sec**	**180sec**	**240sec**	**300sec**	**360sec**
1 cm	86.61417	102.3622	110.2362	118.1102	118.1102	118.1102
2 cm	62.99213	94.48819	102.3622	102.3622	102.3622	102.3622
3 cm	55.11811	78.74016	86.61417	94.48819	94.48819	94.48819
4 cm	39.37008	62.99213	70.86614	70.86614	78.74016	78.74016

Table C.1.2 above gives the data that was plotted for the pressure profile at different position for 20% ethanol blend.

Table C.1.3: Horizontal variation of pressure with distance for E10

10% ethanol horizontal						
	Pressure (KPa)					
Distance	**60sec**	**120sec**	**180sec**	**240sec**	**300sec**	**360sec**
1 cm	110.2362	94.48819	102.3622	110.2362	110.2362	110.2362
2 cm	86.61417	86.61417	94.48819	86.61417	94.48819	94.48819
3 cm	78.74016	70.86614	78.74016	78.74016	78.74016	78.74016
4 cm	55.11811	55.11811	55.11811	55.11811	70.86614	70.86614

Table C.1.3 above gives the data for the 10 % ethanol blend and this data was plotted to give the pressure profile at different position.

C.1.2 Horizontal variation of pressure with time at different position

Table C.1.4: Horizontal variation of pressure with time for E30

30% ethanol				
	Pressure(KPa)			
Time (sec)	**1cm**	**2cm**	**3cm**	**4cm**
60	102.3622	94.48819	86.61417	70.86614
120	118.1102	110.2362	102.3622	78.74016
180	125.9843	110.2362	102.3622	86.61417
240	125.9843	110.2362	102.3622	86.61417
300	133.8583	118.1102	102.3622	94.48819
360	141.7323	125.9843	102.3622	94.48819

Table C.1.4 above gives the data that was plotted for the 30% mixtures and this graph showing this relationship between the pressure and time at different position.

Table C.1.5: Horizontal variation of pressure with time for E20

20% ethanol				
	Pressure(KPa)			
Time (sec)	**1cm**	**2cm**	**3cm**	**4cm**
60	86.61417	62.99213	55.11811	39.37008
120	102.3622	94.48819	78.74016	62.99213
180	110.2362	102.3622	86.61417	70.86614
240	118.1102	102.3622	94.48819	70.86614
300	118.1102	102.3622	94.48819	78.74016
360	118.1102	102.3622	94.48819	78.74016

Table C.1.5 above gives the data that was plotted for the pressure profile with time at different position for 20% ethanol blend.

Table C.1.6: Horizontal variation of pressure with time for E10

10% ethanol				
	Pressure(KPa)			
Time (sec)	1cm	2cm	3cm	4cm
60	110.2362	86.61417	78.74016	55.11811
120	94.48819	86.61417	70.86614	55.11811
180	102.3622	94.48819	78.74016	55.11811
240	110.2362	86.61417	78.74016	55.11811
300	110.2362	94.48819	78.74016	70.86614
360	110.2362	94.48819	78.74016	70.86614

Table C.1.6 above gives the data for a 10% ethanol-petrol blends which was plotted to give the pressure profile with time at different position.

C.1.3 Vertical variation of pressure with distance at different time

The following data was used to plot the vertical pressure profile with distance at different times for E10, E20 and E30.

Table C.1.7: Vertical variation of pressure with distance for E10

10% ethanol vertical						
			Pressure (kPa)			
Distance (cm)	60 sec	120 sec	180 sec	240 sec	300 sec	360 sec
1	70.86614	94.48819	110.2362	118.1102	125.9843	125.9843
2	47.24409	78.74016	78.74016	78.74016	94.48819	94.48819
3	31.49606	55.11811	55.11811	62.99213	62.99213	62.99213
4	23.62205	47.24409	47.244094	55.11811	55.11811	55.11811

Table C.1.8: Vertical variation of pressure with distance for E20

20% ethanol vertical						
			Pressure (kPa)			
Distance (cm)	60 sec	120 sec	180 sec	240 sec	300 sec	360 sec
1	78.74016	102.3622	125.9843	125.9843	133.8583	141.7323
2	70.86614	86.61417	94.48819	102.3622	110.2362	118.1102
3	39.37008	62.99213	62.99213	70.86614	70.86614	70.86614
4	23.62205	55.11811	55.11811	55.11811	55.11811	55.11811

Table C.1.9: Vertical variation of pressure with distance for E30

30% ethanol vertical						
			Pressure (kPa)			
Distance (cm)	**60 sec**	**120 sec**	**180 sec**	**240 sec**	**300 sec**	**360 sec**
1	86.61417	110.2362	133.8583	141.7323	149.6063	149.6063
2	78.74016	102.3622	102.3622	110.2362	118.1102	125.9843
3	55.11811	86.61417	86.61417	94.48819	94.48819	110.2362
4	47.24409	70.86614	78.740157	86.61417	86.61417	94.48819

C.1.4 Vertical variation of pressure with time at different position

The following data was used to plot the pressure profile with time for different ethanol-petrol blends at different position.

Table C.1.10: Vertical variation of pressure with time for E10

10% ethanol				
	Pressure (kPa)			
Time (sec)	**1cm**	**2cm**	**3cm**	**4cm**
60	70.86614	47.24409	31.49606	23.62205
120	94.48819	78.74016	55.11811	47.24409
180	110.2362	78.74016	55.11811	47.24409
240	118.1102	78.74016	62.99213	55.11811
300	125.9843	94.48819	62.99213	55.11811
360	125.9843	94.48819	62.99213	55.11811

Table C.1.11: Vertical variation of pressure with time for E20

20% ethanol				
	Pressure (kPa)			
Time (sec)	**1cm**	**2cm**	**3cm**	**4cm**
60	78.74016	70.86614	39.37008	23.62205
120	102.3622	86.61417	62.99213	55.11811
180	125.9843	94.48819	62.99213	55.11811
240	125.9843	102.3622	70.86614	55.11811
300	133.8583	110.2362	70.86614	55.11811
360	141.7323	118.1102	70.86614	55.11811

Table C.1.12: Vertical variation of pressure with time for E30

30% ethanol				
	Pressure (kPa)			
time (sec)	1cm	2cm	3cm	4cm
60	86.61417	78.74016	55.11811	47.24409
120	110.2362	102.3622	86.61417	70.86614
180	133.8583	102.3622	86.61417	78.74016
240	141.7323	110.2362	94.48819	86.61417
300	149.6063	118.1102	94.48819	86.61417
360	149.6063	125.9843	110.2362	94.48819

C.2 Temperature profile

C.2.1 Horizontal variation of temperature with distance at different time

Table C.2.1: Horizontal variation of temperature with distance for E30

30 vol% ethanol						
			Temperature(^{0}C)			
Distance (cm)	60 sec	120 sec	180 sec	240 sec	300 sec	360 sec
1	28	31	34	36	38	39.5
2	27.5	30	33	35	36.5	38
3	30	32	34	36	38	40
4	29	30	32	35	38	39

Table C.2.1 above gives the data of the temperature variation with the horizontal distance for E30. This data was plotted to give the horizontal temperature profile at different positions and at different times.

Table C.2.2: Horizontal variation of temperature with distance for E20

20 vol% ethanol						
			Temperature(^{0}C)			
Distance (cm)	60 sec	120 sec	180 sec	240 sec	300 sec	360 sec
1	27	30	33.5	35.5	37	39
2	26	28	32	35	36	37.5
3	28	32	34	36	37.5	39
4	26	30	32	35	37	38

Table C.2.2 above gives the data for a 20 % ethanol mixture and this data was plotted to give the relationship between the temperature in the reactor and the horizontal distance from the horn.

Table C.2.3: Horizontal variation of temperature with distance for E10

10 vol% ethanol						
			Temperature(^{0}C)			
Distance (cm)	**60 sec**	**120 sec**	**180 sec**	**240 sec**	**300 sec**	**360 sec**
1	27	28	33	35	36.5	38
2	24	26	30	32	34	36
3	26	29	32	34.5	36	37
4	24	29	31	34	36.5	37

Table C.2.3 above gives the data plotted to give the temperature profile for 10% ethanol.

C.2.2 Horizontal variation of temperature with time at different position

Table C.2.3: Horizontal variation of temperature with time for E30

30 vol% ethanol				
	Temperature (^{0}C)			
Time (sec)	1 cm	2 cm	3 cm	4 cm
60	28	27.5	30	29
120	31	30	32	30
180	34	33	34	32
240	36	35	36	35
300	38	36.5	38	38
360	39.5	38	40	39

Table C.2.3 above gives the `data for the variation of the temperature in the reactor with time for E30.

Table C.2.4: Horizontal variation of temperature with time for E20

30 vol% ethanol				
	Temperature (^{0}C)			
Time (sec)	1 cm	2 cm	3 cm	4 cm
60	27	26	28	26
120	30	28	32	30
180	33.5	32	34	32
240	35.5	35	36	35
300	37	36	37.5	37
360	39	37.5	39	38

Table C.2.4 above gives the data that was used to come up with the temperature profile in the reactor with time for E20.

Table C.2.5: Horizontal variation of temperature with time for E10

10 vol % ethanol				
	Temperature (^{0}C)			
Time (sec)	1 cm	2 cm	3 cm	4 cm
60	27	24	26	24
120	28	26	29	29
180	33	30	32	31
240	35	32	34.5	34
300	36.5	34	36	36.5
360	38	36	39	37

Table C.2.5 above gives the data that was used to plot the relationship between temperature and time in a 10% mixture.

C.2.3 Vertical variation of temperature with position at different time

The following data was used to plot the temperature profile with distance for different times in the reactor for different ethanol blends.

Table C.2.6: Vertical variation of temperature with position for E10

10 vol % ethanol						
	Temperature (^{0}C)					
Distance (cm)	**60 sec**	**120 sec**	**180 sec**	**240 sec**	**300 sec**	**360 sec**
1	27.5	31	33	36	38.5	40
2	26.5	28	30	34.5	35	37
3	25.5	26	28	32	32	35
4	22	24	25	28	30	32

Table C.2.7: Vertical variation of temperature with position for E20

20 vol% ethanol						
	Temperature (^{0}C)					
Distance (cm)	**60 sec**	**120 sec**	**180 sec**	**240 sec**	**300 sec**	**360 sec**
1	28	31.5	33.5	37	39	40
2	27.5	29	32	35	37	38
3	26	27	30	32.5	34	36
4	22.5	25	27	28.5	32	34

Table C.2.8: Vertical variation of temperature with position for E30

30 vol% ethanol						
	Temperature (^{0}C)					
Distance (cm)	**60 sec**	**120 sec**	**180 sec**	**240 sec**	**300 sec**	**360 sec**
1	29	33	34	37.5	40	40.5
2	28.5	30	33.5	35.5	37.5	38
3	27.5	28	31.5	33	35	36.5
4	25	25.5	28.5	30	33	35

C.2.4 Vertical variation of temperature with time at different position

The following data was used to plot the temperature profile with time for different ethanol-petrol blends and distance is presented below

Table C.2.9: Vertical variation of temperature with time at 1cm

1cm	Temperature (^{0}C)		
Time (sec)	**10 vol%**	**20 vol%**	**30 vol%**
60	27.5	28	29
120	31	31.5	33
180	33	33.5	34
240	36	37	37.5
300	38.5	39	40
360	40	40	40.5

Table C.2.10: Vertical variation of temperature with time at 2cm

2cm	Temperature (^{0}C)		
Time (sec)	**10 vol%**	**20 vol%**	**30 vol%**
60	26.5	27.5	28.5
120	28	29	30
180	30	32	33.5
240	34.5	35	35.5
300	35	37	37.5
360	37	38	38

Table C.2.11: Vertical variation of temperature with time at 3cm

3cm	Temperature (^{0}C)		
Time (sec)	**10 vol%**	**20 vol%**	**30 vol%**
60	25.5	26	27.5
120	26	27	28
180	28	30	31.5
240	32	32.5	33
300	32	34	35
360	35	36	36.5

Table C.2.12: Vertical variation of temperature with time at 4cm

4cm	Temperature (^{0}C)		
Time (sec)	**10 vol%**	**20 vol%**	**30 vol%**
60	22	22.5	25
120	24	25	25.5
180	25	27	28.5
240	28	28.5	30
300	30	32	33
360	32	34	35

C.3 Concentration profile

C.3.1 Horizontal variation of ethanol concentration with distance at different time

Table C.3.1: Horizontal variation of ethanol concentration with distance for E30

30 % ethanol(horizontal)						
	Concentration(g/L)					
Distance(cm)	**60sec**	**120sec**	**180sec**	**240sec**	**300sec**	**360sec**
1	162.2418	162.5444	167.1059	163.0219	165.4609	161.1366
2	164.2368	161.5726	165.1176	164.9237	167.102	159.3166
3	162.8189	162.8041	166.1176	165.4771	163.815	162.5257
4	165.5456	162.8204	164.5218	166.8342	166.5612	162.5259

Table C.3.1 gives the data for a 30 % ethanol mixture and thus this data was plotted to show the concentration profiles with horizontal distance.

Table C.3.2: Horizontal variation of ethanol concentration with distance for E20

20 % ethanol(horizontal)						
	Concentration(g/L)					
Distance(cm)	60sec	120sec	180sec	240sec	300sec	360sec
1	129.3081	130.9255	135.0105	132.6833	138.6904	137.1553
2	135.1375	130.3603	124.5252	133.6432	136.4754	133.1533
3	132.5938	134.9851	131.5383	137.4912	133.1785	134.3593
4	133.2884	132.5313	124.6966	135.0564	135.9352	132.8366

The above table gives the data of ethanol concentration in a 20% ethanol mixture at different sonication times and horizontal distance from the sonication horn.

Table C.3.3: Horizontal variation of ethanol concentration with distance for E10

10% ethanol(horizontal)						
	Concentration(g/L)					
Distance(cm)	60sec	120sec	180sec	240sec	300sec	360sec
1	4.96766	87.02344	89.92571	91.75116	89.61368	92.05339
2	90.86672	85.83117	92.06314	92.65269	90.4556	90.67527
3	89.08688	89.03055	87.95571	90.15207	88.53809	91.57969
4	90.78374	86.61147	89.85564	92.01336	91.77212	89.64076

Table C.3.3 above was used to plot the ethanol concentration data in a 10 % ethanol mixture of ethanol and petrol at different positions and times.

C.3.2 Horizontal variation of ethanol concentration with time at different position

Table C.3.4: Horizontal variation of ethanol concentration with time for E30

30% ethanol				
	Concentration (g/L)			
Time (sec)	1cm	2cm	3cm	4cm
60	162.2418	164.2368	162.8189	165.5456
120	162.5444	161.5726	162.8041	162.8204
180	167.1059	165.1176	166.1176	164.5218
240	163.0219	164.9237	165.4771	166.8342
300	165.4609	167.102	163.815	166.5612
360	161.1366	159.3166	162.5257	162.5259

Table C.3.4 above gives the data used to plot for the variation of ethanol concentration with time in a 30% ethanol mixture.

Table C.3.5: Horizontal variation of ethanol concentration with time for E20

20% ethanol				
	Concentration (g/L)			
Time (sec)	**1cm**	**2cm**	**3cm**	**4cm**
60	129.3081	135.1375	132.5938	133.2884
120	130.9255	130.3603	134.9851	132.5313
180	135.0105	124.5252	131.5383	124.6966
240	132.6833	133.6432	137.4912	135.0564
300	138.6904	136.4754	133.1785	135.9352
360	137.1553	133.1533	134.3593	132.8366

Table C.3.5 above gives the data used to plot the concentration profile for 20% ethanol-petrol blend.

Table C.3.6: Horizontal variation of ethanol concentration with time for E10

10% ethanol				
	Concentration (g/L)			
Time (sec)	**1cm**	**2cm**	**3cm**	**4cm**
60	4.96766	90.86672	89.08688	90.78374
120	87.02344	85.83117	89.03055	86.61147
180	89.92571	92.06314	87.95571	89.85564
240	91.75116	92.65269	90.15207	92.01336
300	89.61368	90.4556	88.53809	91.77212
360	92.05339	90.67527	91.57969	89.64076

Table C.3.6 above gives the data that was used to plot the relationship between ethanol concentrations with time in E10.

C.3.3 Vertical variation of ethanol concentration with position at different time

The following data was used to plot the concentration profile with distance for different times for different ethanol blends.

Table C.3.7: Vertical variation of ethanol concentration with position for E10

E10	Concentration (g/L)					
Distance	60 sec	120 sec	180 sec	240 sec	300 sec	360 sec
1 cm	95.15284	88.94209	94.27186	94.63677	90.15356	93.93143
2 cm	90.51039	87.5017	95.88538	92.31549	90.10341	91.26224
3 cm	94.67654	88.99639	94.22356	94.3785	91.25351	92.3222
4 cm	87.85585	88.51967	87.24617	86.37765	85.7189	88.18081

Table C.3.8: Vertical variation of ethanol concentration with position for E20

E20	Concentration (g/L)					
Distance	60 sec	120 sec	180 sec	240 sec	300 sec	360 sec
1 cm	136.16596	136.60641	138.03549	138.8186	138.3498	139.9149
2 cm	134.33341	135.27277	134.1232	136.5738	136.9077	136.9953
3 cm	137.11112	138.03582	138.61878	138.5328	138.0589	139.8697
4 cm	135.37317	138.0482	136.48179	137.5409	136.6613	137.0741

Table C.3.9: Vertical variation of ethanol concentration with position for E30

E30	Concentration (g/L)					
Distance	60 sec	120 sec	180 sec	240 sec	300 sec	360 sec
1 cm	171.18605	169.932794	167.8434	171.2918	170.8465	171.7805
2 cm	168.17846	167.52382	164.24318	168.3043	165.3645	165.9089
3 cm	172.96838	171.45747	172.61268	172.0844	169.2246	173.0986
4 cm	172.22127	170.5812	170.95922	171.2996	174.983	172.3839

C.3.4 Vertical variation of ethanol concentration with time

The following data was used to plot the concentration profile with time for different ethanol-petrol blends and distance is presented below.

Table C.3.10: Vertical variation of ethanol concentration with time at 1 cm

1cm	Concentration (g/L)		
Time (sec)	10 vol%	20 vol%	30 vol%
60	95.15284	136.16596	171.18605
120	88.94209	136.60641	169.932794
180	94.27186	138.03549	167.8434
240	94.63677	138.8186	171.2918
300	90.15356	138.34979	170.84648
360	93.93143	139.91493	171.78053

Table C.3.11: Vertical variation of ethanol concentration with time at 2 cm

2cm	Concentration (g/L)		
Time (sec)	10 vol%	20 vol%	30 vol%
60	90.51039	134.33341	168.17846
120	87.5017	135.27277	167.52382
180	95.88538	134.1232	164.24318
240	92.31549	136.57379	168.30431
300	90.10341	136.9077	165.36453
360	91.26224	136.99533	165.9089

Table C.3.12: Vertical variation of ethanol concentration with time at 3 cm

3cm	Concentration (g/L)		
Time (sec)	10 vol%	20 vol%	30 vol%
60	94.67654	137.11112	172.96838
120	88.99639	138.03582	171.45747
180	94.22356	138.61878	172.61268
240	94.3785	138.53275	172.08436
300	91.25351	138.05886	169.22462
360	92.3222	139.86971	173.09858

Table C.3.13: Vertical variation of ethanol concentration with time at 4 cm

4 cm	Concentration (g/L)		
Time (sec)	10 vol%	20 vol%	30 vol%
60	87.85585	135.37317	172.22127
120	88.51967	138.0482	170.5812
180	87.24617	136.48179	170.95922
240	86.37765	137.54092	171.29961
300	85.7189	136.6613	174.98301
360	88.18081	137.07408	172.38394

C.4 Horizontal and vertical pressure profile

Figure C.1 to C.6 below gives the pressure variation with time comparison graphs at positions of 2cm to 4cm from the ultrasonicator horn.

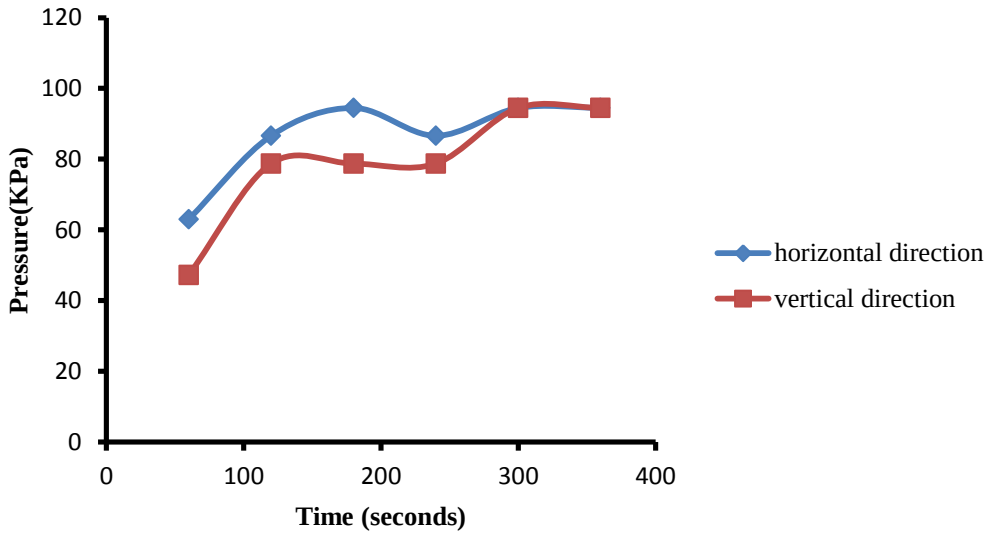

Figure C.1: Variation of pressure with time in both directions (E10 at 2 cm)

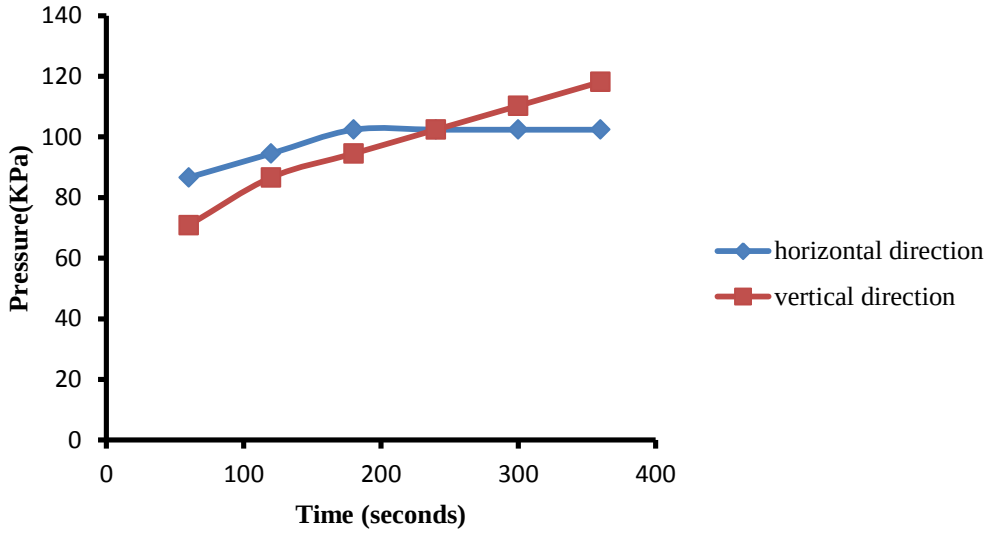

Figure C.2: Variation of pressure with time in both directions (E20 at 2 cm)

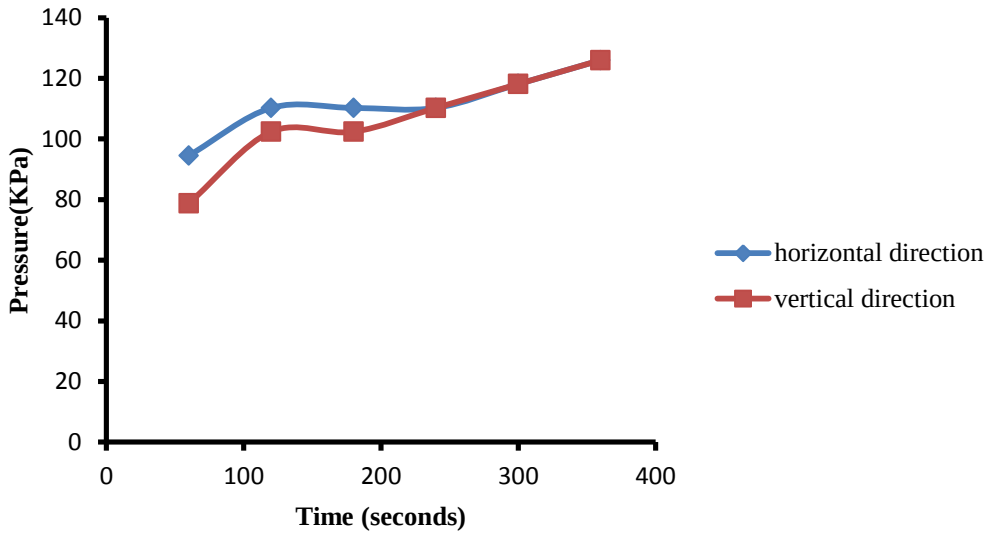

Figure C.3: Variation of pressure with time in both directions (E30 at 2 cm)

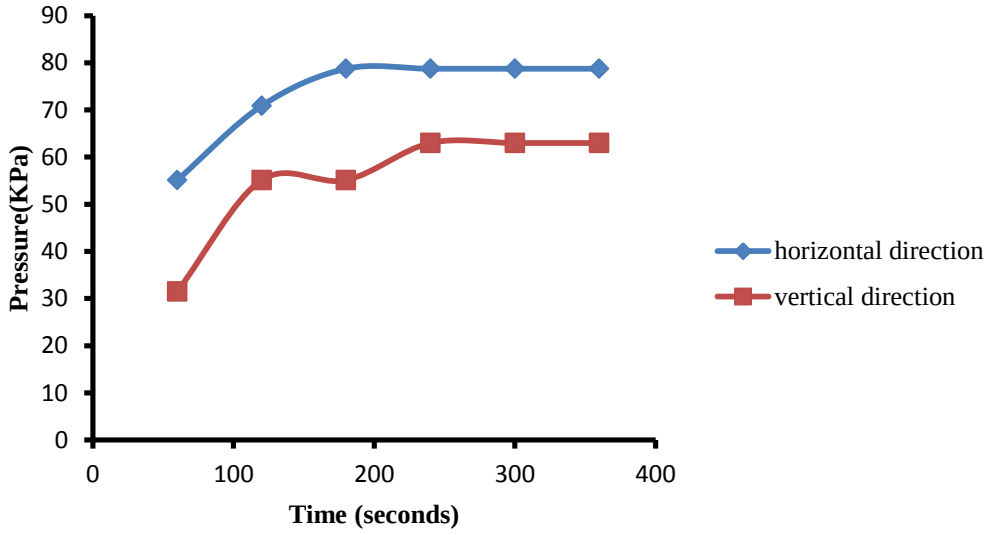

Figure C.4: Variation of pressure with time in both directions (E10 at 3 cm)

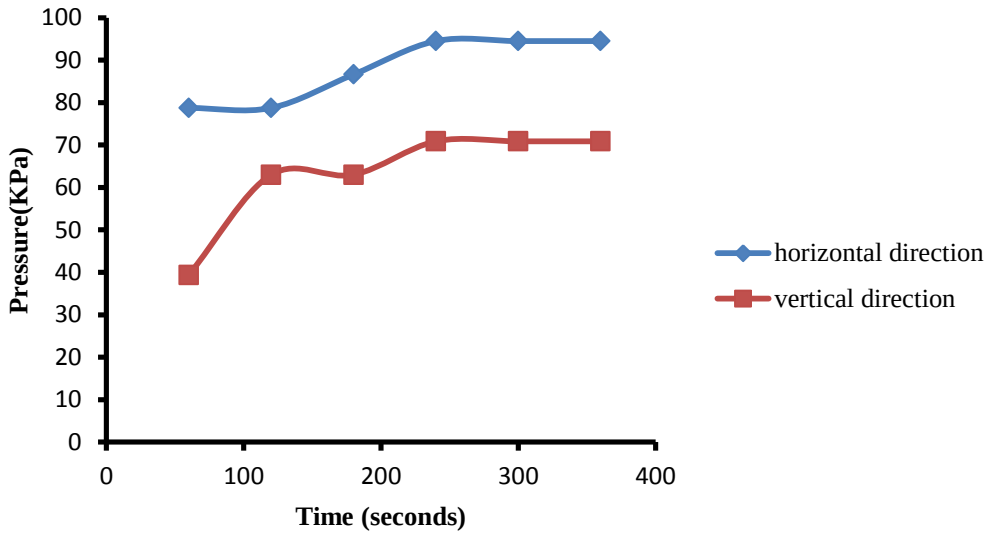

Figure C.5: Variation of pressure with time in both directions (E20 at 3 cm)

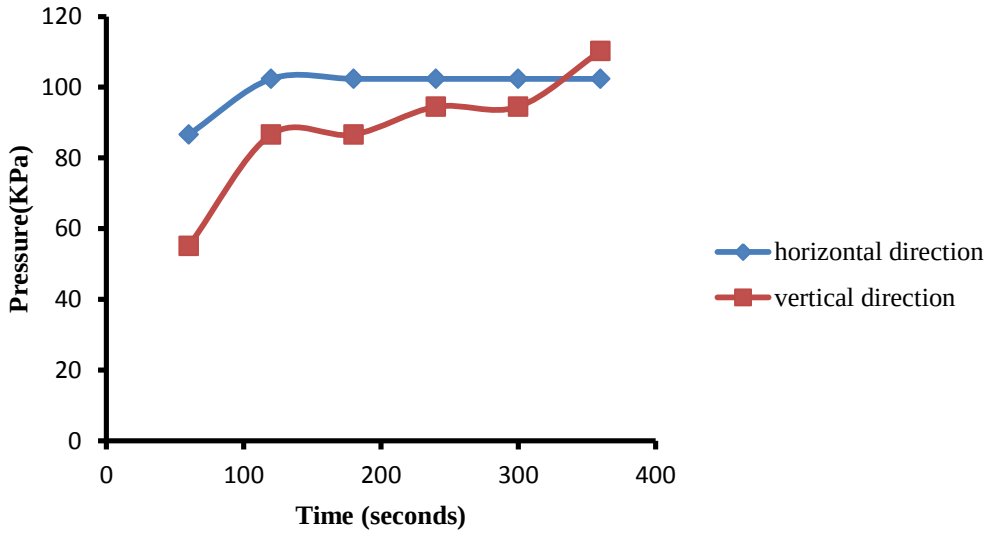

Figure C.6: Variation of pressure with time in both directions (E30 at 3 cm)

C.5 Horizontal and vertical Concentration profile

C.5.1 Horizontal and vertical Concentration profile with distance

Figures C.7 to C.9 below give the comparison for the variation of concentration with distance at different ultrasonication times.

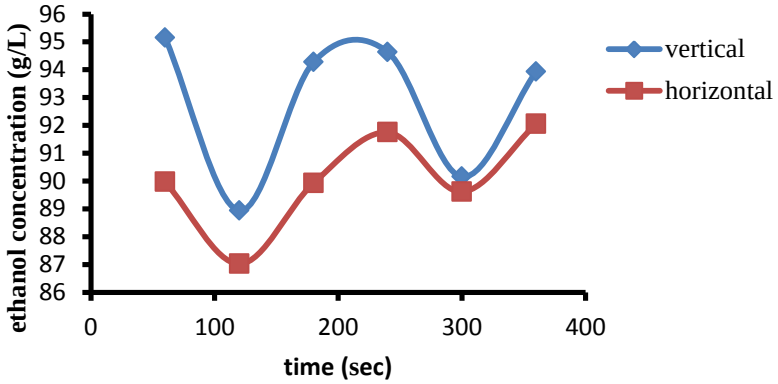

Figure C.7: Variation of concentration with time in both directions for E10 at 1 cm

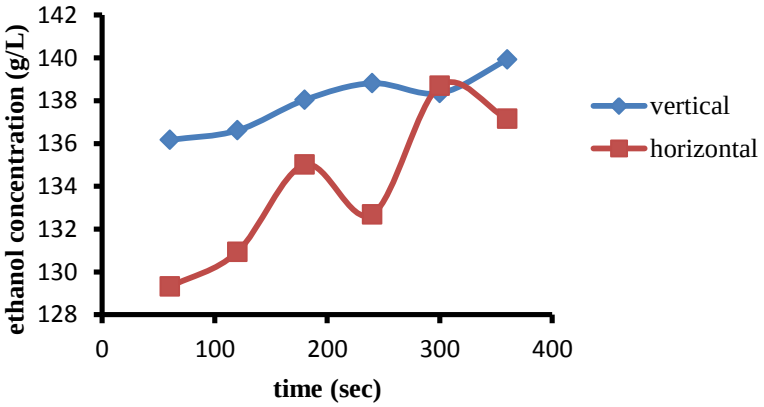

Figure C.8: Variation of concentration with time in both directions for E20 at 1 cm

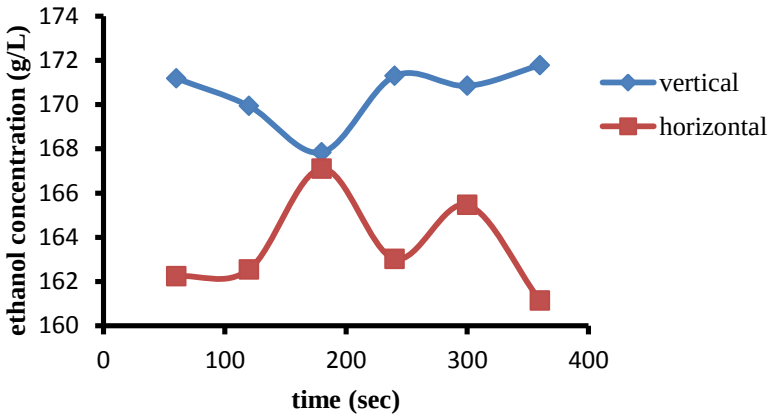

Figure C.9: Variation of concentration with time in both directions for E30 at 1 cm

Figures C.10 to C.13 below show the concentration variation with time in both directions for different at 2 cm

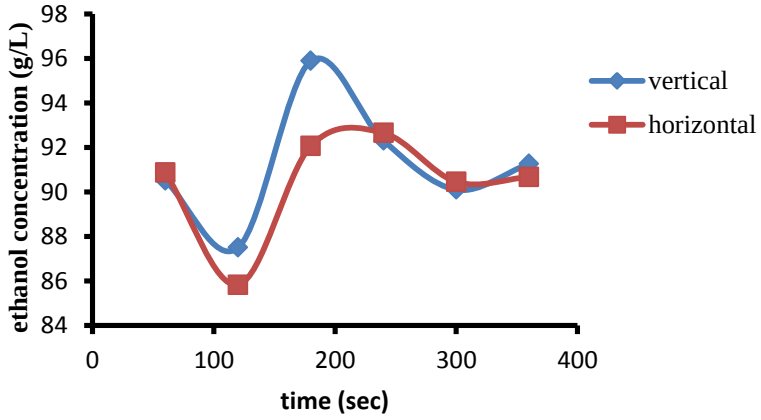

Figure C.10: Variation of concentration with time in both directions for E10 at 2 cm

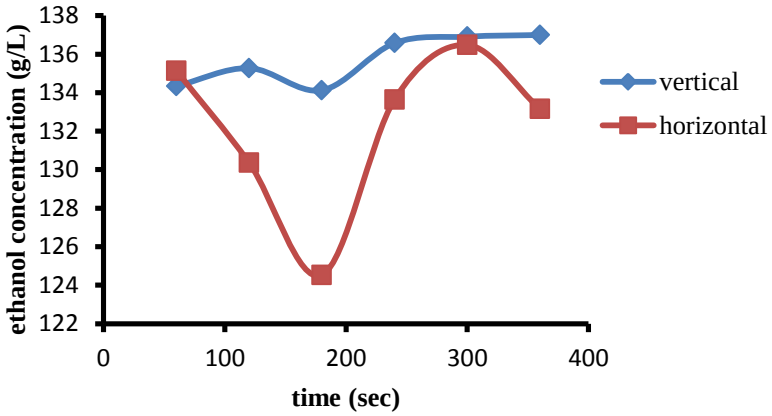

Figure C.11: Variation of concentration with time in both directions for E20 at 2 cm

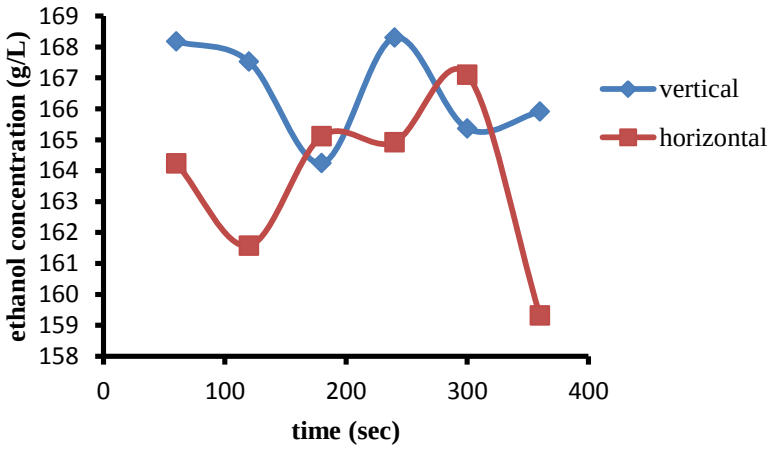

Figure C.12: Variation of concentration with time in both directions for E30 at 2 cm

Figures C.13 to C.15 below show the concentration variation with time in both directions for different at 3 cm

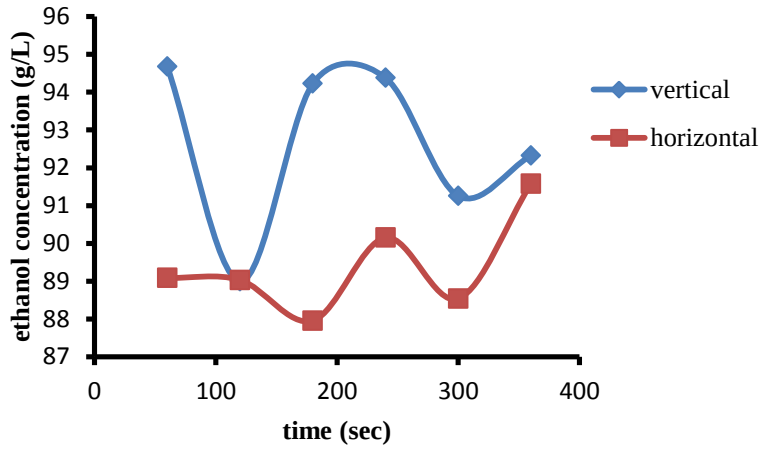

Figure C.13: Variation of concentration with time in both directions for E10 at 3 cm

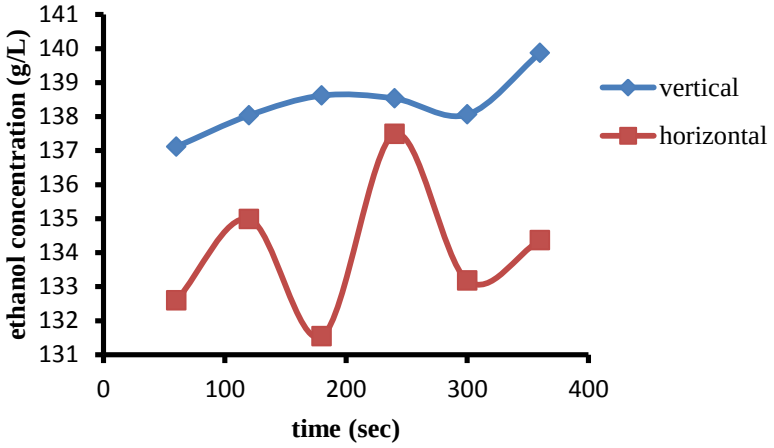

Figure C.14: Variation of concentration with time in both directions for E20 at 3 cm

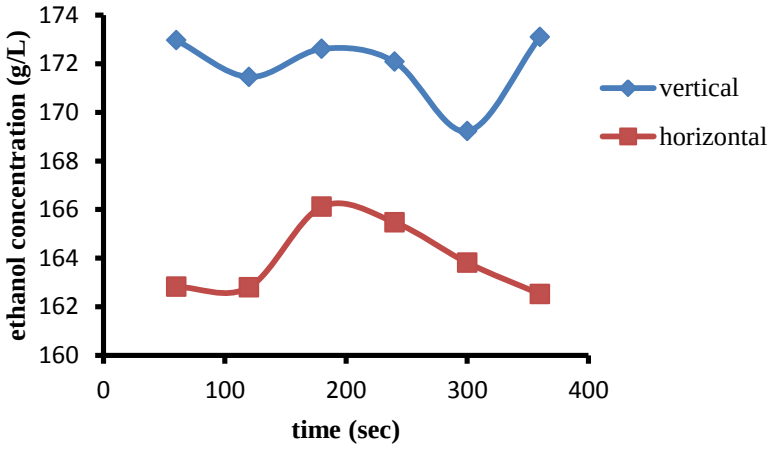

Figure C.15: Variation of concentration with time in both directions E30 at 3 cm

Figures C.16 to C.18 below show the concentration variation with time in both directions for different at 4cm

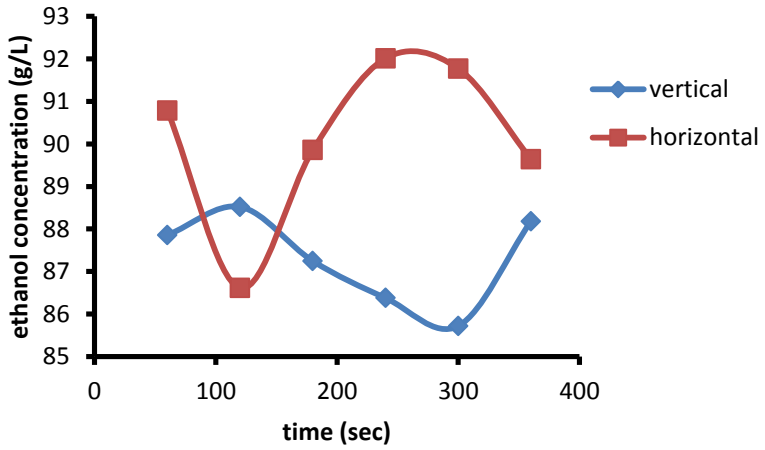

Figure C.16: Variation of concentration with time in both directions for E10 at 4 cm

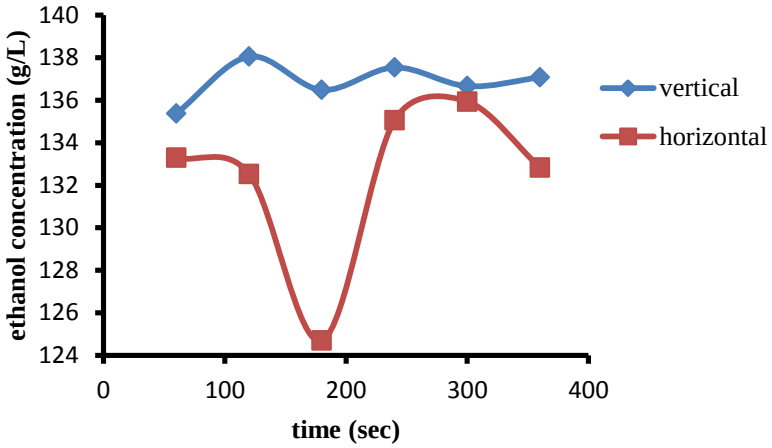

Figure C.17: Variation of concentration with time in both directions for E20 at 4 cm

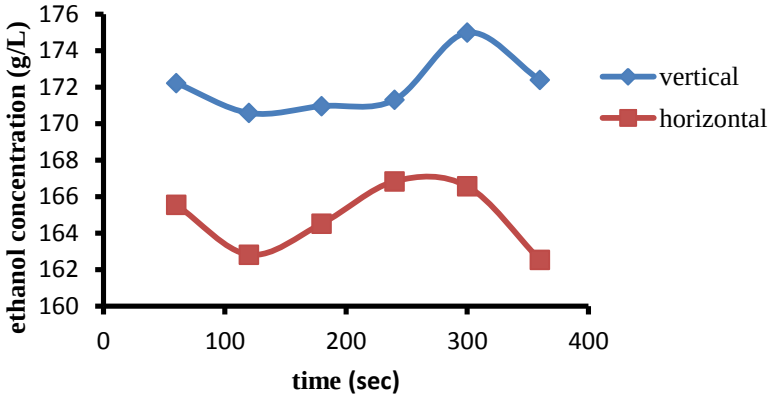

Figure C.18: Variation of concentration with time in both directions for E30 at 4 cm

HPLC calibration curve is given in Figure C.19 which gives the relation between area under the curve and amount in g/L

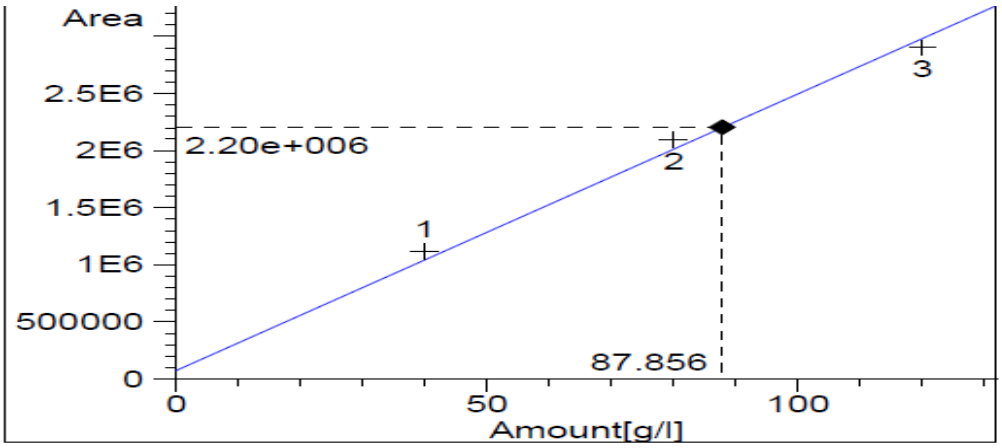

Figure C.19: Calibration curve to determine the concentration

C.6 Refractive index signal for ethanol-HPLC spectrum

Data File C:\CHEM32\1\DATA\ETHANOL 2013-10-10 11-05-07\001-0101.D
Sample Name: Sample 10% 4cm 60 sec

Method Method completed 11:08:23 10/10/13

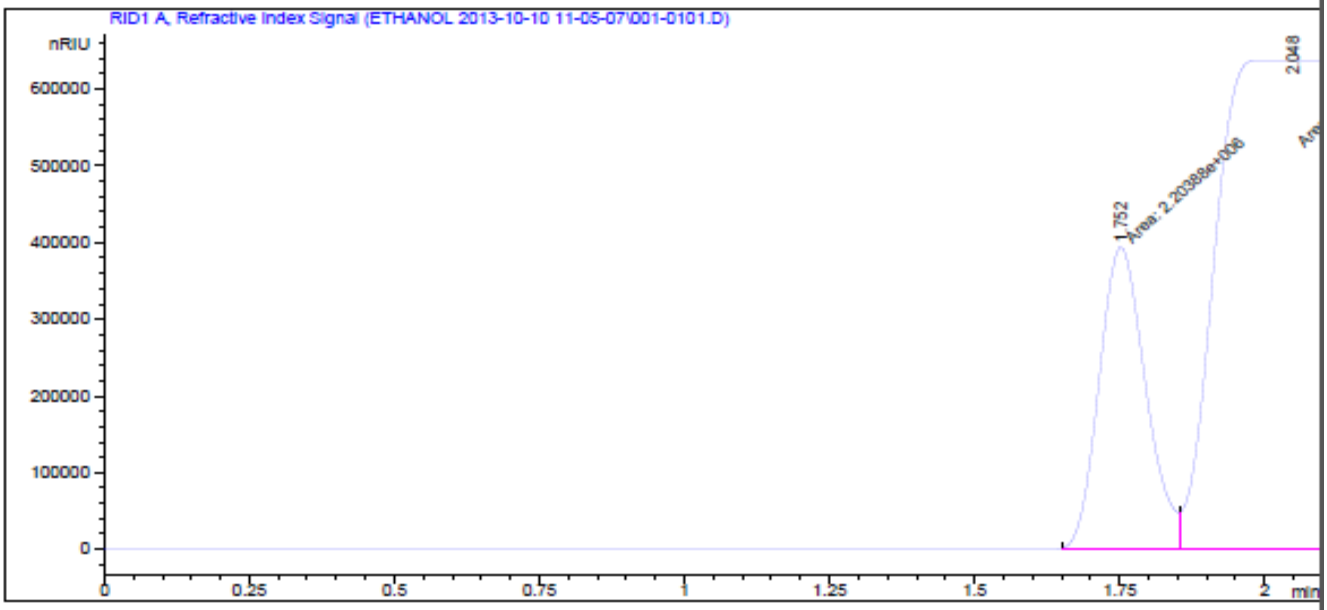

External Standard Report

Sorted By : Signal
Calib. Data Modified : 9/16/2013 14:12
Multiplier: : 1.0000
Dilution: : 1.0000
Use Multiplier & Dilution Factor with ISTDs

Signal 1: RID1 A, Refractive Index Signal

RetTime [min]	Type	Area [nRIU*s]	Amt/Area	Amount [g/l]	Grp	Name
1.752	MF	2.20388e6	3.98641e-5	87.85585		Ethanol A
Totals :				87.85585		

Instrument 1 10/10/2013 13:28 Antony Page 2 of 3

Figure C.20: Refractive index signal for ethanol-HPLC spectrum

- **Effect of the amount of ethanol on the temperature profile as function of distance**

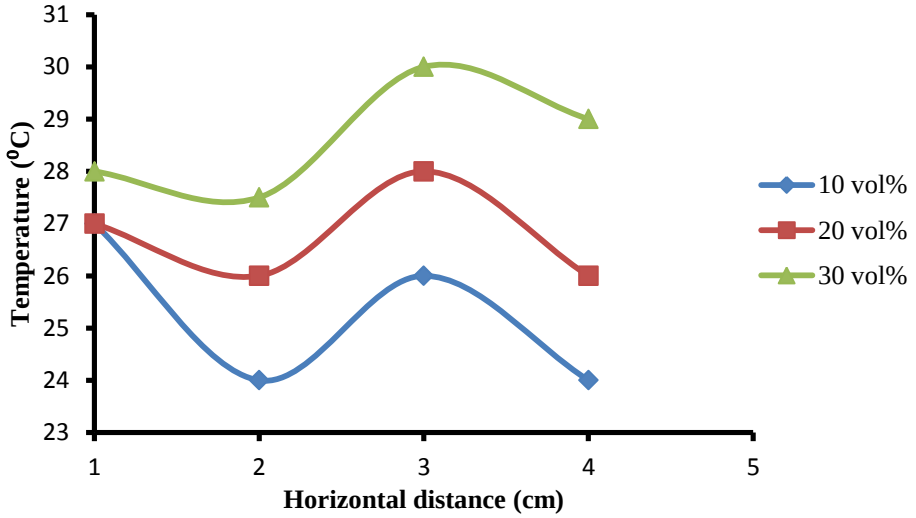

Figure C.21: Temperature as function of distance for 60 second

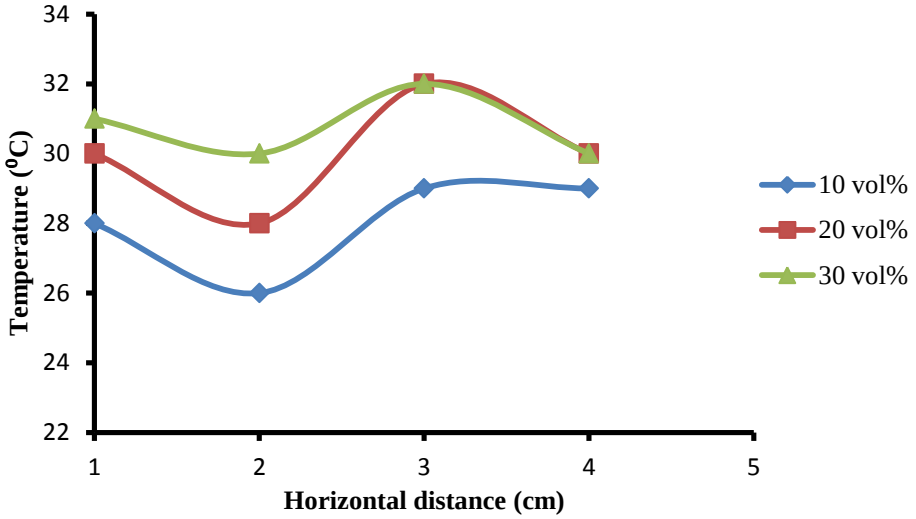

Figure C.22: Temperature as function of distance for 120 second

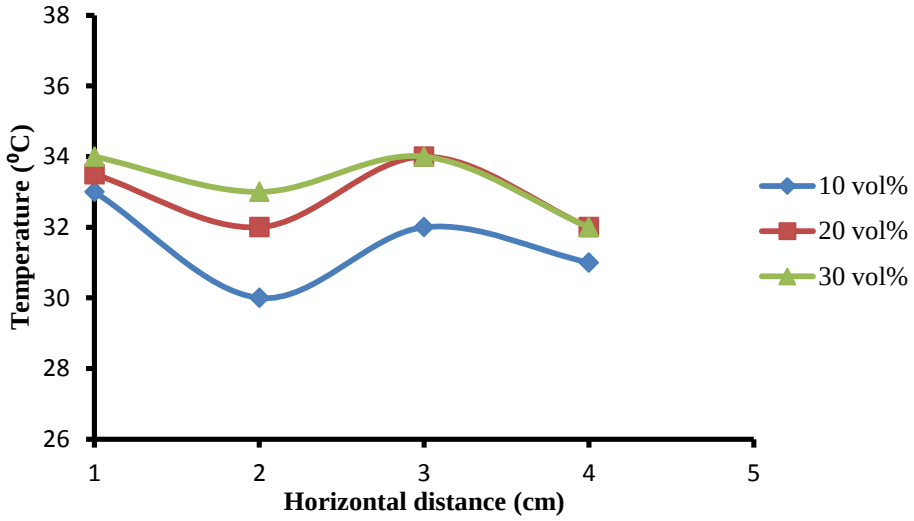

Figure C.23: Temperature as function of distance for 180 second

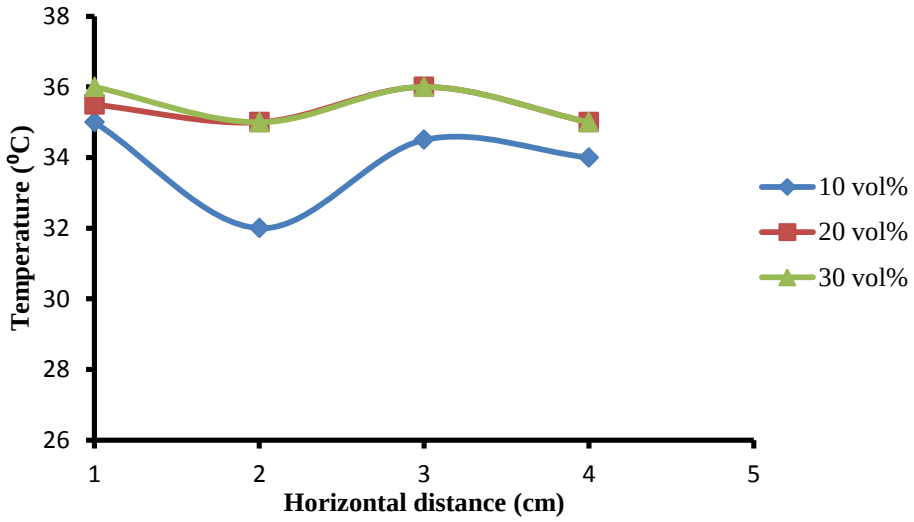

Figure C.24: Temperature as function of distance for 240 second

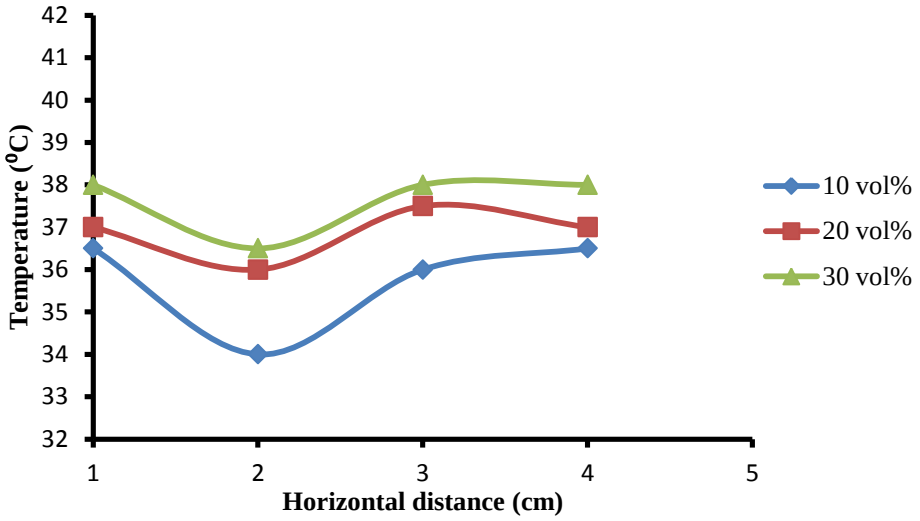

Figure C.25: Temperature as function of distance for 300 second

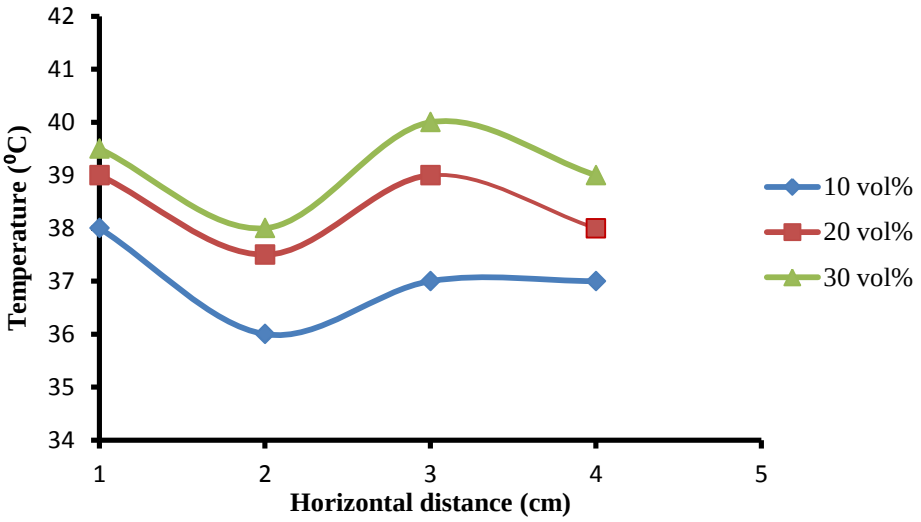

Figure C.26: Temperature as function of distance for 360 second

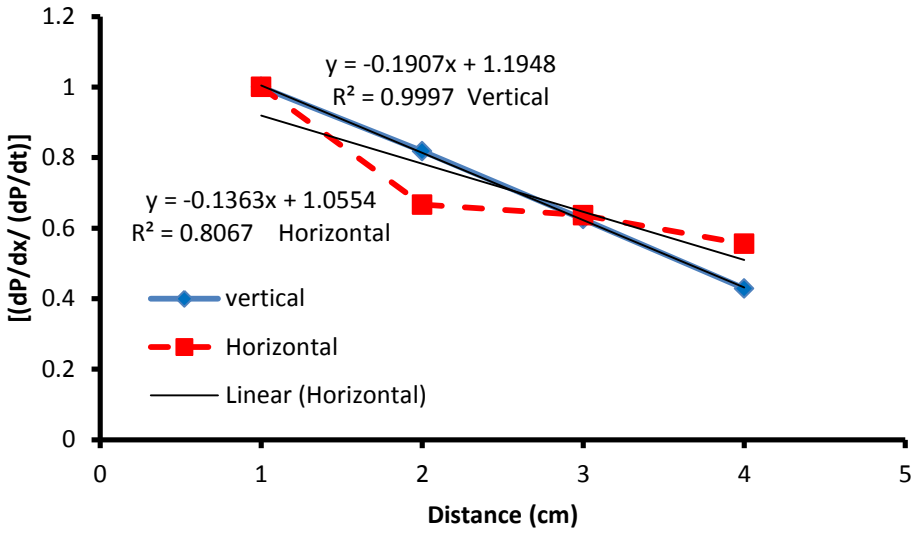

Figure C.26: Mixing efficiency against distance

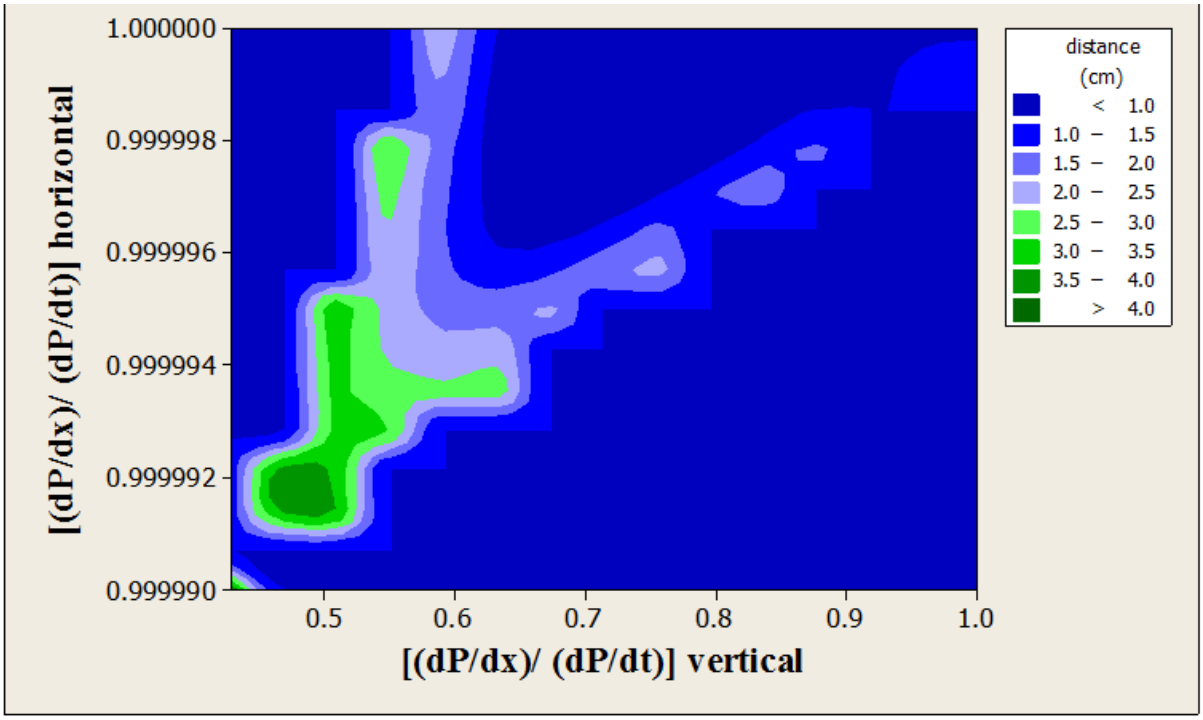

Figure C.27: horizontal mixing efficiency against vertical mixing efficiency

Appendix D

Table D.1: Data obtained from the combustion experiment

Ethanol composition (vol %)	0	20	40	60	80	100
Time (min)	Temperature (^{o} C)	Temperature (^{o} C)	Temperature (^{o} C)	Temperature (^{o} C)	Temperature (^{o} C)	Temperature (^{o} C)
2	55	80	109	80	118	110
4	76	95	131	111	131	134
6	90	108	144	130	140	150
8	101	116	145	139	143	162
10	108	120	146	146	147	165
12	112	122	150	148	149	168
14	115	124	150	148	151	170
16	118	126	152	148	151	171
18	119	127	152	148	152	173
20	120	127	152		151	175
22	121	126				174
24	122					177
26	126					180
28	126					180
30	126					180

D.1 Fuel Consumption

Table D.2: Data showing the consumption of fuel as the ratio of ethanol in the mixture is increased

Ethanol Ratio	Consumed Fuel (mL)	Run time (min)	Fuel Consumption rate (mL/min)
0	5.5	30.83	0.178
20	6.5	23.80	0.273
40	6.5	20.83	0.312
60	7	18.33	0.382
80	8	20.42	0.392
100	13	32.13	0.405

D.2 Exhaust emissions

D.2.1 Chromatograms

The following chromatograms were obtained from a Bruker Gas Chromatographer. The analysis was aimed at checking the composition of the exhaust gas from the combustion process.

Figure D.1 shows a chromatogram of an exhaust gas formed from a fuel with 0 % ethanol and a carbon monoxide peak with a retention time of 1 minute.

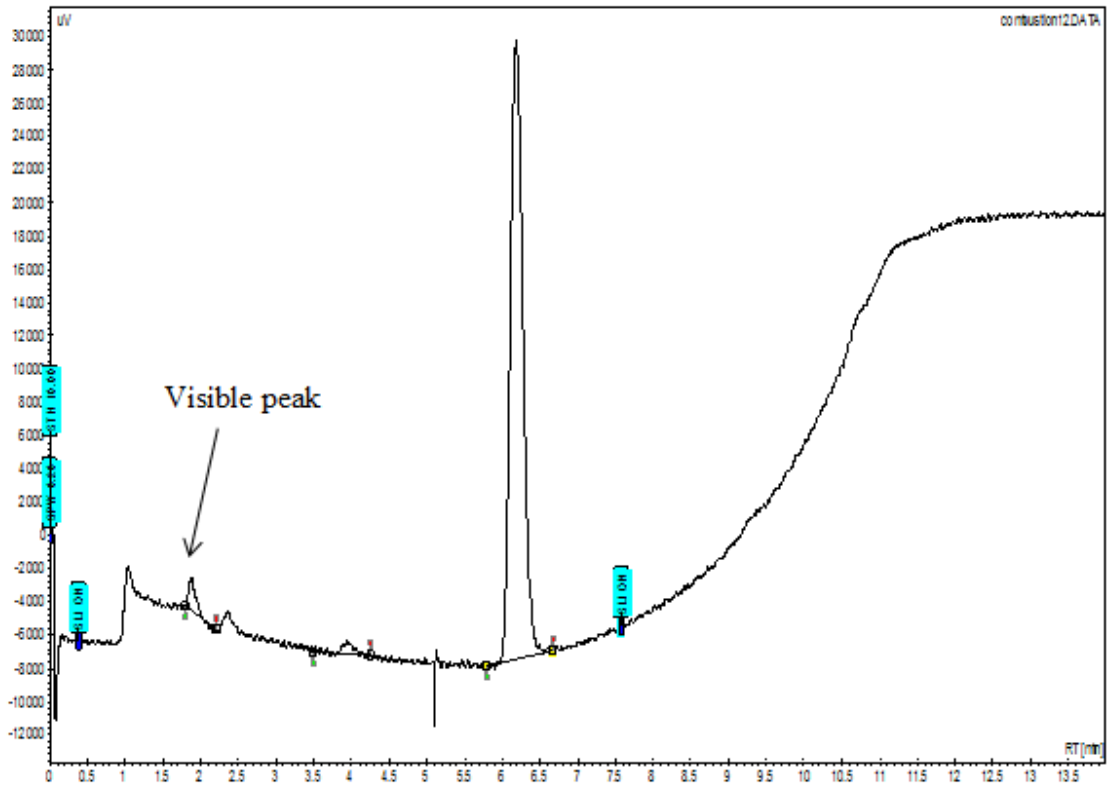

FiguD.1: Chromatogram showing exhaust gases from the combustion of petrol

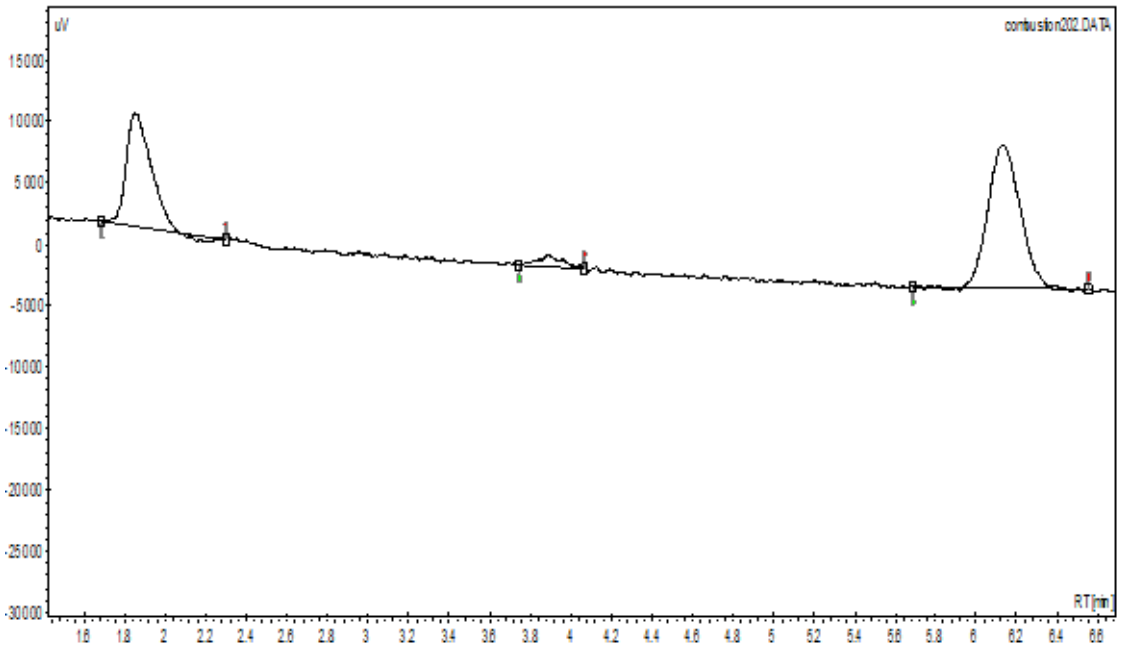

Figure D.2: Chromatogram obtained from the analysis of the exhaust gas that results from 20 % ethanol fuel blend

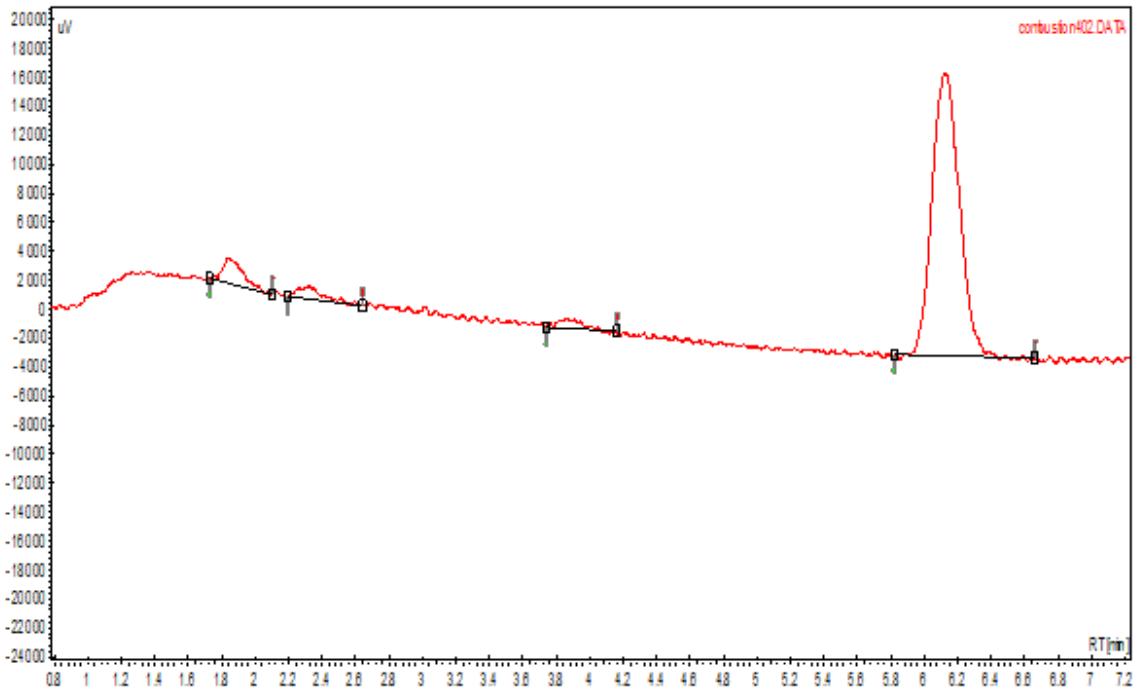

Figure D.3: Chromatogram obtained from the analysis of the exhaust gas that results from 40 % ethanol fuel blend

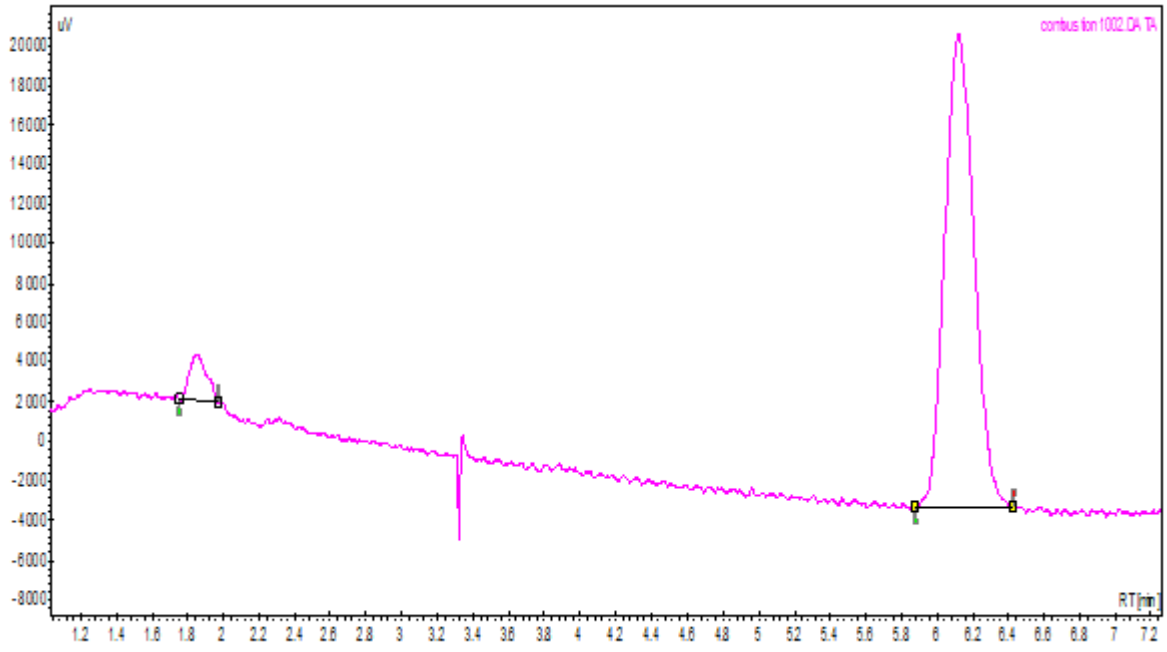

Figure D.4: Chromatogram obtained from the analysis of the exhaust gas that results from 60 % ethanol fuel blend

Table D.3: Data showing the Carbon dioxide composition in the exhaust gas

Ethanol composition	% CO_2	% CO
0	94.43	23.5
20	83.24	9.6
40	69.10	5.4
60	87.63	1.3
80	94.39	4.2
100	97.44	3.3

D.3 Fuel power

The fuel power was determined according to equation 2.37 in the results section. The volume of fuel consumed was converted to mass of fuel consumed by using the mass and density relations:

$$\rho = \frac{m}{V}$$

Where: m is the mass of the fuel

V is the volume of the fuel

ρ is the density of the fuel, ethanol has a density of 789 kg/m^3 and petrol has a density of 737.22 kg/m^3

The mass of the fuel consumed is then multiplied by the calorific value of the fuel and that gives the fuel power. Table D.4 shows the calculated fuel power of the different fuel blends.

Table D.4: Fuel power data

Ethanol Ratio	Consumed Fuel (mL)	Run time (min)	Fuel Consumption rate (mL/min)	Mass of fuel consumed (kg)	Mass consumed per second (kg/s)	Fuel power
0	5.5	30.83	0.178	0.0041	2.1917E-06	0.0973
20	6.5	23.80	0.273	0.0049	3.4028E-06	0.1411
40	6.5	20.83	0.312	0.0049	3.9412E-06	0.1518
60	7	18.33	0.382	0.0054	4.8891E-06	0.1740
80	8	20.42	0.392	0.0062	5.085E-06	0.1660
100	13	32.13	0.405	0.0103	5.32E-06	0.1580

D.4 Indicated power calculation

The evaluation of Indicated power requires the evaluation of mean effective pressure (mep). As shown in 2.4.2 by equation 2.37 and 2.39 that mep is a function of internal energy at all the states during one cycle, the indicated power estimation required that the temperature at each state in the cycle be known. Unfortunately the temperature at the end of the compression stroke and combustion could not be measured due to availability of equipment. Hence the temperature at these states in the cycle was obtained theoretical using equation 2.76 and equation 2.79. The evaluation of equation 2.79 was handled by MATLAB because of large amount of data that needs to be handled. The code has been attached in appendix F. Equation 2.76 was applied a follows;

The fuel entered the cylinder at 25 degrees Celsius and atmospheric pressure. From Table D.5 showing internal energies and critical volumes, the critical volume of air at 25 degrees Celsius and 1 atm was found and used to find the critical volume when the volume of the cylinder occupied by air/fuel mixture had reached the minimum after isentropic compression. The following equation D.1 was used to calculate the critical volume:

$$vr_2 = \frac{v_1}{v_2} vr_1 \qquad \text{(D.1)}$$

A temperature value corresponding to vr_2 was then found from Table D.5 of appendix D.4. This temperature was used as T_2 in equation 2.76 to find the pressure at state 2 in Figure 2.6.

The temperature of the exhaust gas was measured during the experiment to complete the cycle. After determining the temperatures at all the states of the cycle, the internal energy at each state was interpolated from appendix D.4. The internal energies were then plugged into equation 2.39 to find work of one cycle which was the used in equation 1 to determine the mep. The calculated mep was then used in equation D.2 for determining the indicated power (IP) for ethanol-petrol blend at different component content?

$$IP = mep \times L \times A \times N \qquad \text{(D.2)}$$

Table D.5: Ideal gas properties of air (Moran et al, 2005)

T(K), h and u(kJ/kg), s° (kJ/kg · K)												
				when $\Delta s = 0$[1]						when $\Delta s = 0$	
T	h	u	s°	p_r	v_r	T	h	u	s°	p_r	v_r
750	767.29	551.99	2.64737	37.35	57.63	1300	1395.97	1022.82	3.27345	330.9	11.275
760	778.18	560.01	2.66176	39.27	55.54	1320	1419.76	1040.88	3.29160	352.5	10.747
770	789.11	568.07	2.67595	41.31	53.39	1340	1443.60	1058.94	3.30959	375.3	10.247
780	800.03	576.12	2.69013	43.35	51.64	1360	1467.49	1077.10	3.32724	399.1	9.780
790	810.99	584.21	2.70400	45.55	49.86	1380	1491.44	1095.26	3.34474	424.2	9.337
800	821.95	592.30	2.71787	47.75	48.08	1400	1515.42	1113.52	3.36200	450.5	8.919
820	843.98	608.59	2.74504	52.59	44.84	1420	1539.44	1131.77	3.37901	478.0	8.526
840	866.08	624.95	2.77170	57.60	41.85	1440	1563.51	1150.13	3.39586	506.9	8.153
860	888.27	641.40	2.79783	63.09	39.12	1460	1587.63	1168.49	3.41247	537.1	7.801
880	910.56	657.95	2.82344	68.98	36.61	1480	1611.79	1186.95	3.42892	568.8	7.468
900	932.93	674.58	2.84856	75.29	34.31	1500	1635.97	1205.41	3.44516	601.9	7.152
920	955.38	691.28	2.87324	82.05	32.18	1520	1660.23	1223.87	3.46120	636.5	6.854
940	977.92	708.08	2.89748	89.28	30.22	1540	1684.51	1242.43	3.47712	672.8	6.569
960	1000.55	725.02	2.92128	97.00	28.40	1560	1708.82	1260.99	3.49276	710.5	6.301
980	1023.25	741.98	2.94468	105.2	26.73	1580	1733.17	1279.65	3.50829	750.0	6.046
1000	1046.04	758.94	2.96770	114.0	25.17	1600	1757.57	1298.30	3.52364	791.2	5.804
1020	1068.89	776.10	2.99034	123.4	23.72	1620	1782.00	1316.96	3.53879	834.1	5.574
1040	1091.85	793.36	3.01260	133.3	22.39	1640	1806.46	1335.72	3.55381	878.9	5.355
1060	1114.86	810.62	3.03449	143.9	21.14	1660	1830.96	1354.48	3.56867	925.6	5.147
1080	1137.89	827.88	3.05608	155.2	19.98	1680	1855.50	1373.24	3.58335	974.2	4.949
1100	1161.07	845.33	3.07732	167.1	18.896	1700	1880.1	1392.7	3.5979	1025	4.761
1120	1184.28	862.79	3.09825	179.7	17.886	1750	1941.6	1439.8	3.6336	1161	4.328
1140	1207.57	880.35	3.11883	193.1	16.946	1800	2003.3	1487.2	3.6684	1310	3.944
1160	1230.92	897.91	3.13916	207.2	16.064	1850	2065.3	1534.9	3.7023	1475	3.601
1180	1254.34	915.57	3.15916	222.2	15.241	1900	2127.4	1582.6	3.7354	1655	3.295
1200	1277.79	933.33	3.17888	238.0	14.470	1950	2189.7	1630.6	3.7677	1852	3.022
1220	1301.31	951.09	3.19834	254.7	13.747	2000	2252.1	1678.7	3.7994	2068	2.776
1240	1324.93	968.95	3.21751	272.3	13.069	2050	2314.6	1726.8	3.8303	2303	2.555
1260	1348.55	986.90	3.23638	290.8	12.435	2100	2377.4	1775.3	3.8605	2559	2.356
1280	1372.24	1004.76	3.25510	310.4	11.835	2150	2440.3	1823.8	3.8901	2837	2.175
						2200	2503.2	1872.4	3.9191	3138	2.012
						2250	2566.4	1921.3	3.9474	3464	1.864

Source: Tables A-22 are based on J. H. Keenan and J. Kaye, *Gas Tables,* Wiley, New York, 1945.

D.5 MATLAB codes

D.5.1 MATLAB codes used to find the maximum temperature in the cylinder

This code calculates the maximum temperature reached in the cylinder during combustion for each blend:

```
syms T
Cv = constant ('Cv'); % call the constant volume heat capacities stored in the file named 'constant'
Hf = constant ('Hf'); % enthalpies of formation
xE0 = [0.016; 0; 0.209; 0.775; 0; 0; 0; 0]; % composition of the air fuel mixture in the cylinder
xf = [0; 0; 0; 0; 0.462; 0.077; 0.3077; 0.154]; % composition of products from equation 21
Reactants = sum (Hf.*xE0); % the internal energy of the reactants
T1 = 298.15; % temperature of the fuel entering the cylinder
%Internal energy of the of the products at the unknown maximum
%temperature (T)
products1=((Cv(:,1)*(T-T1)+(0.5)*Cv(:,2)*(T^2-T1^2)+(1/3)*Cv(:,3)*(T^3-T1^3)+(1/4)*Cv(:,4)*(T^3-
T1^3)).*(xf/1000));
products2=Hf.*xf;
Products = sum (products1+products2);
To solve = Products-Reactants; % Change in internal energy due to reaction
Y = solve (to solve); % solve for the maximum temperature
%20Ethanol blend

%E20
xE20=[0.0218; 0.01253; 0.2048; 0.760845; 0; 0; 0; 0];% composition of the air fuel mixture in the
cylinder
Reactants E20 = sum (Hf.*xE20); % the internal energy of the reactants
T1=298.15; % temperature of the fuel entering the cylinder
%Internal energy of the of the products at the unknown maximum
%temperature (T)
productsE201=((Cv(:,1)*(T-T1)+(0.5)*Cv(:,2)*(T^2-T1^2)+(1/3)*Cv(:,3)*(T^3-T1^3)+(1/4)*Cv(:,4)*(T^3-
T1^3)).*(xf/1000));
productsE202=Hf.*xf; % the internal energy of the reactants
ProductsE20 = sum (productsE201+productsE202);
tosolveE20=ProductsE20-ReactantsE20; % Change in internal energy due to reaction
yE201=solve (tosolveE20); % solve for the maximum temperature
yE202=double (yE201);
```

%E40

xE40= [0.01101; 0.0169; 0.2062; 0.760845; 0; 0; 0; 0]; % composition of the air fuel mixture in the cylinder

ReactantsE40= sum (Hf.*xE40); % the internal energy of the reactants

T_1=298.15; % temperature of the fuel entering the cylinder

%Internal energy of the of the products at the unknown maximum

%temperature (T)

productsE401=((Cv(:,1)*(T-T_1)+(0.5)*Cv(:,2)*(T^2-T_1^2)+(1/3)*Cv(:,3)*(T^3-T_1^3)+(1/4)*Cv(:,4)*(T^3-T_1^3)).*(xf/1000));

productsE402=Hf.*xf;

ProductsE40= sum (productsE401+productsE402);

tosolveE40=ProductsE40-ReactantsE40; % Change in internal energy due to reaction

yE401= solve (tosolveE40);

yE402= double (yE401);

%E60

xE60= [0.0163; 0.05625; 0.19672; 0.731; 0; 0; 0; 0]; % composition of the air fuel mixture in the cylinder

ReactantsE60= sum (Hf.*xE60); % composition of the air fuel mixture in the cylinder

T_1=298.15; % temperature of the fuel entering the cylinder

%Internal energy of the of the products at the unknown maximum

%temperature (T)

productsE601=((Cv(:,1)*(T-T_1)+(0.5)*Cv(:,2)*(T^2-T_1^2)+(1/3)*Cv(:,3)*(T^3-T_1^3)+(1/4)*Cv(:,4)*(T^3-T_1^3)).*(xf/1000));

productsE602=Hf.*xf;

ProductsE60= sum (productsE601+productsE602);

tosolveE60= ProductsE60-ReactantsE60; % Change in internal energy due to reaction

yE601= solve (tosolveE60); % solve for the maximum temperature

yE602= double (yE601);

%E80

xE80=[0.00768;0.0706;0.1955;0.7262;0;0;0;0];% composition of the air fuel mixture in the cylinder

ReactantsE80= sum (Hf.*xE80); % the internal energy of the reactants

T_1=298.15; % temperature of the fuel entering the cylinder

%Internal energy of the of the products at the unknown maximum

%temperature (T)

productsE801=((Cv(:,1)*(T-T_1)+(0.5)*Cv(:,2)*(T^2-T_1^2)+(1/3)*Cv(:,3)*(T^3-T_1^3)+(1/4)*Cv(:,4)*(T^3-T_1^3)).*(xf/1000));

productsE802=Hf.*xf;

ProductsE80= sum (productsE801+productsE802);

tosolveE80= ProductsE80-ReactantsE80; % Change in internal energy due to reaction

yE801= solve (tosolveE80); % solve for the maximum temperature

yE802= double (yE801);

%E100

xE100= [0.0; 0.077; 0.1957; 0.7271; 0; 0; 0; 0]; % composition of the air fuel mixture in the cylinder

ReactantsE100= sum (Hf.*xE100); % the internal energy of the reactants

T_1= 298.15; % temperature of the fuel entering the cylinder

%Internal energy of the of the products at the unknown maximum

%temperature (T)

productsE1001=((Cv(:,1)*(T-T_1)+(0.5)*Cv(:,2)*(T^2-T_1^2)+(1/3)*Cv(:,3)*(T^3-T_1^3)+(1/4)*Cv(:,4)*(T^3-T_1^3)).*(xf/1000));

productsE1002=Hf.*xf;

ProductsE100= sum (productsE1001+productsE1002);

tosolveE100= ProductsE100-ReactantsE100; % Change in internal energy due to reaction

yE1001= solve (tosolveE100);% solve for the maximum temperature

yE1002= double (yE1001);

T_f= [y2; yE202; yE402; yE602; yE802; yE1002]; % arrange the results in column form

xlswrite('newfile.xls',Tf,'Sheet1','A1')% Export the results to Microsoft excel

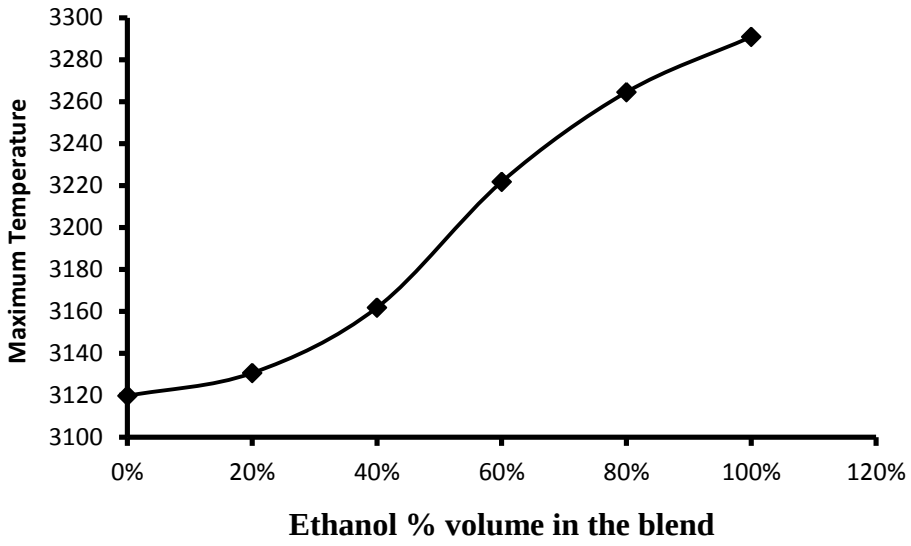

Figure D.5: maximum temperature in the cylinder as a function of ethanol percentage in the blends

D.5.2 MATLAB code used to calculate the amount of nitrogen oxide at different percentages of ethanol.

This code calculates the amount of NO produced during combustion

syms x

PN=7.78E+06; % the partial pressure of oxygen after isentropic compression

PO=1789401.366; % the partial pressure of nitrogen after isentropic compression

c=PO/PN; %Oxygen partial pressure divided by nitrogen partial pressure

% the equilibrium constant of reaction forming NO at different ethanol %

% starting with zero % ethanol at the maximum cylinder temperatures already

% calculated

For k= [2.96353E-30 2.92785E-30 2.83E-30 2.65384E-30 2.53913E-30 2.47223E-30];

F=4*c*x^2-k*x^2+2*k*x-k; % equilibrium constant as a function

B=solve (F); % Solve for the conversion of Nitrogen and Oxygen

C= B(2); % obtains the real solution found above

L= double(C); % converts the solution from fraction to scientific notation

Ans= L(:)*2*1E15% exports the calculated values to the command window

end

D.6 Fuel consumption Tables

Table D.4: Fuel consumption

Ethanol %	Final Depth (cm)	final Vol (ml)	Volume consumed(ml)	Total run time (min)	consumption per min
0%	4.2	396.23	103.77	30.83	3.37
20%	3.8	358.49	141.51	28.80	4.91
40%	4	377.36	122.64	30.83	3.98
60%	3.5	330.19	169.81	22.33	7.60
80%	3.4	320.75	179.25	20.42	8.78
100%	3	283.02	216.98	23.00	9.43
Initial depth (cm)	5.3				
Area (cm^2)	94.34				
Initial volume (mL)	500				

D.7 Procedure for calculating each value in table:

Ethanol percentage was in the first column is the volume percentage of ethanol introduced into the engine tank. Once poured into the tank, the level was measured by a ruler. The initial depth was found to 5.3 cm for 500 ml of fuel poured into the fuel tank.

Using the 500 ml and 5.3 cm as initial volume and fuel level respectively, the area of the tank was calculated by dividing the volume by the level of the fuel in the tank as follows;

$$A = \frac{V}{L} = \frac{500}{5.3} = 94.34\ cm^2 \quad \text{(Shown in Table D.4)}$$

After running the engine for the time shown in column 5 of Table D.4, a constant temperature of the exhaust gas was obtained and this was assumed to be the time the generator stabilized. After this time the engine was stopped and the new level of the fuel was measured. This level was then used to determine the remaining fuel in the tank by multiplying it with the area calculated above as shown below;

Final Volume of fuel at time t $= fuel\ level\ at\ time\ t \times\ Area$

For example the final volume for 0% ethanol composition was calculated as follows:

Fuel level at 30.83 minutes was 4.2 cm. Therefore the Final Volume of fuel at time t $= 4.2 \times 94.34 = 396.23\ ml$ as shown in row 2 and column 2 of Table D.4.

Fuel consumption $= \frac{\text{Initial volume of fuel} - \text{Final Volume of fuel of run time}}{run\ time} = \frac{500-396.23}{30.83} = 3.37 ml/min$ as shown in the first row of the last column of Table D.4.

D.7 Gas Chromatograph (GC) Calibration

The calibration of the GC which enabled the conversion of the percentages provided by the GC to usable percentages was done using air. The GC provided composition of each gas present in the sample as the area under the peak divided by the sum of the areas under all the peaks arising as a consequence of gas detection by the GC. The calibration curve developed related the area to volume percentage as shown in Figure D.5. The calibration using air was done as follows:

Air was assumed to contain nitrogen (79%) and oxygen (21%) because the peaks of other gases present in air like carbon dioxide and argon did not appear as they exist in small amounts. The GC used nitrogen as carrier gas hence the present of nitrogen was not shown by the presence of any peak within the time range used during analysis. So by varying the concentration of oxygen/nitrogen in air by adding nitrogen into it before ejecting into the GC, various peak areas of oxygen were obtained. The volume of nitrogen added was measured to give the exact volume % of oxygen after the addition of nitrogen which was then related to the peak area obtained as shown in Figure D.5. The data obtained during the calibration has been shown in Table D.6.

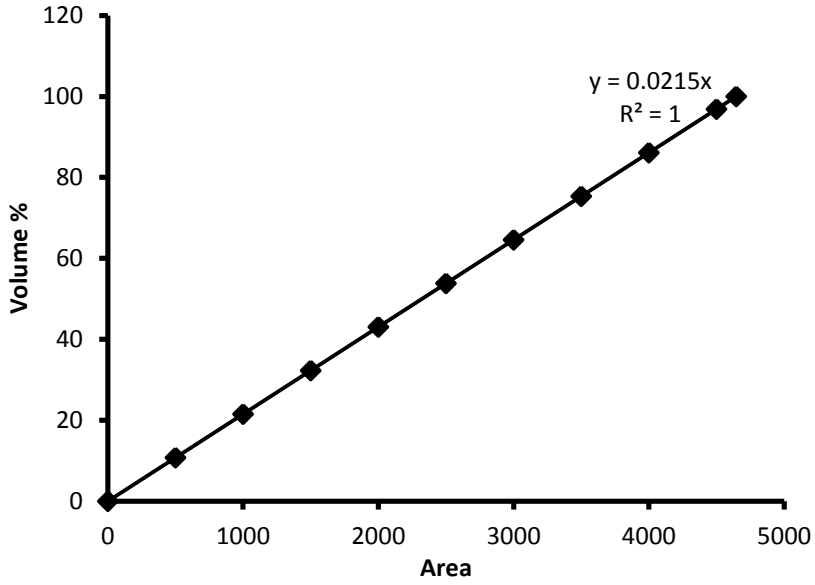

Figure D.6: volume percentage as a function of Area under a peak (GC Calibration curve)

Table D.6: Areas under the peaks corresponding to volume percentages of oxygen

area	% O_2 by volume
0	0.00
500	10.76
1000	21.52
1500	32.29
2000	43.05
2500	53.81
3000	64.57
3500	75.34
4000	86.10
4500	96.86

D.8 Specific heats at constant pressure (C_P) and volume (Cv) (kJ/kmol. K)

Reactants

Petrol (C_8H_{18}): $C_P = 25.3 + 0.162T$

Ethanol (CH_5OH) $C_P = 9.014 + 0.214T - 8.39 \times 10^{-5}T^2 + 13.733 \times 10^{-10}T^3$

Oxygen (O_2): $C_P = 27.0 + 0.0079T$

Nitrogen (N_2): $C_P = 27.6 + 0.0051T$

Products (Sinnott, 2005; Lior*et al*, 1988)

Carbon Dioxide (CO_2): $C_P = 27.4 + 0.0058T$

Carbon monoxide (CO): $C_P = 30.87 - 0.013T + 27.892 \times 10^{-6}T^2 - 1.272 \times 10^{-8}T^3$

Water (H_2O): $C_P = 30.5 + 0.0103T$

Nitrogen oxide (NO): $C_P = 29.45 - 9.38 \times 10^{-4}T + 9.8 \times 10^{-6}T^2 - 4.2 \times 10^{-8}T^3$

The specific heat at constant volume is expressed as a function of the specific heat at constant pressure:

$$C_V = C_P - R \quad \text{(D.3)}$$

D.9 Estimation of nitrogen oxide in the exhaust gas

The effects on NO concentration have been determined theoretically from the equilibrium calculation because of the lack of equipment to measure the low NO emission as follows:

The formation of NO follows the following chemical reaction:

$N_2 + O_2 \rightarrow 2NO$ ΔHrxn = 90.43kJ/mol, ΔG0=86.75 kJ/mol given at 25 ^{0}C

From Levenspiel (1999), the equilibrium constant is calculated using the standard Gibbs free energy at temperature T_1 using the equation D.4:

$$K_1 = Exp\frac{-\Delta G^0}{RT_1} \quad \text{D.4}$$

The equilibrium constant at temperature T is related to K_1 and $-\Delta H_{rxn}$ by equation D.5

$$K = K_1 Exp\frac{-\Delta H_{rxn}}{R}\left(\frac{1}{T} - \frac{1}{T_1}\right) \quad \text{D.5}$$

Where: T the temperature at which combustion occurred (maximum Temperature) and is calculated using the MATLAB code in appendix D.5.2. ΔH_{rxn} is the enthalpy of reaction and R is the ideal gas constant (R=8.314 J/mol K)

$As\Delta H_{rxn}$, T and R are known, the equilibrium constant can be calculated for all blended fuel.

The calculated equilibrium constant is then related to the production of NO at equilibrium by the following equation:

$$K = \frac{{P_{NO}}^2}{P_{N_2}P_{O_2}} \quad \text{D.6}$$

In terms of conversion and as oxygen was the limiting reactant, equation D.6 can be expressed as:

$$K = \frac{P^{o}{}_{O_2} X^2}{P^{o}{}_{N_2} (1-X)^2} \quad \text{D.7}$$

The partial pressures of oxygen and nitrogen were estimated as follows:

The amount of air introduced into the cylinder was assumed to be theoretical amount which is the same as the volume of the cylinder when the piston is at bottom dead center.

The amount of oxygen available for formation of NO was estimated from the results as follows: The amount of oxygen consumed during combustion of ethanol and petrol is equal to the theoretical amount because there was a complete combustion which can be expressed as oxygen reacting in equation 2.59:

$$O_2 \text{ reacting} = O_2 \text{ fed to the cylinder} - 3.5n_{ethanol} - 13.5n_{petrol} \quad \text{D.8}$$

Where $n_{ethanol}$ and n_{petrol} is the number of moles of ethanol and petrol fed to the cylinder at the beginning of each cycle and this was calculated by fuel consumption per minute and dividing by 180 (revolution per min/2) since it takes two revolutions for a four stroke engine to complete one cycle.

The number of moles of oxygen reacting by reaction in equation 2.59 is converted to partial pressure using equation 2.52.

Once partial pressure are known equation D.7 could then be solve using MATLAB as shown in D.5.2 for X. NO formed is found by multiplying X by 2 according to reaction in equation 2.59.

Once NO has been found, the number of moles of oxygen not reacted was found by:

$$\text{Oxygen in the exhaust gas} = O_2 \text{ fed to the cylinder} - 3.5n_{ethanol} - 13.5n_{petrol} - X \quad \text{D.9}$$

As the molar % is the same as the volumetric %, and based on the results (% of O_2) obtained from gas analysis, the total number of moles in the exhaust gas was estimated by:

$$n_{exhaust} = \frac{n_{Oxygen}}{Oxygen\ vol\ \%} \quad \text{D.10}$$

The concentration of NO was then calculated by:

$$\%NO = 2X/n_{exhaust} \quad \text{D.11}$$